Comparative Performance of Different Statistical Models for Predicting Ground-Level Ozone (O_3) and Fine Particulate Matter ($PM_{2.5}$) Concentrations in Montréal, Canada

Edouard Philippe Martin

A Thesis
in
The Department
of
Building, Civil and Environmental Engineering

Presented in Partial Fulfillment of the Requirements
For the Degree of Master of Applied Science (Civil Engineering) at
Concordia University
Montréal, Québec, Canada

May 2011

CONCORDIA UNIVERSITY

School of Graduate Studies

This is to certify that the thesis prepared

By: **Edouard Philippe Martin**

Entitled: **Comparative Performance of Different Statistical Models for Predicting Ground-Level Ozone (O_3) and Fine Particulate Matter ($PM_{2.5}$) Concentrations in Montréal, Canada**

and submitted in partial fulfillment of the requirements for the degree of

Master of Applied Science (Civil Engineering)

complies with the regulations of the University and meets the accepted standards with respect to originality and quality.

Signed by the final Examining Committee:

_____ Chair

Dr. S. Li

_____ Examiner

Dr. C. Mulligan

_____ Examiner

Dr. M. Y. Chen

_____ Supervisor

Dr. Z. Chen

Approved by _____

Dr. K. Ha-Huy, Graduate Program Director
Department of Building, Civil and Environmental Engineering

_____ 2011 _____

R.A.L. Drew, Dean
Faculty of Engineering and Computer Science

ABSTRACT

Comparative Performance of Different Statistical Models for Predicting Ground-Level Ozone (O_3) and Fine Particulate Matter ($PM_{2.5}$) Concentrations in Montréal, Canada

Edouard Philippe Martin

Ground-level ozone (O_3) and fine particulate matter ($PM_{2.5}$) are two air pollutants known to reduce visibility, to have damaging effects on building materials and adverse impacts on human health. O_3 is the result of a series of complex chemical reactions between nitrogen oxides (NOx) and volatile organic compounds (VOCs) in the presence of solar radiation. PM is a class of airborne contaminants composed of sulphate, nitrate, ammonium, crustal components and trace amounts of microorganisms. $PM_{2.5}$ is the respirable subgroup of PM having an aerodynamic diameter of less than 2.5 μm. Development of effective forecasting models for ground-level O_3 and $PM_{2.5}$ is important to warn the public about potentially harmful or unhealthy concentration levels.

The objectives of this study is to investigate the applicability of Multiple Linear Regression (MLR), Principle Component Regression (PCR), Multivariate Adaptive Regression Splines (MARS), feed-forward Artificial Neural Networks (ANN) and hybrid Principal Component – Artificial Neural Networks (PC-ANN) models to predict concentrations of O_3 and $PM_{2.5}$ in Montréal (Canada). Air quality and meteorological data is obtained from the *Réseau de surveillance de la qualité de l'air* (RSQA) for the Airport Station (45°28′N, 73°44′W) and the Maisonneuve Station (45°30′N, 73°34′W) for the period January 2004 to December 2007. Air pollution data include concentration

values for nitrogen monoxide (NO), nitrogen dioxide (NO_2), carbon monoxide (CO) and 142 different volatile organic compounds. Meteorological data include solar irradiation (SR), temperature (Temp), pressure (Press), dew point (DP), precipitation (Precip), wind speed (WS) and wind direction (WD).

Analysis of the available volatile organic compound data expressed on a propylene-equivalent concentration indicated that m/p-xylene, toluene, propylene and (1,2,4)-trimethylbenzene were species with the most significant ozone forming potential in the study area.

Different models and architectures have been investigated through five case studies. Predictive performances of each model have been measured by means of performance metrics and forecast success rates. Overall, MARS models allowing second order interaction of independent basis functions yielded lower error, higher correlation and higher forecast success rates. This study indicates that models based on statistical methods can be cost-effective tools to forecast ground-level O_3 and $PM_{2.5}$ in Montréal and to provide support for decision makers in protecting human health.

AKNOWLEDGEMENTS

I would like to express my appreciation to my thesis supervisor, Dr. Zhi Chen, for his guidance and continuous support throughout my graduate studies at Concordia University. Dr. Chen taught me how to define and develop a research project. He has encouraged me to investigate topics that interest me while providing timely suggestions for improvement. I sincerely thank him for his patience during the time it took me to write this thesis.

I take this opportunity to knowledge Dr. John Hadjinicolaou, who has marked my academic journey with his insatiable questioning of why (and how) things are the way they are. I would like to thank Mr. Conrad Lapensée and Mme. Rodica Motora: they taught me more than calculus and linear algebra in high school, they taught me logic and critical thinking.

I extend my gratitude to Mr. Claude Gagnon (*Réseau de Surveillance de la Qualité de l'Air de Montréal)* for providing the data for this thesis, and the whole team at Salford Systems (San Diego, California, USA) for providing the "Salford Predictive Miner" software.

To my wife Deniz

Aos meus pais e aos meus irmãos
e à toda minha familia

In the hope that others will continue and improve on this work...

TABLE OF CONTENTS

List of Figures

List of Tables

List of Symbols

A	Number of correctly predicted exceedances
BF_i	Generic basis function
c	Generic knot in BF_i
c_p	Penalty factor
d	Effective degrees of freedom
e	Model residual
E	System overall energy
f	Generic activation function
f_{sig}	Sigmoid activation function
i	Generic index, $i = \{1, 2, 3, \ldots, n\}$
F	Number of predicted exceedances
I	Identity matrix
K_{OH}	OH-reactivity
L	Diagonal matrix
$\mathbf{L_{ss}}$	Sum of squares matrix
M	Number of observed exceedances
n	Number of observation
p	Number of independent variables
q	Number of hidden nodes
r	Sample correlation coefficient

R^2	Coefficient of determination
s	Sample standard deviation
s^2	Sample variance
Sy	Variance matrix of matrix **Y**
Sz	Variance matrix of matrix **Z**
t	Time of observation
$\mathbf{u_1}$	Column vector
$\mathbf{v_1}$	First column vector of matrix **V**
V	Orthonormal matrix
w	Weight of hidden node
$\hat{w}$	Estimate of w through the Gradient descent rule
x	Generic independent variable
$\bar{x}$	Mean of x
X	Matrix of generic independent variables
y	Generic dependent variable
$\hat{y}$	Predicted value of y
$\dot{y}$	Geometric mean
y^T	Power transform of y
y^{T*}	Scaled y^T
Z	Matrix of autoscaled generic independent variables
α	Multiplier in hidden layer output
β	Independent variable coefficient in a regression based model
$\hat{\beta}$	Ordinary Least Square estimate of coefficient β

ε	Random error in a regression based model
λ	Eigenvalue
η	Learning rate
φ	Level of power transform
θ	Constant in hidden layer output
θ_w	Wind direction
ψ	Phase shift parameter

List of Abbreviations and Acronyms

ANN	Artificial Neural Network
CI	Confidence Interval
CWS	Canada Wide Standards
EC	Environment Canada
FPR	False Positive Rate
GVC	Generalized Cross Validation
MAE	Mean Absolute Error
MAPE	Mean Absolute Percent Error
MARS	Multivariate Adaptive Regression Splines
MLR	Multiple Linear Regression
NAPS	National Air Pollution Surveillance
OLS	Ordinary Least Squate
PC	Principal Components
PCA	Principal Component Analysis
PCR	Principal Component Regression
RMSE	Root Mean Squared Error
SE	Standard Error
SI	Success Index
SR	Solar Radiation

TPR	True Positive Rate
WD	Wind Direction
WDI	Wind Direction Index
WGAQOG	Working Group on Air Quality Objectives and Guidelines

Chapter 1

Introduction

1.1 Background

In Canada, both the public and private sectors have a long track record in developing strategies to control air pollution. Despite the coordinated implementation of these strategies and advances in technology over the past years, ozone and particulate matter are still prevalent in Eastern Canada (Brook and Dann, 2002). Because these two air pollutants are known to reduce visibility, to have damaging effects on building materials and to have adverse impacts on human health (Seinfeld and Pandis, 1998), they remain important areas of concern for the scientific and engineering communities.

Ground-level ozone is the result of a series of complex chemical reactions between precursor species, namely nitrogen oxides (NO_x) and volatile organic compounds (VOCs) in the presence of solar radiation (Nazaroff and Alvarez-Cohen, 2001).

Particulate matter is an intricate mixture of solid and liquid chemical elements, organic compounds and biological species that vary in size and remain suspended in the

air. Precursor species to particulate matter are known to include NO_x, VOCs, sulphur dioxide (SO_2) and ammoniac (NH_3) (Stanier, 2003).

While ozone and particulate matter are a common problem to almost all major cities in Eastern Canada, the magnitude of the problem varies regionally and locally. Development of effective forecasting models at the local level to predict concentrations of ozone and particulate matter is important because the information provided allows people within a community to take precautionary measures to avoid or limit their exposure to unhealthy levels of air quality (Karatzas and Kaltsatos, 2007).

Air pollution forecasting strategies can be divided in two broad categories: deterministic and statistical. In deterministic models, prior knowledge about the underlying chemical and physical processes governing air pollution is described by means of differential equations with boundary condition (Liu, 2007). Statistical models are more pragmatic mathematical descriptions of how the data can conceivably be produced. Statistical models are used to a greater extent at trend estimation and to a lesser degree at elucidating underlying mechanisms.

Deterministic models are commonly divided in three broad categories, namely: Gaussian, Lagrangian and Eulerian models (Su, 2004). A number of working deterministic platforms have been developed for air pollution monitoring, namely the "Regional Climate Model" (Caya et al., 1995), the "Multiscale Air Quality Simulation Platform" (Odman and Ingram, 1996), the "Goddard Earth Observing System-Chemistry" (Garner et al., 2005) and the "Global Environmental Multi-Scale - Modelling Air Quality and Chemistry" (Talbot et al., 2008), which is

the current operational large-scale model used by Environment Canada to predict ozone and particulate matter.

Deterministic models predict air pollution at the regional scale, but are less suited to capture variance at the local level due to their higher-level spatial resolution (Vautard et al, 2008). In practice, it is seldom feasible to construct a strictly deterministic model to forecast air pollution at the local scale because it requires extensive knowledge of site-specific chemical and physical phenomena, and the collection of a prohibitively large dataset (USEPA, 2003). Often, the complexity of the equations used in deterministic models to represent air pollution dynamics renders analytic solution impossible. In such cases, the model is treated as a black box and numerical algorithms are used to estimate the parameters of the differential equations. One way to improve the computation of parameters in deterministic models is to combine model outputs with measurements from monitoring stations for air pollutants and other meteorological variables (Liu, 2007).

Statistical models offer an alternative to deterministic models for predicting ozone and fine particulate matter as they require only a limited number of mathematical assumptions about the physical behaviour of the system (Turalığlu et al., 2005).

There are two complementary but often overlapping approaches in statistical modelling: model-driven and data-driven (Solaiman et al., 2008). Model driven approaches are based on mathematical or probabilistic methods, simple or sophisticated, that capture the main features of the data. Once the model is specified, analyses are driven by that model. The validity of these analyses depends upon assumptions of additivity of effect and homogeneity of error variance. Some

inferences are strictly valid under further assumptions of normality of residuals. The majority of model-driven approaches are in some sense regression-based, with varying degrees of complexity (Thompson et al., 2001). Model-driven methods include Multiple Linear Regression, Nonlinear Regression, Piecewise Regression and Quantile Regression. Data-driven approaches comprise of analytic processes designed to explore data in search of consistent patterns and/or systematic relationships between variables without an explicit model characterization (Solaiman et al., 2008). Data-driven models are also to a great extent user-centric and interactive processes which leverage analysis technologies and machine computing power. Data-driven methods include Classification and Regression Trees, Cluster Analysis, Fuzzy Inference Systems, Artificial Neural Networks, Bayesian Networks and Multivariate Adaptive Regression Splines.

Over the years, a number of statistical approaches, both model and data driven, have been proposed to forecast ground-level ozone and particulate matter. Despite their evident useful contributions, no *a priori* conclusion can be drawn with respect to their overall performance considering different geographic locations and meteorological conditions (Sousa et al., 2007). In other words, conclusions drawn from a specific study cannot be extrapolated to other sites due to area specificities. Only through model development and performance assessment can we conclude which model is best suited for a specific location.

To this date, no comparative assessment of different statistical models for short-term prediction of ground level ozone and particulate matter in Montréal (Canada) has been undertaken.

While public health imperative provides one motivation for this study, the challenge of developing accurate air pollution forecasting models provides another.

1.2 Objectives and Scope of This study

The main purpose of this study is to gain understanding of air quality and how concentration levels of air pollutants can be forecasted. In order to investigate this, the thesis takes its analytic departure in an extensive amount of empirical data. The data consist of four years of air quality and meteorological data. In this way, we analyse and incorporate both chemical and physical measurements.

The objectives of this study are to determine seasonal and diurnal patterns of ground-level ozone (O_3) and fine particulate matter ($PM_{2.5}$); to investigate the ozone forming potential of different volatile organic compound species in the city and to assess the suitability of different statistical methods for short-term forecast.

The reason for focusing on ozone and fine particulate matter (rather than any other known air pollutants) stems from the fact that O_3 and $PM_{2.5}$ are secondary air pollutants (i.e. not emitted from sources) and highly dependent of precursor species and meteorological conditions.

The study area is limited to the most densely populated areas of Montréal. The air quality and meteorological data used in this thesis has been measured and validated by the *Réseau de surveillance de la qualité de l'air (RSQA)* for the period covering January 2004 to December 2007, inclusively.

Data processing, statistical analysis and model development has been carried out using two commercially available statistical softwares, namely "Salford Predictive Miner" from Salford Systems (San Diego, CA, USA) and "JMP Version 5.1.2" from SAS Institute Inc. (Cary, NC, USA).

1.3 Methodology

The proposed methodology comprises the following eight steps:

1. Review the chemical and physical processes involved in the formation of ozone and particulate matter;
2. Identify the potential air pollution and meteorological variables for building prediction models;
3. Obtain relevant data covering a representative period of time;
4. Develop different predictive models based on statistical methods;
5. Define an appropriate set of performance metrics;
6. Assess each model in terms of performance metrics;
7. Determine the best model for short-term forecasting of ozone and particulate matter; and
8. Gauge the performance the developed models in comparison to literature data.

1.4 Value of Results and Contribution to Research

This work contributes to research by a) increasing domain knowledge related to secondary air pollution in Montréal and b) setting the stage for comparative assessment of different models for short-term forecast of secondary air pollution in Montréal.

The following advances over previous air quality studies will be achieved:

1. Statistical analysis of air pollution and meteorological data putting in evidence seasonal and diurnal patterns in Montréal;
2. Comparison of air pollution levels in different areas of the city;
3. Development of different prediction models based on statistical methods for forecasting of ozone and fine particulate matter;
4. Determination of the ozone-forming potential of different VOC species; and
5. Determination of which statistical method best supports short-term forecast of O_3 and $PM_{2.5}$ locally in Montréal given the area's specific geography and site conditions.

The results of this study can be of interest as a reference and benchmark for future research.

1.5 Organisation of this Thesis

This thesis is organized as follows:

Chapter 1 is the introductory section. It provides the reader with the background and rationale for this study as well this research's objectives and scope. Then, it sheds light on the proposed methodology to achieve our objectives.

The literature survey in Chapter 2 provides the reader with an appropriate level of knowledge about the several topics included in this thesis. First, we review the structure of the Earth's atmosphere. Then, we review the main chemical and physical processes involved in formation of ozone and particulate matter. Thirdly, we review the current understanding of the impacts on health due to different levels of ambient O_3 and $PM_{2.5}$. After that, we review the standards related to air quality standards in Montréal. And lastly, we survey the most recent studies dealing with short-term prediction of ozone and fine particulate matter.

Chapter 3 focuses on the experimental methods of this thesis. It first introduces moment statistics recurrent in this study. Then, it formally introduces the statistical methods used for building forecasting models. After that it describes the models developed in this thesis and the set of metrics for performance assessment.

Chapter 4 presents the investigation area and the set of data collected for this study. We start by discussing the quality of the data, and then follow by characterizing the data and specifying the procedure used for building different datasets.

Chapter 5 is the model validation section of this study. We provide the results of five different case studies with comparison to literature data.

Chapter 6 summarizes the main findings of this research and provides recommendation for future work.

Chapter 2

Literature Review

The purpose of this literature survey is to give the reader sufficient background information on the structure and properties of the different layers in the Earth's atmosphere; on the different chemical and physical processes involved in formation of ozone and fine particulate matter; on the current body of knowledge pertaining to the health impacts of these secondary air pollutants, on the current framework of air quality in Montréal; and finally, to provide the reader with a survey of the most recent studies dealing with short-term prediction of ozone and fine particulate matter. A discussion and a summary are provided at the end of the chapter.

2.1 Earth's Atmosphere

The Earth's atmosphere is composed of four main layers covering our planet to a height of approximately 100 km (Barry and Chorlet, 2003). It consists of a mixture of gases held by gravitational attraction to Earth and that is compressed under its own weight. These four layers vary in density with altitude, temperature and water content. The genesis of Earth's atmosphere dates back some 3 billion years (Dalrymple, 2004). Figure 2.1 shows

the four main layers of the atmosphere (i.e. thermosphere, mesosphere, stratosphere and troposphere) and their temperature profile.

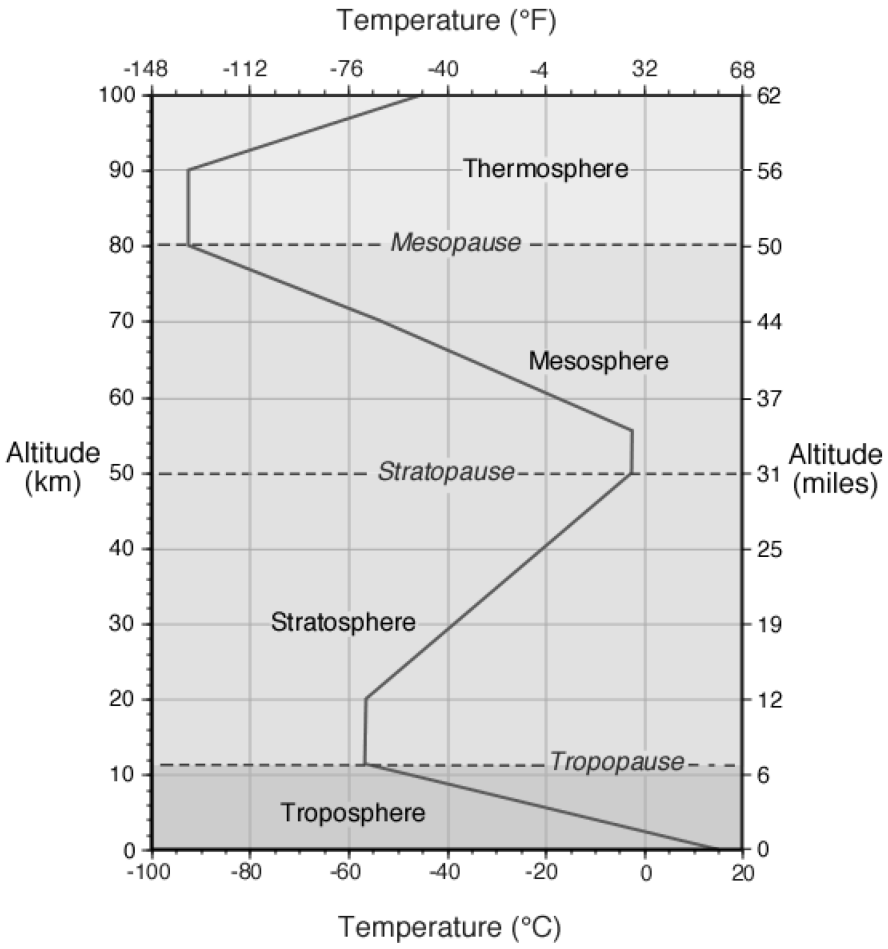

Figure 2.1 Earth's atmosphere (Seinfeld and Pandis, 1998)

The troposphere is the most superficial layer of the atmosphere. It extends from the sea level to an average height of 11 km. Greatest heights occur at the tropics where warm temperatures cause vertical expansion of the lower atmosphere. The thickness of the troposphere varies with solar intensity, as gas expands with increasing levels of absorbed energy. The intensity of solar irradiation is greater near the equator than the

poles. From a mere 7 km at the poles, it becomes gradually thicker to reach 18 km at the equator. All meteorological phenomena (clouds, depressions, rain, thunders, tornados, cyclone, etc…) occur in the troposphere since it is here that approximately 80% of atmospheric air and water vapour are found. At sea level, the composition by volume of dry atmospheric air is composed of 78% nitrogen (N_2), 21% oxygen (O_2), 0.8 argon (Ar), 0.03 carbon dioxide (CO_2), with trace amounts of neon (Ne), helium (He), methane (CH_4), krypton (Kr), hydrogen (H_2), carbon monoxide (CO), xenon (Xe), ozone (O_3) and radon (Rn) totalling less than 0.0003%. The atmosphere contains water vapour in amounts up to 4% by weight (Hutcheon and Handegord, 1995).

The density of the atmosphere decreases exponentially with altitude, but vertical circulation produces vigorous mixing sufficient to maintain an uniform composition up to about 75 km (Hutcheon and Handegord, 1995). The dominant influence is the heating of the earth's surface by incoming solar radiation. Air at the surface is heated, expands, and becomes buoyant. As the buoyancy rises, it expands and cools down in response to the lower atmospheric pressure at elevated heights. As altitude increases, constituent gases become scarcer. Tropospheric temperature decreases with height at a rate of -6.5 ^{o}C/km. This phenomenon is commonly called the "Environmental Lapse Rate" (Seinfeld and Pandis, 1998). At the uppermost height of the troposphere (tropopause), temperature reaches -56^{o}C at an average height of 8.7 km above the sea level. The total mass of the troposphere is estimated to 5.3 x 10^{18} kg (Nazaroff and Alvarez-Cohen, 2001).

Above the troposphere is the stratosphere. This second layer extends from an average altitude of 11 to 50 km. Comparatively, very little weather related events occur in the stratosphere as it contains about 19.9 % of the total mass of the atmospheric

constituent gases (Seinfeld and Pandis, 1998). The lower portion of the stratosphere is influenced by the polar jet stream and subtropical jet stream. It is only on occasion that the top portions of thunderstorms breach the stratosphere.

There is an isothermal layer in the first 9 km, where temperature remains relatively constant with height. From an altitude of 20 to 50 km, temperature increases with an increase in height. The higher temperatures found in this region of the stratosphere occurs because of a localized ozone gas concentration.

This area of localized ozone is paramount to life on Earth as it shields the Earth's surface from excessive solar irradiation (ultraviolet rays) creating heat energy that warms the stratosphere. Ozone is primarily found in the atmosphere at varying concentrations between the altitudes of 10 to 50 km. A transition zone the stratopause separates the mesosphere from the stratosphere.

In the mesosphere, the atmosphere reaches -90°C at an altitude of 80 km. At the top of the mesosphere is another transition zone known as the mesopause.

At an altitude greater than 80 km sits the most external layer of the atmosphere called the thermosphere. Temperatures in this layer can be as high as 1200°C generated from the absorption of solar radiation by oxygen molecules (Barry and Chorlet, 2003). The air in the thermosphere is extremely thin with individual gas molecules being separated from each other by large distances.

2.2 Ozone (O_3)

The ozone (O_3) molecule, also referred to as triatomic oxygen, consists of three oxygen atoms bound together. O_3 is a powerful oxidizing agent unlike diatomic oxygen (O_2).

Ozone is a reactive oxidant that forms in two parts of the atmosphere: the stratosphere and the troposphere. Naturally occurring stratospheric ozone shields life on earth from the harmful effects of the sun's ultraviolet radiation, but at the troposphere, ozone can have damaging effects on building materials and be harmful to human beings.

Tropospheric ozone is a secondary photochemical pollutant: secondary in the sense that ozone in the troposphere is not emitted from anthropogenic or biogenic sources; and photochemical in the sense that the chemical reactions that lead to its production are driven by energy from the sun (Seinfeld and Pandis, 1998).

Ground-level ozone is the result of a series of complex chemical reactions between precursor species, namely nitrogen oxides (NO_x) and volatile organic compounds (VOCs) in the presence of solar irradiation (Nazaroff and Alvarez-Cohen, 2001). While the chemistry of ozone formation is complex, the main features are well established.

The formation and destruction of ground-level O_3 is governed by the following set of three reactions known as the "primary photolytic cycle" (Nazaroff and Alvarez-Cohen, 2001):

$$NO_2 + h\nu \rightarrow NO + O\bullet \quad (2.1)$$

$$O\bullet + O_2 + M \rightarrow O_3 + M \quad (2.2)$$

$$O_3 + NO \rightarrow NO_2 + O_2 \quad (2.3)$$

In the first reaction, nitrogen dioxide (NO_2) absorbs the energy of a photon light ($h\nu$) and dissociates into nitric oxide (NO) and an oxygen radical ($O\bullet$). In the second reaction, the

oxygen radical combines with a diatomic oxygen (O_2) in the presence of a third "body" (M) to form ozone (O_3). In air, the "body" is a non-specific molecule containing nitrogen or oxygen atoms or fine suspended particulate matter. The "body" absorbs energy from the exothermic chemical reaction that combines O• and O_2 into O_3. In the third reaction, ozone oxidises nitric oxide to nitrogen dioxide and is converted back to molecular oxygen.

Reaction (2.1) is the primary source of oxygen radicals. Reaction (2.2) is the only significant means by which ozone is formed and reaction (2.3) is the most important ozone removal mechanism. The NO_2 photolysis reaction (2.1) depends on sunlight and the rate of this reaction (k_1) can be as high as 0.5 min^{-1} during daylight hours. Reactions (2.2) and 2.3 are comparatively fast, the reactions rates (k_2 and k_3) are 21.8 ppm^{-1} min^{-1} and 26.8 ppm^{-1} min^{-1} respectively (Nazaroff and Alvarez-Cohen, 2001).

Considering that the nitrogen cycle operates fast enough to operate in steady state balance, the photostationary-state relation is derived:

$$[O_3] = (k_1 / k_3) \times [NO_2] / [NO] \qquad (2.4)$$

Three important points emerge from the photostationary-state relation. First, the level of O_3 depends directly on sunlight intensity (rate constant k_1). Second, the ozone level depends on the relative amounts of NO_2 and NO. A higher NO_2/NO result in higher O_3 concentration and vice-versa. Third, there must be other reactions allowing NO conversion back into NO_2 without destroying O_3.

The first process allowing NO-to-NO_2 conversion is the oxidation of carbon monoxide (CO):

$$CO + OH\bullet \rightarrow CO_2 + H\bullet \quad (2.5)$$

$$H\bullet + O_2 \rightarrow HO_2\bullet \quad (2.6)$$

$$HO_2\bullet + NO \rightarrow NO_2 + OH\bullet \quad (2.7)$$

In reaction (2.5), CO is oxidized by hydroxyl radical (OH•) to form carbon dioxide (CO_2) and a free hydrogen atom (H•). In reaction (2.6), H• and O_2 combine to form a peroxy radical (HO_2•). In reaction (2.7), NO-to-NO_2 conversion occurs as HO_2• is transformed into OH•.

Recall reactions (2.1) and (2.2):

$$NO_2 + h\nu \rightarrow NO + O\bullet \quad (2.1)$$

$$O\bullet + O_2 + M \rightarrow O_3 + M \quad (2.2)$$

The net effect of the oxidation of CO is:

$$CO + 2O_2 \rightarrow O_3 + CO_2 \quad (2.8)$$

The second process allowing NO-to-NO_2 conversion is the oxidation of VOCs:

$$RH + OH\bullet \rightarrow H_2O + R\bullet \quad (2.9)$$

$$R\bullet + O_2 \rightarrow RO_2\bullet \quad (2.10)$$

$$RO_2\bullet + NO \rightarrow NO_2 + RO\bullet \quad (2.11)$$

In reaction (2.9), the organic compound RH is oxidized by OH• to form a water molecule ($H_2O\bullet$) and an organic fragment (R•). In reaction (2.10), R• combines with oxygen to form an organic peroxy radical ($RO_2\bullet$). In reaction (2.11), NO-to-NO_2 conversion occurs as $RO_2\bullet$ is transformed into an organic alkoxy radical (RO•).

The net effect of the oxidation process of VOCs is:

$$RH + OH\bullet + 2O_2 \rightarrow O_3 + H_2O + RO\ \bullet \quad (2.12)$$

The third process allowing NO-to-NO_2 conversion is photolysis of VOCs:

$$HCHO + h\nu \rightarrow H\bullet + HCO\bullet \quad (2.13)$$

$$H\bullet + O_2 \rightarrow HO_2\bullet \quad (2.14)$$

$$HCO\bullet + O_2 \rightarrow HO_2\bullet + CO \quad (2.15)$$

In reaction (2.13), formaldehyde (HCHO) absorbs the energy of a photon light (*hv*) and dissociates into molecular hydrogen (H•) and aldehyde radical (HCO•). Reactions (2.14) and (2.15) are intermediate but important steps as they show how molecular oxygen reacts with H• and HCO• to form peroxy radicals ($HO_2\bullet$) and CO.

The net effect of the photolysis of formaldehyde is the production of two peroxy radicals ($HO_2\bullet$) as shown in reaction (2.16).

$$HCHO + h\nu + 2O_2 \rightarrow 2HO_2\bullet + CO \quad (2.16)$$

Recall reactions (2.7), (2.1) and (2.2) and multiply by a factor of two and re-write:

$$2NO + 2HO_2\bullet \rightarrow 2NO_2 + 2OH\bullet \quad (2.17)$$

$$2NO_2 + h\nu \rightarrow 2NO + 2O\bullet \quad (2.18)$$

$$2O\bullet + 2O_2 + M \rightarrow 2O_3 + M \quad (2.19)$$

The net effect of the photolysis of VOC (described by formaldehyde reactions) is:

$$HCHO + 4O_2 + h\nu \rightarrow 2O_3 + CO + 2OH\bullet \quad (2.20)$$

Ozone removal from the troposphere takes place primarily in the following manner:

$$O_3 + h\nu \rightarrow O_2 + O\bullet \quad (2.21)$$

$$HO_2\bullet + O_3 \rightarrow OH\bullet + 2O_2 \quad (2.22)$$

$$OH\bullet + O_3 \rightarrow HO_2\bullet + O_2 \quad (2.23)$$

Ozone precursors have both anthropogenic and biogenic origins. In urban and industrialized areas, CO, NO_x and VOCs are produced mainly during the combustion of fossil fuels and thus associated with transportation sector and manufacturing (Barry and

Chorlet, 2003). The dominant CO and NO_x sources are combustion processes, including industrial and electrical generation processes, and mobile sources such as automobiles. Mobile sources, chemical industries and refineries or others that use solvents account for a large portion of VOC emissions. VOCs may be classified under four different groups, namely alkanes, alkenes, alkynes and aromatic hydrocarbons. Biogenic VOCs include the highly reactive compound isoprene (Zheng et al., 2009). Ground-level concentrations of biogenic VOCs are typically lower than anthropogenic VOCs.

2.3 Particulate Matter (PM)

Particulate matter (PM) is a broad and important class of air contaminants comprised of physical, chemical and biological substances existing as discreet particles in the atmosphere (Stanier, 2003). Particulate matter emitted directly from sources is referred to "primary particulate matter"' while particulate matter that is formed from precursor species by means of transformation processes is referred to "secondary particulate matter". Airborne particulate matter (also referred as aerosols) may be in either in the liquid or solid state.

Particulate matter composition includes a wide range of chemical elements, organic compounds and biological species that may occur in the particulate phase. The individual particles may be pure substances or, more typically, complex mixtures of chemical element and compounds. Particulate matter also typically contains a variety of inorganic ions, metals, water, soot, oxides and hundreds of organic compounds found as solids, dilute or highly concentrated solutions and multiphase particles. Major

components include sulphate, nitrate, ammonium, crustal components and trace amounts of microorganisms, such as bacteria and viruses (Akyüz and Çabuk, 2009).

Particulate matter size ranges from a molecular cluster of a few nanometres to particles of size in the order of 1000 μm. Particulate matter can be further categorized with respect to size distribution, either in terms of "number size distribution", "surface size distribution" and "mass size distribution". Particle sizes are often indicated in the literature as a subscript. For example, PM_{10} refers to the PM mass with an aerodynamic diameter of less than 10 μm, while $PM_{2.5}$ refers to the mass of particle matter with sizes smaller than 2.5 μm.

Particulate matter larger than 2.5 μm are mostly the result of physical breakdown of larger particles into smaller ones such as windblown soil, sea salt spray, and dust from quarrying operations. This type of particulate matter is considered coarse mode or sedimentation. Fine particulate matter ($PM_{2.5}$) is the respirable subgroup of airborne particulate matter having an aerodynamic diameter of less than 2.5 μm (Diaz-Roblez et al., 2008). The fine particle mode is often subdivided into the accumulation mode (0.1 – 2.5 μm) and the nucleation mode with particle dimension less than 0.1 μm (Nazaroff and Alvarez-Cohen, 2001).

Some $PM_{2.5}$ is emitted directly into the atmosphere as particles from primary sources but in most cases they are the result of chemical reaction, coagulation and condensation of gases. Some processes that emit fine particle include motor vehicle emissions, incomplete combustion, tire and break wear, vehicular activity resulting in road and pavement dust, erosion, manufacturing processes such as smelting and cement manufacturing. The $PM_{2.5}$ composition is primarily elemental carbon, organic carbon,

mineral components of soil, nitrates and sulphates from reactions involving nitrogen oxides, ammoniac (NH_3) and sulphur dioxide (SO_2). Particulates are commonly classified in the following three classes: sulphates, nitrates and organics (Seinfeld and Pandis, 1998).

Sulphate particulate matter arises mainly from sulphuric acid which can be formed through different pathways. In the atmosphere, sulphuric acid droplets react with ammonia or metal oxides to form sulphate salts, such as:

$$H_2SO_4 + NH_3 \rightarrow NH_4HSO_4 \text{ (ammonium sulphate)} \quad (2.24)$$

Nitrate particulate matter is formed from nitric acid (HNO_3). It is produced in the atmosphere following this series of reaction:

$$NO_2 + O_3 \rightarrow NO_3 + O_2 \quad (2.25)$$

$$NO_2 + NO_3 \rightarrow N_2O_5 \quad (2.26)$$

$$N_2O_5 + H_2O \rightarrow 2HNO_3 \quad (2.27)$$

Nitric acid could also result from the reaction of NO_2 with hydroxyl radicals

$$NO_2 + OH\bullet \rightarrow HNO_3 \quad (2.28)$$

The subsequent reaction of nitric acid with ammonia leads to the formation of ammonium nitrate:

$$HNO_3 + NH_3 \rightarrow NH_4NO_3 \text{ (ammonium nitrate)} \quad (2.29)$$

Reaction times for sulphate precursors show that oxidation of sulphate occurs at an average rate of 0.1 to 1 percent of sulphate per hour. Nitrates continuously change between the gas and condensed phases in the atmosphere, so a reaction time is nearly impossible to quantify (Barnard and Hodan, 2004).

Organic particulate matter spring from highly reactive hydrocarbon species in the atmosphere. Their lifetimes due to the reaction with hydroxyl radical and ozone are relatively short except for low carbon number alkanes. Volatile organic compounds are important sources of fine particular matter. VOCs are removed primarily by oxidation and conversion to CO_2, Oxidation of VOC typically leads to a large number of products. Often, at least some of the products of the VOC oxidation are more volatile than the reactant gas. Accordingly, some of the products partition between the gas and aerosol phases. Measuring and predicting the partitioning of the products is a key problem in understanding secondary organic aerosol formation.

The formation of $PM_{2.5}$ from organic compounds depends on four factors: its atmospheric abundance, its chemical activity, the availability of oxidants, and the volatility of the products. All these factors contribute to reaction times, but volatility plays a predominant role, since highly volatile chemicals such as alkanes and alkenes with less than six carbon atoms are unlikely to form $PM_{2.5}$ (Barnard and Hodan, 2004).

Most recently, there has been increased interest in organic aerosols derived from biogenic volatile organic compounds which are emitted from vegetation. This interest is

due to the reactivity of biogenic compounds, their flux to the atmosphere (7 to 10 times anthropogenic emissions on a global scale) and their potentially large impact on global and regional air pollutions (Griffin et al., 1999).

2.4 Influence of Meteorology on O_3 and PM

The previous two sections have shown that formation mechanisms of ozone and particulate matter are dependent on precursor species. Previous studies have shown that concentration levels do not always increase in direct proportion to amounts of precursor species (Slini et al., 2002; Lu and Wang, 2004; Kuo et al., 2008). The relationship is in fact non-linear and highly dependent on meteorological conditions. Generally speaking, the prime meteorological condition for formation of both of these air pollutants are high temperature, high pressure, light surface winds and low relative humidity (Pires et al., 2008a; Pires et al., 2008b; Salazar-Ruiz et al., 2008).

The reaction rates in ozone formation as well as in sulphate, nitrate and organic aerosol formation, increase as ambient temperature increases. While evaporative emissions of VOCs generally increase with increased temperature, the relationship is different depending if the VOC is volatile or semivolatile. Production of ground-level ozone and fine particulate matter is dependent on meteorological conditions and the supply of VOC species. The rate of O_3 and $PM_{2.5}$ production from a given VOC is a function of the species' volatility, temperature, atmospheric mixing and its OH-reactivity (rate of reaction with hydroxyl radicals).

Aloft temperatures inversions can trap precursor below inversion point and inhibit vertical mixing. Ambient temperature also has an indirect effect on precursor availability. Cloud cover can limit daily temperature rise and maximum temperature. Pressure has an effect on the atmospheric lapse rate, on stability and the extent of vertical mixing.

Precipitation scavenging is the primary processes by which fine particulate are eventually removed from the atmosphere. Relative humidity plays an important role in particulate matter formation. Particles (such as sulphates and nitrates) remain dry with increasing relative humidity until their deliquescent point is reached, at which time a sudden uptake of water occurs with a corresponding increase in particle size (Stanier, 2003).

Particles larger than 2.5 μm (the sedimentation or coarse mode) are efficiently removed by gravitational settling, and therefore remain in the atmosphere for shorter periods of a few hours to a few days (HCEC, 1998). As wind speed and wind direction dictates to a great extent the degree of mixing, the prevalence of wind will ultimately determine the persistence of fine particulate matter and ozone precursor species. Calm or light winds produce weak ventilation and allow localized accumulation of precursor species. Table 2.1 shows the residency time and transport distance versus particle size.
Due to wind and pressure systems, airborne particles found in the nuclei mode are subject to random motion and to coagulation processes in which particles collide to quickly yield larger particles. Consequently, these tiny particles will have short atmospheric residence times. Particles in the size range of 0.1–2.5 μm (the accumulation mode) result from the coagulation of particles in the nuclei mode and from the condensation of vapours onto existing particles which then grow into this size range.

The condensation of vapour is dependent on pressure, wind and temperature. Particulate matter in the accumulation mode account for most of the particle surface area and much of the particle mass in the atmosphere since atmospheric removal processes are least efficient in this size range. These fine particles can remain in the atmosphere for days to weeks depending on favourable weather conditions. The same can be said for ozone precursor species.

Particle Diameter (μm)	Settling Velocity (m/min)	Residence Time (t50%)	Transport Distance (L50%)
1000	200	1 min	1 km
100	20	10 min	10 km
10	0.2	1 day	1,000 km
1	0.002	3 months	100,000 km

Table 2.1 Residency time and transport distance versus PM particle size (Patel, 2004)

2.5 Impact of O_3 and PM on Human Health

The detrimental health effects of ozone and particulate matter on human health are well known and have been extensively documented (Mayer, 1999; Bernstein et al, 2004; Maynard, 2004; Kampa and Castanas, 2008). Tables 2.2 and 2.3 summarize the definite, probable and possible impacts of O_3 and $PM_{2.5}$ on human health.

The symptoms of excessive exposure are cough, shortness of breath, increases in airway resistance and bronchial responsiveness to stimuli; and airway inflammation

(Bernstein et al, 2004), cause-specific mortality (Goldberg et al., 2000a; Goldberg et al., 2006) or non-accidental mortality (Goldberg et al., 2000b; Goldberg et al., 2003).

Correlations between increased levels of ambient air pollution and hospital admissions have been shown for certain sensitive subgroups of the population, specifically those with cardiac and respiratory conditions (Delphino, 1998; Deschamps, 2003). Other epidemiological studies have linked O_3 and $PM_{2.5}$ to changes in pulmonary function, respiratory irritation, asthma, chronic bronchitis and even mortality (Maynard, 2004).

The adverse effects on human health of increased levels of ozone and particulate matter are mainly via the respiratory system (Kampa and Castanas, 2008). $PM_{2.5}$ penetrates the alveolar epithelium (Ghio and Huang, 2004) and ozone initiate lung inflammation (Uysal and Schapira, 2003).

Adverse health effects due to ozone depend on concentration, duration of exposure, and degree of exercise. Ozone exposure of less than 0.50 ppm without exercise typically has no effect on lung function; however, ozone exposure with exercise results in decreased respiratory frequency, decreased forced vital capacity, an increase in airway resistance and symptoms (Bernstein et al., 2004). Ozone exposure ranging from 0.10 to 0.4 ppm is traditionally accompanied with neutrophilic inflammation as early as one hour after exposure and can persist for up to 24 hours (Nightingale et al., 1999).

In a recent Montréal study, it was concluded that the mean percent change of asthma related daily hospital admissions decreased by -4.86 (95% CI: -7.17 - -2.50) given a change of -21.4 $\mu g/m^3$ in ozone concentration (Deschamps, 2003). Ozone's more

dramatic effect in asthmatic subjects is most likely a result of existing chronic inflammation in the lower airways (Vagaggini et al., 2002).

Definite Effect	Probable Effect	Possible Effect
Aggravation of asthma	Aggravation of acute respiratory infections	Decreased birth weight
Increased hospital admissions for respiratory and cardiac conditions	Increased risk of wheezy bronchitis in infants 4-12 months	Increased blood fibrinogen
Acute and chronic depressed lung function in children	Decreased rate of lung growth in children	Increased asthma prevalence
Increased prevalence of bronchitis	Tachycardia in the elderly	
Increased risk of lung cancer	Reduced heart rate variability	
	Increased blood vessel constriction	

Table 2.2 Summary of O_3 impacts on human health (adapted from NRTEE, 2008)

Definite Effect	Probable Effect	Possible Effect
Increase hospital admissions for acute respiratory diseases	Effect on mortality	Aggravation of acute respiratory infections
Aggravation of asthma	Increased sensitivity to allergens	Chronic bronchiolitis with repetitive exposure
Increased bronchial responsiveness		Increased prevalence of asthma
Reduced lung function		

Table 2.3 Summary of $PM_{2.5}$ impacts on human health (adapted from NRTEE, 2008)

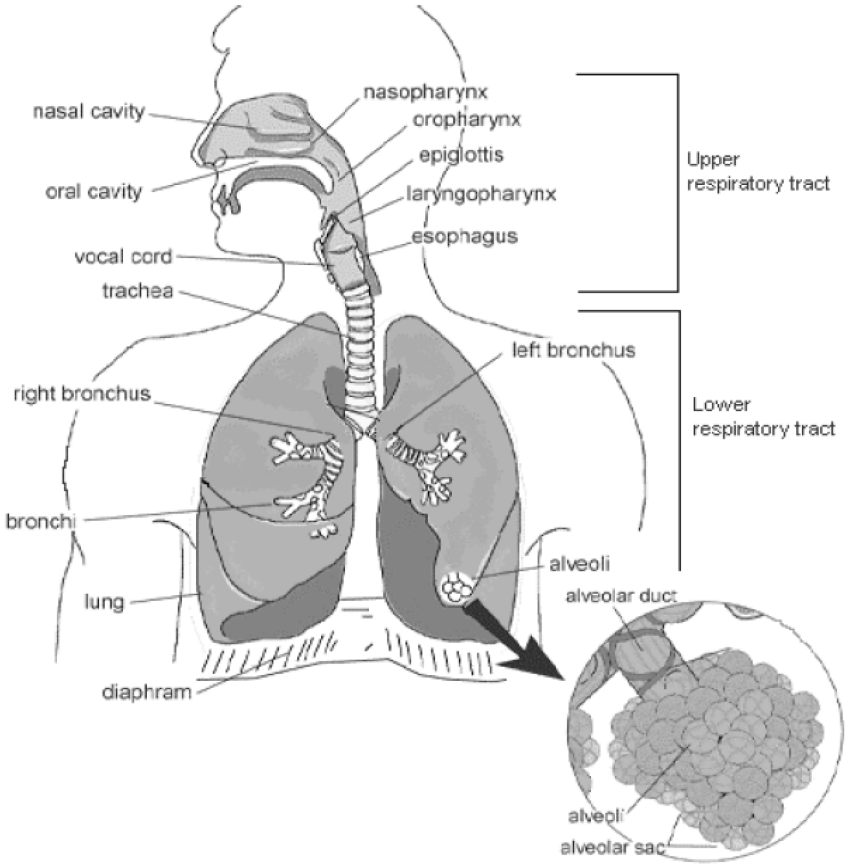

Figure 2.2 Human respiratory system (HCEC, 1998)

Environment Canada has considered the mortality associated with mean ozone concentrations (daily one-hour maximum) that situate between 20 and 75 ppb. There is evidence to show that ozone concentration response relationship is approximately linear, down to 10 ppb, but no evidence of thresholds at low concentration. Furthermore, the risk for non-accidental mortality is 0.79% (95% CI: 0.59-0.99%) for every 10 ppb increase in ozone (daily 1-hour maximum). The weighted mean for respiratory hospitalizations per 10 ppb increase in ozone (daily 1-hour maximum) is 1.12% (95% CI 0.73-1.51%) (HCEC, 1999).

Environment Canada states that the magnitude of the risk of mortality associated with PM_{10} varies by an average 0.8% (95% CI: 0.4% - 1.7%) per 10 μg/m^3 increase for concentrations averaging 25–78 μg/m3; and that overall rate in mortality increases 1.5% (95% CI: 0.85 – 22%) per 10 μg/m^3 increase in $PM_{2.5}$ for concentrations averaging 11 – 30 μg/m^3 (HCEC, 1998). The increase in $PM_{2.5}$ related risk of mortality is thus about twice that for PM_{10}. In a recent Montréal study, it was concluded that the mean percent change of asthma related daily hospital admissions was -0.71 (95% CI: -5.23 – 4.03) given a change of -17.5 μg/m^3 in PM_{10} concentration (Deschamps, 2003). There is little evidence in the PM_{10} and $PM_{2.5}$ data to include a threshold in the dose-response curve. The response was observed to increase monotonically with increasing concentration, in the PM_{10} concentration range below 80–100 μg/m^3 and average $PM_{2.5}$ concentrations 14.7–21 μg/m^3 (HCEC, 1998). The lack of a threshold down to low concentrations suggests that it will be difficult to identify a level at which no adverse effects would be expected to occur as a result of exposure to particulate matter.

So far, no single component has been identified that could explain most of the $PM_{2.5}$ effects. Among the parameters that play an important role for eliciting health effects are the size and surface of particles, their number and their composition. As explained in previous section, the composition of $PM_{2.5}$ varies, as they can absorb and transfer a multitude of pollutants. There is strong evidence to support that ultra fine and fine particles are more hazardous than larger ones (coarse particles), in terms of mortality and cardiovascular and respiratory effects (Kampa and Castanas, 2008). In addition, the metal fraction, the presence of polycyclic aromatic hydrocarbons and other organic components such as endotoxins, mainly contribute to $PM_{2.5}$ toxicity (Maynard, 2004). All

of these constitute the evident epidemiological motivation to consider $PM_{2.5}$ a special class of suspended particulate matter.

The bulk of prior research has focused on mass concentration of fine suspended particles perhaps because a measure of mass of $PM_{2.5}$ in air is straightforward (particles caught in a filter and weighted). Recently, research has begun to focus more on the number concentration of fine suspended particles, the formation and emissions of fresh aerosols particles and the health effects of particles very small, which by their nature can be found in high concentrations without significantly increasing fine particulate matter mass concentration (Stanier, 2003). This focus on particles that can be found in high concentrations but relatively low mass concentrations is supported by recent health studies that show that for a given mass concentration, health effects are larger for smaller particles sizes (Donaldson and McNee, 1998).

2.6 Air Quality Standards for O_3 and PM

In Canada, national ambient air quality objectives (NAAQOs) were first established by the federal government in 1969 under the Clean Air Act. In 1976, standards for ozone and particulate matter were established under this act. In 1988, the Canadian Environmental Protection Act (CEPA) was passed into law, replacing the Clean Air Act. As it was, the NAAQOs were revised under the CEPA by a federal/provincial advisory committee known as the "Working Group on Air Quality Objectives and Guidelines" (WGAQOG).

The WGAQOG's objectives were intended to represent national goals for outdoor air quality, to protect public health and the environment, while ensuring some degree of uniformity across the country. In 1999, the WGAQOG revised the daily 1-hour maxima for O_3 and PM objectives and set a range of levels (rather than specific values) as follows:

- 40 – 50 µg/m3 (20 – 25 ppb) for O_3
- 35 – 40 µg/m3 for PM_{10}
- 20 – 25 µg/m3 for $PM_{2.5}$

In 2000, CEPA was revised, introducing a new framework for setting ambient air quality objectives. It provided a uniform structure for assessing air quality to guide governments in the risk management process by bringing into play local standards and local control strategies. Recognizing the need for a more collaborative national approach on standards setting, Canada's environment ministers, under the auspices of the Canadian Council of Ministers of the Environment (CCME), agreed to new Canada Wide Standards (CWS) in 2000:

- The CWS for ozone is 65 ppb — an 8-hour average, with achievement based on the fourth-highest level measured annually over three years.
- The CWS for $PM_{2.5}$ is 30 µg/m3 — a 24-hour average.

Currently, the actual setting of ambient air quality objectives in Canada is the dual responsibility of both the federal government and provincial/territorial governments. In addition, while provinces have the responsibility and authority to set and enforce air quality objectives, local and regional governments have the authority to pass bylaws that may restrict activities contributing to air pollution emissions in their jurisdiction. Furthermore, provincial and territorial governments have the authority to delegate primary responsibility for air quality management to regional or municipal jurisdictions. For example, the government of Québec has delegated air quality management responsibilities to the Montréal Urban Community.

In Montréal, the 24-hr average objective for O_3 and $PM_{2.5}$ is 50 and 25 $\mu g/m^3$, respectively.

Table 2.4 summarizes a few of the existing Canadian and international objectives, standards, guidelines, goals, and reference levels for ozone.

Pollutant	Period	Montreal		Canada*		United States**	
		ppb	ug/m^3	ppb	ug/m^3	ppb	ug/m^3
NO	**1 h**	1000	1300				
NO2	**1 h**	213	400	213	400		
	24 h	106	200	106	200		
	1 year	53	100	53	100	53	100
CO	**1 h**	30000	35000	30000	35000	35000	40000
	8 h	13000	15000	13000	15000	9000	10000
SO2	**1 h**	500	1300	344			
	24 h	100	260	110		140	
	1 year	20	52	20		30	
O3	**1 h**	82	160	82	160	120	234
	8 h	38	75	65	127***	80	156
	24 h	25	50	25	50		
PM2.5	**3 h**		35				
	24 h		25		30***		35
	1 year						15
*	Maximum acceptable level						
**	US EPA National Ambient Air Quality						
***	CWS						

Table 2.4 Existing air quality objectives, standards and guidelines in Montréal, Canada and United States

2.7 Statistical Models used in O_3 and $PM_{2.5}$ Forecasting

Generally speaking, model-driven statistical approaches are methods aimed at fitting a curve (not necessarily a straight line) through a set of points using some goodness-of-fit criterion. The majority of model-driven approaches are in some sense regression-based, with varying degrees of complexity. Model-driven models include Multiple Linear Regression, Nonlinear Regression, Piecewise Regression and Quantile Regression.

Linear Regression is the most common type of regression. In Linear Regression, the dependent variable is modeled by a function which is a linear combination of the independent variables. The most common techniques to estimate the model parameters are method of moments, Method of Maximum Likelihood and Ordinary Least Squares (OLS). Among these, OLS is the most widely used due to its intuitive derivation and intrinsic simplicity. Linear Regression has been widely used in air quality forecasting (Cuhadaroğlu and Demirci, 1997; Lu and Wang, 2004; Turalığlu et al., 2005).

In Nonlinear Regression, the dependent variable is modeled by a function which is a nonlinear combination of the model parameters and depends on one or more independent variables. Nonlinear models are more difficult to fit than linear models. They require specification of the model and an initial guess for parameter values. Iterative numerical methods are used to search for the least-squares estimates, and there is no guarantee that a solution will be found. Indeed it is possible to diverge, or even to converge on a local solution that is not the least-squares solution. Nonlinear fits do not have some of the nice properties that linear models have, and the results must be interpreted with caution. Nonlinear models have been developed to forecast O_3 (Novara et al., 2007; Xing et al., 2010) and $PM_{2.5}$ (Lin, 2007; Cobourn, 2010).

Piecewise Regression is an extension of the two previous regression approaches. In piecewise regression models, the domain of independent variable space is divided into a number of regions; and for each region, the relationship between the dependent and independent variable is derived by least square fit.

Piecewise regression has been used for the forecast of O_3 (Vyushin et al., 2007) and $PM_{2.5}$ (Lykoudis et al., 2008).

Quantile Regression represents conditional quantiles as functions of predictors. While linear, nonlinear and piecewise regression models specify the change in the conditional mean of the dependent variable associated with a change in the covariates, the quantile-regression model specifies changes in the conditional quantile (Hao and Naiman, 2007). Quantile-regression models can be easily fit by minimizing a generalized measure of distance using algorithms based on linear programming. Potentialities of quantile regression to predict ozone concentrations have been investigated (Sousa et al., 2009).

Multicollinearity (or the high correlation between independent variables) may cause instability in regression models. The instability is in part reflected by large standard errors in the values of regression parameters. Principal Component Analysis (PCA) is one technique used to lessen the degree of multicollinearity from a given dataset. In PCA, a set of correlated variables is transformed into a new set of uncorrelated variables. In Principal Component Regression (PCR), instead of regressing the independent variables on the dependent variable directly, the principal components of the independent variables are used. Often only the principal components with the highest variance are selected (Karatzas and Kaltsatos, 2007). However, the use of low-variance principal components may also be, in some cases, important. Principal Component Regression models have been developed for air quality forecasting (Statherpoulos et al., 1998; Al-Alawi et al., 2008)

In contrast to model-driven, data-driven approaches comprise of analytic processes designed to explore data in search of consistent patterns and/or systematic

relationships between variables without an explicit model characterization. Data-driven approaches use some sort of recurrence relation so that an entire class of objects can be built up from a few initial values and a small number of rules (Solaiman et al., 2008). Data-driven methods include Classification and Regression Trees, Cluster Analysis, Fuzzy Inference Systems, Artificial Neural Networks, Bayesian Networks and Multivariate Adaptive Regression Splines.

Classification and Regression Trees is a non-parametric learning technique (Kim, 2010) that produces either classification or regression trees, depending on whether the dependent variable is categorical or numeric, respectively. Decision trees are formed by a collection of rules based on values of certain variables in the modeling data set. Rules are selected based on how well they split the data into different segment based on variables' values. Each segment is defined by a node. Once a rule and corresponding nodes are selected, matching segments are split into two, and the same logic is applied to each "child" node in a recursive procedure. Splitting stops when no further gain can be made, or some pre-set stopping rules are met. Each branch of the tree ends in a terminal node uniquely defined by a set of rules, and each observation falls into one and exactly one terminal node. Some researchers have proposes the use of classification trees as a suitable technique for forecasting the daily exceedance of ozone (Bruno et al., 2004; Kim, 2010).

Cluster Analysis is an exploratory data-driven approach which aims at sorting different objects into groups in a way that the degree of association between two objects is maximal if they belong to the same group and minimal otherwise. There is some overlapping in the motivation behind Cluster Analysis and

Classification and Regression Trees in the extent that both use algorithms to group objects of similar kind into respective categories and are used to discover structures in data without providing an explanation/interpretation. The main categories of cluster analysis methods include Two-way Joining (Block Clustering), and k-Means Clustering. Recent researchers have applied Cluster Analysis to ozone formation in the atmosphere (Johnson et al., 2007; Tarasova et al., 2007).

In Fuzzy Inference Systems the formulation of the mapping of independent variables to the output variable is achieved using fuzzy logic. This mapping process involves membership functions, logical operations, and if-then rules; and provides a basis from which patterns can be discerned. The most common Fuzzy Inference Systems are Mamdani-type and Sugeno-type. Recent interest in Fuzzy Inference Systems has lead researches to examine its applicability to air pollution modelling (Mintz et al., 2005; Nooria et al., 2010)

In essence, Artificial Neural Networks are a set of simple calculation units that build a non-linear mapping of input vectors to a specified output. Nodes (or neurons) receive an input vector; sums weighted input values and apply a mapping operator to the sum. Nodes are assembled in layers (input, hidden and output) and weights are associated to each node. The objective is to find the optimum set of weights that minimise the overall prediction error. Weight optimization is achieved through an user-specified training algorithm. There are four fundamental types of learning rules: error correction, Hebbian, Boltzmann and competitive learning (Su, 2004). The most commonly used learning algorithm is known as Generalized Delta Rule (or backpropagation). The Generalized Delta Rule is a form of error correction

algorithm. Different artificial neural networks models to forecast O_3 and $PM_{2.5}$ have been proposed. (Prybutok et al., 2000; Slini et al., 2006; Sofuoglu et al., 2006; Wang and Lu, 2006; Brunelli et al., 2007).

Bayesian Networks belong to the family of probabilistic graphical models. These graphical structures are used to represent knowledge about an uncertain domain. In particular, each node in the graph represents a random variable and has a finite set of mutually exclusive states. The edges between the nodes represent probabilistic dependencies among the corresponding random variables. The variables together with the directed edges form an acyclic directed graph networks (Jensen and Nielsen, 2007). The conditional dependencies in the graph are often estimated by using known statistical and computational methods such as maximum likelihood and gradient descent (Ben-Gal, 2007). Solaiman et al. (2008) have investigated a Bayesian neural network model in for ozone forecast in which the conventional learning process is implemented, but probability distribution of weights were considered instead of single set of weights.

Multivariate Adaptive Regression Splines is a nonparametric regression procedure that makes no assumption about the underlying functional relationship between the dependent and independent variables. In this approach, the relationship between the target and predictor variables is constructed by means of basis functions and weights. The basis functions are entirely driven from the dataset and subsequently used in a regression model. Multivariate Adaptive Regression Splines has become particularly popular in the area of data mining because it does not assume or impose any particular type or class of relationship (e.g., linear, logistic)

between the predictor variables and the dependent variable. Instead, models are derived even in situations where the relationship between the predictors and the dependent variables is non-monotone and difficult to approximate with parametric models (Hastie et al., 2001). One study has investigated Multivariate Regression Splines for forecast of 1-hour and 8-hour ahead ozone concentrations in an urban center (Bordignon et al., 2002).

Within the context of statistical modelling of O_3 and $PM_{2.5}$, the data used in the studies surveyed vary widely both in terms of the considered precursor species and meteorological variables. Precursor species include nitrogen monoxide (NO), nitrogen dioxide (NO_2), sulphur dioxide (SO_2) and carbon monoxide (CO). Surface meteorological data includes solar irradiation, temperature, pressure, relative humidity, dew point, precipitation, wind speed (WS) and wind direction (WD).

In some studies (e.g. Solaiman et al., 2008; Tsai et al., 2009) lagged observations of target variables and actual values of precursor species and meteorological inputs corresponding to forecast time are included to account for atmospheric pollution persistence. Su (2004) included dummy variables to represent day of week and time of day.

There are further distinctions within each category as per which method meteorological variables are introduced (i.e. directly or via dimension reduction; using discreet or fuzzy datasets) and the incorporation of temporal and spatial dependence. It has been noted that any time series can be transformed using an appropriate level of power transform as to change the variable's distribution in order to achieve a higher degree of normality (Yeo and Johnson, 2000). In the studies surveyed

relating to air pollution forecasting, some transformations, such as square root or logarithm, are used but data is most often modeled in terms of original concentration scales ($\mu g/m^3$, ppm or ppb). The appropriate transformation depends on the temporal and spatial scale of the particular analysis, with greater spatial and temporal averaging domains generally resulting in more nearly Gaussian distributions.

Studies most commonly consider single monitoring stations located in an urban area as representative of a city. Others consider a network of monitoring stations and compare the underlying patterns. Separate modeling of the impacts of some meteorological parameters on air pollutants concentrations at an unique monitoring station is the simplest and most common approach to analysis (Turalığlu et al., 2005). However, this approach may overlook precursor availability and certain dynamics found at the regional level; and may therefore result in a statistically less significant model and be possibly misleading as an assessment of regional trend. From the conclusions of two previous studies in Montréal (Gilbert et al., 2005; Crouse et al., 2009), it seems clear that, in the context of estimating air pollution, that both spatial and seasonal variability must be considered.

The forecast windows for forecasting air pollution range from 5 min to 48-hour ahead. The most common windows are the 1-hour ahead and daily maximum.

2.8 Discussion

In this study, "ground-level" refers to the "surface boundary layer" which is the region of the lower atmosphere up to about 100 metres in altitude. The surface boundary layer is comprised of the "laminar layer" and "roughness layer" (Rohli and Vega, 2008)

The laminar layer is the part of the atmosphere that is nearest to the surface. The laminar layer is characterized by smooth flow that parallels the features of the surface over which it moves. This layer is only a few millimetres thick. The features of this layer are considered in studies related to plant physiology and durability of building materials because the atmospheric flow over the surfaces is an important factor affecting tissue water loss and chemical oxidation of materials. The parameters describing the laminar layer are less important for processes governing air pollution.

The roughness layer is a zone of strong convection or turbulence. It is characterized by a large component of vertical motion compared to horizontal motion. The turbulence in this layer is almost entirely mechanical in origin. Mechanical turbulence is convection caused by the friction, irregular flow, and vertical gradients of momentum associated with the roughness of topographic elements such as hills and buildings. The roughness layer may extend up to 50 to 100 metres above surface. It is taller by day than by night because of the increased differences of surface heating across space during daylight hours. These processes are important factor governing air pollution processes at the local scale.

The surface boundary layer is very important from an energy perspective. The vertical motion that dominates this zone transports energy used to drive atmospheric

processes between the surface and the atmosphere above this layer. In most cases, especially in daylight hours, the surface is warmer than the atmosphere above it as energy is transported upward via the turbulent flux of sensible heat. The most intense turbulence is associated with situations when the temperature difference between the surface and the air above is large.

From the information in the literature review, ozone concentration in Montréal is expected to be largest during summer months and lowest in winter. Also, ozone levels are expected to be lowest in early morning, to increase gradually (over one or two hours) during the wee hours of the morning with increased vehicular traffic, to peak in late afternoon, and then decrease gradually during evening hours to reach an overnight minimum. Ozone concentrations are expected to vary locally within the Montréal area due to the city's uneven landscape, land use and traffic patterns. Given VOC limited conditions, ozone is expected to be highest in suburban locations than in the downtown core due to ozone scavenging driven by high NO_x levels.

We have seen that, due to its low settling velocity, $PM_{2.5}$ has longer atmospheric lifetime compared to coarse particles. Longer atmospheric lifetime translates into increased residence time and more likelihood to negatively impact human health. Therefore, the $PM_{2.5}$ class of particulate matter is of great concern and will be the object of this study. $PM_{2.5}$ is linked with vehicular traffic, and as such it is expected to be greatest in the city's high-volume and congested areas. Minimal diurnal cycle of $PM_{2.5}$ is expected in Montréal.

At this point, we deliberately ascertain that the meteorological condition does not create ozone or particulate matter by its own. In the strict sense of the term, no causal

relationship can be inferred between meteorology variables and target pollution concentration. While one can argue that this statement can be relaxed when considering solar radiation and temperature because of their direct effect on chemical reaction rates, we will take a more precautionary stand and formally consider that target pollutant concentrations modulates the effect of the precursor emission and the meteorological fluctuation. Since meteorology and topography affect both the reaction rate and transport of ozone as well as precursors, we will consider this urban study on a station-by-station basis.

As hourly means of ozone, fine particulate matter, sulphur dioxide, nitrogen monoxide, nitrogen dioxide and carbon monoxide have been identified as either target pollutants or chemical precursors, they will be considered in this study.

The transport distance of both ozone and fine particulate matter is high, and both local and regional parameters should be considered. However, given that this study is focuses on short-term prediction, no regional parameters will be included. While direct transport of stratospheric ozone is responsible for about 10% of global tropospheric ozone (Bailey et al., 2002), previous studies have shown that its contribution to ground-level O_3 in the North America (even at relatively remote locations) is of minor importance (Altshuller, 1984). Therefore, there is no reason to believe that the forecasting performance of statistical models would be improved at the local scale with inclusion of stratospheric ozone.

Solar radiation, temperature, dew point, pressure, precipitation, wind speed and wind direction values are expected to be correlated at all stations within the city of Montréal therefore the same values will be used throughout this study. Aloft pressure

measurements, higher altitude winds speed and direction are excluded. More than 100 different volatile organic compounds are systematically measured in Montréal; however measurements take place every six days and return as daily averages.

The incorporation of VOC data in O_3 and $PM_{2.5}$ forecasting models is warranted. This can be achieved by means of three contrasting methods. The first comprises introducing VOC data as standalone independent variables. This method is not ideal as inclusion of hundreds of additional independent variables may generate ill-conditioned statistical models. The second, which is the simplest and the most often adopted, is a concentration-based method. The multiple VOC readings are combined into one single independent variable. This is achieved by converting individual VOC species concentration to an equivalent carbon equivalent concentration (Cj) measured in ppbC as shown in equation (2.30) and summing up each value to an equivalent total volatile organic compound (TVOC) measurement expressed in ppbC.

$$\mathrm{C_j} = \mathrm{C_j^*} \times \frac{1}{\mathrm{MW}} \times \mathrm{R_g} \times \frac{\mathrm{T_a}}{\mathrm{P_a}} \times \mathrm{N_c} \tag{2.30}$$

where C^*_j is the quantified concentration of species J in expressed in μg/m^3, MW is molecular weight in g/mole, Rg is the ideal gas constant (8.31 L kPa mol^{-1} K^{-1}), T_a is ambient air temperature in K, P_a is pressure in kPa and N_c is the number of carbon atoms in analyzed species.

The third method is an OH-reactivity-based method which takes into account for the combined effect concentration on carbon-atom basis and OH-reactivity. This method recognizes that VOC species with a large concentration values are not necessarily

important precursor to O_3 or $PM_{2.5}$ if it is unreactive; conversely, another with a small concentration can be important if it is extremely reactive. An example is methane, typically the most abundant VOC in the atmosphere but of negligible importance in producing ozone on urban or regional scales because of its extremely low reactivity. An air mass can have a large total VOC concentration but a low ozone-producing capacity if the VOCs present are relatively unreactive. The concentration-based method described above does not account for the different reactivities of the various VOC species. It can be misleading about the involvement of the various species in ozone formation. As such, TVOC expressed on a carbon-atom concentration basis may not be correlated to ozone. Chameides et al. (1992) proposed a method for normalizing the concentration of each hydrocarbon to that of propylene. In this method, a propylene-equivalent concentration (propy-equiv) for each VOC species is defined by equation (2.31).

$$\text{Propy} - \text{Equiv (J)} = \text{C}_\text{J} \times \frac{\text{K}_{\text{OH}}(\text{J})}{\text{K}_{\text{OH}}(\text{C}_3\text{H}_6)} \tag{2.31}$$

where C_J is the quantified ppbC concentration of species J, K_{OH} is the reaction rate of individual VOC species with OH• radical and $K_{OH}(C_3H_6)$ is equal to the rate constant for propylene with OH•. Rate constants can be obtained from Atkinson (1990). The propy-equiv concentration takes into account the combined effect of hydrocarbon concentration and reactivity with OH•. Choosing the compound propylene for normalizing VOC concentration is justified by the fact that equivalent to propylene corresponds to the upper limit of potential ozone formation (Evtyugina et al., 2009). A compound twice as

reactive as propylene would have a propy-equiv concentration twice its ambient concentration.

The basic assumption made when forecasting ozone and fine particulate matter is that, there is always an underlying pattern which describes the time series. This pattern can be reasonably expected to repeat in the future, given similar conditions. The general idea behind this study involves the following points:

1. Analysis of past data in order to identify (and capture) the pattern of behaviour
2. Assumption that the pattern that has been identified will remain significantly unchanged
3. Extrapolation of the pattern to successive points on the time series

When using statistical models, the assumption of the pattern that has been identified remains significantly unchanged is of vital importance. The forecasting of the proposed models may not hold true if there is a significant change in pattern of ozone and particulate matter formation.

Statistical models are capable of providing a complete and parsimonious description of the relationship between predictor variables and their covariates. Model-driven approaches lead to estimators that possess attractive statistical properties, are easy to calculate, and are straightforward to interpret. Nonlinear, Piecewise and Quantile regression have become increasingly popular because the central-tendency and homoscedasticity assumptions are seldom met in the real world. However, Linear Regression has been applied widely in environmental sciences and is seen as an essential

analysis and prediction tool. For this reason the Multiple Linear Regression model is retained.

The Multiple Linear Regression framework has inherent limitations. First, when summarizing the response for fixed values of predictor variables, the model cannot be readily extended to non-central locations, which is precisely where the interests of air pollution forecast reside. Thus, we will incorporate Piecewise Regression, within the Multivariate Adaptive Regression Splines framework, to this study.

Data-driven models have been shown to perform better under given heavy-tailed distributions which commonly occur in air pollution and meteorology phenomena (Solaiman et al., 2008). Among the data-driven models surveyed, Principal Component Analysis and Artificial Neural Networks are the ones that held our interest. Principal Component Analysis alleviates the expected issues with multicollinearity and principal components can be used as independent variables in linear regression. In this case we build a model based on Principal Component Regression (PCR). Artificial Neural Networks are one of the least black box approaches within this category. Moreover, Artificial Neural Networks have been rigorously demonstrated to be theoretically capable of approximating any measurable function to any desired degree of accuracy (Fonseca, 2003) and have been found extensive utilisation in air pollution forecasting.

Should the underlying mechanisms of ground-level O_3 and $PM_{2.5}$ formation be reasonably captured by these proposed methods; and should these models yield satisfactory results in predicting extreme concentration levels, they could arguably be incorporated into an air quality management framework to assess potential

compliance or non-compliance and most importantly be used for warning the public of unhealthy pollution levels.

With respect to public health; most committees appointed to set standards for ozone and fine particulate matter, recommend a range of 41 to 65 ppb (based on 8-hr average) for O_3 and a range of 25 to 35 $\mu g/m^3$ (based on 24-hour averages) for $PM_{2.5}$. The review of the legislative framework on air quality across Canada and the United States indicated absence of a consensus as to what level the goal of ambient concentrations for this two air pollutants should be. In Canada, different levels of Government try to balance the need to address public health concerns against O_3 and $PM_{2.5}$ levels and what can be reasonably achieved. Provincial and territorial governments are able to adopt the Canada Wide Standards or not, or to use them as benchmarks for differing provincial standards that take into account different priorities and circumstances. In most jurisdictions, the numerical values chosen for particular standards or guidelines reflect political and/or economic considerations. Overall, there are multiple and inconsistent objectives in Canada and it would be to best interest of Canadians if the legislative frameworks were standardized. In Montréal, the 24-hr average objective for O_3 and $PM_{2.5}$ is 50 and 25 $\mu g/m^3$, respectively. These values are well aligned with the other values noted during our benchmarking exercise.

2.9 Summary

In summary, tropospheric ozone is formed when a mixture of nitrogen oxides and other organic gases are exposed to sunlight. The sunlight causes NO_2 to liberate an oxygen radical that combines with O_2, to produce O_3. At the same time, sunlight also causes other

organic gases, such as aldehydes, to dissociate producing in the progress peroxy radicals that ultimately convert NO to NO_2. This step increases the rate at which O_3 is produced by NO_2 photolysis and decreases the rate at which it is consumed by reaction with NO.

Fine particulate matter ($PM_{2.5}$) is the respirable subgroup of airborne particulate matter having an aerodynamic diameter of less than 2.5 μm. $PM_{2.5}$ is mostly the result of physical processes, coagulation and chemical reaction involving sulphates, nitrates and volatile organic compounds. Atmospheric processes such as the oxidation of sulphur dioxide, oxidation of hydrocarbons to low-vapour-pressure organics, and the formation of aerosol salts (e.g. ammonium nitrate and ammonium sulphate) may also contribute to suspended particles.

Chemical processes interact over a wide range of temporal and spatial scales. Fast reactions have a direct impact in the locality of the emissions and can be strongly affected by atmospheric mixing. On the other hand, slow reactions are relatively insensitive to local mixing and affect a wider, regional or global spatial area. The rate of these reactions, in addition to rates of the competing transport and scavenging processes, vary widely in accordance with the site-specific meteorological and photolytic conditions. For all these reasons, the development of forecasting models for maximum daily concentrations of O_3 and $PM_{2.5}$ is acknowledged to be a very challenging undertaking.

Ozone and particulate matter are two air pollutants with non-threshold adverse effects on human beings and the environment. In Montréal, the 24-hr average objective for O_3 and $PM_{2.5}$ is 50 and 25 $\mu g/m^3$, respectively.

Researchers recognized that it is seldom feasible to construct strictly deterministic models to forecast O_3 and $PM_{2.5}$ at the local scale. Previous research show that statistical models yield satisfactory results to when applied in forecasting O_3 and $PM_{2.5}$ using air quality and meteorological data as covariates. Following the review of the statistical methods used in the development of air pollution forecasting models, we have decided to retain the following four methods:

1. Multiple Linear Regression (MLR)
2. Principal Component Regression (PCR)
3. Multivariate Adaptive Regression Splines (MARS)
4. Artificial Neural Networks (ANN)

To this date, no comparative assessment of different statistical models for short-term prediction of ground level ozone and particulate matter in Montréal has been undertaken.

Chapter 3

Methods and Performance Metrics

In this chapter, we first lay out our convention on mathematical notation. Then, we introduce the concept of time series and define the moment statistics recurrent in this study. After that, we describe Principal Component Analysis. Following this, we introduce the seven models considered in this thesis for short-tem forecast of O_3 and $PM_{2.5}$. Then, we formally define the four statistical methods on which our models are based, namely Multiple Linear Regression (MLR), Principal Component Regression (PCR), Multivariate Regression Splines (MARS) and Artificial Neural Networks (ANN). Lastly, we describe the performance metrics considered.

3.1 Preliminaries

3.1.1 Conventions

In the pages that follow, the following conventions will be used:

- Scalars are represented in lower case (e.g. x, σ, s, r)
- Matrices are represented in bold upper case (e.g. **A**, **B**, **S**, **R**, **V**)
- The identity matrix is denoted **I**
- The transpose of a matrix **A** is denoted $\mathbf{A}^T$
- Vectors will be in bold lower case (e.g. **a**, **t**) and assumed to be a column oriented; row vectors are represented with the transpose operator $\mathbf{a}^T$
- It is assumed that the rows of a given data matrix represent observations and columns independent variables

3.1.2 Time Series Data

Time series data, as the name suggests, are data collected over a period of time on one or more variables. Time series data have a particular time interval of observations associated with them. The frequency is simply a measure of the regularity with which the data is collected. In air quality monitoring, the time interval is usually 1 hour.

Let time series denote either the sequence of dependent y or independent x variables. Let n denote the number of observations. Let y_t and y_{t+1} denote observations of y at time t and $t + 1$, respectively.

3.1.3 Moment Statistics and Other Measurements

Moment statistics are those that are formed from sums of power of the data's values. The first moment is the sample mean $\bar{x}$, which is calculated from a sum of values to the first power and measures the center of the distribution.

$$\bar{x} = \frac{1}{n}\sum_{i=1}^{n}(x_i) \tag{3.1}$$

The second moment is the sample variance s^2, which is calculated from sums of the values to the second power and measures the spread of the distribution.

$$s^2 = \frac{1}{n-1}\sum_{i=1}^{n}(x_i - \bar{x})^2 \tag{3.2}$$

The covariance between two variables x_1 and x_2 is given by:

$$s^2_{x_1,x_2} = \frac{1}{n-1}\sum_{i=1}^{n}\left(\left(x_{1,i} - \overline{x_1}\right)\left(x_{2,i} - \overline{x_2}\right)\right) \tag{3.3}$$

The third moment is skewness, which is calculated from sums of values to the third power and measures the asymmetry of the distribution.

$$skewness = \frac{n}{(n-1)(n-2)} \sum_{i=1}^{n} \left(\frac{x_i - \bar{x}}{s} \right)^3 \tag{3.4}$$

where *s* is the sample standard deviation defined below.

The fourth moment is kurtosis, which is calculated from sums of values to the fourth power and measures the relative shape of the middle and tails of the distribution.

$$kurtosis = \frac{n(n+1)}{(n-1)(n-2)(n-3)} \sum_{i=1}^{n} \left(\frac{x_i - \bar{x}}{s} \right)^4 \tag{3.5}$$

The standard deviation *s* is the square-root of the variance.

$$s = \sqrt{s^2} = \sqrt{\frac{1}{n-1} \sum_{i=1}^{n} (x_i - \bar{x})^2} \tag{3.6}$$

Covariance gives little information about the relationship between two variables because it is sensitive to both their standard deviation. By dividing the covariance by the respective two standard deviations, we compute the correlation *r* between the two variables.

$$r_{x_1,x_2} = \frac{s^2_{x_1,x_2}}{s_{x_1} \times s_{x_2}} = \frac{\sum_{i=1}^{n} \left(\left(x_{1,i} - \overline{x_1} \right) \left(x_{2,i} - \overline{x_2} \right) \right)}{\sqrt{\sum_{i=1}^{n} \left(x_{1,i} - \overline{x_1} \right)^2 \times \sum_{i=1}^{n} \left(x_{2,i} - \overline{x_2} \right)^2}} \tag{3.7}$$

Correlation is a measure of the dependence between two variables which indicates that a linear relationship exists between the two variables if the value obtained is different than zero.

3.1.4 Principal Component Analysis (PCA)

PCA is, in principle, a data reduction technique and a tool for information extraction. Specifically, Data compression is achieved with the application of eigenvector decomposition to the covariance of the process variable and finding linear combinations of the original variables. Successive linear combinations or principal components (PC) are extracted in such a way that they are perpendicular (uncorrelated) to one another and account for successive smaller amounts of the total variance.

Given a matrix **X** comprised of p different variables (x_1, x_2, x_3, ... x_p) with n different observations. The matrix **X** can be autoscaled to achieve zero mean and unit variance. Autoscaling is achieved by (a) subtracting from each element the mean of their respective column vector and (b) dividing each mean centered elements by the standard deviation of their respective column vector. Call the autoscaled matrix **Z**. The variance of **Z** is denoted $\mathbf{S_z}$ and is given by:

$$\mathbf{S_z} = \frac{1}{n-1}\mathbf{Z^T Z} \tag{3.8}$$

The main idea behind PCA is to find an orthonormal matrix **V** where

$$\mathbf{Y} = \mathbf{ZV} \tag{3.9}$$

so that the elements of $\mathbf{S_Y}$ are uncorrelated and of maximum variance. This is the same as saying that we want **V** such that $\mathbf{S_Y}$ is a diagonal matrix. This is called an *orthogonalizing transformation*. The correlation matrix $\mathbf{S_Y}$ in terms of **V** is as follows:

$$\mathbf{S_Y} = \frac{1}{n-1}\mathbf{Y^T Y} \tag{3.10}$$

But,

$$\frac{1}{n-1}\mathbf{Y^T Y} = \frac{1}{n-1}(\mathbf{ZV})^{\mathbf{T}}(\mathbf{ZV}) = \mathbf{V^T}(\frac{1}{n-1}\mathbf{Z^T Z})\mathbf{V} \tag{3.11}$$

Therefore,

$$\mathbf{S_Y} = \mathbf{V^T}(\mathbf{S_Z})\mathbf{V} \tag{3.12}$$

There are an infinite number of values for **V** that will produce a diagonal $\mathbf{S_Y}$ for any correlation matrix $\mathbf{S_Z}$, but a unique solution maximizing variance. This unique solution is obtained is given by principal component (Jolliffe, 1989). The principal component solution put forward the sum of the squares of the coefficients in the first

column of $\mathbf{V}$, (denoted by $\mathbf{v}_1$). Expressed mathematically, we wish to maximize equation (3.13) subject to equation (3.14):

$$\mathbf{v_1^T S_z v_1} = \frac{1}{n}\sum_{i=1}^{n}(y_{i,1}^2) \tag{3.13}$$

$$\mathbf{v_1^T\, v_1} = 1 \tag{3.14}$$

Malinowski and Howery (1980) have shown that this optimisation can be achieved by introducing the restriction via the Lagrange multiplier approach as shown in equation (3.15) and then setting the vector of partial derivatives shown in equation (3.16) to zero. By doing so, we get equation (3.17).

$$\mathbf{u_1} = \mathbf{v_1^T S_Z v_1} - \boldsymbol{\lambda}(\mathbf{v_1^T v_1} - 1) \tag{3.15}$$

$$\frac{\delta(\mathbf{u_1})}{\delta \mathbf{v_1}} = 2\mathbf{S_z v_1} - 2\lambda \mathbf{v_1} \tag{3.16}$$

$$(\mathbf{S_Z v_1} - \lambda \mathbf{I})\mathbf{v}_1 = 0 \tag{3.17}$$

where λ is an eigenvalue.

From equation (3.17), we build a set of p homogeneous equation which can be solved by expanding equation (3.18). The solution of this equation is obtained by solving the characteristic equations for the eigenvalues $\lambda_1, \lambda_2, \lambda_3, \ldots, \lambda_p$.

$$|\mathbf{S_Y} - \lambda\mathbf{I}| = 0 \tag{3.18}$$

With these results, we consider a diagonal matrix **L** and a orthonormal matrix **V** such that (a) the diagonal elements of **L** are the eigenvalues $\lambda_1, \lambda_2, \lambda_3, \ldots, \lambda_p$, and (b) the eigenvectors $\boldsymbol{v_1, v_2, v_3, \ldots, v_p}$ are the vector columns of **V**. The relationship between **V** and **L** is given by:

$$\mathbf{V^T}(\mathbf{S_z})\mathbf{V} = \mathbf{L} \tag{3.19}$$

The principal components (PC) of matrix **Z** are the eigenvalues which comprise the diagonal elements of **L**. Finally, the factor score $\widehat{\mathbf{Y}}$ matrix is defined as:

$$\widehat{\mathbf{Y}} = \mathbf{ZV} \tag{3.20}$$

The number of eigenvalues used in computing the factor score matrix determines the dimensionality of the set of factor scores.

If we recapitulate the main steps to obtain the eigenstructure for a correlation matrix and find the principal components:

- Given an original data matrix **X** containing *n* rows and *p* columns, compute the autoscaled data matrix **Z** and the correlation matrix $\mathbf{S_Z}$

- Obtain the characteristic equation of $\mathbf{S_z}$ which is a polynomial of degree p obtained from the expansion of the determinant of $|\mathbf{S_z} - \lambda \mathbf{I}| = 0$ and solve for the roots λ_i, ($\underline{i} = 1, 2, 3, \ldots, p$) called eigenvalues
- Solve for the columns of the $\mathbf{V}$ matrix and ($\mathbf{v_1, v_2, v_3, \ldots, v_p}$) which are called eigenvectors
- For dimensionality reduction, we may select only the principal components with eigenvalues greater than unity

A numerical example of Principal Component Analysis is presented in Appendix B1.

3.2 Methods

These are the seven models included in our study:

1. The Multiple Linear Regression (MLR) model:

The MLR model is based on Multiple Linear Regression method with Ordinary Least Square estimates. It will have air quality and meteorological variables (at time t) as input and either O_3 or $PM_{2.5}$ (at time $t + 1$) as output.

2. The Principal Component Regression (PCR) model:

The PCR model is based on Principal Component Analysis and Multiple Linear Regression method with Ordinary Least Squares. It will have the principal components obtained from the set of air quality and meteorological variables (at time *t*) as input (regardless of the size of their eigenvalue) and either O_3 or $PM_{2.5}$ (at time $t + 1$) as output.

3. The Multivariate Adaptive Regression Splines with First Order Interaction (MARS 1) model:

The MARS 1 model is based on Multiple Linear Regression method with Ordinary Least Squares. It will have basis functions obtained from the set of air quality and meteorological variables (at time *t*) as input (given the constraint of first order interaction) and either O_3 or $PM_{2.5}$ (at time $t + 1$) as output.

4. The Multivariate Adaptive Regression Splines with Second Order Interaction (MARS 2) model:

The MARS 2 model is based on Multiple Linear Regression method with Ordinary Least Squares. It will have basis functions obtained from the set of air quality and meteorological variables (at time *t*) as input (given the constraint of second order interaction) and either O_3 or $PM_{2.5}$ (at time $t + 1$) as output.

5. The Artificial Neural Network (ANN) model:

The ANN model is based on Artificial Neural Networks method. It is a three layered feed-forward ANN. It will have air quality and meteorological variables (at time *t*) as input and either O_3 or $PM_{2.5}$ (at time $t + 1$) as output. Each node in the hidden layer will contain a sigmoid activation function. The optimum number of hidden nodes and model parameters are determined by trial and error using the Gradient Descent Rule while protecting against model overfit.

6. The Hybrid Principal Components and Artificial Neural Network (PC-ANN) model

The PC-ANN model is based Principal Component Analysis and Artificial Neural Network methods. It will have all the principal components (i.e. regardless of the size of their eigenvalue) obtained from the set of air quality and meteorological variables (at time *t*) as input to a three layered ANN. The output of the ANN is either O_3 or $PM_{2.5}$ (at time $t + 1$). Each node in the hidden layer will contain a sigmoid activation function. The optimum number of hidden nodes and model parameters are determined by trial and error using the Gradient Descent Rule while protecting against model overfit.

7. The Reduced Hybrid Principal Components and Artificial Neural Network (PC*-ANN) model

The PC*-ANN model is based Principal Component Analysis and Artificial Neural Network methods. It will have principal components with eigenvalues greater than unity obtained from the set of air quality and meteorological variables (at time *t*) as input to a three layered ANN. The output of the ANN is either O_3 or $PM_{2.5}$ (at time $t + 1$). Each node in the hidden layer will contain a sigmoid activation function. The optimum number of hidden nodes and model parameters are determined by trial and error using the Gradient Descent Rule while protecting against model overfit.

We will run MLR, PCR, ANN, PC-ANN and PC*-ANN with "JMP Version 5.1.2". Then, we will run MARS 1 and MARS 2 with "Salford Predictive Miner".

3.2.1 Multiple Linear Regression (MLR)

Multiple linear regression is concerned with describing and evaluating the relationships between a given variable and one or more other variables. More specifically MLR attempts to explain movements in a variable by reference to movements in one or more variables by fitting a straight line through the time series.

The general form of the MLR model is:

$$y = \beta_0 + \sum_{i=1}^{p} (\beta_i x_i) + \varepsilon \tag{3.21}$$

where y is the dependent variable, x are the independent variables, β is a coefficient, p is the number of dependent variables and ε is the random error. The multiple linear regression is built under the four assumptions with respect to the disturbance term ε, namely

1. the random errors have zero mean;
2. the variance of the random errors is constant and finite;
3. the random errors are linearly independent of one another; and
4. there is no relationship between the error and the covariates.

In mathematical notation:

$$E(\varepsilon_t) = 0 \tag{3.22}$$

$$\text{var}\ (\varepsilon_t) = \sigma^2 \tag{3.23}$$

$$\text{cov}\ (\varepsilon_t\ ,\ \varepsilon_{t-1}) = 0 \tag{3.24}$$

$$\text{cov}\ (\varepsilon_t\ ,\ x_t) = 0 \tag{3.25}$$

There are a number of methods for determining the appropriate values of the coefficients β given a sample with n different observations. Ordinary least square method entails taking vertical distance from points to the fitted line, squaring it and then minimising the total sum of the areas of the squares. The least square estimate equation is:

$$\hat{y} = \widehat{\beta_o} + \sum_{i=1}^{p} \left(\widehat{\beta_i} x_i\right) + e \tag{3.26}$$

where $\hat{y}_t$ is the estimated dependent variable, x are the independent variables, $\widehat{\beta_i}$ are the estimated coefficient, p is the number of dependent variables and e is the sample error (or residual). Note that the residual is the difference between the observed and estimated – i.e (y_t - $\hat{y}_t$).

There are various ways to describe the ordinary least squares technique. In the lines that follow, we will summarize this simple yet often misunderstood technique. In matrix form we can write:

$$\mathbf{Y} = \mathbf{X\beta} \tag{3.27}$$

$$\widehat{\mathbf{Y}} = \mathbf{X}\widehat{\boldsymbol{\beta}} + \mathbf{e} \tag{3.28}$$

$$\mathbf{e} = \mathbf{Y} - \widehat{\mathbf{Y}} \tag{3.29}$$

Let L be the sum of squares cost function which is the sum of the squares of residuals

$$\mathbf{L_{ss}} = \mathbf{e^T e} = \left(\mathbf{Y} - \mathbf{X}\widehat{\boldsymbol{\beta}}\right)^{\mathbf{T}}\left(\mathbf{Y} - \mathbf{X}\widehat{\boldsymbol{\beta}}\right) = \mathbf{Y^T Y} - 2\widehat{\boldsymbol{\beta}}^{\mathbf{T}}\mathbf{X^T Y} + \widehat{\boldsymbol{\beta}}^{\mathbf{T}}\mathbf{X^T X}\widehat{\boldsymbol{\beta}} \tag{3.30}$$

In order to obtain the parameter estimates the residual sum of squares cost function must be minimized with respect to all the elements. By differentiating L and

setting all partial derivatives to zero, we find the parameter values that minimise the residual sum of squares.

$$\frac{\partial \mathbf{L_{ss}}}{\partial \widehat{\boldsymbol{\beta}}} = -2\mathbf{X^T Y} + 2\mathbf{X^T X}\widehat{\boldsymbol{\beta}} = 0 \tag{3.31}$$

This leads to:

$$\mathbf{X^T Y} = \mathbf{X^T X}\widehat{\boldsymbol{\beta}} \tag{3.32}$$

Multiplying both sides by the inverse of $\mathbf{X^T X}$, we get:

$$\widehat{\boldsymbol{\beta}} = (\mathbf{X^T X})^{-1}\mathbf{X^T Y} \tag{3.33}$$

Statistical significance at 0.05 confidence level is established by two-tailed p-test statistic and overall significance by F-test.

3.2.2 Principal Component Regression (PCR)

Principal component regression models it the response variable by means of a multiple linear regression based on principal components PC_i instead of using x_i to obtain:

$$\hat{y} = \widehat{\beta_0} + \sum_{i=1}^{p} \left(\widehat{\beta_i} PC_i\right) + e \tag{3.34}$$

Statistical significance at 0.05 confidence level is established by two-tailed p-test statistic and overall significance by F-test.

3.2.3 Multivariate Adaptive Regression Splines (MARS)

The MARS algorithm consists in fitting multiple piecewise linear functions at different regions of the domain of each independent variables. Through the additive effect of these different linear functions, a global non-linear relationship between the independent variables and the target variable can be established. The MARS model is a spline regression model that uses a specific class of basis functions as predictors in place of the original data.

The linear functions used in the MARS approach are hinge-type basis functions which have the form:

$$\begin{aligned} BF_i(x) &= \max(0, x - c) \text{ or} \\ &= \max(0, c - x) \end{aligned} \tag{3.35}$$

where x is one value of the independent variables and c is one knot. The returned value of $BF_i(x)$ is 0 for all values of x_i up to some threshold value c and $BF_i(x_i)$ is equal to x_i for all values of x_i greater than c. The hinge-type basis functions partition the data space into disjoint regions, each of which can be treated independently. A knot marks the end of one region and the beginning of another. Thus, the knot is where the behaviour of the function changes.

In classical splines, the knots are predetermined and evenly spaced. Finding the best basis functions given a predetermined number (and location) of knots is a straightforward optimisation problem consisting in examining a number of potential basis functions and selecting the one with the best coefficient of determination. However, finding the best basis functions when the location and number of knots are unknown is a more challenging task (Nedjah and Mourelle, 2005). This is exactly what MARS achieves through its stepwise forward/backward search procedure.

In the forward pass, MARS starts the model with just a constant. The constant (or intercept term) is the mean of the response values. Then, MARS begins to search for a variable-knot combination that most improves the model's performance. In this context, performance improvement means maximum reduction in sum-of-squares residual error. Adding a basis function always reduces the MSE. MARS searches for a pair of hinge-type basis functions, the primary and mirror image. This search is then repeated, with MARS searching for the best variable to add given the basis functions already in the model. This process of adding terms continues until the change in residual error is too small to continue or until the maximum number of terms is reached. The maximum number of terms is specified by the user before model building starts.

A key property of MARS, is its ability to uncover a number of subregions of predictors with different interaction patterns. This allows MARS to pragmatically model non-linear relationships between variables. MARS achieves that by allowing inclusion of interaction terms, such that any given basis function can be a function of another basis functions which is active in a localized region of the variables involved.

After implementing the forward stepwise selection of basis functions, a backward procedure is applied in which the model is pruned by removing those basis functions that are associated with the smallest increase in the (least squares) goodness-of-fit. The so-called Generalized Cross Validation error is a measure of the goodness of fit that takes into account not only the residual error but also the model complexity (Hastie et al., 2001). It is given by:

$$GCV = \frac{\sum_{i=1}^{n}(y_i - \hat{y}_i)^2}{\left(1 - \frac{1 + c_p d}{n}\right)^2} \tag{3.36}$$

where n is the number of observations in the data set, d is the effective degrees of freedom, which is equal to the number of independent basis functions. The quantity c_p is the penalty for adding a basis function. The penalty factor is usually between 2 and 3 (Hastie et al, 2001). The model that minimises GCV is chosen as "best" and defined as final fit.

MARS will ultimately fit y by means of a multiple linear regression on BF_j (x_i) (instead of using x_i) to obtain:

$$\hat{y} = \hat{\beta}_0 + \sum_{i=1}^{p}\left(\hat{\beta}_i BF_i\right) + e \tag{3.37}$$

Statistical significance at 0.05 confidence level is established by two-tailed p-test statistic and overall significance by F-test.

3.2.4 Artificial Neural Networks (ANN)

A general definition of artificial neural networks (ANN) is a set of simple calculation units, which can mimic complex global behaviour by computing a solution based on its relationship to other units and exterior stimulus. These calculation units are called neurons (or nodes). Each neuron receives an input vector, sums weighted input values and apply a mapping operator, *F*, to the sum. Thus artificial neurons build a non-linear mapping of input vectors xi to output y.

$$y = F\left(\sum_{i=1}^{p} w_i\, x_i\right) \tag{3.38}$$

In this most general form, artificial neural networks model are designed to mimic the behaviour of the brain. These networks resemble the human brain in two respects. First, they can recognize trends and patterns; and second, they can learn from their interactions with the environment. It is however important not to take this resemblance too far, because there is only limited similarities between artificial and biological neural networks. In particular, while the human brain contains billions of neurons, ANN usually contain less then 100 equivalent units. The way in which artificial networks store and manipulate information is an over simplification of the way in which networks of biological neurons functions. The analogy, while not literal, is a strong one and it allows us to refer to models based on artificial networks as *intelligent models*.

The information-processing properties of neural networks depend mainly on two factors: the network architecture (i.e. the scheme used to connect elements), and the

training algorithm (rules) employed to specify the values of the weights connecting the nodes.

In multilayer neural network, there is one input layer, a number of hidden layers and one output layer; each consisting of a number of nodes (i.e. artificial neurons) as shown in Figure 3.1. The input nodes are the interface through which a dataset is entered in the network. Input nodes transmit real-valued signal to each of the nodes in the first hidden layer. Each hidden node produces a single real-valued output and transmits in turn to nodes in successive hidden layers. The number of nodes in the input layer is equal to the number of input variables, with each node paired to a single input variable. The number of nodes in the output layer is equal to the number of output variables, with each of the nodes expressing the value of one distinct parameter being modelled. By parsimony, networks are built to model a specific dependent variable and therefore there is often a single node in the output layer.

The most widely studied activation functions having infinite domain of input values are the hyperbolic tangent (tanh) and sigmoid (logistic) functions. There is no *a priori* method known in choosing which of these functions is most suited to a given problem (Su, 2004).

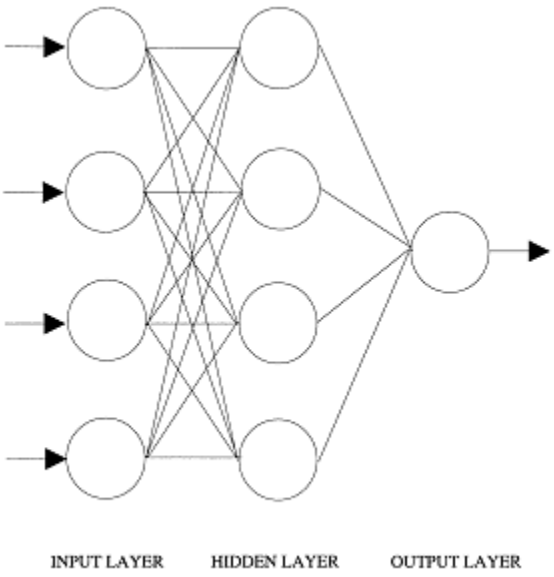

Figure 3.1 Artificial Neural Network architecture

Training neural networks requires optimising the synaptic weights so that the systems' overall energy *E* is minimized. Expressed mathematically:

$$min(E) = min(\sum_{i=1}^{n} E_i) = \frac{1}{2} min \sum_{i=1}^{n} (\hat{y}_i - y_i)^2 \tag{3.39}$$

where *y* real observed data and $\hat{y}$ is output.

The most popular method used for minimising the overall energy is the Gradient Descent Rule (sometimes referred to as the Delta Rule algorithm). Gradient Descent is based on evaluating the direction of the error function, and updating the weight by backpropagation.

$$\Delta w_1 = \eta \frac{\delta E}{\delta w_1} \tag{3.40}$$

where η is the learning rate.

The algorithm starts at the last output neuron, evaluates the error energy at the neurons, minimises the energy by changing the weights. Then evaluates the next neuron in the chain until reaching the first hidden neuron. The training process is repeated until the outputs have reached a satisfactory level.

The final form of the artificial neural network containing one hidden layer is:

$$\hat{y} = \sum_{j=0}^{q} \sum_{i=1}^{p} \left(\alpha_{i,j} f\left(\widehat{w}_{i,j} x_{i,j} \right) + \theta_q \right) + e \tag{3.41}$$

where $\hat{y}$ is the forecasted dependent variable, x is independent variable, p is the number of independent variables, q is the number of hidden nodes, f is activation function and (α, θ) are a set of parameters determined using the observed data (training phase) and minimizing the prediction error function (Nedjah and Mourelle, 2006).

We provide the derivation of the Gradient Descent Rule using the sigmoid activation function in Appendix A. Also, we provide a numerical example of Artificial Neural Network methodology in Appendix B2.

3.3 Performance Metrics

The analysis of prediction performance typically involves calculation of errors between observed y and predicted $\hat{y}$ values. Some of the traditional statistical forecasting error measures are listed below:

1. MBE: Mean Bias Error

$$MBE = \frac{1}{n}\sum_{i=1}^{n}(y_i - \hat{y}_i) \tag{3.42}$$

MBE averages the prediction error averaged over n points. MBE indicates if the observed concentrations are being over or under-estimated.

2. MAE: Mean Absolute Error

$$MAE = \frac{1}{n}\sum_{i=1}^{n}|y_i - \hat{y}_i| \tag{3.43}$$

MAE is the absolute value of prediction error averaged over n points. MAE indicates the mean order of magnitude of residuals.

3. MAPE: Mean Absolute Percent Error

$$MAPE = \frac{1}{n}\sum_{i=1}^{n}\left|\frac{y_i - \hat{y}_i}{y_i}\right| \text{ x } 100\% \tag{3.44}$$

MAPE averages the ratio of the prediction error to the observed value over *n* points. MAPE allows comparison between different models with different means of response.

4. RMSE: Root Mean Squared Error

$$RMSE = \sqrt{\frac{1}{n}\sum_{i=1}^{n}(y_i - \hat{y}_i)^2} \tag{3.45}$$

RMSE averages the square of the prediction error over n points.

5. R^2: Coefficient of Determination

$$R^2 = \frac{n\sum_{i=1}^{n}(y_i\hat{y}_i) - \sum_{i=1}^{n}(y_i)\sum_{i=1}^{n}(\hat{y}_i)}{\sqrt{n[\sum_{i=1}^{n}(y_i^2) - (\sum_{i=1}^{n}(y_i))^2]\left[n\sum_{i=1}^{n}(\hat{y}_i^{\,2}) - (\sum_{i=1}^{n}(\hat{y}_i))^2\right]}} \tag{3.46}$$

R^2 measures the variability of the data that is accounted for by the statistical model.

In addition to the five traditional metrics listed above, three other metrics are used for performance evaluation of forecasting models.

6. TPR: True Positive Rate

$$TPR = \frac{A}{M} \tag{3.47}$$

TPR corresponds to the fraction of correctly predicted exceedances, where A represents the correctly predicted exceedances and M is all observed exceedances.

7. FPR: False Positive Rate

$$FPR = \frac{F - A}{n - M} \tag{3.48}$$

FPR corresponds to the fraction of falsely predicted exceedances, where F is all predicted exceedances.

8. SI: Success Index

$$SI = TPR - FPR \tag{3.49}$$

The SI is the difference between TPR and FPR.

All the above performance metrics will be considered in this study and will be reported for each prediction model for O_3 and $PM_{2.5}$ with respect to training and validation phase.

3.4 Discussion

O_3 and $PM_{2.5}$ formation are time dependent. O_3 follows the photostationary-state relation described in equation (2.4), which is a function of two reaction rates. The time required for the $PM_{2.5}$ precursors to react and form $PM_{2.5}$ is highly variable, and depends on the specific precursor chemical, temperature, and humidity.

Inclusion of lagged values of the target variable (or of the independent variables) in statistical models may capture important dynamic structure of O_3 and $PM_{2.5}$ formation. Often a change in the value of one of the air quality or meteorological data (explanatory variables) does not affect the dependent variable immediately during one time period, but rather with a lag over several time periods. Should we include lagged values, then by definition the values of O_3 (or $PM_{2.5}$) at time *t* would be partly determined by the random error term, and so its lagged values could not be non-stochastic. Moving from a purely static model to one which allows for lagged effect is likely to reduce serial correlation; however, inclusion of lagged values of the dependent variables violates the mathematical assumptions of the statistical methods included in this thesis. Precisely, the assumption that the explanatory variables are non-stochastic (i.e. there is no relationship between the error and the corresponding dependent variable) is being violated. For that reason, we decided to exclude lagged values. Moreover, a model which contains lagged values may

solve a statistical problem (autocorrelated residuals) at the expense of creating an interpretational one.

Su (2004) noted that forecast models should exclude actual values of precursor species and meteorological inputs corresponding to forecast time. The inclusion of dummy variables to represent time of day (or day of week) improves the performance of forecasting models, but on the other it is difficult to argue that either O_3 or $PM_{2.5}$ is truly a function of "hour" (or "day of week"). For these reasons, we decided to exclude actual values and dummy variables in this study.

From the literature survey, we identified that forecasting windows examined by previous studies study range from 5 minutes to 24 hours ahead, with 1-hour ahead being the most common. This choice is justified because chemical and physical processes governing ozone and fine particulate matter can be observed within this time frame. Also within this time frame, forecast models based on statistical methods yield satisfactory results with the exclusion of lagged variables. Moreover, it allows relatively ample time to regulatory bodies to issue warnings and for the public to take precautionary measures to avoid exposure to unhealthy levels of air pollution.

There are no formal requirements with respect to Gaussian distribution of variables employed in models based on MLR, PCR, MARS or ANN. MLR, PCR and MARS rely on central-tendencies of the data. Transformation of the data through an appropriate level of a power transform alleviates deviations to normality (Yeo and Johnson, 2000) and may yield air pollution forecasting models with improved performance (Al-Alawi et al., 2008). We found through literature review that it is not unusual to pre-process the data for ozone and particulate matter by means of power

transforms (usually square root and log), though this practice was found to be sporadic and non-standard.

In the preliminary stages of this study, the following parametric power transform was considered:

$$y^T = \begin{cases} \dfrac{y^{\varphi} - 1}{\varphi \times \dot{y}^{(\varphi-1)}} & if\ \varphi \neq 0 \\ \\ \dot{y} \ln(y) & if\ \varphi \neq 0 \end{cases} \tag{3.50}$$

where $\dot{y}$ is the geometric mean of the data series. Then, the transformed data was rescaled to fall in the 0.1 to 0.9 range as follows:

$$y^{T*} = 0.8 \times \left(\frac{y^T - y^T_{min}}{y^T_{max} - y^T} \right) + 0.1 \tag{3.51}$$

We found minimal improvements in the forecasting capabilities. Also, this pre-processing modifies the units of the variables and renders model interpretation more difficult. For this reason, we decided to exclude it from this study. We acknowledge, however, its importance and benefits.

There are a number of statistical tools available to determine the contribution of an independent variable in a regression model. One of the popular ones is the t-ratio.

$$t - ratio = \frac{\hat{\beta}_i}{SE_i} \tag{3.52}$$

where $\hat{\beta}$ is the least square estimate of the coefficient β_i, and SE_i is the standard error of the estimate. The t-ratio described in equation (3.52) measures the importance of a particular independent variable x_i in describing the dependent variable y, in the multiple regression model. As a rule of thumb, the independent variable x_i is said have a significant importance if

$$|t - ratio| > t_{2.5}(n - (p - 1)) \tag{3.53}$$

where $t_{2.5}(n - (p - 1))$ is the point on the scale of t-distribution having $(n - (p - 1))$ degrees of freedom such that an area of 0.025 exists under the curve of this t-distribution between $t_{2.5}$ and ∞.

This brings us to our next point in this discussion. The strength of principal component analysis is that it is a non-parametric analysis yielding an unique answer independent of the user. In other words, there are no parameters that need to be optimized or coefficients to be adjusted based on user experience. On the other hand, there are three assumptions that need some clarifications.

First, PCA is based on the Principle of Linearity. There is no *a priori* reason to challenge the applicability of principal component analysis for air quality modelling based on PCA's reliance on Principles of Linearity. Mathematically speaking, this is what allows us to (a) interpolate between individual data points, (b) to establish a transformation relationship between the input variables and principal component and (c) re-express the data as a linear combination of its basis vectors. Second, is the assumption

that principal components are truly orthogonal. This assumption provides an intuitive simplification that makes PCA solvable with linear algebra decomposition techniques. Third, is that the variance of the noise in the original dataset is negligible compared to the variance of the principal components. This is what leads us to say that the covariance and underlying dynamics between column vectors of the dataset can be effectively singled out from noise.

It has been suggested to retain the number of principal components with eigenvalues larger than unity (Karatzas and Kaltsatos, 2007). This practice is warranted for achieving reduction in the dimensionality of the dataset. On the other hand, it hinders the forecasting capabilities of the models. We will give this special consideration in our case studies.

The attractiveness of feed-forward artificial neural networks comes from their remarkable information processing characteristics pertinent mainly to nonlinearity, high parallelism, fault and noise tolerance, and learning and generalization capabilities (Basheer and Hajmeer, 2000). The main disadvantage of feed-forward neural networks is that the error associated with the network's computed output can potentially be large since they cannot look forward and correct estimates. Also, the training phase may take quite a long time before completion and may not find an optimal configuration. However, when there are outliers or multicollinearity in the data, neural networks significantly outperforms linear regression models (Al-Alawi et al., 2008).

As previously noted, the process of building data-driven models, such as the feed-forward Artificial Neural Network, is to a great extent user centric. Therefore, we must consider the following issues.

1. The composition and size of the learning set

Networks with significantly different performances can result from training using different learning cases. Some studies have suggested the cross validation technique, in which an algorithm makes different learning and testing datasets from available observations (Setiono, 2006). In such cases, ANN models are trained multiple times with different datasets and their predictive performance assessed given the multiple testing datasets and outputs. The architecture yielding the overall best performance (i.e. best generalization capability) is retained.

In our study, we have decided to employ a random two-way split of the observations into learning and testing (validation) dataset, while ensuring that high and low concentration values are included in each.

2. The number of hidden layers and the number of nodes for each hidden layer

Determining the optimum number of hidden layers and number of nodes in each hidden layer is not straightforward (Su, 2004). Algorithms that automatically determine the optimum number of hidden nodes in single hidden layer ANN have been proposed (Setiono, 2006). Yet, most models for forecasting ozone and particulate matter have one hidden layer with variable number of hidden nodes.

In our study, we have opted to investigate the one single hidden layer architecture. Furthermore, we will resort to the trial and error technique, that is, starting with only one hidden node and then adding additional nodes stepwise while ensuring that the network's

predictive accuracy has improved. The ANN based model will eventually overfit using the training dataset and lose its generalisation abilities. This can be seen by the continuous increase in R^2 using the training dataset and decrease in R^2 using the testing dataset. It is useful also to consider an error metric (such as RMSE) for both the training and validation run to check for overfit.

3. The learning rate (η)

The learning algorithm searches the space of weight values for an optimal solution, using a gradient descent approach. In all gradient methods, a small value for the learning rate will make the convergence of the network towards a solution slow, whereas a large value may cause the weights in the network to 'jump' back and forth over the appropriate value. We will assume slow convergence and therefore use a small learning rate of 0.001.

4. The type of nonlinear activation function.

As there is no theoretical argument why one function is better than the other, we have selected sigmoid activation function. The sigmoid function described by equation (3.54) is a standard choice due to its attractive properties, namely unipolarity (i.e. $0 < f_{sig}(x) < 1$) and simple differentiation as shown in equation (3.55).

$$f_{sig}(x) = \frac{1}{1 + e^{-\propto x}} \tag{3.54}$$

$$f'_{sig}(x) = \alpha f_{sig}(x)\left(1 - f_{sig}(x)\right) \tag{3.55}$$

When using the sigmoid activation function equation (3.40) reduces to:

$$\Delta w_1 = \alpha \hat{y}_i \eta \sum_{i=i}^{p} \left(\hat{y}_i(1 - y_i)(\hat{y}_i - y_i)\right) \tag{3.56}$$

More detailed information on training ANN model can be found elsewhere (Egmont-Petersen et al., 1994; Nedjah and Mourelle, 2006).

The identification of patterns in model-driven approaches is based on the optimisation of a cost function while in data-driven techniques such as Multivariate Regression Splines and Artificial Neural Networks, on training. The performance of regression models is largely dependent on the complexity of the pattern itself. On the other hand, the performance of the ANN approach depends largely on the learning algorithm and on the architecture of the network and its parameters. The strength of data-driven approaches is that the analysis yields an unique answer independent (to some extent) of the user.

3.5 Summary

In this section, we formally defined the concepts of time series, moment statistics, correlation and standard deviation. Then, laid the mathematical foundation and formulation for principal component analysis and discussed how it could be applied to reduce the dimensionality and address potential multicollinearity in the dataset.

After that, we introduced the seven different models included in this study, namely: MLR, PCR, MARS 1, MARS 2, ANN, PC-ANN and PC*-ANN. Then, we directed our efforts in describing in mathematical terms Multiple Linear Regression (MLR), Principal Component Regression (PCR) Multivariate Regression Splines (MARS) and Artificial Neural Networks (ANN). Following this, we presented the seven different metrics to be used in the comparative model performance assessment.

Our discussion focused first on the benefits of power transform which can be an important tool to improve linear models. Then, we developed on the implicit assumptions of the Principal Component Analysis. And finally we considered both the attractiveness and challenges associated with the user-centric exploratory ANN development process.

In spite of its evident success in many applications, linear model-driven approaches such as MLR and PCR face serious shortcomings. To a great extent, their inadequacy arises from its linear representation of non-linear systems and multicollinearity. Multicollinearity, or the high correlation between independent variables in a regression equation, makes it difficult to correctly identify the most important contributors for prediction; and given the pre-assumed linear form, no complex nonlinear patterns can be captured. PCR is not expected to be affected by multicollinearity and yield better results than MLR.

Data-driven models such as MARS and ANN are empirical in nature. They can provide pragmatic accurate solutions for phenomena forecasted through experimental data and field observations. The attractiveness of applying MARS and ANN to air pollution forecasting includes their ability to handle nonlinearity and high parallelism as well as imprecise information. Both MARS and ANN are considered are considered in

this study. The use of these two data-driven models is desirable because (i) bring nonlinearity may allows a better fit to the input data, (ii) noise-insensitivity might provide more accurate prediction in the presence of measurement errors, (iii) their high parallelism implies fast processing and hardware failure-tolerance, (iv) they allow generalization enabling application of the model to unlearned data.

Chapter 4

Investigation Area and Data

4.1 Investigation Area

Montréal (45°30′N, 73°35′W) is situated in the southwest of the province of Québec, in Eastern Canada. The city is situated on the Island of Montréal on the Saint Lawrence River.

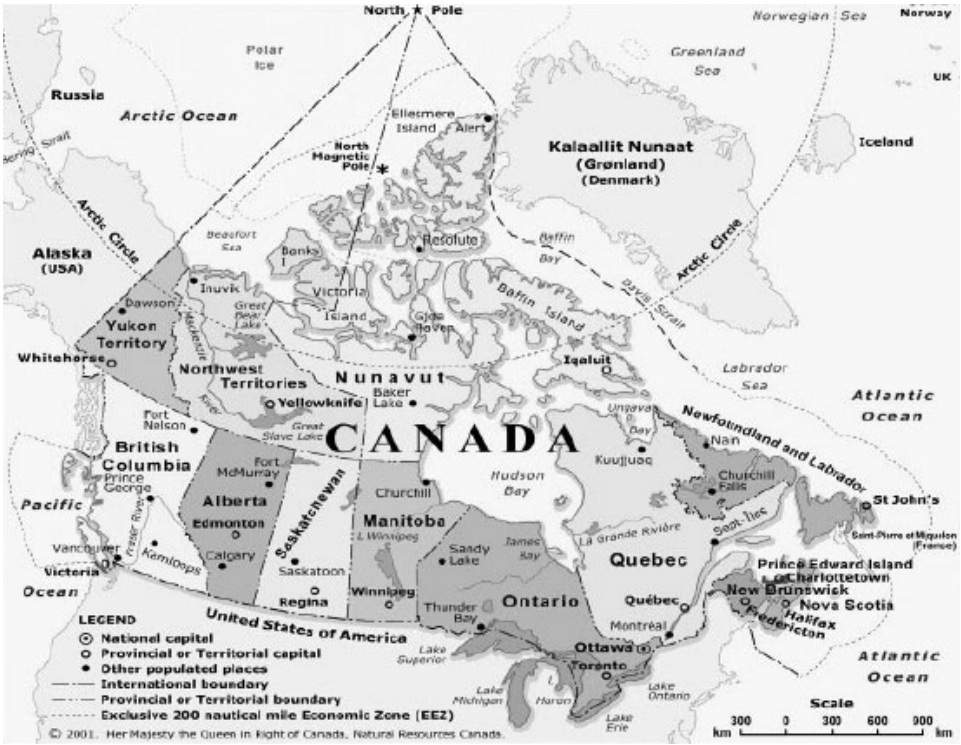

Figure 4.1 Map of Canada (HRSDC, 2004)

The 30-year (1971-2000) monthly daily means, maxima, minima and extremes temperatures are shown in Table 4.1 below. The mean 30-year average annual temperature is 6.2°C. Typical temperatures in the summer range from 16°C – 26°C and in the winter from -5°C to -15°C. Temperature in spring and fall are mild, but with frequent dire differentials. Extreme temperatures are experienced in mid-August and mid-January, when extreme temperatures have reached 37.6°C and -37.8°C respectively.

Temperature	Jan	Feb	Mar	Apr	May	Jun	Jul	Aug	Sep	Oct	Nov	Dec	Year
Daily (°C)	-10.2	-8.4	-2.3	5.7	13.4	18.2	20.9	19.6	14.6	8.1	1.6	-6.3	6.2
Stand. Deviation	2.9	3.0	2.3	1.7	1.7	1.2	1.0	1.1	1.4	1.6	1.6	3.2	0.9
Daily Max (°C)	-5.7	-3.9	2.2	10.7	19.0	23.6	26.2	24.8	19.7	12.7	5.3	-2.2	11.1
Daily Min (°C)	-14.7	-12.9	-6.7	0.6	7.7	12.7	15.6	14.3	9.4	3.4	-2.1	-10.4	1.4
Extreme Max (°C)	13.9	15.0	25.6	30.0	33.9	35.0	35.6	37.6	33.5	28.3	21.7	18.0	
Extreme Min (°C)	-37.8	-33.9	-29.4	-15.0	-4.4	0.0	6.1	3.3	-2.2	-7.2	-19.4	-32.4	

Table 4.1 Montréal 30-year (1971-2000) temperature averages (EC, 2011)

Total 30-year (1971-2000) monthly cumulative means of rainfall, snowfall and precipitation are shown in Table 4.2. Precipitation as rainfall and snowfall average 763.8 mm and 217.5 cm respectively.

Precipitation	Jan	Feb	Mar	Apr	May	Jun	Jul	Aug	Sep	Oct	Nov	Dec	Year
Rainfall (mm)	27.2	19.8	35.8	63.9	76.1	83.1	91.3	92.7	92.6	75.4	71.2	35.1	763.8
Snowfall (cm)	52.5	43.3	36	13.1	0.2	0	0	0	0	2.2	21.9	48.3	217.5
Precipitation (mm)	78.3	61.5	73.6	78	76.3	83.1	91.3	92.7	92.6	77.8	92.6	81.3	978.9

Table 4.2 Montréal 30-year (1971-2000) rainfall, snowfall and precipitation averages (EC, 2011)

In 2001, the population in Montréal was estimated at 1,812,723 inhabitants (City of Montréal, 2003). The density of the population is shown in Figure 4.2.

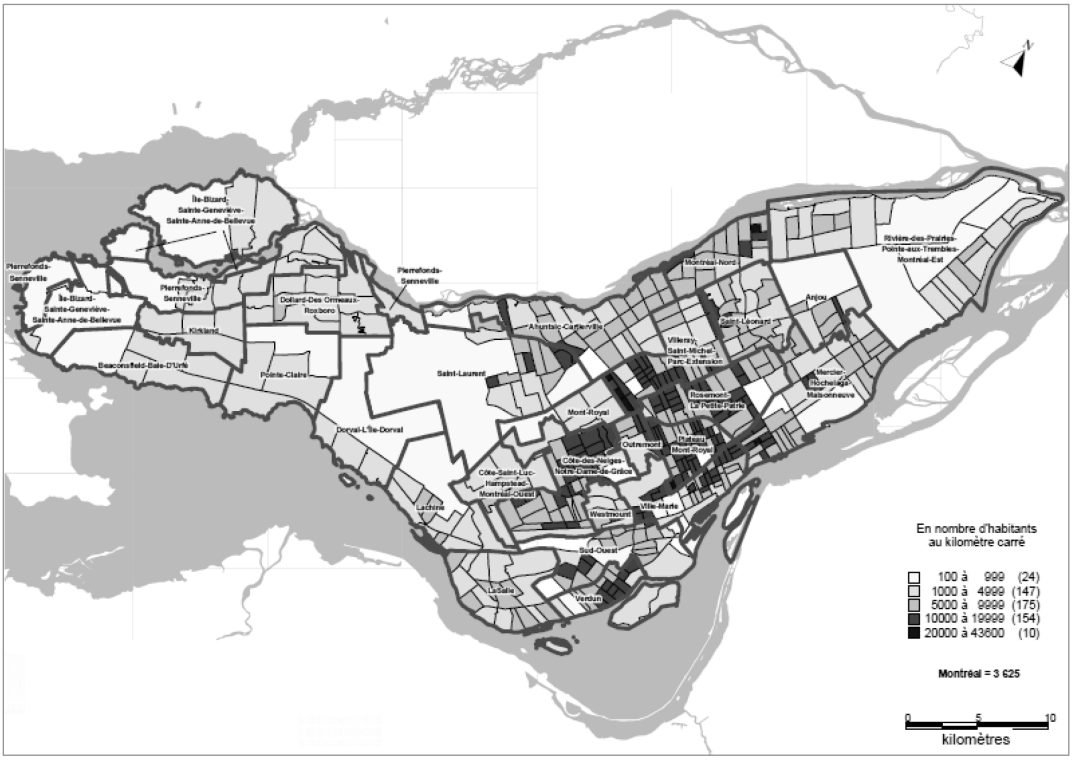

Figure 4.2 Population density Montréal (MTL, 2003)

Some 600,000 people live within the boundaries of the boroughs of Mont-Royal, Côte-Saint-Luc, Ville-Marie and Le Plateau. Population densities in these boroughs range from 20,000 to 40,000 inhabitants per km^2. It is in this south-eastern region of the island where most of the businesses, academic institutions and entertainment centers are located. Another 400,000 people live in the western region of the city. The density in the west ranges from 1,000 to 5,000 inhabitants per km^2. The Kirkland – Ville-Marie corridor is an important commuter's route.

There air quality monitoring stations in Montréal as shown in Figure 4.3. These monitoring stations are part of the *Réseau de surveillance de la qualité de l'air de la ville de Montréal* (RSQA) and integrated to Environment Canada's National Air Pollution Surveillance (NAPS) network.

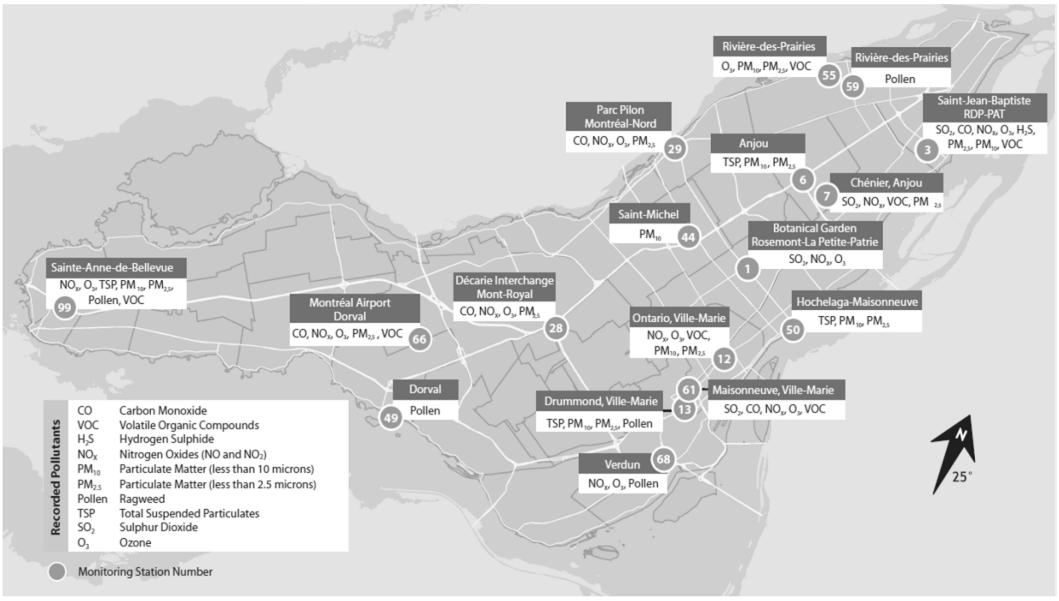

Figure 4.3 RSQA Monitoring Stations in Montréal, adapted from (RSQA, 2007)

Given the demographic considerations explained earlier, we collected meteorological and air quality data from the (Montréal Pierre Elliott Trudeau) Airport Station (45°28′N, 73°44′W) and the Maisonneuve Station (45°30′N, 73°34′W) for the period January 2004 to December 2007.

4.2 Data Collection and Quality Analysis

Hourly means of ozone (O_3), fine particulate matter ($PM_{2.5}$), nitrogen monoxide (NO), nitrogen dioxide (NO_2), and carbon monoxide (CO) are available daily at the Airport and Maisonneuve monitoring stations. As these pollutants have been identified as either target pollutants or chemical precursors, they are considered in this study. In addition, solar irradiation (SR), temperature (Temp), pressure (Press), dew point (DP), precipitation (Precip), wind speed (WS) and wind direction (WD) are monitored at Airport station. As these were identified as having an influence in the formation of both O_3 and $PM_{2.5}$, they are also considered in this study.

O_3 concentrations are monitored by ultra-violet absorption photometry; $PM_{2.5}$ concentrations are monitored by dichotomous sampling; NO and NO_2 concentrations are monitored by chemiluminescence method; and CO concentrations are monitored by infrared absorption photometry. All equipments are calibrated periodically and submitted to rigorous preventive maintenance program. Monitoring is continuous and hourly mean values are recorded.

All observations have been validated by RSQA and used for reporting (RSQA, 2004; RSQA, 2005; RSQA 2006; RSQA, 2007). We cross checked the monthly and annual averages obtained by our statistical analysis with values reported by RSQA and have obtained agreement at three decimal digits.

There would be a total of 35,064 hourly observations within the period January 1st, 2004 to December 31st, 2007, but there were missing values. The completeness of the data (expressed by percent, by month) for air pollution readings at Airport and

Maisonneuve stations as well as for meteorological data at Airport station are shown in Appendix C.

It is noted that at least 50% of the air quality data is missing at the Airport station for:

1. O_3 (from January to June 2004);
2. $PM_{2.5}$ (for June – July 2004);
3. NO (for March and June 2004);
4. NO_2 (in June 2004); and
5. CO (in June 2004).

Also, it is noted that at least 50% of the air quality data are missing at the Maisonneuve station for $PM_{2.5}$ (for June – August 2005 and December 2007).

In addition, it is noted that at least 50% of the meteorological data are missing at Airport Station for:

1. SR (October – November 2006, February – May 2007 and October – December 2007); and
2. DP (in November 2006).

To ensure consistency with the values reported by RSQA, these months have not been removed from the main dataset. This writer and the reader will exercise caution when interpreting moment statistics presented in the next section.

VOC data is available for 142 different species as daily (24-hour) averages, computed from 0h00-23h00 on each day at six days intervals. As such, the maximum number of observations during the period January 2004 to December 2007 is 243. There are 22 days with missing values.

4.3 Data Characterization

Monthly means of O_3 are consistently higher at Airport than at the Maisonneuve station, see Figure 4.4. Ozone demonstrates a clear seasonal pattern for both stations, with highest monthly means in March to June and lowest in November to January. There is a moderate correlation between values at the two stations ($r = 0.70$). Figure 4.5 show the monthly means of O_3 at Airport and Maisonneuve stations by month. Monthly mean O_3 concentration is highest at Airport in May at 57.4 $\mu g/m^3$ (95% CI: 56.2 – 58.6 $\mu g/m^3$) and lowest in November at 27.5 $\mu g/m^3$ (95% CI: 26.8 – 28.2 $\mu g/m^3$). Monthly mean O_3 at Maisonneuve is highest in June at 37.5 $\mu g/m^3$ (95% CI: 36.6 – 38.5 $\mu g/m^3$) and lowest in November at 15.1 $\mu g/m^3$ (95% CI: 14.7 – 15.5 $\mu g/m^3$).

Monthly daily-means of $PM_{2.5}$ are generally higher at Maisonneuve than at the Airport station, see Figure 4.6. Fine particulate matter monthly daily-means do not show

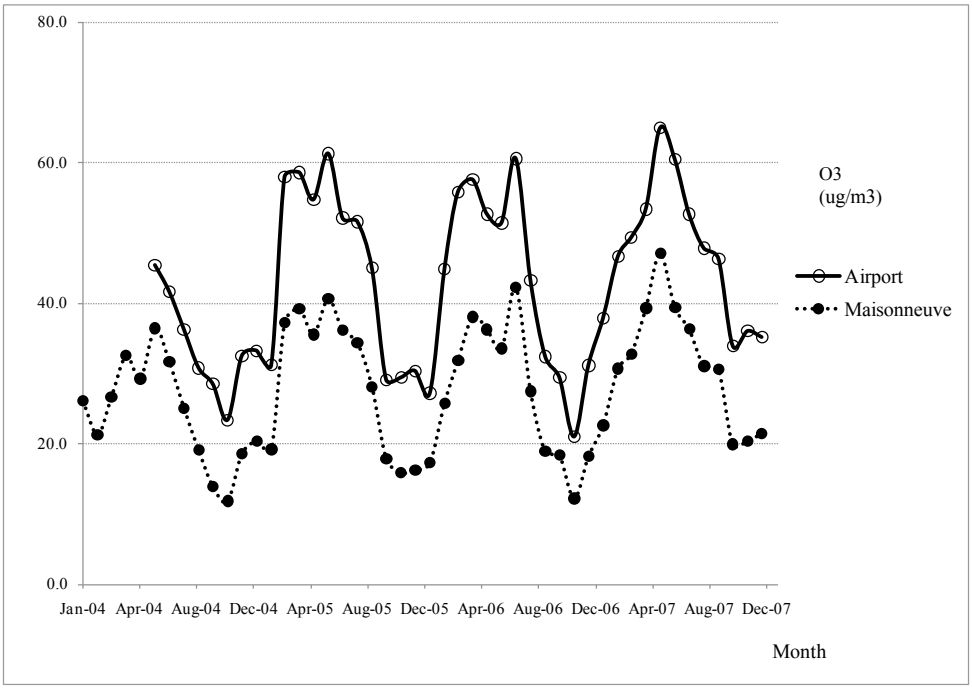

Figure 4.4 Monthly means of O_3 at Airport and Maisonneuve stations

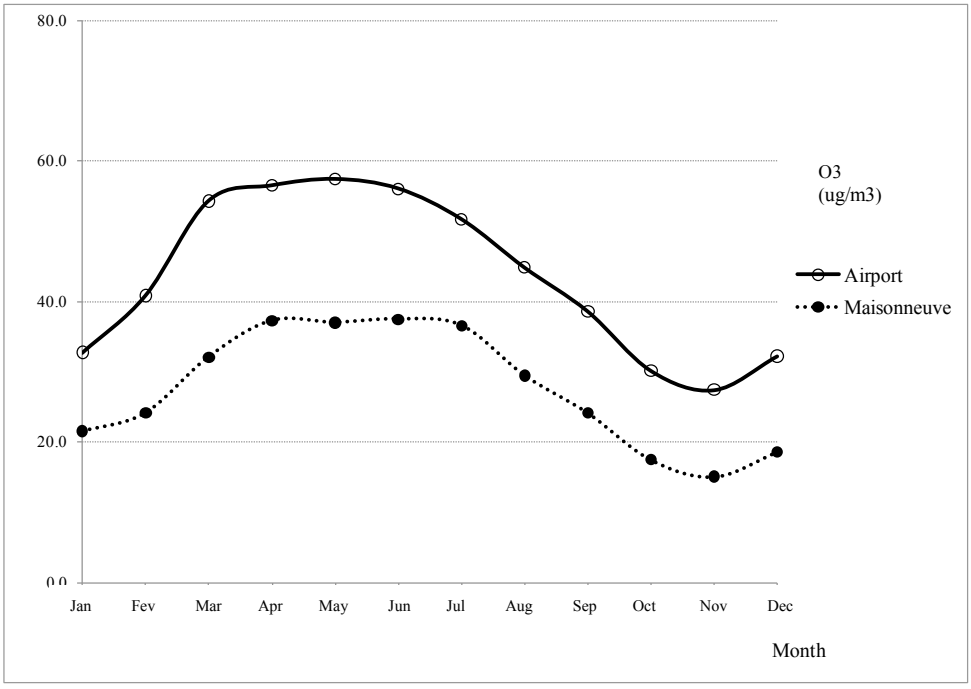

Figure 4.5 Monthly means of O_3 at Airport and Maisonneuve stations by month

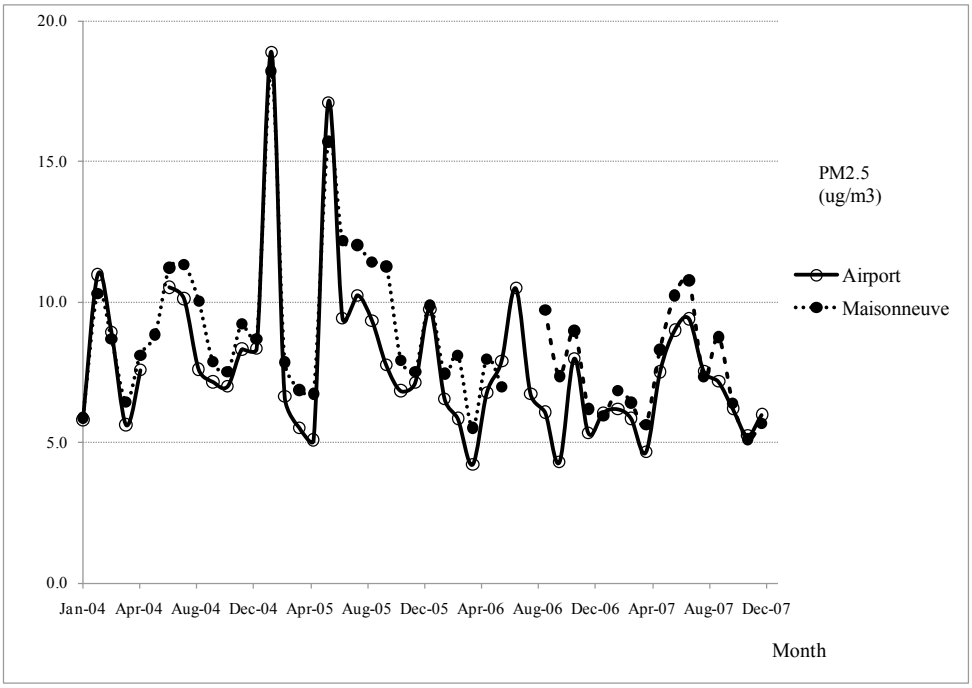

Figure 4.6 Monthly means of $PM_{2.5}$ at Airport and Maisonneuve stations

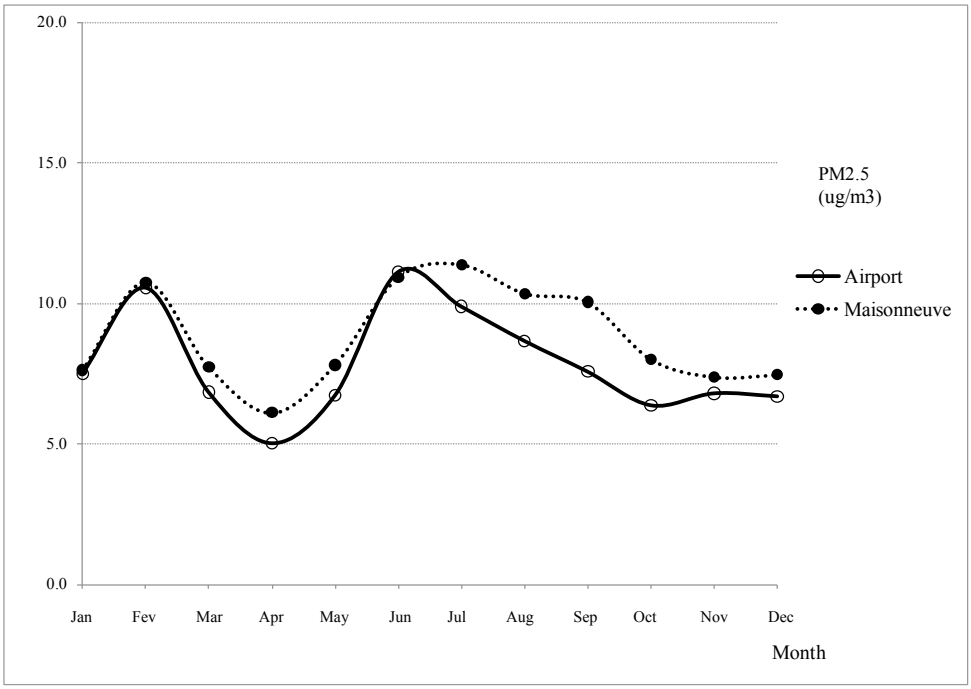

Figure 4.7 Monthly means of $PM_{2.5}$ at Airport and Maisonneuve stations by month

clear seasonal pattern for either stations. There is a weak correlation between values at the two stations (r = 0.20). Figure 4.7 show the monthly means of $PM_{2.5}$ at Airport and Maisonneuve stations by month.

Monthly means of NO are consistently higher at Maisonneuve than at the Airport station, see Figure 4.8. NO demonstrates a clear seasonal pattern for both stations, with highest monthly means in October to February and lowest in June to August. There is a moderate correlation between values at the two stations (r = 0.63). Figure 4.9 show the monthly means of NO at Airport and Maisonneuve stations by month. Monthly mean NO concentration is highest at Airport in February at 17.5 $\mu g/m^3$ (95% CI: 17.1 – 17.9 $\mu g/m^3$) and lowest in July at 2.7 $\mu g/m^3$ (95% CI: 2.8 – 2.9 $\mu g/m^3$). Monthly mean NO at Maisonneuve is highest in February at 43.1 $\mu g/m^3$ (95% CI: 42.2 – 44.0 $\mu g/m^3$) and lowest in July at 15.9 $\mu g/m^3$ (95% CI: 15.5 – 16.2 $\mu g/m^3$).

Monthly means of NO_2 are consistently higher at Maisonneuve than at the Airport station, see Figure 4.10. NO_2 demonstrates a clear seasonal pattern for both stations, with highest monthly means in November to March and lowest in July to September. There is a moderate correlation between values at the two stations (r = 0.58). Figure 4.11 show the monthly means of NO_2 at Airport and Maisonneuve stations by month. Monthly mean NO_2 concentration is highest at Airport in January at 33.0 $\mu g/m^3$ (95% CI: 32.3 – 33.7). $\mu g/m^3$) and lowest in July at 17.0 $\mu g/m^3$ (95% CI: 16.6 – 17.4 $\mu g/m^3$). Monthly mean NO_2 at Maisonneuve is highest in March at 54.0 $\mu g/m^3$ (95% CI: 52.8 – 55.2 $\mu g/m^3$) and lowest in July at 35.7 $\mu g/m^3$ (95% CI: 34.9 – 36.5 $\mu g/m^3$).

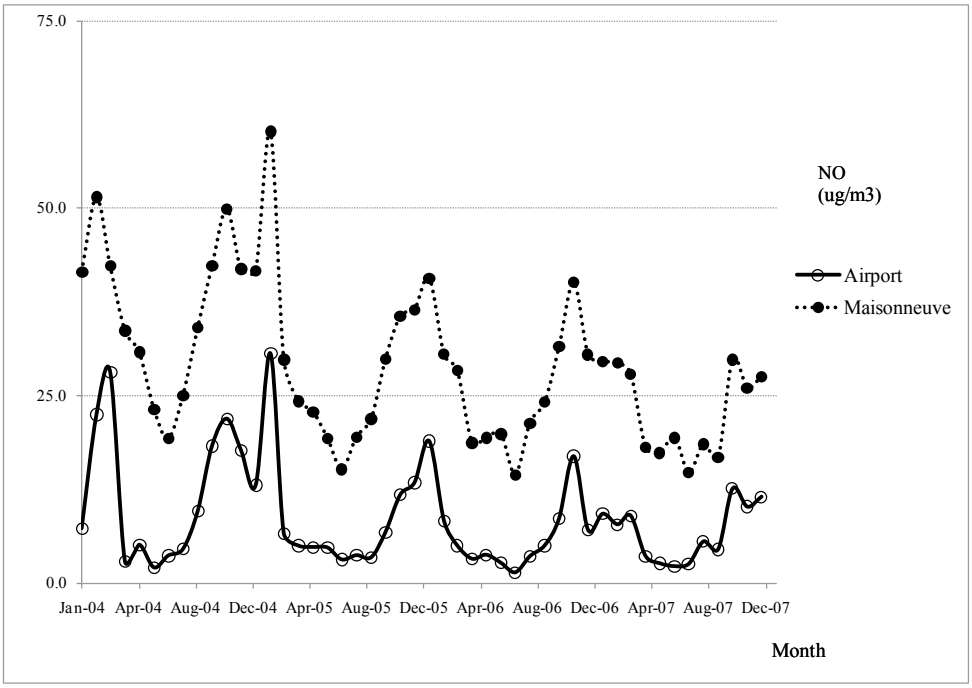

Figure 4.8 Monthly means of NO at Airport and Maisonneuve stations

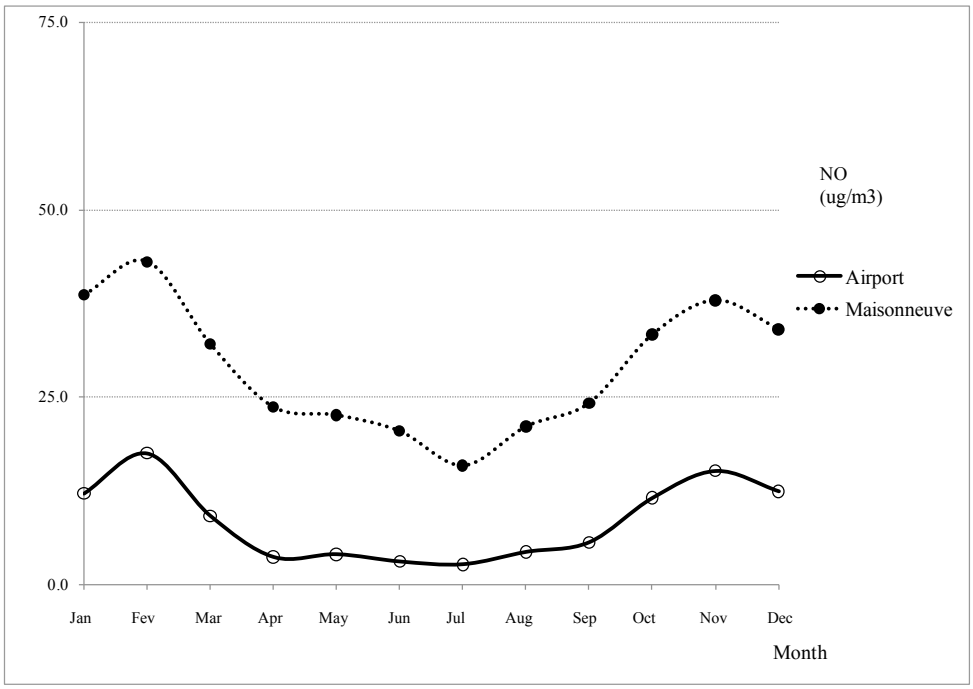

Figure 4.9 Monthly means of NO at Airport and Maisonneuve stations by month

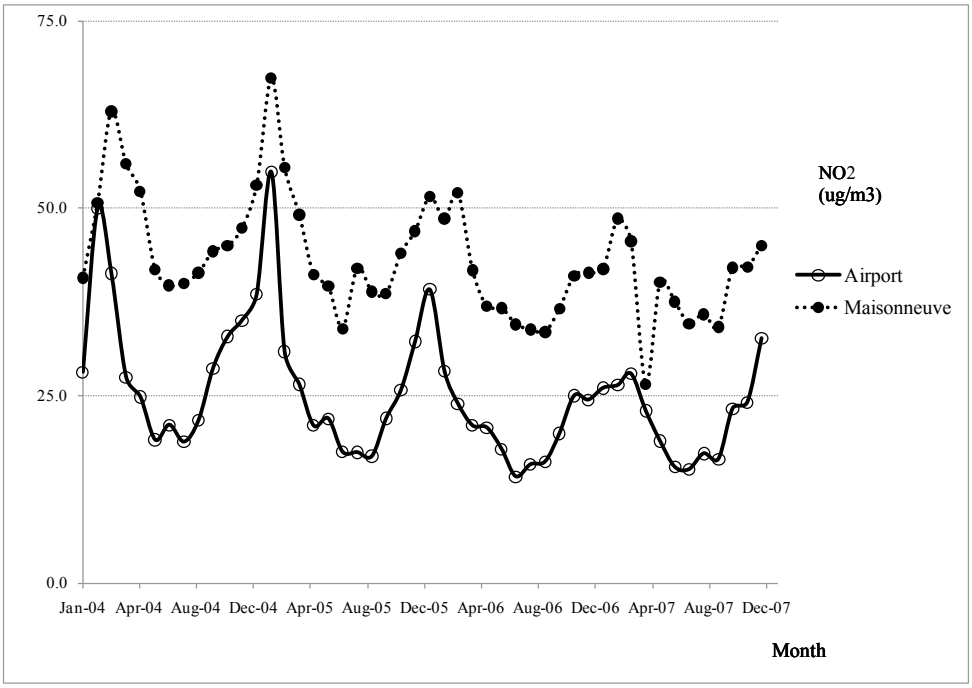

Figure 4.10 Monthly means of NO_2 at Airport and Maisonneuve stations

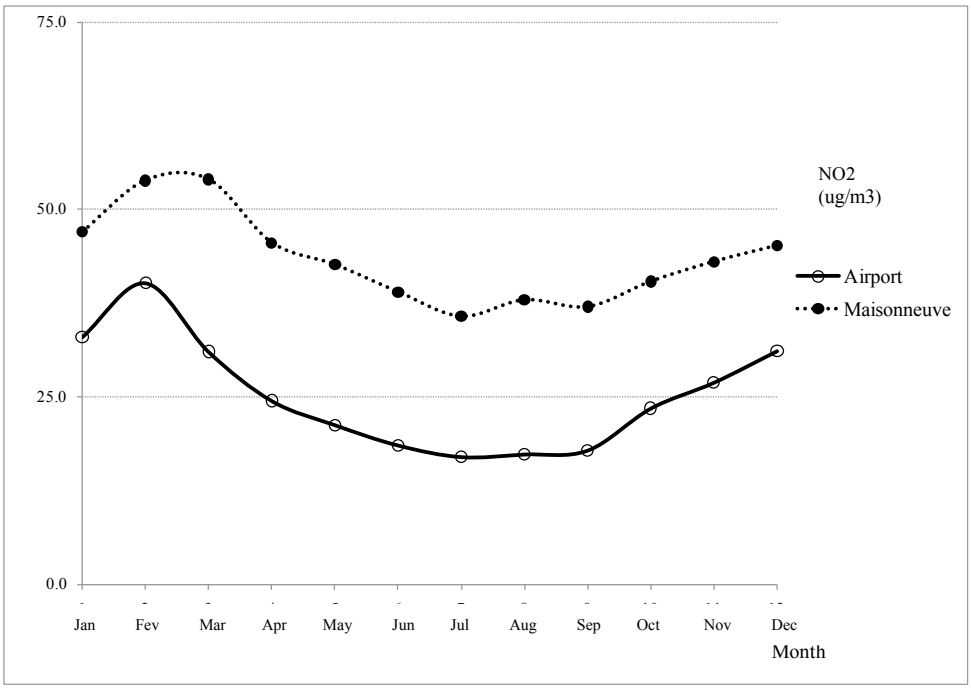

Figure 4.11 Monthly means of NO_2 at Airport and Maisonneuve stations by month

Monthly means of CO are consistently higher at Maisonneuve than at the Airport station, see Figure 4.12. Fine particulate matter monthly daily-means do not show clear seasonal pattern for either stations. Carbon monoxide does not show clear seasonal pattern for either stations. There is a moderate correlation between values at the two stations (r = 0.61). Figure 4.13 show the monthly means of CO at Airport and Maisonneuve stations by month.

SR demonstrates a clear seasonal pattern (see Figure 4.14) with highest monthly means in October to December and lowest in March to May. Figure 4.15 show the monthly means of SR at Airport stations by month. Monthly mean SR levels is highest in November at 934.7 (95% CI: 920.6 – 948.7 W/m^2) and lowest in April at 156.5 $\mu g/m^3$ (95% CI: 154.1 – 158.8 $\mu g/m^3$).

Temp and DP demonstrate a clear seasonal pattern (see Figures 4.16 and 4.18) with highest monthly means in June to August and lowest in March to May. Figure 4.17 and 4.19 show the monthly means of Temp and DP at Airport stations by month, respectively. Monthly mean Temp and DP levels are highest in July at 21.9 ^oC (95% CI: 21.4 – 22.4 ^oC) and 15.8 ^oC (95% CI: 15.3 – 16.3 ^oC), in that order. Monthly mean Temp and DP levels are lowest in January -9.2 ^oC (95% CI: -9.6 – -8.8 ^oC) and -13.7 $\mu g/m^3$ (95% CI: -14.1 – -13.2 ^oC), respectively.

Monthly means of Press and Precip do not show clear seasonal pattern for either station, see Figures 4.20 and 4.22.

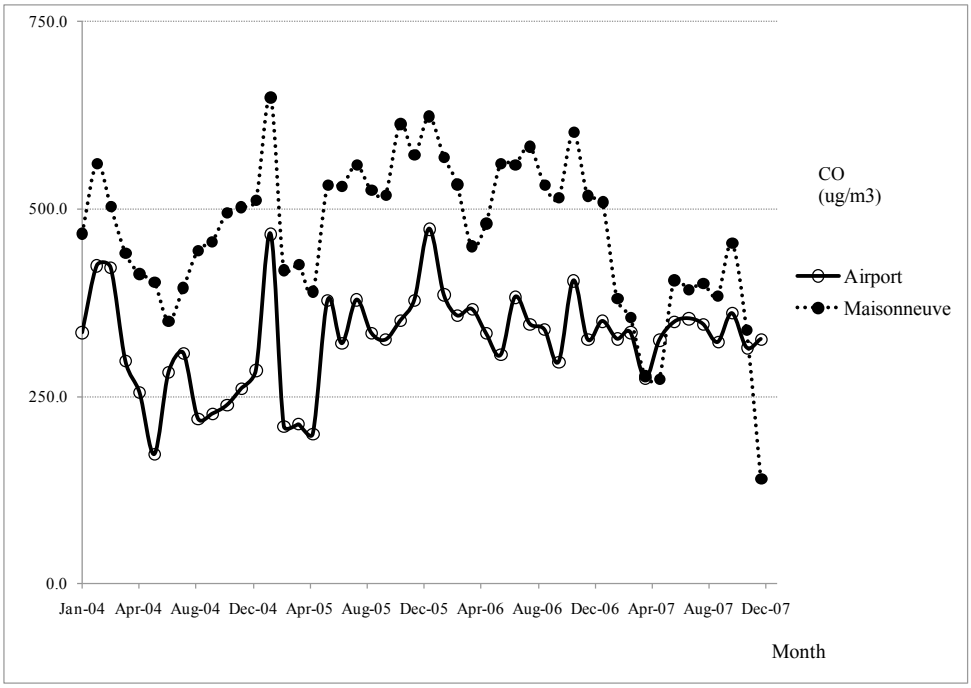

Figure 4.12 Monthly means of CO at Airport and Maisonneuve stations

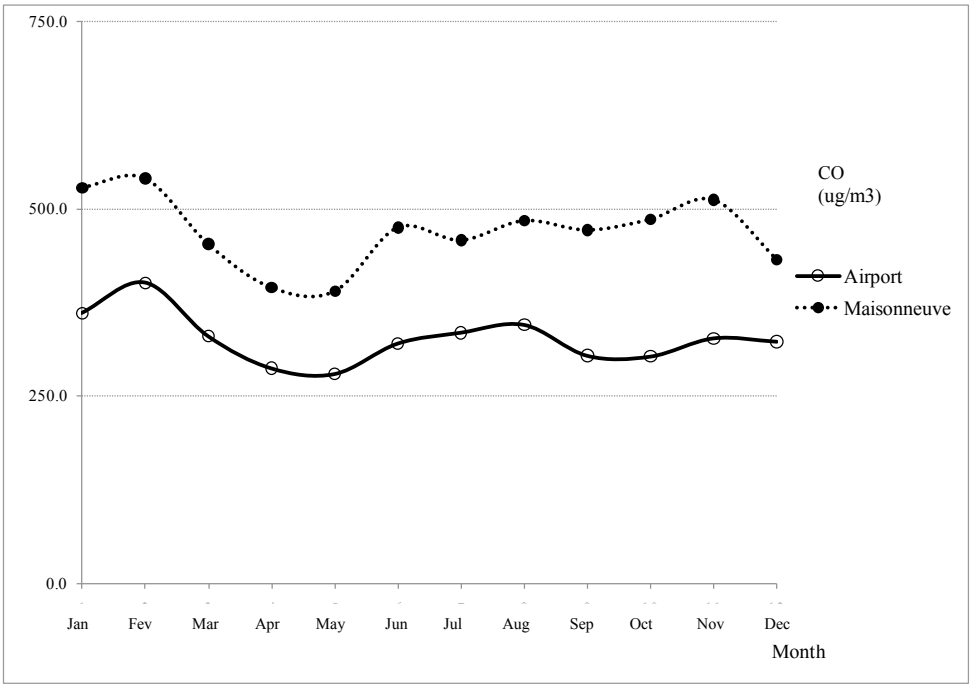

Figure 4.13 Monthly means of CO at Airport and Maisonneuve stations by month

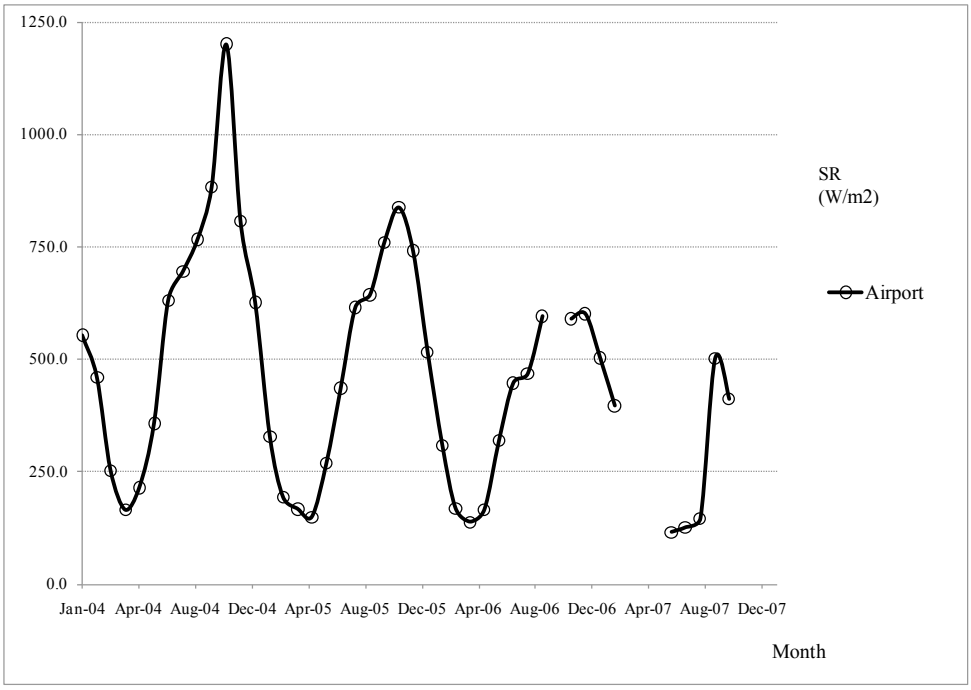

Figure 4.14 Monthly means of SR at Airport station

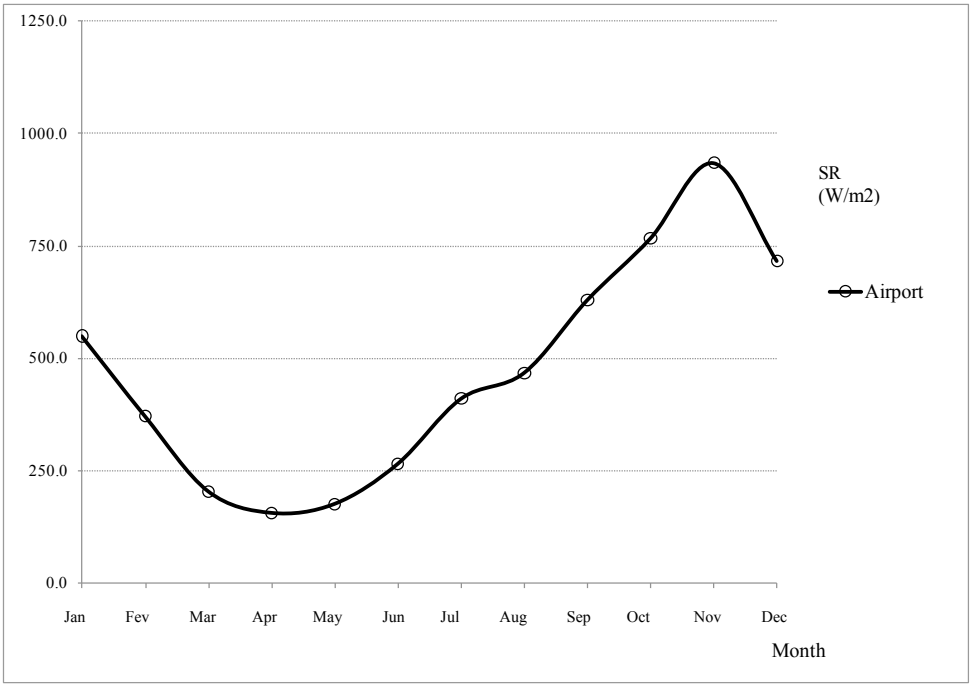

Figure 4.15 Monthly means of SR at Airport station by month

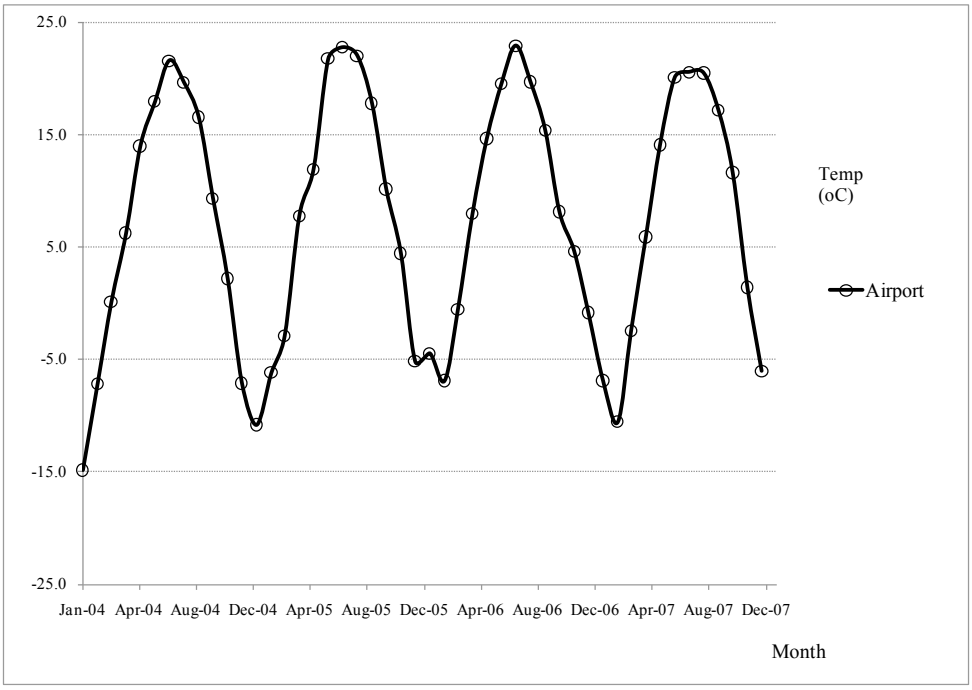

Figure 4.16 Monthly means of Temp at Airport station

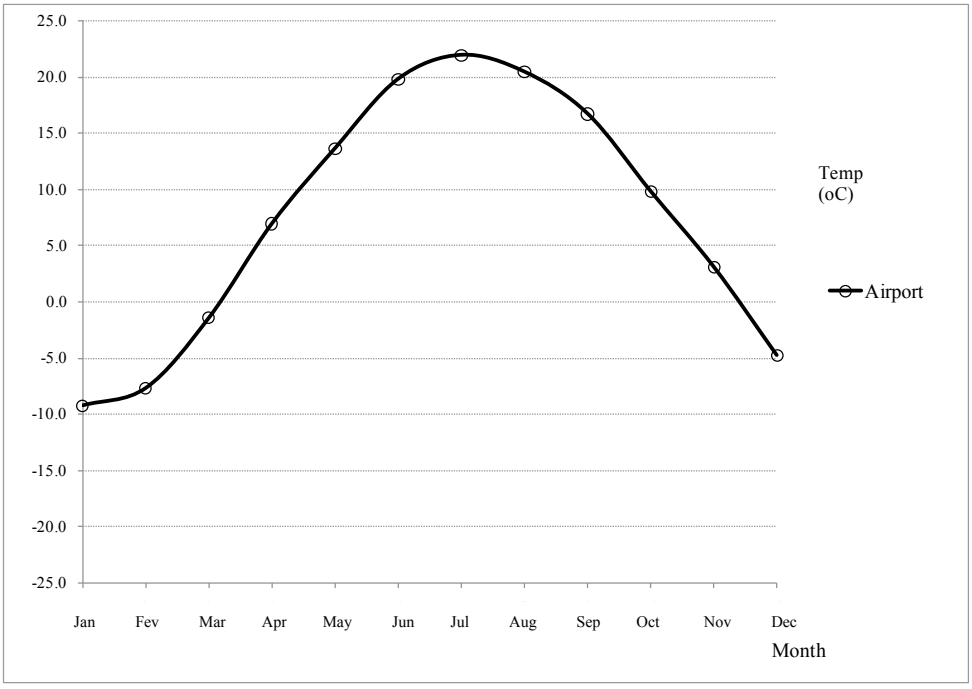

Figure 4.17 Monthly means of Temp at Airport station by month

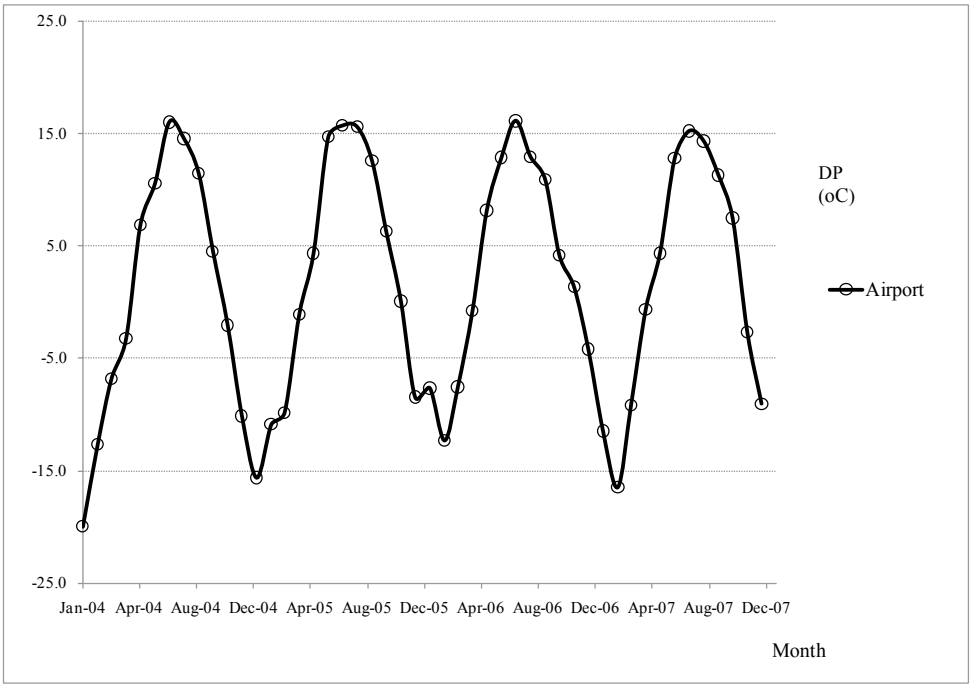

Figure 4.18 Monthly means of DP at Airport station

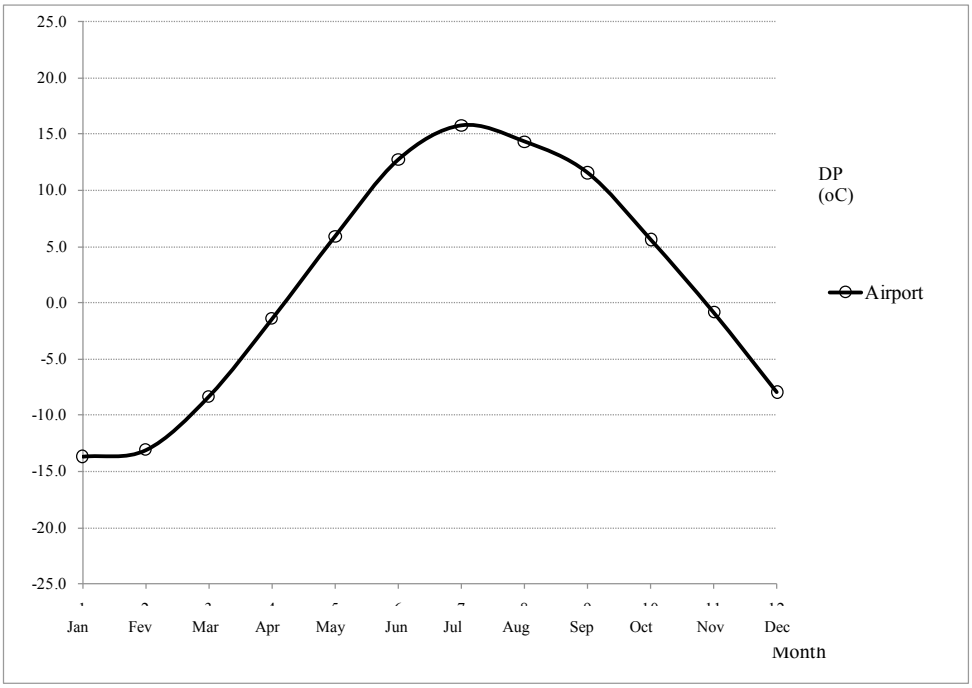

Figure 4.19 Monthly means of DP at Airport station by month

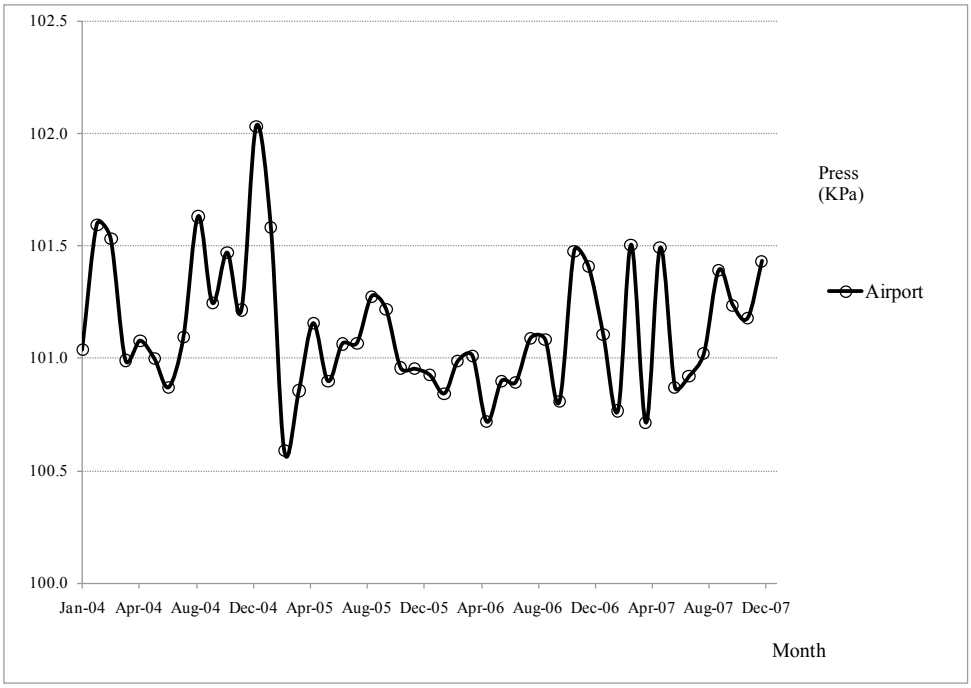

Figure 4.20 Monthly means of Press at Airport station

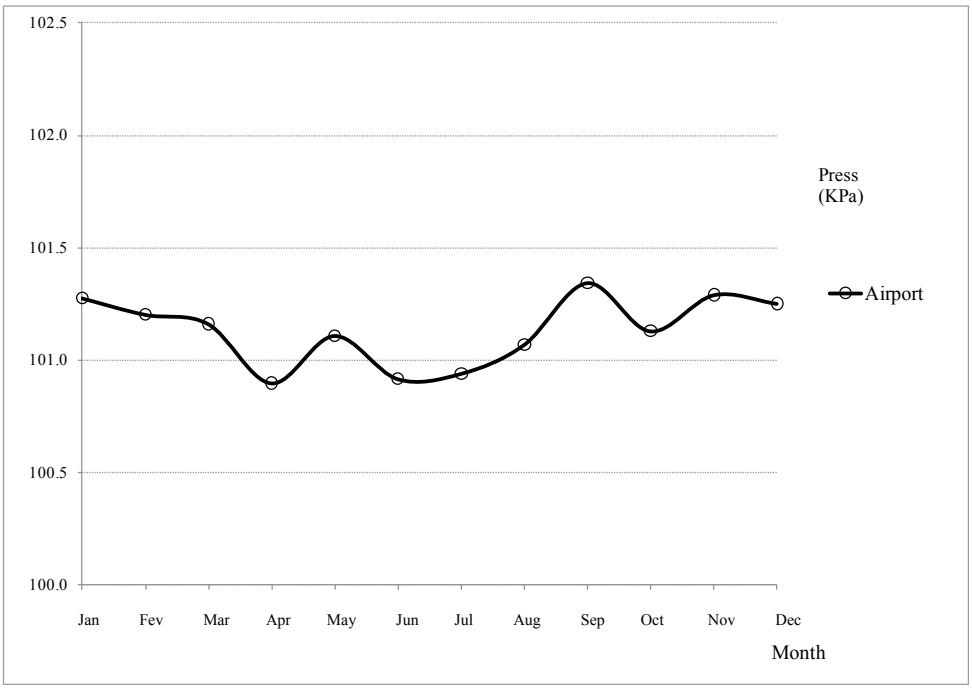

Figure 4.21 Monthly means of Press at Airport station by month

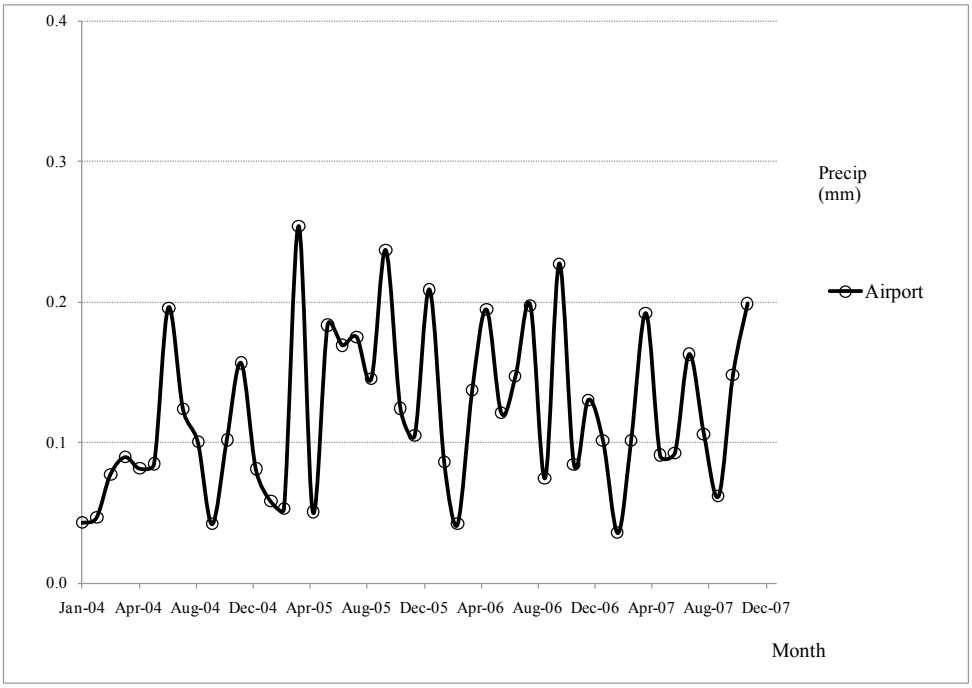

Figure 4.22 Monthly means of Precip at Airport station

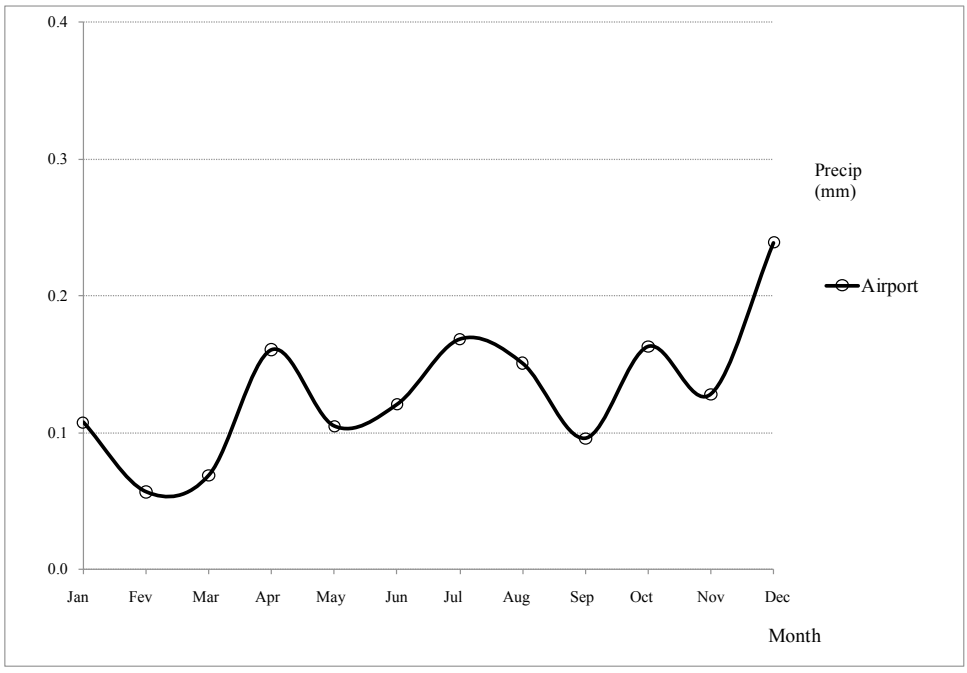

Figure 4.23 Monthly means of Precip at Airport and stations by month

The wind direction is reported by RSQA as (NE, E, SE, S, SW, W, NW, N). We transformed these values to (1, 2, 3, 4, 5, 6, 7, 8) respectively. The corresponding mean values of the daily maximum 1-h ozone concentration between January 2004 and December 2007 were plotted as a function of the transformed numerical values of wind direction. Results are tabulated in Appendix G. Then, we followed the procedure described in Chaloulakou et. al (2003) to derive the wind direction index (WDI). The rationale of this procedure is to remove the discontinuity of the wind direction angle at 360^o by fitting the following sinusoidal function:

$$WDI = 1 + \sin(\psi - \theta_w \pi) \tag{4.1}$$

where θ_w is the wind direction expressed in radians (with 0^o corresponding to the North) and ψ is an estimated parameter accounting for the phase shift.

The inclusion of wind speed and wind direction in this study does not violate the assumption of non-stochasticity of input variablesfor the regression models. The pseudo-randomness of WS and WDI is smoothed over the 1-hour averaging period of the data collection. Both variables WS and WDI point out to the role, which is primarily of physical transport of precursor species and mixing, that wind plays in the surface boundary layer with respect to the formation of ozone and fine particulate matter.

The value of ψ has been determined to be -0.79 for both Airport and Maisonneuve stations. From the definition of the index, it emerges that when the wind is southwesterly (i.e. WD is 5), WDI is 2.0 (maximum value). Conversely, when the wind is northeasterly (i.e. WD is 1), WDI is 0.0 (minimum value). These wind directions correspond to the maximum and minimum values of the daily 1-h maximum O_3, respectively.

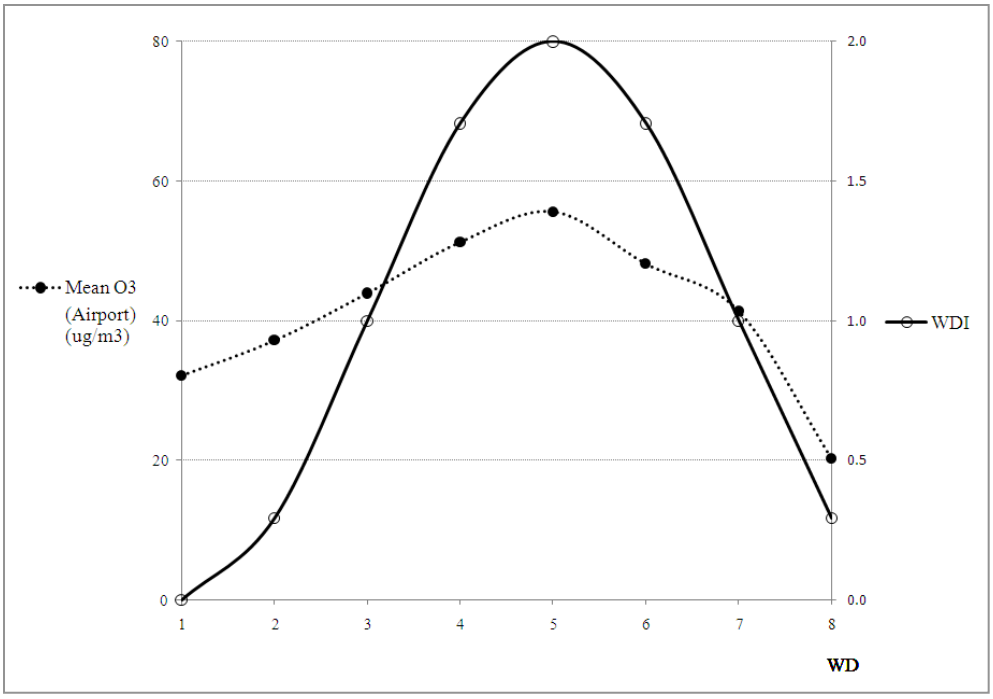

Figure 4.24 WDI and maximum 1-hour O_3 at Airport station by WD

The monthly means of all variables considered in this study for each month in the January 2004 to December 2007 period are presented in Appendix D. The typical monthly averages observed in the 2004-2007 time series are presented in Appendix E.

Given the seasonal pattern of air pollution and meteorological data at both stations, we have decided to consider two different seasons, namely summer and winter. The summer season corresponds to May, June and July. In summer; O_3 and Temp are especially high, and NO, NO_2 are especially low. The winter season corresponds to months of November, December and January. In winter, O_3 and Temp are especially low, and NO, NO_2 are especially high. This confirms the working of the photostationary equations.

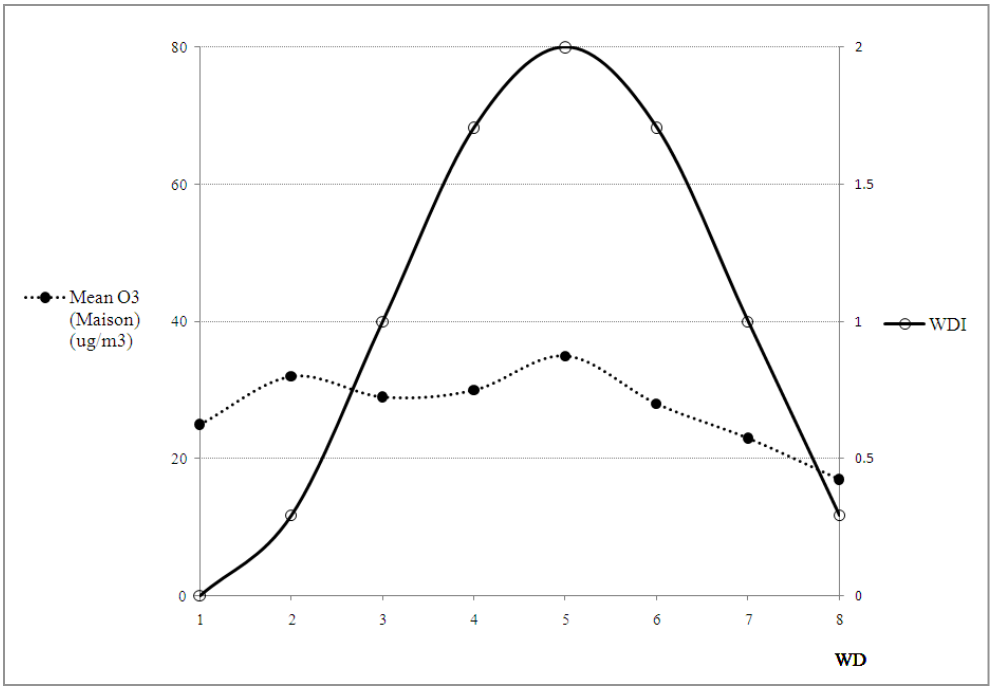

Figure 4.25 WDI and maximum 1-hour O_3 at Maisonneuve station by WD

4.4 Diurnal Cycles

Summer hourly means of air quality data at Airport and Maisonneuve stations are given in Figures 26 and 28, respectively. Winter hourly means of air quality data at Airport and Maisonneuve stations are given in Figures 27 and 29, respectively. Hourly means of meteorological data at Airport station are given in Figures 30 to 33. Numerical values for each hour are given in Appendix F and the distribution by season is given in Appendix H.

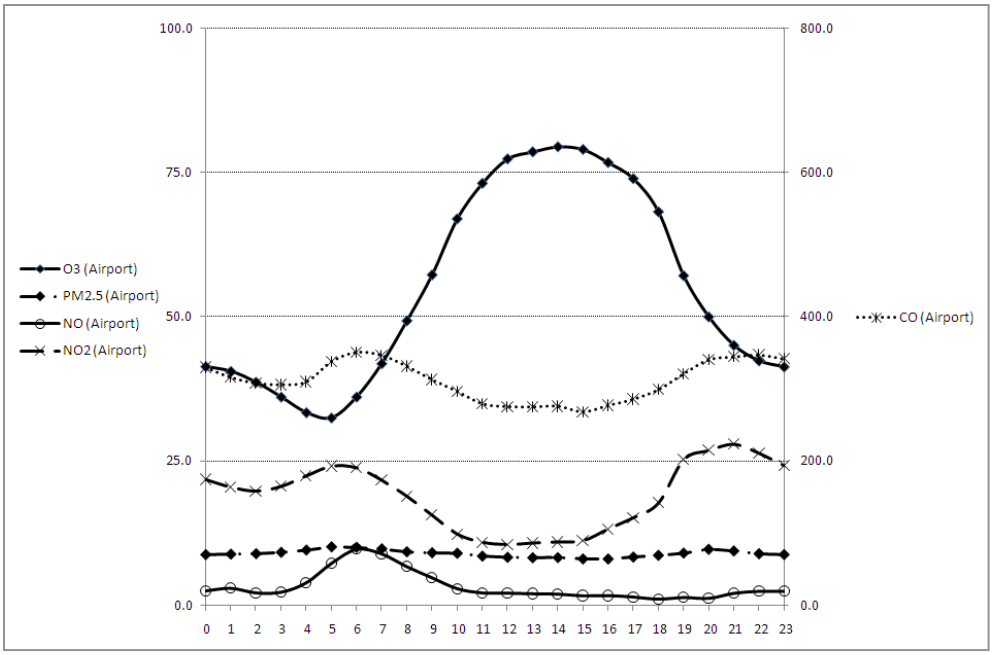

Figure 4.26 Diurnal cycle of O_3, $PM_{2.5}$, NO, NO_2 and CO (in $\mu g/m^3$) at Airport station (Summer)

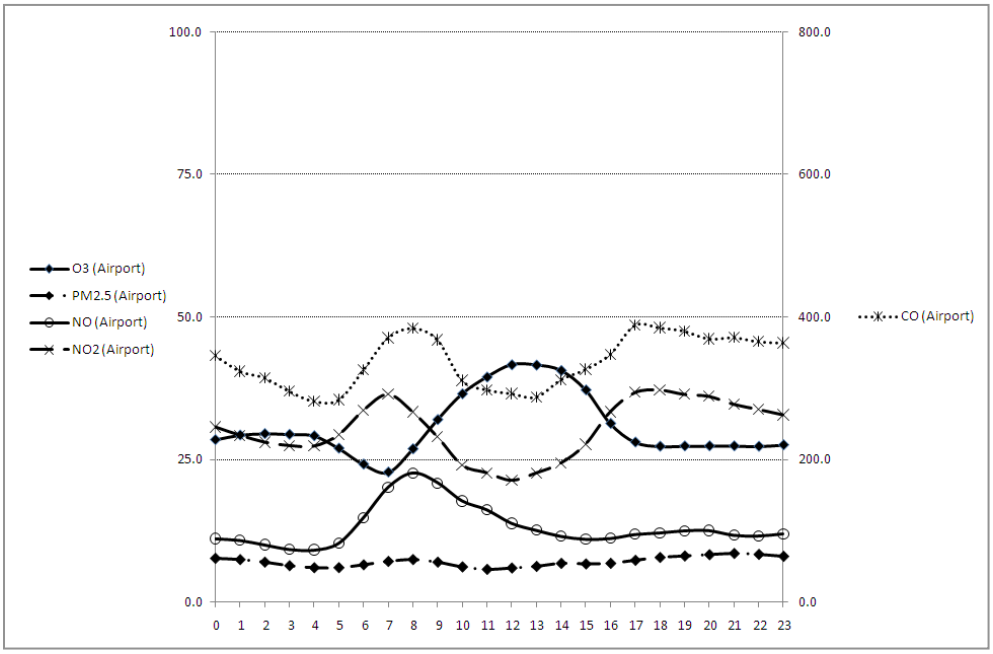

Figure 4.27 Diurnal cycle of O_3, $PM_{2.5}$, NO, NO_2 and CO (in $\mu g/m^3$) at Airport station (Winter)

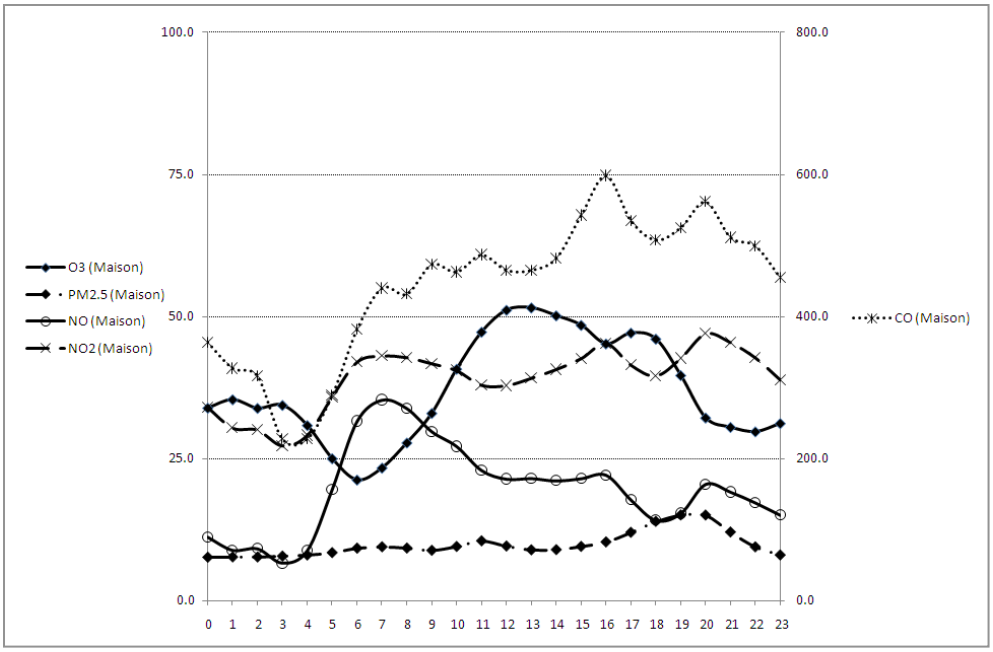

Figure 4.28 Diurnal cycle of O_3, $PM_{2.5}$, NO, NO_2 and CO (in $\mu g/m^3$) at Maisonneuve station (Summer)

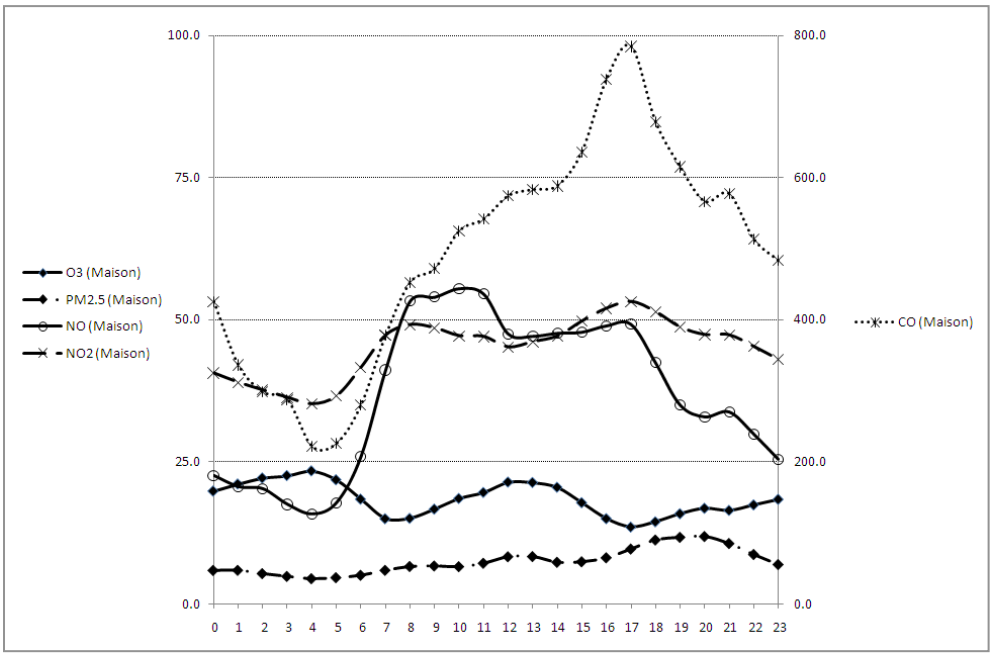

Figure 4.29 Diurnal cycle of O_3, $PM_{2.5}$, NO, NO_2 and CO (in $\mu g/m^3$) at Maisonneuve station (Winter)

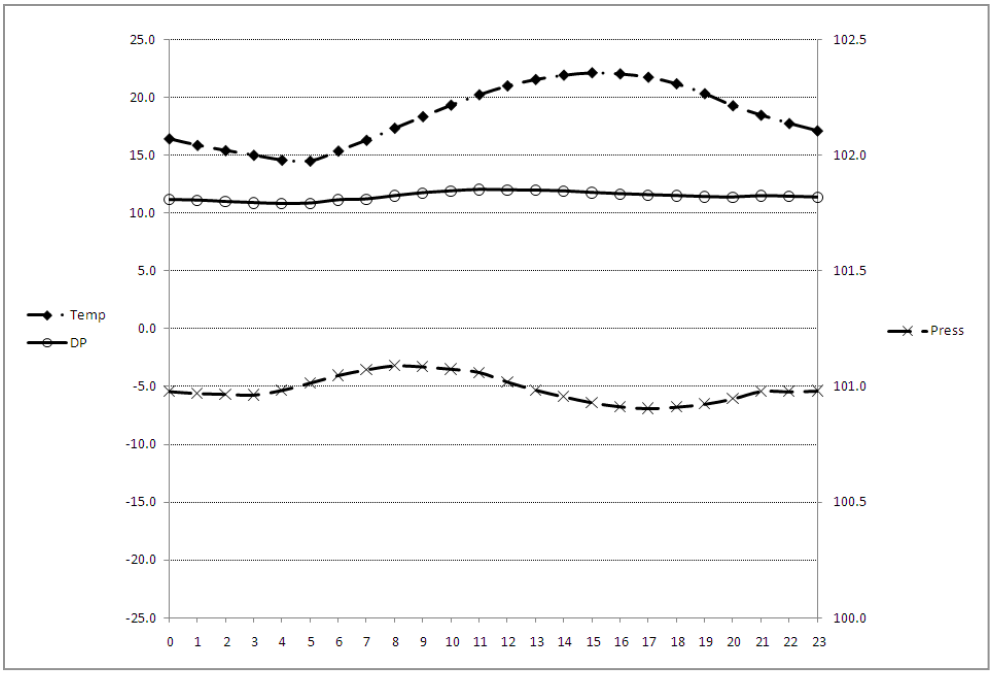

Figure 4.30 Diurnal cycle of Temp and DP (^{o}C); and Press (kPa) at Airport station (Summer)

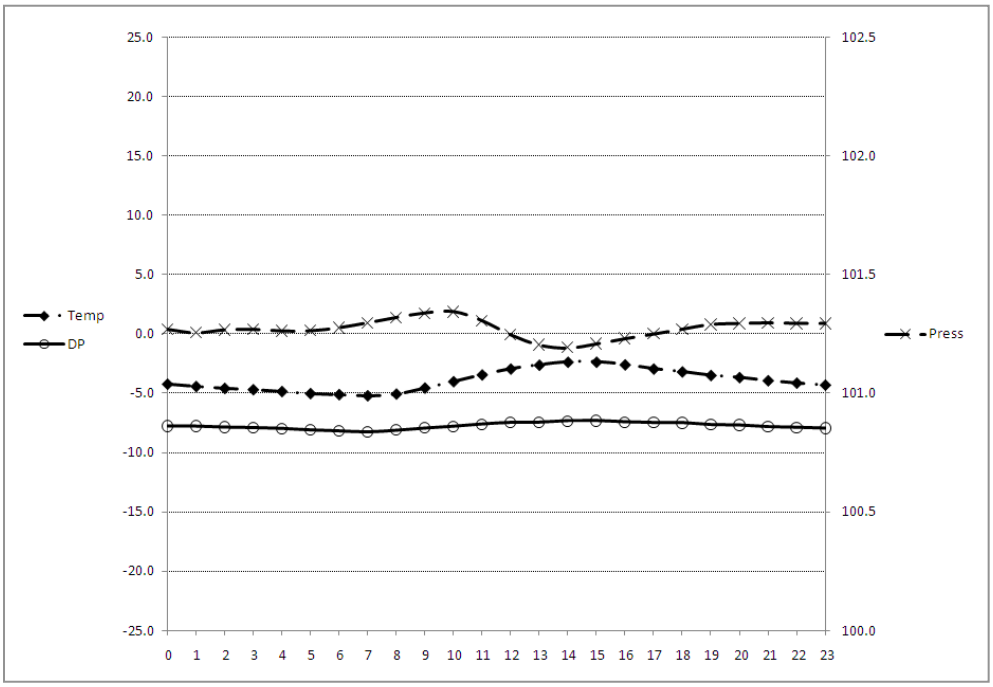

Figure 4.31 Diurnal cycle of Temp and DP (^{o}C); and Press (kPa) at Airport station (Winter)

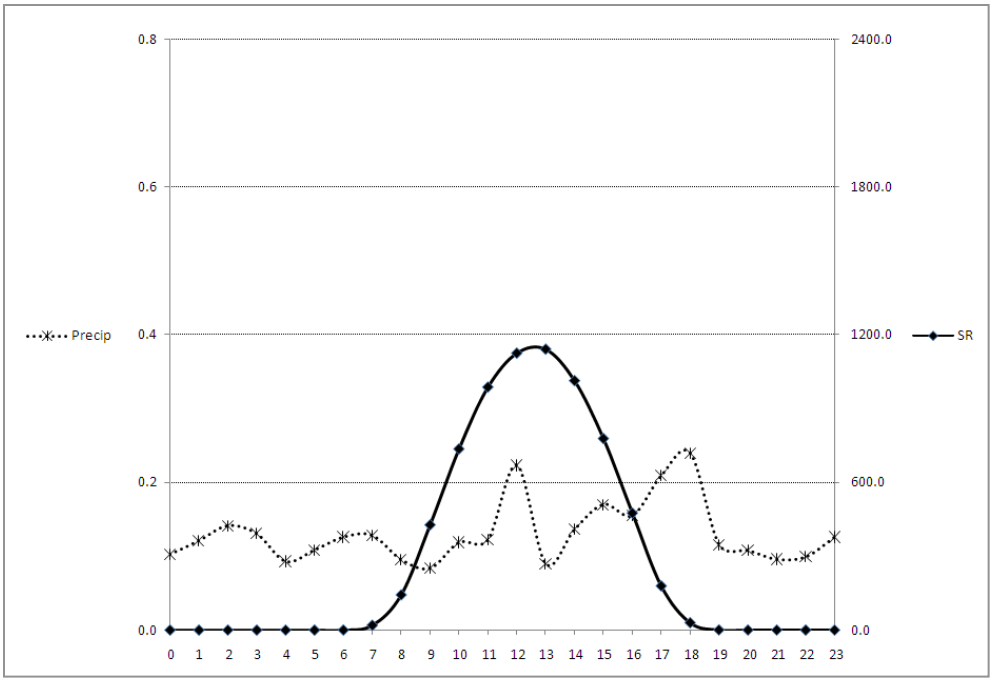

Figure 4.32 Diurnal cycle of Precip (mm) and SR (W/m^2) at Airport station (Summer)

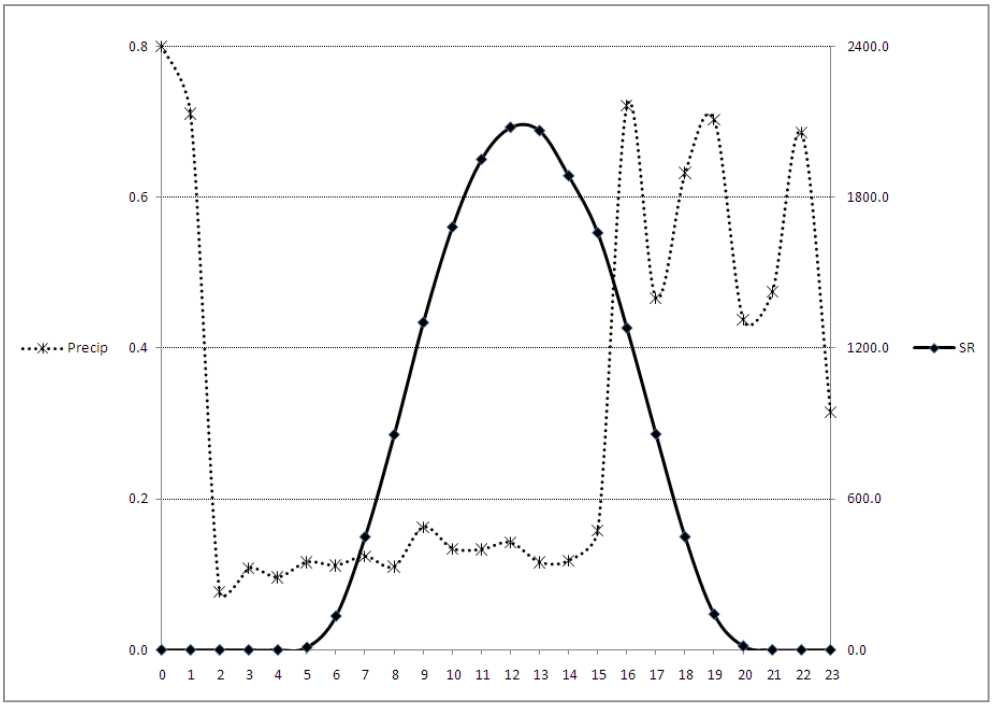

Figure 4.33 Diurnal cycle of Precip (mm) and SR (W/m^2) at Airport station (Winter)

On a typical early-morning in Montréal - that is between 05h00 and 07h00; NO, NO_2 and CO concentrations peak with increased vehicular traffic. At twilight, the nitrogen dioxide photolysis (dissociation of nitrogen dioxide into nitric oxide and oxygen radical) is limited due to low solar radiation (and temperature). At the same time, O_3 concentrations decreases because i) ozone oxidises NO to NO_2 and is converted back to molecular oxygen, ii) solar radiation and temperature are still low limiting the amount of free energy for NO_2 dissociation, iii) to low VOC levels (given low VOC volatility), and iii) limited photolysis of VOC allowing the alternate pathway of NO conversion to NO_2.

After 07h00, with increased solar irradiation and temperature, NO and NO_2 decrease and O_3 concentrations increase. O_3 increases because during the day light hours, i) NO_2 absorbs the energy of a photon light and dissociates into NO and an oxygen radical, then the oxygen radical combines with O_2 to form O_3, and ii) because of the increased VOC levels (higher volatility) which enables the oxidation process of hydrocarbons by hydroxyl radical (OH•) offering another pathway which converts NO to NO_2.

We note that O_3 peaks at 15h00. Then, in the afternoon, with decreasing solar irradiation, ozone concentrations decrease to stabilize at 21h00 in summer and 17h00 in winter. NO, NO_2 and CO increases with vehicular traffic peak at 21h00 in summer and 18h00 in winter. At sunset, the NO_2 dioxide photolysis is again limited due to low solar irradiation. At these times of day, ozone and nitric oxide combine to yield nitrogen dioxide and oxygen. The data confirms these important ozone formation mechanisms in Montréal.

O_3 levels in Maisonneuve are lower than at Airport. The data indicates that at Airport, with lower NO and NO_2 concentrations, NO_x makes a net positive contribution to photochemical ozone formation, but at Maisonneuve with higher concentrations, typical of downtown Montréal, the balance is shifted to ozone consumption. The data confirms that NO_x scavenging occur in the city as higher NO_x emissions locally decrease ozone.

Given the diurnal pattern of air pollution and meteorological data at both stations, we have decided consider two different periods in our study, namely day and night. The day period corresponds to 11h00 to 16h00. The night period corresponds to 22h00 to 04h00.

Tables 4.3 to 4.6 show the correlation between variables for summer and winter seasons by day and night periods. Correlation coefficients between pollutants and meteorological variables were analysed to evaluate the influence of each variable on O_3 and $PM_{2.5}$ concentration. These coefficients provide a measure of the linear relation between two variables and also indicate the existence of collinearity between the explanatory variables.

At Airport station, summer ozone concentrations were correlated with $PM_{2.5}$ and temperature during day time; and with NO_2 and wind speed during night time. Winter ozone concentrations were negatively correlated with $PM_{2.5}$, NO, NO_2 and CO during both day and night time. At Maisonneuve station, ozone concentrations were correlated with NO during both day and night periods. During daylight hours, ozone was correlated with temperature. Overall, the correlations of ozone with meteorological variables were generally weak.

At Airport station, summer $PM_{2.5}$ concentrations were correlated with O_3, CO and temperature during both day and night periods. Winter $PM_{2.5}$ concentrations were negatively correlated with $PM_{2.5}$, NO, NO_2 and CO during both day and night time. High correlation was found between $PM_{2.5}$ and O_3, NO, NO_2 at Maisonneuve during both periods in winter. The correlations of $PM_{2.5}$ with meteorological variables were generally weak.

Cross correlation between precursor species were identified, such as NO and CO (0.70), O3 and NO2 (-0.70) and NO and NO2 (0.65), demonstrating the existence of collinearity between the variables. Also, the correlation between temperature and dew point was positive and highly significant, as expected.

Summer/Day	O3 (Airport)	PM2.5 (Airport)	O3 (Maison)	PM2.5 (Maison)
O3 (Airport)	1.00	0.51	0.90	0.49
PM2.5 (Airport)	0.51	1.00	0.44	0.92
NO (Airport)	-0.34	0.09	-0.28	0.03
NO2 (Airport)	-0.16	0.31	-0.18	0.28
CO (Airport)	0.10	0.62	0.08	0.60
O3 (Maison)	0.90	0.44	1.00	0.39
PM2.5 (Maison)	0.49	0.92	0.39	1.00
NO (Maison)	-0.55	-0.18	-0.71	-0.14
NO2 (Maison)	0.32	0.37	0.01	0.46
CO (Maison)	-0.09	0.21	-0.30	0.27
SR	-0.05	0.01	0.04	0.00
Temp	0.62	0.50	0.58	0.48
DP	0.27	0.55	0.26	0.55
Press	0.27	-0.05	0.30	-0.08
Precip	-0.20	-0.07	-0.22	-0.04
WS	-0.05	-0.13	-0.03	-0.15
WDI	0.30	0.12	0.25	0.11

Table 4.3 Correlation of variables (Summer / Day)

Summer/Night	O3 (Airport)	PM2.5 (Airport)	O3 (Maison)	PM2.5 (Maison)
O3 (Airport)	1.00	0.12	0.85	0.21
PM2.5 (Airport)	0.12	1.00	0.23	0.89
NO (Airport)	-0.35	0.09	-0.22	0.05
NO2 (Airport)	-0.54	0.34	-0.29	0.23
CO (Airport)	-0.22	0.61	-0.09	0.53
O3 (Maison)	0.85	0.23	1.00	0.23
PM2.5 (Maison)	0.21	0.89	0.23	1.00
NO (Maison)	-0.31	-0.03	-0.49	0.03
NO2 (Maison)	-0.22	0.33	-0.31	0.36
CO (Maison)	-0.04	0.09	-0.15	0.13
SR	-0.04	0.04	-0.07	0.06
Temp	0.26	0.50	0.23	0.51
DP	0.09	0.46	0.06	0.47
Press	-0.19	0.07	-0.07	0.02
Precip	0.05	0.05	0.02	0.07
WS	0.44	-0.28	0.31	-0.25
WDI	0.37	0.06	0.26	0.12

Table 4.4 Correlation of variables (Summer / Night)

Winter/Day	O3 (Airport)	PM2.5 (Airport)	O3 (Maison)	PM2.5 (Maison)
O3 (Airport)	1.00	-0.54	0.80	-0.51
PM2.5 (Airport)	-0.54	1.00	-0.40	0.79
NO (Airport)	-0.48	0.74	-0.32	0.51
NO2 (Airport)	-0.74	0.74	-0.53	0.62
CO (Airport)	-0.64	0.79	-0.43	0.61
O3 (Maison)	0.80	-0.40	1.00	-0.48
PM2.5 (Maison)	-0.51	0.79	-0.48	1.00
NO (Maison)	-0.43	0.43	-0.61	0.58
NO2 (Maison)	-0.26	0.42	-0.52	0.53
CO (Maison)	-0.53	0.48	-0.66	0.64
SR	-0.03	0.03	-0.07	0.06
Temp	-0.36	0.05	-0.41	0.09
DP	-0.51	0.14	-0.52	0.17
Press	0.24	0.04	0.24	-0.01
Precip	-0.20	-0.03	-0.13	-0.04
WS	0.31	-0.38	0.34	-0.39
WDI	0.41	-0.32	0.13	-0.30

Table 4.5 Correlation of variables (Winter / Day)

Winter/Night	O3 (Airport)	PM2.5 (Airport)	O3 (Maison)	PM2.5 (Maison)
O3 (Airport)	1.00	-0.60	0.79	-0.52
PM2.5 (Airport)	-0.60	1.00	-0.53	0.74
NO (Airport)	-0.46	0.70	-0.39	0.41
NO2 (Airport)	-0.80	0.70	-0.56	0.55
CO (Airport)	-0.55	0.79	-0.43	0.49
O3 (Maison)	0.79	-0.53	1.00	-0.59
PM2.5 (Maison)	-0.52	0.74	-0.59	1.00
NO (Maison)	-0.44	0.46	-0.56	0.60
NO2 (Maison)	-0.56	0.57	-0.69	0.61
CO (Maison)	-0.39	0.46	-0.52	0.57
SR	-0.03	-0.06	-0.02	-0.04
Temp	-0.13	-0.07	-0.24	0.00
DP	-0.21	-0.01	-0.30	0.06
Press	-0.11	0.19	-0.01	0.12
Precip	-0.03	-0.08	0.00	-0.07
WS	0.60	-0.42	0.50	-0.34
WDI	0.27	-0.19	0.08	-0.15

Table 4.6 Correlation of variables (Winter / Night)

4.5 Dataset Preparation

Data from Airport station (O_3, $PM_{2.5}$, NO, NO_2, CO, SR, Temp, Press, DP, Precip, WS and WDI) and from Maisonneuve station (O_3, $PM_{2.5}$, NO, NO_2 and CO) observed in summer/winter seasons and in day/night periods at time *t* (present time) were set in a matrix form. Then we added columns to indicate the observed values of O_3 and $PM_{2.5}$ at *t* + 1 (future time, 1-hour window). The 1-hour ahead values of O_3 and $PM_{2.5}$ were referred to as OP and PP, respectively. Each variable carried a subscript "Airport" or "Maison" to indicate its source.

We eliminated the rows of each pattern where there was at least one observation missing, from either station. The resulting matrix contained 17 columns and 4,976 rows. At this point, we made an informed decision not to include a "production" subset in order to simplify subsequent analysis. Then, we randomly selected rows in the matrix for either learning or testing in such a way that the selection was uniformly distributed. We applied a subroutine such that:

1. at least 50% (but no more than 55%) of the observations were tagged as "learning";
2. 50% of the top 50 observations for each variable were tagged "testing";
3. 50% of the bottom 50 observations for each variable were tagged "testing"

The learning dataset was used for model training and the testing dataset was used for model validation. All models were trained and validated using the same datasets. Table.

4.7 summarises the final split count of the main observation matrix into the learning and testing datasets used for forecasting (Case Studies 1 through 4 inclusively).

Period	Cases	Learning	Testing
Summer			
Day	1002	506	496
Night	1224	629	595
Winter			
Day	1231	650	581
Night	1519	796	723
Total	4976	2581	2395

Table 4.7 Learning and testing counts

The dataset used in Case Study 5 differed from the previous datasets as the objective of this case study was to model daily means of ozone at Maisonneuve station with inclusion of available VOC data. In addition to the set of air quality and meteorological data used in the previous four case studies, the concentration values of 142 different VOC species that were available at six days interval were included. The original dataset with no missing values contained 186 rows of observations. The same subroutine was applied. The dataset was split into training and validation datasets containing 102 and 84 observations, respectively.

Chapter 5

Results

In this section we present the result of four case studies. In Case Study 1, we investigate O_3 at Airport. In Case Study 2, we investigate $PM_{2.5}$ at Airport. In Case Study 3, we investigate O_3 at Maisonneuve. In Case Study 4, we investigate $PM_{2.5}$ at Maisonneuve.

For each case study we consider different model configuration for summer-day, summer-night, winter-day and winter-night. The model outputs for Case Study 1 are presented in Appendix I. Error diagnostics for Case Study 1 are presented in Appendix J.

5.1 Case Study 1: O_3 Forecast at Airport Station

5.1.1 Summer

Different models to forecast 1-hour ahead O_3 concentrations at Airport station during the summer season were developed. We considered two distinct periods, namely day and night-time. The developed models were based on MLR, PCR, MARS 1, MARS 2, ANN, PC-ANN and PC*-ANN methods.

The observed means of the O_3 responses were 78.9 and 37.0 $\mu g/m^3$ during the day and night-time respectively. The 75% percentile of O_3 concentrations were 96 and 55 $\mu g/m^3$ for the day and night-time period, in that order. The overall performance metrics and the success forecasting rates at the 75% percentile concentrations obtained with the learning dataset are shown in Table 5.1 (PCR and MARS 1), Table 5.2 (MLR, MARS 2 and ANN) and Table 5.3 (PC-ANN and PC*-ANN).

Model suitability was assessed considering the overall performance metrics and the success forecasting rates at the 75% percentile concentrations obtained in the validation phase. These results are shown in Table 5.4 (PCR and MARS 1), Table 5.5 (MLR, MARS 2 and ANN) and Table 5.6 (PC-ANN and PC*-ANN).

Closely studying day-time results, the following inferences have been made:

1. R^2 ranged (0.48 – 0.68) with a corresponding *r* in the (0.69 – 0.82) range. In terms of these two metrics, PC-ANN performed the best, closely followed by MARS 1.
2. MAPE ranged (14% – 15%). All models yielded values in the same order of magnitude.
3. MBE ranged (-3.0 – -0.8), MAE ranged (13.0 – 15.5) and RMSE ranged (16.6 – 21.5). In terms of these three metrics, MARS 1 performed the best, closely followed by PC-ANN and MARS 2.
4. TPR ranged (0.59 – 0.73), FPR ranged (0.07 – 0.12) and SI ranged (0.51 – 0.65). In terms of these three metrics, MARS 1 performed the best, closely followed by MARS 2 and PC-ANN.

Similarly, the following inferences have been made with respect to night-time results:

1. R^2 ranged (0.51 – 0.69) with a corresponding *r* in the (0.71 – 0.83) range. In terms of these two metrics, ANN performed the best, closely followed by MARS 2 and PC-ANN.
2. MAPE ranged (20% – 31%). In terms of this metric, MARS 2 performed the best closely followed by PC-ANN.
3. MBE ranged (-0.9 – 0.3), MAE ranged (11.5 – 14.1) and RMSE ranged (15.2 – 18.9). In terms of these three metrics, ANN performed the best, closely followed by MARS 2.
4. TPR ranged (0.46 – 0.67), FPR ranged (0.07 – 0.12) and SI ranged (0.39 – 0.59). In terms of these three metrics, PC-ANN performed the best, closely followed by MARS 2.

O3 Airport (Training) Summer	Day PCR	Day MARS 1	Night PCR	Night MARS 1
Overall Performance Metrics				
Coefficient of Determination (R^2)	0.68	0.74	0.55	0.64
Correlation Coefficient (r)	0.82	0.86	0.74	0.80
Mean Absolute Percent Error (MAPE)	15%	14%	28%	25%
Mean Bias Error (MBE)	0.0	0.0	0.0	0.0
Mean Absolute error (MAE)	13.9	12.3	13.5	12.0
Root Mean Squared Error (RMSE)	17.3	15.5	17.0	15.3
Exceedance of 75% Precentile				
True Positive Rate (TPR)	0.62	0.71	0.47	0.55
False Positive Rate (FPR)	0.06	0.09	0.08	0.07
Success Index (SI)	0.55	0.62	0.39	0.48

Table 5.1 Forecasting summer O_3 at Airport with PCR and MARS 1 (Training)

O3 Airport (Training) Summer	Day MLR	Day MARS 2	Day ANN	Night MLR	Night MARS 2	Night ANN
Overall Performance Metrics						
Coefficient of Determination (R^2)	0.68	0.73	0.80	0.55	0.66	0.73
Correlation Coefficient (r)	0.82	0.85	0.89	0.74	0.82	0.85
Mean Absolute Percent Error (MAPE)	15%	14%	12%	29%	25%	20%
Mean Bias Error (MBE)	0.0	0.0	0.0	0.0	0.0	0.0
Mean Absolute error (MAE)	14.0	12.3	9.8	13.4	11.4	10.5
Root Mean Squared Error (RMSE)	17.3	15.7	13.0	17.0	14.7	13.3
Exceedance of 75% Precentile						
True Positive Rate (TPR)	0.63	0.74	0.75	0.49	0.57	0.64
False Positive Rate (FPR)	0.07	0.08	0.06	0.07	0.07	0.07
Success Index (SI)	0.57	0.66	0.69	0.42	0.50	0.57

Table 5.2 Forecasting summer O_3 at Airport with MLR, MARS 2 and ANN (Training)

O3 Airport (Training) Summer	Day PC - ANN	Day PC*-ANN	Night PC - ANN	Night PC*-ANN
Overall Performance Metrics				
Coefficient of Determination (R^2)	0.86	0.64	0.70	0.48
Correlation Coefficient (r)	0.93	0.80	0.83	0.69
Mean Absolute Percent Error (MAPE)	11%	15%	22%	31%
Mean Bias Error (MBE)	0.0	0.0	0.0	0.0
Mean Absolute error (MAE)	9.1	14.2	10.8	14.1
Root Mean Squared Error (RMSE)	11.2	18.3	14.0	18.3
Exceedance of 75% Precentile				
True Positive Rate (TPR)	0.77	0.62	0.59	0.37
False Positive Rate (FPR)	0.07	0.09	0.07	0.08
Success Index (SI)	0.71	0.53	0.52	0.29

Table 5.3 Forecasting summer O_3 at Airport with PC-ANN and PC*-ANN (Training)

O3 Airport (Validation) Summer	Day PCR	Day MARS 1	Night PCR	Night MARS 1
Overall Performance Metrics				
Coefficient of Determination (R^2)	0.48	0.68	0.60	0.65
Correlation Coefficient (r)	0.69	0.82	0.78	0.81
Mean Absolute Percent Error (MAPE)	14%	14%	25%	22%
Mean Bias Error (MBE)	-3.0	-1.3	-0.6	0.3
Mean Absolute error (MAE)	15.5	13.0	13.2	12.3
Root Mean Squared Error (RMSE)	21.5	16.6	17.0	16.0
Exceedance of 75% Precentile				
True Positive Rate (TPR)	0.62	0.72	0.54	0.59
False Positive Rate (FPR)	0.08	0.07	0.08	0.07
Success Index (SI)	0.54	0.65	0.46	0.52

Table 5.4 Forecasting summer O_3 at Airport with PCR and MARS 1 (Validation)

O3 Airport (Validation) Summer	Day MLR	Day MARS 2	Day ANN	Night MLR	Night MARS 2	Night ANN
Overall Performance Metrics						
Coefficient of Determination (R^2)	0.48	0.66	0.58	0.60	0.68	0.69
Correlation Coefficient (r)	0.69	0.81	0.76	0.77	0.83	0.83
Mean Absolute Percent Error (MAPE)	14%	14%	15%	25%	20%	21%
Mean Bias Error (MBE)	-2.5	-1.3	-1.7	-0.6	-0.2	-0.1
Mean Absolute error (MAE)	15.4	13.2	13.1	13.2	11.5	11.8
Root Mean Squared Error (RMSE)	21.5	17.2	18.9	17.2	15.2	15.2
Exceedance of 75% Precentile						
True Positive Rate (TPR)	0.59	0.73	0.65	0.53	0.63	0.65
False Positive Rate (FPR)	0.08	0.10	0.09	0.08	0.08	0.12
Success Index (SI)	0.51	0.63	0.54	0.45	0.55	0.53

Table 5.5 Forecasting summer O_3 at Airport with MLR, MARS 2 and ANN (Validation)

O3 Airport (Validation) Summer	Day PC - ANN	Day PC*-ANN	Night PC - ANN	Night PC*-ANN
Overall Performance Metrics				
Coefficient of Determination (R^2)	0.68	0.56	0.68	0.51
Correlation Coefficient (r)	0.83	0.75	0.83	0.71
Mean Absolute Percent Error (MAPE)	15%	15%	21%	31%
Mean Bias Error (MBE)	-0.8	-1.8	-0.9	0.0
Mean Absolute error (MAE)	13.3	15.0	11.8	14.1
Root Mean Squared Error (RMSE)	16.9	19.5	15.3	18.9
Exceedance of 75% Precentile				
True Positive Rate (TPR)	0.72	0.66	0.67	0.46
False Positive Rate (FPR)	0.09	0.12	0.08	0.07
Success Index (SI)	0.63	0.54	0.59	0.39

Table 5.6 Forecasting summer O_3 at Airport with PC-ANN and PC*-ANN (Validation)

These results indicate that i) the performance of PCR is not significantly better than the performance of MLR, ii) MARS 2 marginally outperforms MARS 1, iii) PC-ANN marginally outperforms ANN, iv) while successfully achieving reduction in the dimensionality of the input vector, PC*-ANN is outperformed by ANN. Therefore, we have opted to focus our attention on MLR, MARS 2 and ANN models for subsequent analysis related to ozone.

5.1.2 Winter

MLR, MARS 2 and ANN models were developed to forecast 1-hour ahead O_3 concentrations at Airport station during the winter season. We considered two distinct periods, namely day and night-time.

The observed means of the O_3 responses were 36.9 and 29.5 $\mu g/m^3$ during the day and night-time respectively. The 75% percentile of O_3 concentrations were 55 and 44 $\mu g/m^3$ for the day and night-time period, in that order. The overall performance metrics and the success forecasting rates at the 75% percentile concentrations obtained with the learning dataset are shown in Table 5.7.

Model suitability was assessed considering the overall performance metrics and the success forecasting rates at the 75% percentile concentrations obtained in the validation phase. These results are shown in Table 5.8.

Closely studying day-time results, the following inferences have been made:

1. R^2 ranged (0.70 – 0.78) with a corresponding *r* in the (0.84 – 0.88) range. In terms of these two metrics, MARS 2 performed the best.
2. MAPE ranged (11% – 16%). In terms of this metric, MARS 2 performed the best.
3. MBE ranged (-3.0 – -0.5), MAE ranged (7.1 – 8.3) and RMSE ranged (9.1 – 10.7). In terms of these three metrics, MARS 2 performed the best.
4. TPR ranged (0.43 – 0.66), FPR ranged (0.05 – 0.07) and SI ranged (0.39 – 0.59). In terms of these three metrics, ANN performed the best.

Similarly, the following inferences have been made with respect to night-time results:

1. R^2 ranged (0.73 – 0.77) with a corresponding *r* in the (0.85 – 0.88) range. In terms of these two metrics, ANN model performed the best.
2. MAPE ranged (14% – 17%). In terms of this metric, MARS 2 performed the best.
3. MBE ranged (-0.5 – 0.6), MAE ranged (7.0 – 7.9) and RMSE ranged (9.1 – 10.1). In terms of these three metrics, ANN performed the best.
4. TPR ranged (0.65 – 0.75), FPR ranged (0.08 – 0.09) and SI ranged (0.57 – 0.65). In terms of these three metrics, ANN performed the best.

O3 Airport (Training) Winter	Day MLR	Day MARS 2	Day ANN	Night MLR	Night MARS 2	Night ANN
Overall Performance Metrics						
Coefficient of Determination (R^2)	0.73	0.81	0.82	0.74	0.80	0.82
Correlation Coefficient (r)	0.85	0.90	0.91	0.86	0.89	0.90
Mean Absolute Percent Error (MAPE)	13%	9%	9%	15%	12%	12%
Mean Bias Error (MBE)	0.0	0.0	0.0	0.0	0.0	0.0
Mean Absolute error (MAE)	7.9	6.7	6.6	7.7	6.6	6.3
Root Mean Squared Error (RMSE)	10.4	8.7	8.4	9.6	8.5	8.0
Exceedance of 75% Precentile						
True Positive Rate (TPR)	0.54	0.74	0.78	0.62	0.72	0.76
False Positive Rate (FPR)	0.04	0.06	0.07	0.04	0.04	0.07
Success Index (SI)	0.49	0.68	0.71	0.58	0.68	0.69

Table 5.7 Forecasting winter O_3 at Airport with MLR, MARS 2 and ANN (Training)

O3 Airport (Validation) Winter	Day MLR	Day MARS 2	Day ANN	Night MLR	Night MARS 2	Night ANN
Overall Performance Metrics						
Coefficient of Determination (R^2)	0.70	0.78	0.77	0.73	0.76	0.77
Correlation Coefficient (r)	0.84	0.88	0.88	0.85	0.87	0.88
Mean Absolute Percent Error (MAPE)	16%	11%	11%	17%	14%	15%
Mean Bias Error (MBE)	0.5	-0.3	-0.3	-0.6	-0.5	-0.6
Mean Absolute error (MAE)	8.3	7.1	7.2	7.9	7.3	7.0
Root Mean Squared Error (RMSE)	10.7	9.1	9.3	10.1	9.4	9.1
Exceedance of 75% Precentile						
True Positive Rate (TPR)	0.43	0.63	0.66	0.65	0.69	0.75
False Positive Rate (FPR)	0.05	0.06	0.07	0.08	0.09	0.09
Success Index (SI)	0.39	0.56	0.59	0.57	0.60	0.65

Table 5.8 Forecasting winter O_3 at Airport with MLR, MARS 2 and ANN (Validation)

5.2 Case Study 2: $PM_{2.5}$ Forecast at Airport Station

5.2.1 Summer

Different models to forecast 1-hour ahead $PM_{2.5}$ concentrations at Airport station during the summer season were developed. We considered two distinct periods, namely day and night-time. The developed models were based on MLR, PCR, MARS 1, MARS 2, ANN, PC-ANN and PC*-ANN methods.

The observed means of the $PM_{2.5}$ responses were 10.7 and 8.2 $\mu g/m^3$ during the day and night-time respectively. The 75% percentile of $PM_{2.5}$ concentrations were 11 and 12 $\mu g/m^3$ for the day and night-time period, in that order. The overall performance metrics and the success forecasting rates at the 75% percentile concentrations obtained with the learning dataset are shown in Table 5.9 (PCR and MARS 1), Table 5.10 (MLR, MARS 2 and ANN) and Table 5.11 (PC-ANN and PC*-ANN).

Model suitability was assessed considering the overall performance metrics and the success forecasting rates at the 75% percentile concentrations obtained in the validation phase. These results are shown in Table 5.12 (PCR and MARS 1), Table 5.13 (MLR, MARS 2 and ANN) and Table 5.14 (PC-ANN and PC*-ANN).

Closely studying day-time results, the following inferences have been made:

1. R^2 ranged (0.48 – 0.74) with a corresponding *r* in the (0.69 – 0.86) range. In terms of these two metrics, PC-ANN performed the best.

2. MAPE ranged (44% – 67%). In terms of this metrics, MARS 2 performed the best.
3. MBE ranged (-3.0 – 0.5), MAE ranged (3.1 – 4.0) and RMSE ranged (4.9 – 6.7). In terms of these three metrics, PC-ANN performed the best, closely followed by MARS 2.
4. TPR ranged (0.77 – 0.88), FPR ranged (0.06 – 0.13) and SI ranged (0.70 – 0.75). In terms of these three metrics, MARS 2 performed the best, closely followed by ANN.

Similarly, the following inferences have been made with respect to night-time results:

1. R^2 ranged (0.47 – 0.57) with a corresponding *r* in the (0.68 – 0.75) range. In terms of these two metrics, ANN model performed the best, closely followed by MARS 2.
2. MAPE ranged (47% – 56%). In terms of this metric, ANN performed the best.
3. MBE ranged (-0.2 – 0.1), MAE ranged (3.7 – 4.0) and RMSE ranged (5.6 – 6.5). In terms of these three metrics, ANN performed the best, closely followed by MARS 1.
4. TPR ranged (0.73 – 0.86), FPR ranged (0.08 – 0.16) and SI ranged (0.64 – 0.70). In terms of these three metrics, ANN performed the best, closely followed by MARS 2.

These results indicate that i) the performance of PCR is not significantly better than the performance of MLR, ii) MARS 2 marginally outperforms MARS 1, iii) PC-ANN marginally outperforms ANN, iv) while successfully achieving reduction in the dimensionality of the input vector, PC*-ANN is outperformed by ANN. Therefore, we have opted to focus our attention on MLR, MARS 2 and ANN models for subsequent analysis related to particulate matter.

PM2.5 Airport (Training) Summer	Day PCR	Day MARS 1	Night PCR	Night MARS 1
Overall Performance Metrics				
Coefficient of Determination (R^2)	0.66	0.77	0.51	0.57
Correlation Coefficient (r)	0.81	0.88	0.71	0.75
Mean Absolute Percent Error (MAPE)	60%	39%	60%	51%
Mean Bias Error (MBE)	0.0	0.0	0.0	0.0
Mean Absolute error (MAE)	3.7	2.8	4.3	3.8
Root Mean Squared Error (RMSE)	5.0	4.1	6.1	5.8
Exceedance of 75% Precentile				
True Positive Rate (TPR)	0.90	0.91	0.85	0.76
False Positive Rate (FPR)	0.14	0.08	0.18	0.14
Success Index (SI)	0.77	0.83	0.67	0.62

Table 5.9 Forecasting summer $PM_{2.5}$ at Airport with PCR and MARS 1 (Training)

PM2.5 Airport (Training) Summer	Day MLR	Day MARS 2	Day ANN	Night MLR	Night MARS 2	Night ANN
Overall Performance Metrics						
Coefficient of Determination (R^2)	0.66	0.84	0.84	0.51	0.60	0.56
Correlation Coefficient (r)	0.81	0.92	0.91	0.71	0.78	0.75
Mean Absolute Percent Error (MAPE)	59%	35%	36%	59%	50%	48%
Mean Bias Error (MBE)	0.0	0.0	0.0	0.0	0.0	0.0
Mean Absolute error (MAE)	3.7	2.4	2.5	4.2	3.8	3.9
Root Mean Squared Error (RMSE)	5.0	3.4	3.5	6.1	5.5	5.8
Exceedance of 75% Precentile						
True Positive Rate (TPR)	0.90	0.90	0.90	0.83	0.73	0.73
False Positive Rate (FPR)	0.14	0.05	0.06	0.15	0.09	0.12
Success Index (SI)	0.77	0.84	0.84	0.69	0.64	0.61

Table 5.10 Forecasting summer $PM_{2.5}$ at Airport with MLR, MARS 2 and ANN (Training)

PM2.5 Airport (Training) Summer	Day PC - ANN	Day PC*-ANN	Night PC - ANN	Night PC*-ANN
Overall Performance Metrics				
Coefficient of Determination (R^2)	0.88	0.73	0.60	0.50
Correlation Coefficient (r)	0.94	0.85	0.77	0.70
Mean Absolute Percent Error (MAPE)	33%	43%	45%	49%
Mean Bias Error (MBE)	0.0	0.0	-0.2	0.0
Mean Absolute error (MAE)	2.2	3.0	3.6	4.1
Root Mean Squared Error (RMSE)	3.0	4.4	5.6	6.2
Exceedance of 75% Precentile				
True Positive Rate (TPR)	0.91	0.87	0.75	0.72
False Positive Rate (FPR)	0.05	0.06	0.12	0.16
Success Index (SI)	0.86	0.80	0.63	0.56

Table 5.11 Forecasting summer $PM_{2.5}$ at Airport with PC-ANN and PC*-ANN (Training)

PM2.5 Airport (Validation) Summer	Day		Night	
	PCR	MARS 1	PCR	MARS 1
Overall Performance Metrics				
Coefficient of Determination (R^2)	0.48	0.48	0.54	0.55
Correlation Coefficient (r)	0.69	0.69	0.74	0.74
Mean Absolute Percent Error (MAPE)	67%	46%	56%	52%
Mean Bias Error (MBE)	0.3	0.5	0.1	-0.1
Mean Absolute error (MAE)	4.0	3.4	4.0	3.9
Root Mean Squared Error (RMSE)	6.7	6.7	5.7	5.7
Exceedance of 75% Precentile				
True Positive Rate (TPR)	0.88	0.80	0.86	0.77
False Positive Rate (FPR)	0.13	0.08	0.16	0.14
Success Index (SI)	0.75	0.72	0.70	0.63

Table 5.12 Forecasting summer $PM_{2.5}$ at Airport with PCR and MARS 1 (Validation)

PM2.5 Airport (Validation) Summer	Day			Night		
	MLR	MARS 2	ANN	MLR	MARS 2	ANN
Overall Performance Metrics						
Coefficient of Determination (R^2)	0.48	0.63	0.55	0.54	0.54	0.57
Correlation Coefficient (r)	0.69	0.79	0.74	0.74	0.74	0.75
Mean Absolute Percent Error (MAPE)	67%	44%	45%	56%	51%	47%
Mean Bias Error (MBE)	0.3	0.3	-0.2	0.1	0.0	0.0
Mean Absolute error (MAE)	4.0	3.2	3.3	3.9	3.9	3.7
Root Mean Squared Error (RMSE)	6.7	5.7	6.6	5.7	5.8	5.6
Exceedance of 75% Precentile						
True Positive Rate (TPR)	0.88	0.83	0.81	0.82	0.75	0.73
False Positive Rate (FPR)	0.13	0.08	0.06	0.13	0.10	0.08
Success Index (SI)	0.75	0.75	0.75	0.69	0.64	0.65

Table 5.13 Forecasting summer $PM_{2.5}$ at Airport with MLR, MARS 2 and ANN (Validation)

PM2.5 Airport (Validation) Summer	Day		Night	
	PC - ANN	PC*-ANN	PC - ANN	PC*-ANN
Overall Performance Metrics				
Coefficient of Determination (R^2)	0.74	0.48	0.47	0.51
Correlation Coefficient (r)	0.86	0.69	0.69	0.71
Mean Absolute Percent Error (MAPE)	47%	51%	50%	50%
Mean Bias Error (MBE)	-0.3	0.0	-0.2	-0.1
Mean Absolute error (MAE)	3.1	3.7	4.0	4.0
Root Mean Squared Error (RMSE)	4.9	6.7	6.5	6.0
Exceedance of 75% Precentile				
True Positive Rate (TPR)	0.83	0.77	0.76	0.74
False Positive Rate (FPR)	0.08	0.07	0.09	0.15
Success Index (SI)	0.75	0.70	0.67	0.59

Table 5.14 Forecasting summer $PM_{2.5}$ at Airport with PC-ANN and PC*-ANN (Validation)

5.2.2 Winter

MLR, MARS 2 and ANN models were developed to forecast 1-hour ahead $PM_{2.5}$ concentrations at Airport station during the winter season. We considered two distinct scenarios, namely day and night-time.

The observed means of the $PM_{2.5}$ responses were 8.3 and 5.5 $\mu g/m^3$ during the day and night-time respectively. The 75% percentile of $PM_{2.5}$ concentrations were 8.0 and 10.0 $\mu g/m^3$ for the day and night-time period, in that order. The overall performance metrics and the success forecasting rates at the 75% percentile concentrations obtained with the learning dataset are shown in Table 5.15.

Model suitability was assessed considering the overall performance metrics and the success forecasting rates at the 75% percentile concentrations obtained in the validation phase. These results are shown in Table 5.16.

Closely studying day-time results, the following inferences have been made:

1. R^2 ranged (0.64 – 0.71) with a corresponding *r* in the (0.80 – 0.84) range. In terms of these two metrics, ANN performed the best.
2. MAPE ranged (44% – 50%). In terms of this metric, MARS 2 performed the best.
3. All models averaged 0.1 for MBE, MAE ranged (2.8 – 3.1) and RMSE ranged (3.9 – 4.4). In terms of these three metrics, ANN performed the best.
4. TPR ranged (0.67 – 0.75), FPR ranged (0.10 – 0.14) and SI ranged (0.54 – 0.65). In terms of these three metrics, ANN performed the best.

Similarly, the following inferences have been made with respect to night-time results:

1. R^2 ranged (0.66 – 0.68) with a corresponding *r* in the (0.81 – 0.83) range. In terms of these two metrics, MARS 2 model performed the best.
2. MAPE ranged (46% – 50%). In terms of this metric, MARS 2 performed the best.
3. MBE ranged (0.0 – 0.2), MAE ranged (3.0 – 3.3) and RMSE ranged (4.3 – 4.5). In terms of these three metrics, MARS 2 performed the best.
4. TPR ranged (0.75 – 0.78), FPR ranged (0.10 – 0.11) and SI ranged (0.65 – 0.68). In terms of these three metrics, MARS 2 performed the best.

PM2.5 Airport (Training) Winter	Day MLR	Day MARS 2	Day ANN	Night MLR	Night MARS 2	Night ANN
Overall Performance Metrics						
Coefficient of Determination (R^2)	0.68	0.74	0.76	0.62	0.70	0.64
Correlation Coefficient (r)	0.82	0.86	0.87	0.79	0.84	0.80
Mean Absolute Percent Error (MAPE)	45%	38%	41%	53%	46%	47%
Mean Bias Error (MBE)	0.0	0.0	0.0	0.0	0.0	0.0
Mean Absolute error (MAE)	2.9	2.6	2.5	3.1	2.8	3.0
Root Mean Squared Error (RMSE)	4.3	3.9	3.8	4.3	3.8	4.2
Exceedance of 75% Precentile						
True Positive Rate (TPR)	0.74	0.69	0.75	0.75	0.77	0.71
False Positive Rate (FPR)	0.13	0.09	0.10	0.11	0.10	0.10
Success Index (SI)	0.60	0.60	0.65	0.64	0.67	0.62

Table 5.15 Forecasting winter $PM_{2.5}$ at Airport with MLR, MARS 2 and ANN (Training)

PM2.5 Airport (Validation) Winter	Day MLR	Day MARS 2	Day ANN	Night MLR	Night MARS 2	Night ANN
Overall Performance Metrics						
Coefficient of Determination (R^2)	0.64	0.70	0.71	0.66	0.68	0.67
Correlation Coefficient (r)	0.80	0.83	0.84	0.81	0.83	0.82
Mean Absolute Percent Error (MAPE)	50%	44%	45%	53%	46%	47%
Mean Bias Error (MBE)	0.1	0.1	0.1	0.1	0.2	0.0
Mean Absolute error (MAE)	3.1	2.9	2.8	3.3	3.0	3.1
Root Mean Squared Error (RMSE)	4.4	4.0	3.9	4.5	4.3	4.4
Exceedance of 75% Precentile						
True Positive Rate (TPR)	0.69	0.67	0.75	0.77	0.78	0.75
False Positive Rate (FPR)	0.14	0.13	0.10	0.11	0.10	0.10
Success Index (SI)	0.55	0.54	0.65	0.66	0.68	0.65

Table 5.16 Forecasting winter $PM_{2.5}$ at Airport with MLR, MARS 2 and ANN (Validation)

5.3 Case Study 3: O_3 Forecast at Maisonneuve Station

5.3.1 Summer

Different models to forecast 1-hour ahead O_3 concentrations at Maisonneuve station during the summer season were developed. We considered two distinct scenarios, namely day and night-time. The developed models were based on MLR, MARS 2 and ANN.

The observed means of the O_3 responses were 49.5 and 31.1 $\mu g/m^3$ during the day and night-time respectively. The 75% percentile of O_3 concentrations were 65 and 44 $\mu g/m^3$ for the day and night-time period, in that order. The overall performance metrics and the success forecasting rates at the 75% percentile concentrations obtained with the learning dataset are shown in Table 5.17.

Model suitability was assessed considering the overall performance metrics and the success forecasting rates at the 75% percentile concentrations obtained in the validation phase. These results are shown in Table 5.18.

Closely studying day-time results, the following inferences have been made:

1. R^2 ranged (0.61 – 0.70) with a corresponding *r* in the (0.78 – 0.84) range. In terms of these two metrics, MARS 2 performed the best.
2. MAPE ranged (24% – 30%). In terms of these two metrics, MARS 2 performed the best.
3. MBE ranged (0.3 – 0.7), MAE ranged (10.0 – 11.6) and RMSE ranged (12.9 – 14.8). In terms of these three metrics, MARS 2 performed the best.

4. TPR ranged (0.50 – 0.62), FPR ranged (0.07 – 0.10) and SI ranged (0.41 – 0.56). In terms of these three metrics, MARS 2 performed the best.

Similarly, the following inferences have been made with respect to night-time results:

1. R^2 ranged (0.48 – 0.65) with a corresponding *r* in the (0.70 – 0.80) range. In terms of these two metrics, ANN performed the best.
2. MAPE ranged (36% – 42%). In terms of this metric, ANN performed the best.
3. MBE ranged (-0.6 – -0.3), MAE ranged (9.8 – 11.8) and RMSE ranged (12.5 – 15.1). In terms of these three metrics, MARS 2 performed the best.
4. TPR ranged (0.47 – 0.57), FPR ranged (0.05 – 0.07) and SI ranged (0.41 – 0.50). In terms of these three metrics, MARS 2 performed the best.

O3 Maisonneuve (Training) Summer	Day MLR	Day MARS 2	Day ANN	Night MLR	Night MARS 2	Night ANN
Overall Performance Metrics						
Coefficient of Determination (R^2)	0.61	0.73	0.64	0.44	0.62	0.68
Correlation Coefficient (r)	0.78	0.85	0.80	0.66	0.79	0.83
Mean Absolute Percent Error (MAPE)	30%	24%	28%	39%	32%	30%
Mean Bias Error (MBE)	0.0	0.0	0.0	0.0	0.0	0.0
Mean Absolute error (MAE)	11.6	9.9	11.1	11.7	9.5	8.7
Root Mean Squared Error (RMSE)	15.2	12.7	14.6	15.0	12.3	11.2
Exceedance of 75% Precentile						
True Positive Rate (TPR)	0.55	0.64	0.63	0.43	0.57	0.58
False Positive Rate (FPR)	0.08	0.08	0.11	0.09	0.07	0.05
Success Index (SI)	0.47	0.56	0.52	0.35	0.50	0.53

Table 5.17 Forecasting summer O_3 at Maisonneuve with MLR, MARS 2 and ANN (Training)

O3 Maisonneuve (Validation) Summer	Day MLR	Day MARS 2	Day ANN	Night MLR	Night MARS 2	Night ANN
Overall Performance Metrics						
Coefficient of Determination (R^2)	0.61	0.70	0.65	0.48	0.65	0.63
Correlation Coefficient (r)	0.78	0.84	0.81	70%	80%	80%
Mean Absolute Percent Error (MAPE)	29%	24%	26%	0.4	0.4	0.4
Mean Bias Error (MBE)	0.3	0.4	0.7	-0.3	-0.3	-0.6
Mean Absolute error (MAE)	11.6	10.0	11.0	11.8	9.8	10.2
Root Mean Squared Error (RMSE)	14.8	12.9	14.0	15.1	12.5	13.0
Exceedance of 75% Precentile						
True Positive Rate (TPR)	0.50	0.62	0.62	0.47	0.57	0.53
False Positive Rate (FPR)	0.09	0.07	0.10	0.07	0.07	0.05
Success Index (SI)	0.41	0.56	0.53	0.41	0.50	0.48

Table 5.18 Forecasting summer O_3 at Maisonneuve with MLR, MARS 2 and ANN (Validation)

5.3.2 Winter

MLR, MARS 2 and ANN models were developed to forecast 1-hour ahead O_3 concentrations at Maisonneuve station during the winter season. We considered two distinct scenarios, namely day and night-time.

The observed means of the O_3 responses were 17.4 and 21.1 $\mu g/m^3$ during the day and night-time respectively. The 75% percentile of O_3 concentrations were 27.0 and 31.0 $\mu g/m^3$ for the day and night-time period, in that order. The overall performance metrics and the success forecasting rates at the 75% percentile concentrations obtained with the learning dataset are shown in Table 5.19.

Model suitability was assessed considering the overall performance metrics and the success forecasting rates at the 75% percentile concentrations obtained in the validation phase. These results are shown in Table 5.20.

Closely studying day-time results, the following inferences have been made:

1. R2 ranged (0.58 – 0.68) with a corresponding r in the (0.76 – 0.82) range. In terms of these two metrics, ANN performed the best.
2. MAPE ranged (25% – 29%). In terms of this metric, MARS 2 performed the best.
3. MBE ranged (-0.1 – 0.3), MAE ranged (4.7 – 5.6) and RMSE ranged (6.4 – 6.5). In terms of these three metrics, MARS 2 performed the best.
4. TPR ranged (0.53 – 0.67), FPR ranged (0.05 – 0.06) and SI ranged (0.47 – 0.61). In terms of these three metrics, MARS 2 performed the best.

Similarly, the following inferences have been made with respect to night-time results:

1. R^2 ranged (0.63 – 0.71) with a corresponding *r* in the (0.80 – 0.84) range. In terms of these two metrics, MARS 2 model performed the best.
2. MAPE ranged (25% – 28%). In terms of this metric, MARS 2 performed the best.
3. MBE ranged (-0.9 – 0.8), MAE ranged (5.4 – 6.1) and RMSE ranged (7.1 – 7.9). In terms of these three metrics, MARS 2 performed the best.
4. TPR ranged (0.61 – 0.67), FPR ranged (0.05 – 0.09) and SI ranged (0.55 – 0.60). In terms of these three metrics, MARS 2 performed the best.

O3 Maisonneuve (Training) Winter	Day MLR	Day MARS 2	Day ANN	Night MLR	Night MARS 2	Night ANN
Overall Performance Metrics						
Coefficient of Determination (R^2)	0.67	0.80	0.83	0.65	0.72	0.75
Correlation Coefficient (r)	0.82	0.89	0.91	0.81	0.85	0.87
Mean Absolute Percent Error (MAPE)	26%	23%	22%	27%	26%	25%
Mean Bias Error (MBE)	0.0	0.0	0.0	0.0	0.0	0.0
Mean Absolute error (MAE)	5.2	4.2	3.9	5.9	5.3	4.9
Root Mean Squared Error (RMSE)	6.8	5.3	4.9	7.4	6.7	6.3
Exceedance of 75% Precentile						
True Positive Rate (TPR)	0.68	0.77	0.78	0.58	0.68	0.69
False Positive Rate (FPR)	0.04	0.04	0.04	0.05	0.05	0.07
Success Index (SI)	0.65	0.73	0.75	0.53	0.63	0.62

Table 5.19 Forecasting winter O_3 at Maisonneuve with MLR, MARS 2 and ANN (Training)

O3 Maisonneuve (Validation) Winter	Day MLR	Day MARS 2	Day ANN	Night MLR	Night MARS 2	Night ANN
Overall Performance Metrics						
Coefficient of Determination (R^2)	0.58	0.67	0.68	0.63	0.71	0.71
Correlation Coefficient (r)	0.76	0.82	0.82	0.80	0.84	0.84
Mean Absolute Percent Error (MAPE)	29%	25%	27%	28%	25%	26%
Mean Bias Error (MBE)	0.3	0.0	-0.1	-0.9	-0.8	-0.8
Mean Absolute error (MAE)	5.6	4.7	4.9	6.1	5.5	5.4
Root Mean Squared Error (RMSE)	7.3	6.5	6.4	7.9	7.1	7.1
Exceedance of 75% Precentile						
True Positive Rate (TPR)	0.53	0.67	0.64	0.61	0.67	0.66
False Positive Rate (FPR)	0.05	0.06	0.06	0.05	0.07	0.09
Success Index (SI)	0.47	0.61	0.58	0.55	0.60	0.57

Table 5.20 Forecasting winter O_3 at Maisonneuve with MLR, MARS 2 and ANN (Validation)

5.4 Case Study 4: $PM_{2.5}$ Forecast at Maisonneuve

5.4.1 Summer

Different models to forecast 1-hour ahead $PM_{2.5}$ concentrations at Maisonneuve station during the summer season were developed. We considered two distinct scenarios, namely day and night-time. The developed models were based on MLR, MARS 2 and ANN.

The observed means of the $PM_{2.5}$ responses were 8.6 and 9.2 $\mu g/m^3$ during the day and night-time respectively. The 75% percentile of $PM_{2.5}$ concentrations were 13 and 11 $\mu g/m^3$ for the day and night-time period, in that order. The overall performance metrics and the success forecasting rates at the 75% percentile concentrations obtained with the learning dataset are shown in Table 5.21.

Model suitability was assessed considering the overall performance metrics and the success forecasting rates at the 75% percentile concentrations obtained in the validation phase. These results are shown in Table 5.22.

Closely studying day-time results, the following inferences have been made:

1. R^2 ranged (0.44 – 0.47) with a corresponding *r* in the (0.66 – 0.68) range. In terms of these two metrics, MARS 2 performed the best.
2. MAPE ranged (48% – 58%). In terms of this metrics, MARS 2 performed the best.
3. MBE ranged (-0.1 – 0.2), MAE ranged (4.0 – 4.4) and RMSE ranged (6.7 – 6.9). In terms of these three metrics, MARS 2 performed the best.

4. TPR ranged (0.69 – 0.82), FPR ranged (0.11 – 0.15) and SI ranged (0.58 – 0.67). In terms of these three metrics, ANN performed the best.

Similarly, the following inferences have been made with respect to night-time results:

1. R^2 ranged (0.44 – 0.53) with a corresponding *r* in the (0.66– 0.73) range. In terms of these two metrics, MARS 2 model performed the best.
2. MAPE ranged (48% – 57%). In terms of this metric, ANN performed the best.
3. MBE ranged (-0.1 – 0.1), MAE ranged (3.6 – 3.9) and RMSE ranged (5.2 – 5.7). In terms of these three metrics, MARS 2 performed the best.
4. TPR ranged (0.71 – 0.74), FPR ranged (0.11 – 0.16) and SI ranged (0.56 – 0.62). In terms of these three metrics, MARS 2 performed the best.

PM2.5 Maisonneuve (Training)	Day			Night		
Summer	MLR	MARS 2	ANN	MLR	MARS 2	ANN
Overall Performance Metrics						
Coefficient of Determination (R^2)	0.61	0.72	0.67	0.41	0.56	0.51
Correlation Coefficient (r)	0.78	0.85	0.82	0.64	0.75	0.72
Mean Absolute Percent Error (MAPE)	57%	44%	46%	61%	54%	50%
Mean Bias Error (MBE)	0.0	0.0	0.0	0.0	0.0	0.0
Mean Absolute error (MAE)	4.2	3.5	3.7	4.0	3.4	3.7
Root Mean Squared Error (RMSE)	5.8	4.9	5.3	5.9	5.1	5.4
Exceedance of 75% Precentile						
True Positive Rate (TPR)	0.83	0.76	0.74	0.75	0.75	0.72
False Positive Rate (FPR)	0.13	0.07	0.08	0.16	0.11	0.13
Success Index (SI)	0.70	0.68	0.66	0.59	0.64	0.59

Table 5.21 Forecasting summer $PM_{2.5}$ at Maisonneuve with MLR, MARS 2 and ANN (Training)

PM2.5 Maisonneuve (Validation)	Day			Night		
Summer	MLR	MARS 2	ANN	MLR	MARS 2	ANN
Overall Performance Metrics						
Coefficient of Determination (R^2)	0.44	0.47	0.46	0.44	0.53	0.48
Correlation Coefficient (r)	0.66	0.68	0.68	0.66	0.73	0.69
Mean Absolute Percent Error (MAPE)	58%	48%	48%	57%	56%	48%
Mean Bias Error (MBE)	-0.1	0.2	0.0	0.0	-0.1	0.1
Mean Absolute error (MAE)	4.4	4.0	4.0	3.9	3.6	3.8
Root Mean Squared Error (RMSE)	6.9	6.7	6.8	5.7	5.2	5.4
Exceedance of 75% Precentile						
True Positive Rate (TPR)	0.82	0.69	0.78	0.72	0.74	0.71
False Positive Rate (FPR)	0.15	0.11	0.11	0.16	0.11	0.12
Success Index (SI)	0.67	0.58	0.67	0.56	0.62	0.59

Table 5.22 Forecasting summer $PM_{2.5}$ at Maisonneuve with MLR, MARS 2 and ANN (Validation)

5.4.2 Winter

MLR, MARS 2 and ANN models were developed to forecast 1-hour ahead $PM_{2.5}$ concentrations at Maisonneuve station during the winter season. We considered two distinct scenarios, namely day and night-time.

The observed means of the $PM_{2.5}$ responses were 6.9 $\mu g/m^3$ in both day and night-time periods. The 75% percentile of $PM_{2.5}$ concentrations were 10.0 and 9.0 $\mu g/m^3$ for the day and night-time period, respectively. The overall performance metrics and the success forecasting rates at the 75% percentile concentrations obtained with the learning dataset are shown in Table 5.23.

Model suitability was assessed considering the overall performance metrics and the success forecasting rates at the 75% percentile concentrations obtained in the validation phase. These results are shown in Table 5.24.

Closely studying day-time results, the following inferences have been made:

1. R^2 ranged (0.44 – 0.47) with a corresponding *r* in the (0.66 – 0.68) range. In terms of these two metrics, MARS 2 performed the best.
2. MAPE ranged (48% – 58%). In terms of this metric, MARS 2 performed the best.
3. MBE ranged (-0.1 – 0.2), MAE ranged (4.0 – 4.4) and RMSE ranged (6.7 – 6.9). In terms of these three metrics, MARS 2 performed the best.
4. TPR ranged (0.82 – 0.78), FPR ranged (0.11 – 0.15) and SI ranged (0.58 – 0.67). In terms of these three metrics, ANN performed the best.

Similarly, the following inferences have been made with respect to night-time results:

1. R^2 ranged (0.44 – 0.53) with a corresponding *r* in the (0.66 – 0.73) range. In terms of these two metrics, MARS 2 model performed the best.
2. MAPE ranged (48% – 57%). In terms of this metric, MARS 2 performed the best.
3. MBE ranged (-0.1 – 0.1), MAE ranged (3.6 – 3.9) and RMSE ranged (5.2 – 5.7). In terms of these three metrics, MARS 2 performed the best.
4. TPR ranged (0.71 – 0.74), FPR ranged (0.11 – 0.16) and SI ranged (0.56 – 0.62). In terms of these three metrics, MARS 2 performed the best.

PM2.5 Maisonneuve (Training) Winter	Day MLR	Day MARS 2	Day ANN	Night MLR	Night MARS 2	Night ANN
Overall Performance Metrics						
Coefficient of Determination (R^2)	0.52	0.65	0.59	0.42	0.60	0.62
Correlation Coefficient (r)	0.72	0.81	0.77	0.65	0.78	0.79
Mean Absolute Percent Error (MAPE)	57%	46%	47%	58%	50%	46%
Mean Bias Error (MBE)	0.0	0.0	0.0	0.0	0.0	0.0
Mean Absolute error (MAE)	3.7	3.1	3.3	3.0	2.5	2.4
Root Mean Squared Error (RMSE)	4.8	4.1	4.4	4.1	3.4	3.3
Exceedance of 75% Precentile						
True Positive Rate (TPR)	0.69	0.71	0.60	0.50	0.63	0.68
False Positive Rate (FPR)	0.16	0.12	0.12	0.09	0.06	0.05
Success Index (SI)	0.54	0.59	0.48	0.42	0.57	0.62

Table 5.23 Forecasting winter $PM_{2.5}$ at Maisonneuve with MLR, MARS 2 and ANN (Training)

PM2.5 Maisonneuve (Validation) Winter	Day MLR	Day MARS 2	Day ANN	Night MLR	Night MARS 2	Night ANN
Overall Performance Metrics						
Coefficient of Determination (R^2)	0.49	0.51	0.55	0.50	0.57	0.57
Correlation Coefficient (r)	0.70	0.71	0.74	0.71	0.75	0.76
Mean Absolute Percent Error (MAPE)	59%	55%	51%	53%	48%	45%
Mean Bias Error (MBE)	-0.1	-0.3	-0.2	0.2	0.3	0.1
Mean Absolute error (MAE)	3.9	3.7	3.5	3.1	2.8	2.7
Root Mean Squared Error (RMSE)	5.2	5.2	4.9	4.3	3.9	3.9
Exceedance of 75% Precentile						
True Positive Rate (TPR)	0.74	0.75	0.66	0.56	0.60	0.64
False Positive Rate (FPR)	0.18	0.14	0.12	0.09	0.07	0.09
Success Index (SI)	0.56	0.61	0.54	0.48	0.53	0.55

Table 5.24 Forecasting winter $PM_{2.5}$ at Maisonneuve with MLR, MARS 2 and ANN (Validation)

5.5 Case Study 5: Daily O_3 at Maisonneuve and VOC Data

The objective of this case study was to model daily means of ozone at Maisonneuve station. In addition to the set of air quality and meteorological data used in the previous four case studies, the concentration values of 142 different VOC species that were available at six days interval were included. The original dataset with no missing values contained 186 rows of observations. The dataset was split into training and validation datasets containing 102 and 84 observations, respectively.

The observed mean of the O_3 response was 26.9 $\mu g/m^3$. The 75% percentile of O_3 concentrations was 35 $\mu g/m^3$. TVOC concentration measured a carbon-atom basis ranged (30.1 – 294.8 ppbC) with an average of 34.4.6 ppbC. TVOC measured by OH-reactivity weighted method ranged (9.6 – 106.6 propy-equiv ppbC) with an average of 34.4 propy-equiv ppbC.

Tables 5.25 and 5.26 show VOC ranked by concentration in carbon-atom basis (ppbC) and by concentration normalized by OH-reactivity (propy-equiv ppbC) respectively. In these tables, molecular weight (MW) is in g mol^{-1}, K_{OH} (from Atkinson (1990)) is in 10^{12} cm^3 $molecule^{-1}$ s^{-1}.Toluene, isopentane, ethylene and m/p-xylene were found to be, in that order, the most abundant VOC species measured by ppbC. In another hand, m/p-xylene, toluene, propylene and (1,2,4)-trimethylbenzene were found to be the most reactive as measured by propy-equiv ppbC.

VOC species	MW	K_{OH}	ppbc	Propy-Equiv	ppbc rank	Propy-Equiv rank
Toluene	92.1	5.96	11.6	2.63	1	2
Isopentane	72.2	3.94	7.2	1.08	2	10
Ethylene	28.1	8.52	6.3	2.05	3	5
m/p-Xylene	106.2	18.95	5.8	4.16	4	1
Butane	58.1	2.54	5.6	0.54	5	18
Ethane	30.1	0.268	5.2	0.05	6	1
Propane	44.1	1.15	5.0	0.22	7	1
Isobutane	58.1	2.54	4.8	0.47	8	23
Acetylene	26.0	0.9	3.5	0.12	9	1
Benzene	78.1	1.23	3.1	0.15	10	1
Pentane	72.2	3.94	3.0	0.45	11	24
2-Methylpentane	86.2	5.6	2.4	0.52	12	19
Propylene	42.1	26.3	2.2	2.21	13	3
o-Xylene	106.2	13.7	1.9	0.99	14	14
Ethylbenzene	106.2	7.1	1.9	0.50	15	20
1,2,4-Trimethylbenzene	120.2	32.5	1.7	2.15	16	4
3-Methylpentane	86.2	5.7	1.7	0.36	17	25
Hexane	86.2	5.61	1.5	0.33	18	26
1-Butene/Isobutene	56.1	31.4	1.4	1.73	19	7
3-Ethyltoluene	120.2	15	1.0	0.57	20	17

Table 5.25 VOC species at Maisonneuve ranked by ppbC (K_{OH} from Atkinson (1990))

VOC species	MW	K_{OH}	ppbc	Propy-Equiv	ppbc rank	Propy-Equiv rank
m/p-Xylene	106.2	18.95	5.8	4.16	4	1
Toluene	92.1	5.96	11.6	2.63	1	2
Propylene	42.1	26.3	2.2	2.21	13	3
1,2,4-Trimethylbenzene	120.2	32.5	1.7	2.15	16	4
Ethylene	28.1	8.52	6.3	2.05	3	5
Isoprene	68.1	101	0.5	1.82	30	6
1-Butene/Isobutene	56.1	31.4	1.4	1.73	19	7
2-Methyl-2-butene	70.1	61	0.5	1.22	26	8
trans-2-Butene	56.1	64	0.5	1.20	28	9
Isopentane	72.2	3.94	7.2	1.08	2	10
1,3,5-Trimethylbenzene	120.2	57.5	0.5	1.07	29	11
trans-2-Pentene	72.2	67	0.4	1.06	32	12
1,3-Butadiene	54.1	66.6	0.4	1.04	33	13
o-Xylene	106.2	13.7	1.9	0.99	14	14
cis-2-Butene	56.1	56.4	0.4	0.79	38	15
2-Methyl-1-butene	70.1	61	0.3	0.68	40	16
3-Ethyltoluene	120.2	15	1.0	0.57	20	17
Butane	58.1	2.54	5.6	0.54	5	18
2-Methylpentane	86.2	5.6	2.4	0.52	12	19
Ethylbenzene	106.2	7.1	1.9	0.50	15	20

Table 5.26 VOC species at Maisonneuve ranked by propy-equiv ppbC (K_{OH} from Atkinson (1990))

Alkanes were found to be the most abundant hydrocarbon group but also the least reactive. As a group, alkanes represented approximately 47% of TVOC as ppbC and 16% as propy-equiv ppbC. Alkenes were found to be the least abundant group but most reactive. Alkenes represented approximately 15% of TVOC as ppbC and 44% as propy-

equiv ppbC. Aromatic hydrocarbons contributed to 33% of TVOC and 39% of propy-equiv concentrations. Alkynes contributed to less than 4% of TVOC but did not influence total propy-equiv levels.

The potential influence of OH• radical reactivity on ozone production is most evident for the biogenic species isoprene. Isoprene ranked 30th for ppbC and sixth for average propy-equiv ppbC concentration. As evidence by these rankings, isoprene has more impact on ozone production in Montréal than some of the most common anthropogenic VOC such as butane (ranked fifth as ppbC and 18th as propy-equiv), propane (ranked seventh as ppbC and 31st as propy-equiv) or ethane (ranked 6th as ppbC and 47th as propy-equiv). The Isoprene is an important biogenic VOC high reactivity with OH• radical (K_{OH} = 78×10^{12} cm^3 molecule^{-1} s^{-1}) suggest that isoprene may be the most important naturally emitted compound in Montréal.

A MLR model without inclusion of VOC data was first considered to model O_3 levels at Maisonneuve. The resulting model (which included $PM_{2.5}$, NO, Temp, DP, and WS as statistically significant independent variables) yielded a R^2 of 0.75 and RMSE of 6.5 μg/m^3.

Then, VOC data was introduced in MLR by including TVOC concentrations first on a carbon-atom basis (i.e ppbC) and then on weighted OH-reactivity (i.e propy-equiv ppbC). TVOC on a carbon-atom basis was not found to be statistically significant. TVOC measured on weighted OH-reactivity was found to be statistically significant in the regression model with an associated t-ratio of -2.06. The resulting MLR model yielded an improved R^2 of 0.76 and RMSE of 6.4 μg/m^3.

Subsequent analysis involved MARS 2 and ANN models including TVOC measured as propy-equiv ppbC. The overall performance metrics and the success forecasting rates at the 75% percentile concentrations obtained with the learning dataset are shown in Table 5.27. Model suitability was assessed considering the overall performance metrics and the success forecasting rates at the 75% percentile concentrations obtained in the validation phase. These results are shown in Table 5.28.

Closely studying the results obtained using the test dataset (which incorporated OH-reactivity of VOC data), the following inferences have been made:

1. R^2 ranged (0.63 – 0.75) with a corresponding *r* in the (0.79 – 0.87) range. In terms of these two metrics, MARS 2 performed the best.
2. MAPE ranged (29% – 46%). In terms of this metric, MARS 2 performed the best.
3. MBE ranged (-0.8 – 0.2), MAE ranged (5.4 – 7.3) and RMSE ranged (7.5 – 9.1). In terms of these three metrics, MARS 2 performed the best.
4. TPR ranged (0.70 – 0.75), FPR ranged (0.02 – 0.03) and SI ranged (0.67 – 0.73). In terms of these three metrics, MARS 2 performed the best.

O3 Maisonneuve (Training)	Without VOC data			With VOC data (as propy-equiv)		
	MLR	MARS 2	ANN	MLR	MARS 2	ANN
Overall Performance Metrics						
Coefficient of Determination (R^2)	0.75	0.87	0.83	0.76	0.88	0.84
Correlation Coefficient (r)	0.86	0.93	0.91	0.87	0.94	0.92
Mean Absolute Percent Error (MAPE)	26%	20%	22%	25%	18%	21%
Mean Bias Error (MBE)	0.0	0.0	0.0	0.0	0.0	0.0
Mean Absolute error (MAE)	5.0	3.8	4.3	4.8	3.6	4.1
Root Mean Squared Error (RMSE)	6.5	4.7	5.3	6.4	4.5	5.2
Above 75% Quantile						
True Positive Rate (TPR)	0.58	0.62	0.65	0.58	0.73	0.69
False Positive Rate (FPR)	0.09	0.09	0.13	0.11	0.11	0.13
Success Index (SI)	0.48	0.52	0.52	0.47	0.63	0.56

Table 5.27 Predicting O_3 at Maisonneuve with MLR, MARS 2 and ANN including VOC data (Training)

O3 Maisonneuve (Validation)	Without VOC data			With VOC data (as propy-equiv)		
	MLR	MARS 2	ANN	MLR	MARS 2	ANN
Overall Performance Metrics						
Coefficient of Determination (R^2)	0.62	0.70	0.69	0.63	0.75	0.70
Correlation Coefficient (r)	0.79	0.84	0.83	0.79	0.87	0.83
Mean Absolute Percent Error (MAPE)	44%	37%	35%	46%	29%	37%
Mean Bias Error (MBE)	-0.3	-0.7	-0.5	-0.7	0.2	-0.8
Mean Absolute error (MAE)	7.2	6.3	6.3	7.3	5.4	6.5
Root Mean Squared Error (RMSE)	9.2	8.2	8.4	9.1	7.5	8.3
Above 75% Quantile						
True Positive Rate (TPR)	0.70	0.75	0.70	0.75	0.75	0.70
False Positive Rate (FPR)	0.05	0.06	0.03	0.03	0.02	0.03
Success Index (SI)	0.65	0.69	0.67	0.72	0.73	0.67

Table 5.28 Predicting O_3 at Maisonneuve with MLR, MARS 2 and ANN including VOC data (Validation)

Overall, the inclusion of VOC data measured on weighted OH-reactivity yielded improved results during both training and validation phases. There is however an implicit assumption stemming from the fact that i) VOC data was available only as mean daily values and that ii) corresponding daily averages for air pollution and meteorological data was used for modelling O_3 at Maisonneuve station. This assumption is that VOC/NOx and total OH-reactivity at Maisonneuve is constant. Anthropogenic VOC flux at Maisonneuve is expected to be correlated to traffic flow, and biogenic VOC flux is expected to peak with increased temperature and solar radiation. As such, VOC and NOx

fluxes are expected to vary depending on time of day, so are the values of the VOC/NOx ratio and the relative importance of VOC measured as propy-equiv ppbC in ozone formation. Due to data availability, we were not able to characterize diurnal patterns of VOC fluxes at Maisonneuve station.

From the available data, we can infer that the area near Maisonneuve station is characterized by low propy-equiv ppbC levels and low average daily VOC/NOx ratios, which suggests that area is VOC-limited. In this region, hydroxyl radicals (OH•) are scavenged by NO_2. NO_2 scavenging of OH• slows down the oxidation process of hydrocarbons. The alternative pathway for NO-to-NO_2 conversion which yields organic peroxy radical (RO_2) as by-products is limited. As the OH• radical pool is exhausted, ozone formation is dictated primarily by NO_2 photolysis.

The fact that ozone formation process at Maisonneuve is driven by NO_2 photolysis and that levels of reactive VOC are relatively low explains why the inclusion of propy-equiv ppbC values during model training resulted in marginal improvement of the forecasting performance.

5.6 Comparison to Literature Data

The performance of the models developed in this thesis are compared with results from similar studies found in the literature. Table 5.29 and 5.30 summarizes the performance of O_3 and $PM_{2.5}$, respectively, from other studies.

Source	Year	Season	Period	Window	Site	Type	Target	Mean	R2	MAE	RMSE
Agirre-Basurko et al.	2006	All	All	1	Bilbao (Spain)	MLR	O3	43	0.771	-	-
Kovac-Andic et al.	2009	Spring	Day	0	Osijek (Croatia)	MLR	O3	78	0.680	-	-
Kovac-Andic et al.	2009	Summer	Day	0	Osijek (Croatia)	MLR	O3	46	0.780	-	-
Bordignon et al.	2002	All	All	1	Padova (Italy)	MARS 2	O3	110	0.659	15.5	-
Bordignon et al.	2002	All	All	1	Padova (Italy)	ANN	O3	110	0.623	15.99	-
Su	2004	All	All	1	Calgary (Canada)	ANN	O3	63	0.870	4.00	5.00
Su	2004	All	All	1	Edmonton	ANN	O3	72	0.890	4.00	5.00
Patel	2004	Summer	Day	0	Port Arthur (USA)	ANN	O3	80	0.770	-	-
Patel	2004	Summer	Night	0	Port Arthur (USA)	ANN	O3	42	0.750	-	-
Corani	2005	All	All	1	Milan (italy)	ANN	O3	52	0.689	17.02	-
Agirre-Basurko et al.	2006	All	All	1	Bilbao (Spain)	ANN	O3	43	0.835	-	-
Tsai et al.	2009	All	All	0	Chou Ying (Taiwan)	ANN	O3	-	0.846	-	-
Tsai et al.	2009	All	All	0	Chou Ying (Taiwan)	PC-ANN	O3	-	0.879	-	-

Table 5.29 Performance of O_3 forecasting methods from other studies

Source	Year	Season	Period	Window	Site	Type	Target	Mean	R2	MAE	RMSE
Ordieres et al.	2005	All	All	8	El Paso (United States)	MLR	PM2.5	24	0.398	0.02	0.27
Diaz-Robles et al.	2008	Summer	All	8	Temuco (Chile)	MLR	PM10	48.5	0.779	20.83	28.39
Akyuz and Cabuk	2009	Winter	All	0	Zonguldak (Turkey)	MLR	PM10	44.1	0.805	4.07	5.36
Akyuz and Cabuk	2009	Winter	All	0	Zonguldak (Turkey)	MLR	PM2.5	28.1	0.811	3.74	5.00
He	2004	All	All	0	Fort McKay (Canada)	ANN	PM2.5	4	0.430	-	-
Patel	2004	Summer	Day	0	Port Arthur (USA)	ANN	PM2.5	7	0.735	-	-
Patel	2004	Summer	Night	0	Port Arthur (USA)	ANN	PM2.5	15	0.470	-	-
Corani	2005	All	All	1	Milan (italy)	ANN	PM10	52	0.774	8.59	-
Ordieres et al.	2005	All	All	8	El Paso (United States)	ANN	PM2.5	24	0.381	0.00	0.00
Diaz-Robles et al.	2008	Summer	All	8	Temuco (Chile)	ANN	PM10	48.5	0.777	20.65	28.57

Table 5.30 Performance of $PM_{2.5}$ forecasting methods from other studies

The performance of MLR models for O_3 in this study are comparable to the results obtained by Agirre-Basurko et al. (2006) and Kovac-Andric et al. (2009) in terms of R^2. Kovac-Andric et al. (2009) obtained better results in the season of lowest mean O_3, which correlates to our own findings. It should be noted that while Agirre et al.

(2006) forecasted O_3 at 1 to 8-hour window, they incorporated observed NO_2 values corresponding to the forecast window.

Patel (2004) and Tsai et al. (2009) O_3 ANN models outperformed our models in terms of R^2. However, their result refers to performance of ANN models in the training phase which includes meteorological data observed at the same time when ozone was being predicted. Our O_3 ANN models underperformed in terms of R^2 compared to Agirre-Basurko et al. (2006). Agirre-Basurko et al. (2006) included 15 lagged observations of O_3.

The ANN models to forecast O_3 developed in this thesis outperform the similar model developed by Bordignon et al. (2002) in terms of R^2 and RMSE. Our models are comparable to Su (2004) in terms of MAE and RMSE, but inferior in terms of R^2. Su (2004) included additional independent variables, namely "time of day", "mixing height" and "total hydrocarbons".

The MARS 2 model developed by Bordignon et. al (2009) outperformed the ANN model, which supports the findings of this thesis. Moreover, the R^2 in our both studies are comparable. The PC-ANN model proposed by Tsai et al. (2009) outperformed the ANN model developed in the same study, which is aligned with our own findings.

Generally speaking, $PM_{2.5}$ forecasting models achieve lower performance when compared to O_3 models. This is due chaotic nature of $PM_{2.5}$ time series which stems from the random motion of airborne particles found in the nuclei mode in addition to the complex formation mechanisms of and nitrate particulate matter in the size range of 0.1–2.5 μm (the accumulation mode) in the atmosphere. For that reason, caution must be exercised when comparing forecasting performances of $PM_{2.5}$ and PM_{10} models.

Our MLR models outperformed the model developed by Ordieres et al. (2005) to forecast $PM_{2.5}$ with a 8 hour window with MLR which yielded an R^2 of 0.398. Akyuz and Cabuk (2009) achieved high R^2 with relatively low RMSE and MAE for MLR to predict $PM_{2.5}$ and PM_{10}. In that study, polycyclic aromatic hydrocarbons were included as independent variables and forecast window was 0. Diaz-Roblez et al. (2008) PM_{10} MLR model achieved high R^2 for an 8-hour window. Our $PM_{2.5}$ MLR models achieved comparable MAE and RMSE values compared to Diaz-Roblez et al. (2008) mean of response.

Diaz-Roblez et al. (2008) PM_{10} ANN models performed comparably to their own MLR models. Ordieres et al. (2005) $PM_{2.5}$ ANN model underperformed in terms of R^2 compared to their MLR models, but yielded better performance in terms of MAE and RMSE. In this thesis, $PM_{2.5}$ ANN models outperformed MLR models in terms of all performance metrics and success rates. Corani (2005) included SO_2 as input and achieved a relatively high R^2 and low RMSE for PM_{10} ANN model. In addition, Corani (2005) reported SI of 0.68, 0.73 and 0.60 for exceedances above and 40, 50 and 60 $\mu g/m^3$ respectively. Patel (2004) considered different ANN architectures for summer day and night periods and achieved high R^2, but this model includes meteorological data observed at the same time when $PM_{2.5}$ was being predicted. In addition to all precursor species and meteorological inputs included in this thesis; He (2004) included total hydrocarbon, total reduced sulphur and SO_2 but obtained a relatively low R^2 for year round $PM_{2.5}$ ANN model. While the $PM_{2.5}$ ANN developed in the course of our case studies performed comparably regardless of season or period of day (at both Airport and Maisonneuve), our findings should not be generalized.

5.7 Summary

We developed seven model types in this thesis namely: MLR, PCR, MARS 1, MARS 2, ANN, PC-ANN and PC*-ANN. All models were developed with the learning datasets and their performance considered with the testing dataset.

We assessed the performance of MLR models, and used their results as baseline. Then, we conducted principal component analysis. The calculated principal components were used in regression (PCR) for the both O_3 and $PM_{2.5}$ at Airport station. We did not see benefits in terms of improved performance using PC, but saw increase in the statistical significance of the independent variables as measured by the t-ratio. After, we introduced the MARS method. We considered first and second order interaction and thus developed MARS 1 and MARS 2 models respectively. We applied both MARS models to prediction of O_3 and $PM_{2.5}$ at Airport station during summer season (day and night periods). MARS 1 model yielded less satisfactory results than MARS 2, and was ruled out from subsequent analysis. After, we applied the trial and error methodology to train ANN models. The results of ANN models were comparable of these of MARS 2 models. Finally we considered two hybrid approaches, which are the PC-ANN and PC*-ANN models. In PC-ANN, all principal components were used as input into ANN, while only the principal components with eigenvalues greater than unity were employed in PC*-ANN. Our rationale for PC*-ANN was to reduce the dimensionality of the dataset while keeping knowledge of most of the variability in the data. PC-ANN outperformed PC*-ANN and only outperformed ANN marginally. Given these results, MLR, MARS 2 and ANN models were retained for further analysis.

For ozone, MLR models yielded better results in winter for both stations. MLR performance at Airport was superior compared to Maisonneuve in day and night periods. For $PM_{2.5}$, MLR models yielded comparable results at Airport and Maisonneuve, regardless of season or period considered.

ANN models outperformed MLR models for O_3 and $PM_{2.5}$ forecasting at both stations. For ozone, ANN models performed comparably at both stations, but for $PM_{2.5}$ performance was best at Airport.

MARS 2 models outperformed ANN models. For O_3, MARS 2 yielded comparable results in both station. For $PM_{2.5}$, MARS 2 models yielded consistently better results at Airport.

Overall, the MARS 2 and ANN models demonstrated better forecasting potential then MLR. This is attributed to the more flexible and data driven learning algorithms employed by MARS and ANN. Also, MARS and ANN have more flexibility in terms of internal structure to best fit the data. This flexibility, combined with data-driven learning algorithms, allow both MARS and ANN to account for nonlinearities in the dataset.

MARS 2 outperformed ANN. The better performance of MARS 2 over ANN is attributed to inclusion of second order interactions of covariates. Second order interactions in MARS 2 models allow basis functions to be input into other basis functions. MARS 2 was empowered the uncovering of subregions in the time series where precursors of O_3 and $PM_{2.5}$ have recursive in addition to nonlinear relationships.

Case Study 5 was concerned with characterizing VOC data at Maisonneuve station and with modelling of daily averages of ozone. VOC concentration levels were considered as measure by ppbC and propy-equiv ppbC. For ozone modeling, we first

considered a MLR without the inclusion of VOC data. We observed a marginal improvement of the model's performance (higher R^2 and SI, with lower RMSE) with the inclusion of VOC data as measured by propy-equiv ppbC. In addition, we considered a MARS 2 and ANN models which included VOC data as propy-equiv ppbC values and saw that the best model was MARS 2.

The detailed comparisons between performance of models developed in this thesis and literature data prove that statistical models based on multiple linear regression, multivariate adaptive splines and artificial neural networks can perform accurately to forecast 1-hour O_3 and $PM_{2.5}$ in Montréal without the inclusion of lagged variables or dummy variables as well as daily O_3 at Maisonneuve with the inclusion of VOC data measured as propy-equiv ppbC. It can therefore be concluded that the parameters in each of the models have been correctly estimated to support air pollution forecasting in Montréal.

Chapter 6

Conclusion

6.1 Conclusions

The objectives of this study were to examine air pollution and to evaluate the suitability of different models based on statistical methods for short-term prediction of O_3 and $PM_{2.5}$ at two different locations within Montréal, namely: Airport Station (45°28′N, 73°44′W) and the Maisonneuve Station (45°30′N, 73°34′W). We collected relevant air pollution and meteorological data from January 2004 to December 2007.

To achieve these objectives, the collected data was characterized and underlying formation mechanisms of O_3 and $PM_{2.5}$ were identified; models based on Multiple Linear Regression (MLR), Multivariate Adaptive Regression Splines (MARS) and Artificial Neural Network (ANN) were developed and assessed in terms of predictive performance through five different case studies.

The raw data was analysed using conventional descriptive statistics. The dataset was randomly split into a training and validation. Model performance was assessed independently for winter/summer seasons as well as day/night periods. For forecasting, four different case studies were presented and 64 models were built: 16 were based on

MLR, 16 on MARS 2, 16 on ANN, 4 on PCR, 4 on MARS 1, 4 on PC-ANN and 4 on PC*-ANN. In total, we conducted 280 forecasting experiments. For modeling, one case study was presented and four models were built: two were based on MLR, one MARS 2, one on ANN. In total, we conducted 284 experiments. Statistical analysis and modelling was carried out using the commercially available statistical software "Salford Predictive Miner" from Salford Systems (San Diego, CA, USA) and "JMP Version 5.1.2" from SAS Institute Inc. (Cary, NC, USA)

Stepwise regression technique was used to build MLR models. The different MARS models were built using an optimum number of basis functions so that the generalized cross validation (GCV) criterion was minimised. Different network configurations for ANN were considered and the retained model was the one that presented the best goodness of fit and lowest error values. The statistical significance of MLR, PCR, MARS 1 and MARS 2 models was analysed. Performance of each model was assessed by means of performance metrics and success rates at the 75% percentile concentrations.

Performance metrics included the coefficient of determination (R^2), correlation coefficient (r), mean bias error (MBE), mean absolute error (MAE), mean absolute percent error (MAPE) and square root of the mean square error (RMSE). The optimal model for each trial was selected when R^2 and *r* approached unit value and MBE, MAE, MAPE and RMSE minimized. Exceedance indicators included true positive rate (TPR), false positive rate (FPR) and success index. The optimal model was the one that showed evidence of high TPR and low FPR, for a combined highest SI.

The forecasting methods discussed in this thesis gave reasonably good predictions in terms of the key metrics of error and exceedance levels. The values of the key performance indicators were comparable to these found in the literature. MARS 2 models performed the best, in terms of accuracy and parsimony, for forecasting ozone and fine particulate matter in Montréal in both winter/summer seasons as well as night/day periods.

TVOC measured by OH-reactivity weighted method ranged (9.6 – 106.6 propy-equiv ppbC) with an average of 34.4 propy-equiv ppbC. The most reactive VOC species as measured by propy-equiv ppbC were found to be m/p-xylene, toluene, propylene and (1,2,4)-trimethylbenzene. The modeling methods discussed in this thesis also gave reasonably good results in terms of the key metrics of error and exceedance levels. TVOC measured as propy-equiv ppbC was found to be statistically significant for inclusion in statistical modeling. MARS 2 model for modeling O_3 at Maisonneuve yielded the best performance in terms of accuracy and parsimony.

This study is the first comparative assessment of different statistical models for short-term prediction of ground level ozone and particulate matter in Montréal and the first to investigate the ozone forming potential of different volatile organic compound species in Montréal.

This work contributed to research by

1. Statistical analysis of air pollution and meteorological data putting in evidence seasonal and diurnal patterns in Montréal;
2. Comparison of air pollution levels in different areas of the city;

3. Development of different prediction models based on statistical methods for forecasting of ozone and fine particulate matter;
4. Determination of the ozone-forming potential of different VOC species; and
5. Determination of which statistical method best supports short-term forecast of O_3 and $PM_{2.5}$ locally in Montréal given the area's specific geography and site conditions.

The results of this study can be of interest as a reference and benchmark for future research.

6.2 Recommendations for Future Work

Further research is warranted to increase the collective knowledge of the applicability of statistical methods for forecasting ozone and particulate matter in Montréal. The following are eight recommendations for future study:

1. Include hourly-average of H_2SO_4, HNO_3, NH_3, SO_2 and VOC (measured as propy-equiv ppbC) as independent variables;
2. Investigate forecast windows up to 8-hours ahead;
3. Extend the study area to Montréal East, to South Shore (Longueil, Brossard) and North Shore (Laval) as these become increasingly more populated areas;
4. Investigate the effect on forecasting performance of ANN models by varying number of hidden layers, hidden nodes and corresponding activation functions

(e.g. step, piece-wise, bipolar sigmoid, hyperbolic tangent, radial basis or conic section);

5. Investigate the effect on forecasting performance of MARS models by allowing higher order interaction of basis function;
6. Quantify uncertainty in both target and prediction variables by using a fuzzy-set approach;
7. Perform sensitivity analysis of target variables to prediction variables;
8. Investigate performance of models based on other statistical methods (e.g. Quantile Regression, Classification and Regression Trees, and Fuzzy Inference Systems).

References

Agirre-Basurko, E., Ibarra-Berastegi, G. and Madariaga, G., 2006. Regression and multilayer perceptron-based models to forecast hourly O_3 and NO_2 levels in the Bilbao area. E*nvironmental Modelling & Software*, 21 (4): 430-446.

Akyuz, M. and Cabuk, H., 2009. Meteorological variations of $PM_{2.5}/PM_{10}$ concentrations and particle-associated polycyclic aromatic hydrocarbons in the atmospheric environment of Zonguldak, Turkey. *Journal of Hazardous Materials,* 170 (1): 13-21.

Al-Alawi, S.M., Abdul-Wahab, S.A. and Bakheit, C.S., 2008. Combining principal component regression and artificial neural networks for more accurate predictions of ground-level ozone. *Environmental Modelling & Software.* 23: 396 – 403.

Altshuller, A.P., 1984. *Assessment of the Contribution of Stratospheic Ozone to Ground-Level Ozone Concentrations*. Environmental Research Brief, U.S. Environmental Protection Agency, Washington (United States).

Atkinson, R., 1990. Gas-phase Tropospheric Chemistry of Organic Compounds: A Review. *Atmospheric Environment,* 24 (1): 1–41.

Bailey, R.A. Clark, H.M., Ferris, J.P. and Krause, S., 2002. *Chemistry of the Environment*. Academic Press, New York (United States).

Barnard, W.R. and Hodan, W.M., 2004. *Evaluating the Contribution of $PM_{2.5}$ Precursor Gases and Re-entrained Road Emissions to Mobile Source $PM_{2.5}$ Particulate Matter Emission*. Proceedings of the13th International Emission Inventory Conference, United States Environmental Protection Agency, Washington (United States).

Barry, R.G. and Chorley, R.J., 2003. *Atmosphere, Weather and Climate*. Routledge, London (England).

Basheer, I.A. and Hajmeer, M., 2000. Artificial neural networks: fundamentals, computing, design, and application. *Journal of Microbiological Methods,* 43: 3–31.

Ben-Gal. I., 2007. *Bayesian Networks*, Encyclopaedia of Statistics in Quality & Reliability, Wiley & Sons, New York (United States).

Bernstein, J.A., Alexis, N., Barnes, C., Bernstein, L.I., Nel, A., Peden, D., Diaz-Sanches, D., Tarlo, M.S. and Williams, P.B., 2004. Health effects of air pollution. *Journal of Allergy and Clinical Immunology,* 114: 1116–1123.

Bordignon, S., Gaetan, C. and Lisi, F., 2002. Nonlinear models for ground-level ozone forecasting. *Statistical Methods & Applications,* 11 (2) : 227-245.

Brook, J. and Dann, T., 2002. *Major Sources of Air Pollution in Eastern Canada and Transboundary Pollution*. Proceedings of the Symposium on Air Pollution and Public Health, Québec National Institute of Public Health, Québec (Canada).

Brunelli, U., Piazza, V., Pignato, L., Sorbello, F. and Vitabile, S., 2007. Two-days ahead prediction of daily maximum concentrations of SO_2, O_3, PM_{10}, NO_2, CO in the urban area of Palermo, Italy. *Atmospheric Environment,* 41: 2967–2995.

Bruno, F., Cocchi, D. and Trivisano, C., 2004. Forecasting daily high ozone concentrations by classification trees. *Environmetrics,* 15(2) : 141-153.

Caya, D., Laprise, R., Gigure, M., Bergeron, G., Blanchet, J., Stocks, B.,Boer, G. and McFarlane, N., 1995. Description of the Canadian regional climate model. *Water, Air and Soil Pollution* 82: 477-482.

Chaloulakou, A., Saisanaa, M. and Spyrellisa, N., 2003. Comparative assessment of neural networks and regression models for forecasting summertime ozone in Athens. *The Science of the Total Environment*, 313: 1–13.

Chameides, W. L., Fehsenfeld, F., Rodgers, M.O, Cardelino, C., Martinez, J., Parrish, D., Lonneman, W., Lawson, D.R., Rasmussen, R.A., Zimmerman, P., Greenberg, J., Middleton, P. and Wang, T. 1992. Ozone Precursor Relationships in the Ambient Atmosphere. *Journal of Geophysical Research*, 97 (5): 6037-6055.

Cobourn, W.G., 2010. An enhanced $PM_{2.5}$ air quality forecast model based on nonlinear regression and back-trajectory concentrations. *Atmospheric Environment*, 44(25): 3015-3023.

Corani, G., 2005. Air quality prediction in Milan: neural networks, pruned neural networks and lazy learning. *Ecological Modelling*, 185: 513-529.

Crouse, D., Goldberg, M.S. and Ross, N., 2009. A Prediction-based Approach to Modelling Temporal and Spatial Variability of Traffic-related Air Pollution in Montreal, Canada. *Atmospheic Environment,* 43 (32): 5075-5084.

Cuhadaroğlu, B. and Demirci, E., 1997. Influence of some meteorological factors on air pollution in Trabzon city. *Energy and Buildings,* 25: 179-184.

Dalrymple, G.B., 2004. *The age of Earth and Its Cosmic Surroundings*. Stanford University Press, Palo Alto (United States).

Delfino, R.J., Murphy-Moulton, A.M. and Becklake, M.R., 1998. Emergency Room Visits for Respiratory Illnesses among the Elderly in Montreal: Association with Low Level Ozone Exposure. *Environmental Research,* 76: 67 – 77.

Deschamps, K.M., 2003. *Associations between Asthma Hospital Admissions and Ambient Air Pollutants in Montréal, 1992 to 1999*. M.A. dissertation, Concordia University, Montréal (Canada).

Diaz-Robles, L.A. Ortega, J.C, Fub, J.S., Reed, G.D., Chow, J.C., Watson, J.G. and Moncada-Herrera, J.A., 2008. A hybrid ARIMA and artificial neural networks model to forecast particulate matter in urban areas: The case of Temuco, Chile. *Atmospheric Environment*, 42 (35): 8331-8340.

Donaldson, K. and MacNee, W., 1998. *The mechanism of lung injury caused by PM_{10} in issues in environmental science and technology*. Ed. R.E. Hester & R.M. Harisson, The Royal Society of Chemistry, London.

Egmont-Petersen M., Talmon J. L., Brender J., and NcNair, P., 1994. On the quality of neural net classifiers. *Artificial Intelligence in Medicine*, 6 (5): 359–381.

Evtyugina, M.G., Nunes, T., Alves, C. and Marques, M.C., 2009. Photochemical pollution in a rural mountainous area in the northeast of Portugal. *Atmospheric Research,* 92 (2): 151-158.

Fonseca, D.J., Navaresse, D.O. and Moynihan, G.P., 2003. Simulation metamodeling through artificial neural networks. *Engineering Applications of Artificial Intelligence,* 16: 177–183.

Garner, J., Lewis, T., Hogsett, W. and Andersen, C., 2005. *Air quality criteria for ozone and related photochemical oxidants (second external review draft) volume iii*. Technical report, U.S. Environmental Protection Agency, Washington (United States).

Ghio, A.J. and Huang, Y.C., 2004. Exposure to concentrated ambient particles (CAPs): a review. *Inhalation Toxicology,* 16: 53 – 59.

Gilbert, N.L., Goldberg, M.S., Beckerman, B., Brook, J.R and Jerrett, M., 2005. Assessing Spatial Variability of Ambient Nitrogen Dioxide in Montreal, Canada, with a Land-Use Regression Model. *Journal of the Air & Waste Management Association,* 55: 1059 – 1063.

Goldberg, M.S., Burnett, R.T., Bailar, J.C., Brook, J.R., Bonvalot, Y., Tamblyn, R., Singh, R. and Valois, M.-F. , 2001a. The Association between Daily Mortality and Ambient Air Particle Pollution in Montreal, Quebec: 1. Nonaccidental Mortality. *Environmental Research,* 86: 12 – 25.

Goldberg, M.S., Burnett, R.T., Bailar, J.C., Brook, J., Bonvalot, Y., Tamblyn, R., Singh, R., Valois, M.-F. and Vincent, R., 2001b. The Association between Daily Mortality and Ambient Air Particle Pollution in Montreal, Quebec: 2. Cause-Specific Mortality. *Environmental Research,* 86: 26 – 36.

Goldberg, M.S., Burnett, R.T., Valois, M.-F., Flegel, K., Bailar, J.C., Brook, J., Vincent, R. and Radon, K., 2003. Associations between ambient air pollution and daily mortality among persons with congestive heart failure. *Environmental Research,* 91: 8 – 20.

Goldberg, M.S., Burnett, R.T., Yale, J.-F, Valois, M.-F. and Brook, J.R., 2006. Associations between ambient air pollution and daily mortality among persons with diabetes and cardiovascular disease. *Environmental Research,* 100: 255 – 267.

Griffin, R.J. Cocker, D.R. Flagan, R.C. and Seinfeld, J.H., 1999. Organic aerosol formation from oxidation of biogenic hydrocarbons. *Journal of Geophysical Research,* 104: 3555-3567.

Hao, L. and Naiman, D. Q., 2007. *Quantile Regression*. Sage Publications, Thousand Oaks (United States).

Hastie, T., Tibshirani, R. and Friedman, J., 2001. *The Elements of Statistical Learning: Data Mining, Inference and Prediction*. Springer, New York (United States).

HCEC, 1998. *National Ambient Air Quality Objectives for Particular Matter: A report by the CEPA/FPAC on Air Quality Objectives and Guidelines*. Health Canada & Environmental Canada (HCEC), Ottawa (Canada).

HCEC, 1999. *National Ambient Air Quality Objectives for Ground-Level Ozone : A report by the CEPA/FPAC on Air Quality Objectives and Guidelines.* Health Canada & Environmental Canada (HCEC), Ottawa (Canada).

He, Y., 2004. *ANN Modeling of Ambient $PM_{2.5}$ in Fort McKay, Alberta*. M.Sc. Dissertation, University of Alberta, Edmonton (Canada).

HRSDC, 2004. *Early Childhood Education and Care Policy***.** Human Resources and Skills Development Canada, Ottawa (Canada).

Hutcheon, N.B. and Handegord, G.O.P., 1995. *Building Science for a Cold Climate*. National Research Council Canada, Ottawa (Canada).

Jensen, F. V. and Nielsen, T.D., 2007. *Bayesian Networks and Decision Graphs*. Springer, New York (United States).

Johnson. D., Mignacca, D., Herod, D., Jutzi, D. and Miller, H., 2007. Characterization and identification of trends in average ambient ozone and fine particulate matter levels through trajectory cluster analysis in eastern Canada. *Journal of the Air & Waste Management Association*, 57 (8): 907-18.

Jolliffe, I.T., 1989. *Principal Component Analysis*. Springer-Verlag, New York (United States).

Kampa, M. and Castanas, E., 2008. Human health effects of air pollution, *Environmental Pollution,* 151: 362–367.

Karatzas, K and Kaltsatos, S., 2007. Air pollution modeling with aid of computational intelligence methods in Thessaloniki, Greece. *Simulation Modelling Practice and Theory,* 15: 1310–1319.

Kim, S.E., 2010. Tree-based threshold modeling for short-term forecast of daily maximum ozone level. *Stochastic Environmental Research and Risk Assessment*, 24 (1): 19-28.

Kovac-Andric, E., Branab, J. and Gvozdica V., 2009. Impact of meteorological factors on ozone concentrations modelled by time series analysis and multivariate statistical methods. *Ecological Informatics*, 4 (2): 117-122.

Kuo, C.-Y., Chen, P.-T., Lin, Y.-C., Lin C.Y., Chen, H.H. and Shih, J.F, 2008. Factors affecting the concentrations of PM_{10} in central Taiwan, *Chemosphere* 70: 1273–1279.

Lin, Y., 2007. *Development of fuzzy system and nonlinear regression models for ozone and $PM_{2.5}$ air quality forecasts*. Ph.D. dissertation, University of Louisville, Louisville (United States).

Liu, Z., 2007. *Combing Measurements With Deterministic Model Outputs: Predicting Ground-Level Ozone*. Ph.D. dissertation. University Of British Columbia, Vancouver (Canada).

Lu, W.Z. and Wang, X.K., 2004. Interaction patterns of major air pollutants in Hong Kong territory. *Science of Total Environment,* 324: 247–259.

Lykoudis, S., Psounis, N., Mavrakis, A. and Christides, A., 2008. Predicting photochemical pollution in an industrial area. *Environmental Monitoring and Assessment,* 142: 279 -288.

Malinowski, E.R. and Howery, D.G., 1980. *Factor analysis in chemistry*. John Wiley & Sons, New York (United States).

Mayer, H., 1999. Air pollution in cities. *Atmospheric Environment,* 33: 4029–4037.

Maynard, R., 2004. Key airborne pollutants—the impact on health. *Science of Total Environment,* 335: 9–13.

Mintz, R., Young, B.R. and Svrcek, W.Y., 2005. Fuzzy logic modeling of surface ozone concentrations. *Computers & Chemical Engineering,* 29 (10): 2049-2059.

MTL, 2003. *Atlas démographique et socio-économique de Montréal*. Ville de Montréal, Montréal (Canada).

Nazaroff, W. and Alvarez-Cohen, L., 2001. *Environmental Engineering Science*. John Wiley & Sons, New York (United States).

Nedjah, N. and Mourelle, L.M., 2005. *Fuzzy Systems Engineering: Theory and Practice*, Springer, New York (United States).

Nedjah, N. and Mourelle, L.M., 2006. *Genetic Systems Programming Theory and Experiences.* Springer, New York (United States).

Nightingale, J.A., Rogers, D.F. and Barnes, P.J., 1999. Effect of inhaled ozone on exhaled nitric oxide, pulmonary function, and induced sputum in normal and asthmatic subjects. *Thorax,* 54: 1061 – 1069.

Nooria, R., Hoshyaripoura, G., Ashrafia, K. and Araabib, B. N., 2010. Uncertainty analysis of developed ANN and ANFIS models in prediction of carbon monoxide daily concentration. *Atmospheric Environment*, 44(4): 476-482.

Novara, C., Volta, M. and Finzi, G., 2007. Nonlinear Models to Forecast Ozone Peaks. *Air Pollution Modeling and Its Application XVII,* 11: 721-723.

NRTEE, 2008. *Developing ambient air quality objectives for Canada : advice to the Minister of Environment*. National Round Table on the Environment and the Economy, Ottawa (Canada).

Odman, M. and Ingram, C., 1996. *Multiscale air quality simulation plat-form (maqsip) source code documentation and validation.* Technical report, Environmental Programs, MCNC-North Carolina Supercomputing Center, Raleigh (United States).

Ordieres, J. B., Vergara, E. P., Capuz, R. S., and Salazar, R. E., 2005. Neural network prediction model for fine particulate matter ($PM_{2.5}$) on the US–Mexico border in El Paso (Texas) and Ciudad Juárez (Chihuahua). *Environmental Modelling & Software*, 20 (5) : 547-559.

Patel, P., 2004. *Neural Network Analysis of 8-hr Ozone and Particulate Matter in the Texas Upper Gulf Coast Region*. M.Eng. dissertation, Lamar University, Beaumont (United States).

Pires, J.C.M., Sousa, S.I.V., Pereira, M.C., Alvim-Ferraz, M.C.M. and Martins, F.G., 2008a. Management of air quality monitoring using principal component and cluster analysis—Part II: CO, NO_2 and O_3. *Atmospheric Environment*, 42: 1261-1274.

Pires, J.C.M., Sousa, S.I.V., Pereira, M.C., Alvim-Ferraz, M.C.M. and Martins, F.G., 2008b. Management of air quality monitoring using principal component and cluster analysis—Part I: SO_2 and PM_{10}. *Atmospheric Environment,* 42: 1249-1260.

Prybutok, B., Yi, J. and Mitchell, D., 2000. Comparison of neural network models with ARIMA and regression models for prediction of Houston's daily maximum ozone concentrations. *European Journal of Operational Research,* 122: 31-40.

Rohli, R.V. and Vega, A.J., 2008. *Climatology*. Jones and Bartlett Publishers, Sudbury.

RSQA, 2004. *Rapport environnemental annuel de la Qualité de l'air à Montréal (2004).* Réseau de Surveillance de la Qualité de l'air (RSQA), Montréal (Canada).

RSQA, 2005. *Rapport environnemental annuel de la Qualité de l'air à Montréal (2005).* Réseau de Surveillance de la Qualité de l'air (RSQA), Montréal (Canada).

RSQA, 2006. *Rapport environnemental annuel de la Qualité de l'air à Montréal (2006).* Réseau de Surveillance de la Qualité de l'air (RSQA), Montréal (Canada).

RSQA, 2007. *Rapport environnemental annuel de la Qualité de l'air à Montréal (2007).* Réseau de Surveillance de la Qualité de l'air (RSQA), Montréal (Canada).

Salazar-Ruiz, E., Ordieres, J.B., Vergara, E.P. and Capuz-Rizo, S.F., 2008. Development and comparative analysis of tropospheric ozone prediction models using linear and artificial intelligence-based models in Mexicali, Baja California (Mexico) and Calexico, California (US). *Environmental Modelling and Software* 23: 1056–1069.

Setiono, R., 2006. Feedforward Neural Network Construction Using Cross Validation. *Neural Computation*, 13 (12): 2865-2877.

Seinfeld, J.H. and Pandis, S.N., 1998. *Atmospheric Chemistry and Physics*. John Wiley & Sons, New York (United States).

Slini, T., Karatzas, K. and Moussiopoulos, N., 2002. Statistical analysis of environmental data as the basis of forecasting: an air quality application. *Science of Total Environment,* 288: 227 – 237.

Slini, T., Kaprara, A., Karatzas, K. and Moussiopoulos, N., 2006. PM_{10} forecasting for Thessaloniki, Greece. *Environmental Modelling & Software,* 21: 559 – 565.

Sofuoglu, S.C., Sofuoglu, A., Birgili, S. and Tayfur, G., 2006. Forecasting ambient air SO_2 concentrations using artificial neural networks. *Energy Source,* 1: 127–136.

Solaiman, T.A, Coulibaly, P. and Kanaroglou, P., 2008. Ground-level ozone forecasting using data-driven methods. *Air quality, Atmosphere and Health*, 1: 179-193.

Sousa, S., Martins, F., Alvim-Ferraz, M. and Pereira, M., 2007. Multiple linear regression and artificial neural networks based on principal components to predict ozone concentrations. *Environmental Modelling and Software,* 22: 97-103.

Sousa, S., Pires, J., Martins, F., Pereira, M. and Alvim-Ferraz, M., 2009. Potentialities of quantile regression to predict ozone concentrations. *Environmetrics*, 20 (2): 147–158.

Stanier, C.O., 2003. *Ultrafine Particles in the Atmosphere: Formation, Emissions and Growth.* Ph.D. dissertation, Carnegie Mellon University, Pittsburgh (United States).

Statheropoulos, M., Vassiliadis, N. and Pappa, A., 1998. Principal Component and Canonical Correlation Analysis for examining air pollution and meteorological data. *Atmospheric Environment*, 32: 1087-1095.

Su, D. 2004. *Artificial Neural Networks for Modelling Ground-Level Ozone*. M.Sc. dissertation, University of Alberta, Edmonton (Canada).

Talbot, D., Moran, M. D., Bouchet, V., Crevier, L.-P., Ménard, S. and Kallaur, A., 2008. Development of a New Canadian Operational Air Quality Forecast Model. *Air Pollution Modeling and Its Application*, 4: 470-478.

Tarasova, O. A., Brenninkmeijer, C. A. M., Jockel1, P., Zvyagintsev, A. M., and Kuznetsov, G. I., 2007. A climatology of surface ozone in the extra tropics:

cluster analysis of observations and model results. *Atmospheric Chemistry and Physics,* 7: 6099–6117.

Thompson, M.L., Reynolds, J., Cox, L.H., Guttorp, P., and Sampson, P.D., 2001. A review of statistical methods for the meteorological adjustment of tropospheric ozone. A*tmospheric Environment,* 35: 617-630.

Tsai, C., Changa, L. and Chiang, H., 2009. Forecasting of ozone episode days by cost-sensitive neural network methods. *Science of the Total Environment*, 407 (6): 2124-2135.

Turalıoğlu, F., Nuhoğlu, A. and Bayraktar, H., 2005. Impacts of some meteorological parameters on SO_2 and TSP concentrations in Erzurum, Turkey. *Chemosphere*, 55: 1633–1642.

USEPA, 2003. *Guidelines for developing an air quality (ozone and $PM_{2.5}$) forecasting program*. United States Environmental Protection Agency, Washington (United States).

Uysal, N. and Schapira, R.M., 2003. Effects of ozone on lung function and lung diseases, *Current Opinion in Pulmonary Medicine,* 9: 144 – 150.

Vagaggini, B., Taccola, M., Cianchetti, S., Carnevali, S., Bartoli, M.L. and Bacci, E., 2002. Ozone exposure increases eosinophilic airway response induced by previous allergen challenge. *American Journal of Respiratory and Critical Care Medicine.* 16: 1073 –1077.

Vautard, R., Schaap, M., Bergström, R., Bessagnet, B., Brandt, J., Builtjes, P.J.H. and Krol, M.C, 2008. Skill and uncertainty of a regional air quality model ensemble. *Atmospheric Environment,* 43: 4822 - 4832.

Vyushin, D. I., Fioletov, V. E., and Shepherd, T.G., 2007. Impact of long-range correlations on trend detection in total ozone. *Journal of Geophysical Research*, 112, D14307.

Wang, D. and Lu, W.Z., 2006. Ground-level ozone prediction using multilayer perceptron trained with an innovative hybrid approach. *Ecological Modelling,* 198: 332 – 340.

Xing, J., Wang, S. X., Jang, C., Zhu, Y., and Hao, J. M., 2010. Nonlinear response of ozone to precursor emission changes in China: a modeling study using response surface methodology. *Atmospheric Chemistry and Physics*, 10: 29809-29851.

Yeo, I.-K. and Johnson, R. A. (2000) A new family of power transformations to improve normality or symmetry. *Biometrika*, 87: 954–959.

Zheng, J., Shao, M., Che, W., Zhang, L., Zhong, L., Zhang, Y. and David Streets, 2009. Speciated VOC Emission Inventory and Spatial Patterns of Ozone Formation Potential in the Pearl River Delta, China. *Environmental Science & Technology*, 43 (22) : 8580–8586.

Websites:

EC, 2011: National Climate Data and Information Archive website:
http://climate.weatheroffice.gc.ca/climateData/canada_e.html
Accessed on January 15th 2011.

RSQA: *Réseau de surveillance de la qualité de l'air* (RSQA) website :
http://ville.montreal.qc.ca/portal/page?_pageid=7237,74687650&_dad=portal&_schema=PORTAL. Accessed on January 15th 2011.

Appendix A Derivation of the Gradient Descents Rule Using the Sigmoid Activation Function

Given:

$$y_p = f_{sig}\left(\sum_{i=1}^{n}\left(w_i x_i\right)\right) = \frac{1}{1+e^{-\alpha\left(\sum_{i=1}^{n}\left(w_i x_i\right)\right)}} \tag{A.1}$$

$$E_p = \frac{1}{2}\left(\hat{y}_p - y_p\right)^2 \tag{A.2}$$

$$E = \sum_{p=1}^{P} E_p \tag{A.3}$$

Derive:

$$\Delta w_i(t) = w_i(t) - \eta\frac{\partial E}{\partial w_i} \tag{A.4}$$

Step 1 Write:

$$\Delta w_i(t) = -\eta\sum_{p=1}^{P}\left(\frac{\partial E_p}{\partial w_i}\right) \tag{A.5}$$

Step 2 Apply chain rule:

$$\frac{\partial E_p}{\partial w_i} = \frac{\partial E_p}{\partial y_p}\times\frac{\partial y_p}{\partial w_i} \tag{A.6}$$

Step 3 Obtain:

$$\begin{aligned}\frac{\partial E_p}{\partial y_p} &= \frac{1}{2}\frac{\partial}{\partial y_p}\left(\hat{y}_p - y_p\right)^2 \\ &= \frac{1}{2}\times 2\times\left(\hat{y}_p - y_p\right)\times(-1) \\ &= -\left(\hat{y}_p - y_p\right)\end{aligned} \tag{A.7}$$

Step 4 Obtain:

$$
\begin{aligned}
\frac{\partial y_p}{\partial w_i} &= \frac{\partial}{\partial w_i}\left(\frac{1}{1+e^{-\alpha\left(\sum_{i=1}^{n}(w_i x_i)\right)}}\right) \\
&= \frac{0\times\left(1+e^{-\alpha\left(\sum_{i=1}^{n}(w_i x_i)\right)}\right)-(1)\times\left(\left(0+e^{-\alpha\left(\sum_{i=1}^{n}(w_i x_i)\right)}\times(-\alpha\ x_i)\right)\right)}{\left(1+e^{-\alpha\left(\sum_{i=1}^{n}(w_i x_i)\right)}\right)^2} \\
&= \alpha\ x_i \frac{e^{-\alpha\left(\sum_{i=1}^{n}(w_i x_i)\right)}}{1+e^{-\alpha\left(\sum_{i=1}^{n}(w_i x_i)\right)}}\times\frac{1}{1+e^{-\alpha\left(\sum_{i=1}^{n}(w_i x_i)\right)}} \\
&= \alpha\ x_i \frac{1-1+e^{-\alpha\left(\sum_{i=1}^{n}(w_i x_i)\right)}}{1+e^{-\alpha\left(\sum_{i=1}^{n}(w_i x_i)\right)}}\times\frac{1}{1+e^{-\alpha\left(\sum_{i=1}^{n}(w_i x_i)\right)}} \\
&= \alpha\ x_i\left(\frac{1+e^{-\alpha\left(\sum_{i=1}^{n}(w_i x_i)\right)}}{1+e^{-\alpha\left(\sum_{i=1}^{n}(w_i x_i)\right)}}-\frac{1}{1+e^{-\alpha\left(\sum_{i=1}^{n}(w_i x_i)\right)}}\right)\times\frac{1}{1+e^{-\alpha\left(\sum_{i=1}^{n}(w_i x_i)\right)}} \\
&= \alpha\ x_i\left(1-f_{sig}\left(\sum_{i=1}^{n}(w_i x_i)\right)\right)\left(f_{sig}\left(\sum_{i=1}^{n}(w_i x_i)\right)\right) \\
&= \alpha\ x_i(1-y_p)(y_p)
\end{aligned}
\tag{A.8}
$$

Step 5 Rewrite:

$$\begin{aligned}\Delta w_i(t) &= -\eta \frac{\partial E}{\partial w_i} \\ &= -\eta \sum_{p=1}^{P} \left(\frac{\partial E_p}{\partial w_i} \right) \\ &= -\eta \sum_{p=1}^{P} \left(\frac{\partial E_p}{\partial y_p} \times \frac{\partial y_p}{\partial w_i} \right) \\ &= -\eta \sum_{p=1}^{P} \left(-\left(\hat{y}_p - y_p \right) \times \alpha \; x_i \left(1 - y_p \right) \left(y_p \right) \right) \\ &= \alpha \; x_i \; \eta \sum_{p=1}^{P} \left(\left(y_p \right) \times \left(1 - y_p \right) \times \left(\hat{y}_p - y_p \right) \right)\end{aligned} \tag{A.9}$$

Step 6 Conclude:

$$\Delta w_i(t) = \alpha \; x_i \; \eta \sum_{p=1}^{P} \left(\delta_p \right) \tag{A.10}$$

$$w_i(t) = w_i(t-1) + \alpha \; x_i \; \eta \sum_{p=1}^{P} \left(\delta_p \right) \tag{A.11}$$

where

$$\delta_p = \left(y_p \right) \times \left(1 - y_p \right) \times \left(\hat{y}_p - y_p \right) \tag{A.12}$$

Appendix B Numerical Examples

B.1 A Numerical Example for Principal Component Analysis

Consider Matrix **X** from the data in Table B.1

Pattern	$x_{1,p}$	$x_{2,p}$	$x_{3,p}$
1	7	4	3
2	4	1	8
3	6	3	5
4	8	6	1
5	8	5	7
6	7	2	9
7	5	3	3
8	9	5	8
9	7	4	5
10	8	2	2

Table B.1 Data for PCA numerical example

Step 1 Calculate the means of each column vector $\mathbf{x_{i,p}}$ of matrix **X**

$$\bar{x}_j = \frac{1}{n}\sum_{i=1}^{n} x_{j,i} \tag{A.13}$$

$$\bar{x}_1 = \frac{1}{p}\sum_{i=1}^{p} x_{1,i} = \frac{1}{10}(7+4+...+8) = 6.9$$

$$\bar{x}_2 = \frac{1}{p}\sum_{i=1}^{p} x_{2,i} = \frac{1}{10}(4+1+...+2) = 3.5$$

$$\bar{x}_3 = \frac{1}{p}\sum_{i=1}^{p} x_{3,i} = \frac{1}{10}(3+8+...+2) = 5.1$$

Step 2 Calculate the standard deviation σ of each column vector of matrix X

$$\sigma_j = \sqrt{\sigma_j^2} = \sqrt{\frac{1}{n-1}\sum_{i=1}^{n}\left(x_{j,i} - \bar{x}_j\right)^2} \tag{A.14}$$

$$\sigma_1 = \sqrt{\sigma_1^2} = \sqrt{\frac{1}{n-1}\sum_{i=1}^{n}\left(x_{1,i} - \bar{x}_1\right)^2}$$

$$= \sqrt{\frac{1}{10-1}\left((7-6.9)^2 + (4-6.9)^2 + \ldots + (8-6.9)^2\right)} = 1.52$$

$$\sigma_2 = \sqrt{\sigma_2^2} = \sqrt{\frac{1}{n-1}\sum_{i=1}^{n}\left(x_{2,i} - \bar{x}_2\right)^2}$$

$$= \sqrt{\frac{1}{10-1}\left((4-3.5)^2 + (1-3.5)^2 + \ldots + (2-3.5)^2\right)} = 1.58$$

$$\sigma_3 = \sqrt{\sigma_3^2} = \sqrt{\frac{1}{n-1}\sum_{i=1}^{n}\left(x_{3,i} - \bar{x}_3\right)^2}$$

$$= \sqrt{\frac{1}{10-1}\left((3-5.1)^2 + (8-5.1)^2 + \ldots + (2-5.1)^2\right)} = 2.81$$

Step 3 Normalize observation data by subtracting from each element the mean and by dividing the result by the standard deviation of its respective column vector. Thus creating the normalized autoscaled matrix **Z**

$$z_{j,i} = \frac{\left(x_{j,i} - \bar{x}_j\right)}{\sigma_j} \tag{A.15}$$

$$z_{1,1} = \frac{(7-6.9)}{1.52} = 0.07 \qquad z_{2,1} = \frac{(4-3.5)}{1.58} = 0.32 \qquad z_{3,1} = \frac{(3-5.1)}{2.81} = -0.75$$

$$z_{1,2} = \frac{(4-6.9)}{1.52} = -1.90 \qquad z_{2,2} = \frac{(1-3.5)}{1.58} = -1.58 \qquad z_{3,2} = \frac{(8-5.1)}{2.81} = 1.03$$

$$z_{1,10} = \frac{(8-6.9)}{1.52} = 0.72 \quad \cdots \qquad z_{2,10} = \frac{(2-3.5)}{1.58} = -0.32 \quad \cdots \qquad z_{3,10} = \frac{(2-5.1)}{2.81} = -1.10 \quad \cdots$$

Pattern	$z_{1,p}$	$z_{2,p}$	$z_{3,p}$
1	0.07	0.32	-0.75
2	-1.90	-1.58	1.03
3	-0.59	-0.32	-0.04
4	0.72	1.58	-1.46
5	0.72	0.95	0.68
6	0.07	-0.95	1.39
7	-1.25	-0.32	-0.75
8	1.38	0.95	1.03
9	0.07	0.32	-0.04
10	0.72	-0.95	-1.10

Table B.2 Data for matrix Z in PCA numerical example

Step 4 Calculate the covariance s between the j^{th} and k^{th} columns of each column vector of the normalized autoscaled matrix Z. Note that $s_{j,k} = s_{k,j}$.

$$s_{j,k} = \frac{1}{n-1}\sum_{i=1}^{n}\left(a_{j,i} \cdot a_{k,i}\right) \tag{A.16}$$

For j = 1

$$s_{1,1} = \frac{1}{n-1}\sum_{i=1}^{n}\left(z_{1,i}\cdot z_{1,i}\right)$$
$$= \frac{1}{10-1}\left(0.07\times 0.07 + (-1.90)\times(-1.90) + ... + 0.72\times 0.72\right) = 1.00$$
$$s_{1,2} = \frac{1}{n-1}\sum_{i=1}^{n}\left(z_{1,i}\cdot z_{2,i}\right)$$
$$= \frac{1}{10-1}\left(0.07\times 0.32 + (-1.90)\times(-1.58) + ... + 0.72\times(-1.10)\right) = 0.67$$
$$s_{1,3} = \frac{1}{n-1}\sum_{i=1}^{n}\left(z_{1,i}\cdot z_{3,i}\right)$$
$$= \frac{1}{10-1}\left(0.07\times(-0.75) + (-1.90)\times 1.03 + ... + 0.72\times(--1.10)\right) = -0.10$$

For j = 2

$$s_{2,2} = \frac{1}{n-1}\sum_{i=1}^{n}\left(z_{2,i}\cdot z_{2,i}\right)$$
$$= \frac{1}{10-1}\left(0.32\times 0.32 + (-1.58)\times(-1.58) + ... + (-0.95)\times(-0.95)\right) = 1.00$$
$$s_{2,3} = \frac{1}{n-1}\sum_{i=1}^{n}\left(z_{2,i}\cdot z_{3,i}\right)$$
$$= \frac{1}{10-1}\left(0.32\times(-0.75) + (-1.58)\times 1.03 + ... + (-0.95)\times(-1.10)\right) = -0.29$$

For j = 3

$$s_{3,3} = \frac{1}{n-1}\sum_{i=1}^{n}\left(z_{3,i}\cdot z_{3,i}\right)$$
$$= \frac{1}{10-1}\left((-0.75)\times(-0.75) + 1.03\times 1.03 + ... + (-1.10)\times(-1.10)\right) = 1.00$$

Recognise that the covariance s between the j^{th} and k^{th} column of the normalized autoscaled matrix **Z** s equal to the correlation r . Note that $r_{j,k} = r_{k,j}$.

Build the correlation (or covariance) matrix **S**

	$z_{1,p}$	$z_{2,p}$	$z_{3,p}$
$z_{1,p}$	1.00	0.67	-0.10
$z_{2,p}$	0.67	1.00	-0.29
$z_{3,p}$	-0.10	-0.29	1.00

Table B.3 Data for matrix S in PCA numerical example

Step 5 Find the 3 different eigenvalues λ_i (i.e. scalars λ_1, λ_2 and λ_3) and the 3 different respective eigenvectors $\mathbf{v_i}$ (i.e vectors $\mathbf{v_1}$, $\mathbf{v_2}$ and $\mathbf{v_3}$) such that

$$\mathbf{(S - \lambda_i I) v_i} = 0 \qquad \text{(A.17)}$$

Expand:

$$\begin{aligned} &\mathbf{(S - \lambda_i I) v_i} = 0 \\ &\mathbf{S v_i - \lambda_i v_i} = 0 \\ &\mathbf{S v_i - \lambda_i I v_i} = 0 \end{aligned} \qquad \text{(A.18)}$$

Recall:

For all $\mathbf{v_i}$ which are non-zero, the characteristic equation of **S** (shown below) is satisfied.

$$\det (\mathbf{S - \lambda_i I}) = 0 \qquad \text{for all } i = 1 \text{ to } 3 \qquad \text{(A.19)}$$

In this numerical example, the characteristic equation is a 3rd order polynomial in λ yielding 3 roots. These roots are the 3 distinct eigenvalues of **S**; and for each of these eigenvalue there is an associated eigenvector.

Expand det (**S** - λ **I**):

$$\det(\mathbf{S} - \lambda_i \mathbf{I}) = 0$$

$$\Leftrightarrow \det\left(\begin{bmatrix} 1.00 & 0.67 & -0.10 \\ 0.67 & 1.00 & -0.29 \\ -0.10 & -0.29 & 1.00 \end{bmatrix} - \lambda_i \begin{bmatrix} 1.00 & 0 & 0 \\ 0 & 1.00 & 0 \\ 0 & 0 & 1.00 \end{bmatrix}\right) = 0$$

$$\Leftrightarrow \det\left(\begin{bmatrix} 1.00 - \lambda_i & 0.67 & -0.10 \\ 0.67 & 1.00 - \lambda_i & -0.29 \\ -0.10 & -0.29 & 1.00 - \lambda_i \end{bmatrix}\right) = 0$$

$$\Leftrightarrow (1.00 - \lambda_i) \times \det\begin{pmatrix} (1.00 - \lambda_i) & -0.29 \\ -0.29 & (1.00 - \lambda_i) \end{pmatrix}$$
$$- (0.67) \times \det\begin{pmatrix} 0.67 & -0.29 \\ -0.10 & (1.00 - \lambda_i) \end{pmatrix}$$
$$+ (-0.10) \det\begin{pmatrix} 0.67 & (1.00 - \lambda_i) \\ -0.10 & -0.29 \end{pmatrix} = 0$$

$$\Leftrightarrow (1.00 - \lambda_i) \times ((1.00 - \lambda_i) \times (1.00 - \lambda_i) - (-0.29) \times (-0.29))$$
$$- (0.67) \times ((0.67) \times (1.00 - \lambda_i) - (-0.29) \times (-0.10)) = 0$$
$$+ (-0.10) \times ((0.67) \times (-0.29) - (1.00 - \lambda_i) \times (-0.10))$$

$$\Leftrightarrow \quad \lambda_i^3 - 3.00\,\lambda_i^2 + 2.46\,\lambda_i - 0.50 = 0$$

The roots of the characteristic equation (i.e. λ_1, λ_2 and λ_3) are the 3 different eigenvalues λ_i

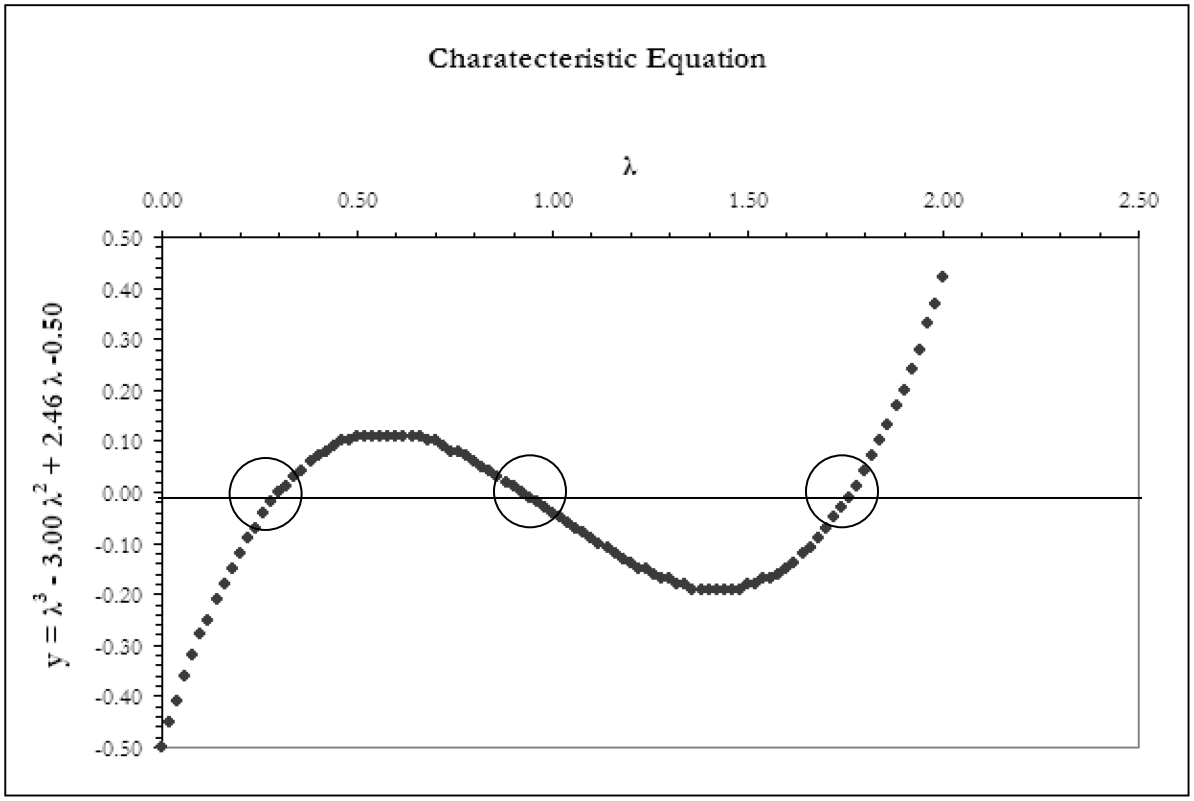

Figure B.1 Roots of the characteristic equation

Find the local maximum and local minimum

$$\frac{\partial}{\partial\lambda}\left(\lambda_i^3 - 3.00\,\lambda_i^2 + 2.46\,\lambda_i - 0.50\right) = 0$$

$$\Leftrightarrow \quad 3.00\lambda_i^2 - 6.00\,\lambda_i + 2.46 = 0$$

$$\Leftrightarrow \quad \lambda_i = \begin{cases} \dfrac{-(-6.00)+\sqrt{(-6.00)^2 - 4\times(3.00)[-0.50]}}{2\times(3.00)} \\ \dfrac{-(-6.00)-\sqrt{(-6.00)^2 - 4\times(3.00)[-0.50]}}{2\times(3.00)} \end{cases}$$

$$\Leftrightarrow \quad \lambda_i = \begin{cases} 1.42 & \min \\ 0.58 & \max \end{cases}$$

Solve for the roots by False Position Method

Consider:

$$x_r = x_u - \frac{f(x_u)(x_l - x_u)}{f(x_l) - f(x_u)} \qquad \text{(A.20)}$$

The value of x_r computed with equation replaces whichever of the two initial guesses, x_l or x_u, yields a function value with the same sign as $f(x_r)$. In this way, the values of x_l and x_u always bracket the true root. The process is repeated until the root is estimated adequately. The approximate percent error ε_a is be calculated as in

$$\varepsilon_a = \left| \frac{x_r^{new} - x_r^{old}}{x_r^{old}} \right| \times 100\,\% \;\geq\; 1.0\% \qquad \text{(A.21)}$$

For the left-hand root (λ_l), take

$$\begin{aligned} x_l &= \lambda_{max} - 0.5 \\ &= 0.58 - 0.50 \\ &= 0.08 \end{aligned}$$

and

$$\begin{aligned} x_u &= \lambda_{max} \\ &= 0.58 \end{aligned}$$

Initialisation

$$x_r = x_u - \frac{f(x_u)(x_l - x_u)}{f(x_l) - f(x_u)}$$

$$x_r = 0.58 - \frac{(0.11)(0.08 - 0.58)}{(-0.33) - (0.11)}$$

$$x_r = 0.45$$

Iteration 1

Reconsider

$x_l = 0.08$

$x_u = x_r$
$= 0.44$

$$x_r^{new} = x_u - \frac{f(x_u)(x_l - x_u)}{f(x_l) - f(x_u)}$$

$$x_r^{new} = 0.45 - \frac{(0.09)(0.08 - 0.45)}{(-0.33) - (0.09)} = 0.37$$

$$\varepsilon_a = \left| \frac{x_r^{new} - x_r^{old}}{x_r^{old}} \right| \times 100\ \% \ \geq \ 1.0\%$$

$$\varepsilon_a = \left| \frac{0.37 - 0.44}{0.44} \right| \times 100\ \% = 21.87 \ \geq \ 1.0\%$$

Iteration 2

Reconsider

$x_l = 0.08$

$x_u = x_r$
$= 0.37$

$$x_r^{new} = x_u - \frac{f(x_u)(x_l - x_u)}{f(x_l) - f(x_u)}$$

$$x_r^{new} = 0.37 - \frac{(0.05)(0.08 - 0.37)}{(-0.33) - (0.05)} = 0.33$$

$$\varepsilon_a = \left| \frac{x_r^{new} - x_r^{old}}{x_r^{old}} \right| \times 100\ \% \ \geq \ 1.0\%$$

$$\varepsilon_a = \left| \frac{0.33 - 0.37}{0.37} \right| \times 100\ \% = 11.53 \ \geq \ 1.0\%$$

Left-hand root (λ_1)

Iteration	x_l	x_r	x_u	f (x_l)	f (x_r)	f (x_u)	ε_a
0	0.08	0.4472	0.58	-0.33	0.091	0.11	-
1	0.08	0.3670	0.45	-0.33	0.049	0.09	21.87
2	0.08	0.3290	0.37	-0.33	0.021	0.05	11.53
3	0.08	0.3136	0.33	-0.33	0.010	0.02	4.93
4	0.08	0.3076	0.31	-0.33	0.003	0.01	1.92
5	0.08	**0.3042**	0.31	-0.33	**0.000**	0.01	**0.72**

Table B.4 False Position Method iterations for λ_1 in PCA numerical example

For the left-hand root (λ_2), take

$$x_l = \lambda_{max} = 0.58$$

$$x_u = \lambda_{min} = 1.42$$

Middle root (λ_2)

Iteration	x_l	x_r	x_u	f (x_l)	f (x_r)	f (x_u)	ε_a
0	0.58	0.8917	1.42	0.11	0.018	-0.19	-
1	0.89	0.9379	1.42	0.02	-0.06	-0.19	4.93
2	0.89	0.9269	0.94	0.02	0.001	-0.01	1.19
3	0.93	0.9271	0.94	0.00	0.000	-0.01	0.02

Table B.5 False Position Method iterations for λ_2 in PCA numerical example

For the left-hand root (λ_3), take

$$x_l = \lambda_{min} = 1.42$$

$$x_u = \lambda_{max} + 0.5 = 1.42 + 0.50 = 1.92$$

Right-hand root (λ_3)

Iteration	xl	Xr	xu	fxl	fxr	fxu	ε_a
0	1.42	1.6408	1.92	-0.19	-0.122	0.25	-
1	1.64	1.7335	1.92	-0.12	-0.0407	0.25	5.348
2	1.73	1.7601	1.92	-0.04	-0.011	0.25	1.510
3	1.76	1.7688	1.92	-0.01	0.000	0.25	0.375

Table B.6 False Position Method iterations for λ_3 in PCA numerical example

Therefore scalars (λ_1, λ_2 , λ_3) = (0.3042, 0.9271, 1.7688)

Now, recall that **(S - λ_i I) $\mathbf{v_i}$** = 0 for all *i* = 1 to 3; can be solved by Cramer's rule or by developing the system of three equations and three unknows.

Solution of first column vector v_1

$$(\mathbf{S} - \lambda_1 \mathbf{I})\mathbf{v_1} = 0$$

$$\Leftrightarrow \left(\begin{bmatrix} 1.00 & 0.67 & -0.10 \\ 0.67 & 1.00 & -0.29 \\ -0.10 & -0.29 & 1.00 \end{bmatrix} - 0.3042 \begin{bmatrix} 1.00 & 0 & 0 \\ 0 & 1.00 & 0 \\ 0 & 0 & 1.00 \end{bmatrix} \right) \begin{bmatrix} v_1 \\ v_2 \\ v_3 \end{bmatrix} = \begin{bmatrix} 0.00 \\ 0.00 \\ 0.00 \end{bmatrix}$$

$$\Leftrightarrow \begin{bmatrix} v_1 \\ v_2 \\ v_3 \end{bmatrix} = \begin{bmatrix} 0.6420 \\ 0.6864 \\ -0.3417 \end{bmatrix}$$

Solution of second column vector v_2

$$(\mathbf{S} - \lambda_2 \mathbf{I})\mathbf{v_2} = 0$$

$$\Leftrightarrow \left(\begin{bmatrix} 1.00 & 0.67 & -0.10 \\ 0.67 & 1.00 & -0.29 \\ -0.10 & -0.29 & 1.00 \end{bmatrix} - 0.9271 \begin{bmatrix} 1.00 & 0 & 0 \\ 0 & 1.00 & 0 \\ 0 & 0 & 1.00 \end{bmatrix} \right) \begin{bmatrix} v_1 \\ v_2 \\ v_3 \end{bmatrix} = \begin{bmatrix} 0.00 \\ 0.00 \\ 0.00 \end{bmatrix}$$

$$\Leftrightarrow \begin{bmatrix} v_1 \\ v_2 \\ v_3 \end{bmatrix} = \begin{bmatrix} 0.3847 \\ 0.0971 \\ 0.9179 \end{bmatrix}$$

Solution of third column vector v_3

$$(\mathbf{S} - \lambda_3 \mathbf{I})\mathbf{v_3} = 0$$

$$\Leftrightarrow \left(\begin{bmatrix} 1.00 & 0.67 & -0.10 \\ 0.67 & 1.00 & -0.29 \\ -0.10 & -0.29 & 1.00 \end{bmatrix} - 1.7688 \begin{bmatrix} 1.00 & 0 & 0 \\ 0 & 1.00 & 0 \\ 0 & 0 & 1.00 \end{bmatrix} \right) \begin{bmatrix} v_1 \\ v_2 \\ v_3 \end{bmatrix} = \begin{bmatrix} 0.00 \\ 0.00 \\ 0.00 \end{bmatrix}$$

$$\Leftrightarrow \begin{bmatrix} v_1 \\ v_2 \\ v_3 \end{bmatrix} = \begin{bmatrix} -0.6632 \\ 0.7207 \\ 0.2017 \end{bmatrix}$$

$$\therefore V = \begin{bmatrix} 0.64 & 0.38 & -0.66 \\ 0.69 & 0.10 & 0.72 \\ -0.34 & 0.92 & 0.20 \end{bmatrix}$$

Conclude

The eigenvalues ($\lambda_1, \lambda_2, \lambda_3$) = (0.3042, 0.9271, 1.7688)

Eigenvector $\mathbf{V} = < \mathbf{v_1} \ \mathbf{v_2} \ \mathbf{v_3} >$

$$= \begin{bmatrix} 0.64 & 0.38 & -0.66 \\ 0.69 & 0.10 & 0.72 \\ -0.34 & 0.92 & 0.20 \end{bmatrix}$$

Step 6 Get the factor score matrix $\mathbf{F} = \mathbf{Z}\,\mathbf{V}^*$, where $\mathbf{V}^* = [\,\mathbf{v_1}, \mathbf{v_2}\,]$ as the third principal component has been disregarded.

Pattern	$F_{1,p}$	$F_{2,p}$
1	0.51	-0.63
2	-2.66	0.06
3	-0.58	-0.29
4	2.05	-0.91
5	0.88	0.99
6	-1.08	1.21
7	-0.76	-1.20
8	1.18	1.57
9	0.27	0.02
10	0.19	-0.83

Table B.7 Data for matrix F in PCA numerical example

Recognise that in this step, we have achieved data compression by transforming matrix **Z** [10 x 3] into matrix **F** [10 x 2].

B.2 A Numerical Example for Artificial Neural Network using the Gradient Descent Rule and Sigmoid Activation Function

Consider

Pattern	$x_{1,p}$	$x_{2,p}$	$x_{3,p}$	$\hat{y}_p$
1	0.93	0.79	0.66	0.62
2	0.83	0.80	0.63	0.54
3	0.96	0.12	0.98	1.20
4	0.71	0.84	0.03	0.03
5	0.98	0.14	0.47	0.84
6	0.59	0.98	0.72	0.37
7	0.43	0.92	0.61	0.22
8	0.03	0.90	0.48	-0.10
9	0.78	0.43	0.79	0.80
10	0.81	0.46	0.42	0.55

Table B.8 Data for matrix X in ANN numerical example

Initialisation

Set (randomly):

$w_1 = 0.80$
$w_2 = 0.40$
$w_3 = 1.00$

*** Iteration 1**

Calculate the summed weighted inputs N_p for each pattern.

$$N_p = \sum_{i=1}^{n} \left(w_i x_{i,p} \right) \tag{A.22}$$

$$N_1 = \sum_{i=1}^{3} \left(w_i x_{i,1} \right) = 0.80 \times 0.93 + 0.40 \times 0.79 + 1.00 \times 0.66 = 1.72$$

$$N_2 = \sum_{i=1}^{3} \left(w_i x_{i,2} \right) = 0.80 \times 0.83 + 0.40 \times 0.80 + 1.00 \times 0.63 = 1.61$$

...

$$N_{10} = \sum_{i=1}^{3} \left(w_i x_{i,10} \right) = 0.80 \times 0.81 + 0.40 \times 0.46 + 1.00 \times 0.42 = 1.25$$

Calculate the networks output y_p for each pattern

$$y_p = f_{sigmoid}\left(N_p\right) = \frac{1}{1+e^{-N_p}} \tag{A.23}$$

$$y_1 = f_{sigmoid}\left(N_1\right) = \frac{1}{1+e^{-N_p}} = \frac{1}{1+e^{-1.72}} = 0.85$$

$$y_2 = f_{sigmoid}\left(N_2\right) = \frac{1}{1+e^{-N_p}} = \frac{1}{1+e^{-1.61}} = 0.83$$

...

$$y_{10} = f_{sigmoid}\left(N_{15}\right) = \frac{1}{1+e^{-N_p}} = \frac{1}{1+e^{-1.25}} = 0.78$$

Calculate the energy level E each output p

$$E_p = \frac{1}{2}\left(\hat{y}_p - y_p\right)^2 \tag{A.24}$$

$$E_1 = \frac{1}{2}\left(\hat{y}_1 - y_1\right)^2 = \frac{1}{2}\left(0.62 - 0.85\right)^2 = 0.03$$

$$E_2 = \frac{1}{2}\left(\hat{y}_2 - y_2\right)^2 = \frac{1}{2}\left(0.54 - 0.83\right)^2 = 0.04$$

...

$$E_{10} = \frac{1}{2}\left(\hat{y}_{10} - y_{10}\right)^2 = \frac{1}{2}\left(0.55 - 0.78\right)^2 = 0.03$$

Pattern	$\hat{y}_p$	N_p	Y_p	E_p
1	0.62	1.72	0.85	0.03
2	0.54	1.61	0.83	0.04
3	1.20	1.80	0.86	0.06
4	0.03	0.94	0.72	0.24
5	0.84	1.31	0.79	0.00
6	0.37	1.58	0.83	0.11
7	0.22	1.32	0.79	0.16
8	-0.10	0.86	0.70	0.32
9	0.80	1.58	0.83	0.00
10	0.55	1.25	0.78	0.03

Table B.9 Internal energies at first iteration in ANN numerical example

Calculate the network's total energy E_T

$$E_T = \sum_{p=1}^{P} E_p \qquad \text{(A.25)}$$
$$= 0.03 + 0.04 + \ldots + 0.03$$
$$= 0.98$$

Compute the weight correction coefficients δ_p.

$$\delta_p = (y_p) \times (1 - y_p) \times (\hat{y}_p - y_p) \qquad \text{(A.26)}$$

$$\delta_1 = (y_1) \times (1 - y_1) \times (\hat{y}_1 - y_1) = (0.85) \times (1 - 0.85) \times (0.62 - 0.85) = -0.03$$
$$\delta_2 = (y_2) \times (1 - y_2) \times (\hat{y}_2 - y_2) = (0.83) \times (1 - 0.83) \times (0.54 - 0.83) = -0.04$$
$$\ldots$$
$$\delta_{10} = (y_{10}) \times (1 - y_{10}) \times (\hat{y}_{10} - y_{10}) = (0.78) \times (1 - 0.78) \times (0.55 - 0.78) = -0.04$$

Compute the summed product of the weight correction coefficient δ_p and x_i.

With respect to first variable $x_{1,p}$

$$\sum_{p=1}^{N} (\delta_p \cdot x_{1,p})$$
$$= (-0.03 \times 0.93) + (-0.04 \times 0.83) + \ldots + (-0.04 \times 0.81) = -0.23$$

With respect to second variable $x_{2,p}$

$$\sum_{p=1}^{N}\left(\delta_p \cdot x_{2,p}\right)$$
$$=\left(-0.03\times 0.79\right)+\left(-0.04\times 0.80\right)+\ldots+\left(-0.04\times 0.46\right)=-0.49$$

With respect to second variable $x_{3,p}$

$$\sum_{p=1}^{N}\left(\delta_p \cdot x_{3,p}\right)$$
$$=\left(-0.03\times 0.66\right)+\left(-0.04\times 0.63\right)+\ldots+\left(-0.04\times 0.42\right)=-0.21$$

Find the weight differential

$$\Delta w_i(t)=\alpha\ \eta\sum_{p=1}^{P}\left(\delta_p \cdot x_{p,i}\right) \tag{A.27}$$

$$\Delta w_1(t)=\alpha\ \eta\sum_{p=1}^{P}\left(\delta_p \cdot x_{p,1}\right)=1.0\times 0.2\times\left(-0.23\right)=-0.05$$

$$\Delta w_2(t)=\alpha\ \eta\sum_{p=1}^{P}\left(\delta_p \cdot x_{p,2}\right)=1.0\times 0.2\times\left(-0.49\right)=-0.10$$

$$\Delta w_3(t)=\alpha\ \eta\sum_{p=1}^{P}\left(\delta_p \cdot x_{p,3}\right)=1.0\times 0.2\times\left(-0.21\right)=-0.04$$

Correct the weights

$$w_i(t+1)=w_i(t)+\Delta w_i(t) \tag{A.28}$$

$$w_1(t+1)=w_1(t)+\Delta w_1(t)=0.80-0.05=0.75$$
$$w_2(t+1)=w_2(t)+\Delta w_2(t)=0.40-0.10=0.30$$
$$w_3(t+1)=w_3(t)+\Delta w_3(t)=1.00-0.04=0.96$$

Reset :

$w_1 = 0.75$
$w_2 = 0.30$
$w_3 = 0.96$

Summary

Iteration	w_1	w_2	w_3	E_T
0	0.80	0.40	1.00	0.98
1	0.75	0.30	0.96	0.91
2	0.71	0.20	0.92	0.85
3	0.67	0.10	0.88	0.78
4	0.63	0.01	0.84	0.72
5	0.59	-0.09	0.80	0.66
6	0.56	-0.18	0.77	0.61
7	0.53	-0.27	0.75	0.56
8	0.51	-0.36	0.72	0.53
9	0.49	-0.43	0.70	0.50
10	0.48	-0.51	0.69	0.47

Table B.10 Weight correction up to 10 iterations in ANN numerical example

Appendix C Completeness of the Data

Month	O3 (Airport)	PM2.5 (Airport)	NO (Airport)	NO2 (Airport)	CO (Airport)
Jan-04	0%	100%	100%	100%	100%
Feb-04	0%	99%	100%	100%	100%
Mar-04	0%	99%	36%	100%	97%
Apr-04	0%	99%	100%	100%	100%
May-04	0%	85%	85%	85%	85%
Jun-04	46%	0%	48%	46%	48%
Jul-04	99%	36%	99%	99%	99%
Aug-04	94%	95%	99%	99%	99%
Sep-04	99%	95%	99%	99%	99%
Oct-04	100%	100%	100%	100%	96%
Nov-04	98%	100%	98%	98%	98%
Dec-04	100%	95%	100%	100%	100%
Jan-05	100%	100%	100%	100%	100%
Feb-05	100%	94%	100%	100%	100%
Mar-05	100%	95%	100%	100%	100%
Apr-05	100%	98%	99%	96%	100%
May-05	99%	99%	99%	99%	96%
Jun-05	100%	85%	100%	100%	100%
Jul-05	100%	89%	100%	100%	100%
Aug-05	100%	97%	100%	100%	100%
Sep-05	100%	100%	100%	100%	100%
Oct-05	100%	98%	100%	100%	100%
Nov-05	99%	95%	99%	99%	99%
Dec-05	100%	100%	100%	100%	100%
Jan-06	100%	98%	100%	100%	100%
Feb-06	100%	99%	100%	100%	98%
Mar-06	100%	98%	100%	100%	95%
Apr-06	100%	100%	100%	100%	100%
May-06	100%	98%	100%	100%	100%
Jun-06	100%	97%	100%	100%	100%
Jul-06	99%	99%	99%	99%	99%
Aug-06	100%	99%	100%	100%	99%
Sep-06	99%	98%	99%	99%	99%
Oct-06	100%	100%	100%	100%	100%
Nov-06	99%	96%	98%	98%	98%
Dec-06	99%	99%	99%	99%	97%
Jan-07	100%	99%	100%	100%	100%
Feb-07	100%	99%	94%	94%	100%
Mar-07	100%	100%	100%	100%	100%
Apr-07	100%	100%	100%	100%	100%
May-07	99%	99%	99%	99%	98%
Jun-07	99%	97%	99%	99%	100%
Jul-07	99%	96%	99%	99%	99%
Aug-07	100%	96%	100%	100%	100%
Sep-07	100%	98%	100%	100%	100%
Oct-07	99%	95%	100%	100%	100%
Nov-07	100%	92%	100%	100%	100%
Dec-07	99%	99%	99%	99%	94%

Table C.1 Completeness of the data for air pollution readings at Airport station

Month	SR	Temp	DP	Press	Precip	WS	WD
Jan-04	100%	100%	100%	100%	100%	100%	100%
Feb-04	100%	100%	100%	100%	100%	100%	100%
Mar-04	100%	100%	100%	100%	99%	100%	100%
Apr-04	100%	99%	99%	100%	99%	99%	99%
May-04	100%	100%	99%	99%	99%	100%	100%
Jun-04	100%	100%	99%	100%	100%	100%	100%
Jul-04	100%	100%	91%	91%	91%	100%	100%
Aug-04	76%	99%	99%	100%	99%	99%	99%
Sep-04	100%	100%	99%	98%	98%	100%	100%
Oct-04	99%	100%	95%	100%	100%	100%	100%
Nov-04	98%	93%	93%	93%	93%	93%	93%
Dec-04	100%	100%	100%	100%	100%	100%	100%
Jan-05	100%	100%	100%	99%	99%	100%	100%
Feb-05	100%	99%	99%	100%	100%	99%	99%
Mar-05	100%	94%	94%	93%	93%	94%	94%
Apr-05	100%	92%	92%	68%	68%	92%	92%
May-05	100%	100%	100%	100%	100%	100%	100%
Jun-05	100%	100%	99%	99%	99%	100%	100%
Jul-05	100%	100%	100%	100%	99%	100%	100%
Aug-05	100%	100%	97%	100%	100%	100%	100%
Sep-05	99%	100%	100%	99%	99%	100%	100%
Oct-05	100%	100%	97%	100%	99%	100%	100%
Nov-05	100%	73%	70%	73%	73%	73%	73%
Dec-05	100%	100%	100%	100%	100%	100%	100%
Jan-06	100%	100%	100%	96%	95%	100%	100%
Feb-06	100%	100%	96%	96%	96%	100%	100%
Mar-06	100%	100%	100%	100%	100%	100%	100%
Apr-06	100%	100%	100%	100%	100%	100%	100%
May-06	100%	100%	100%	99%	100%	100%	100%
Jun-06	100%	100%	100%	100%	100%	100%	100%
Jul-06	100%	100%	100%	100%	100%	100%	100%
Aug-06	97%	100%	100%	100%	100%	100%	100%
Sep-06	67%	100%	100%	100%	100%	100%	100%
Oct-06	0%	100%	100%	97%	97%	100%	100%
Nov-06	48%	100%	100%	100%	100%	100%	0%
Dec-06	100%	100%	100%	100%	100%	100%	100%
Jan-07	99%	100%	100%	100%	100%	100%	100%
Feb-07	55%	100%	100%	100%	100%	100%	100%
Mar-07	0%	100%	100%	100%	100%	100%	100%
Apr-07	0%	100%	100%	97%	97%	100%	100%
May-07	0%	100%	100%	97%	97%	100%	100%
Jun-07	100%	100%	100%	100%	100%	100%	100%
Jul-07	99%	100%	97%	83%	83%	100%	100%
Aug-07	100%	100%	78%	100%	100%	100%	100%
Sep-07	100%	100%	100%	100%	100%	100%	100%
Oct-07	30%	100%	99%	99%	98%	100%	100%
Nov-07	0%	100%	99%	100%	100%	100%	100%
Dec-07	0%	100%	98%	100%	92%	100%	100%

Table C.2 Completeness of the data for air pollution readings at Maisonneuve station

Month	SR	Temp	DP	Press	Precip	WS	WD
Jan-04	100%	100%	100%	100%	100%	100%	100%
Feb-04	100%	100%	100%	100%	100%	100%	100%
Mar-04	100%	100%	100%	100%	99%	100%	100%
Apr-04	100%	99%	99%	100%	99%	99%	99%
May-04	100%	100%	99%	99%	99%	100%	100%
Jun-04	100%	100%	99%	100%	100%	100%	100%
Jul-04	100%	100%	91%	91%	91%	100%	100%
Aug-04	76%	99%	99%	100%	99%	99%	99%
Sep-04	100%	100%	99%	98%	98%	100%	100%
Oct-04	99%	100%	95%	100%	100%	100%	100%
Nov-04	98%	93%	93%	93%	93%	93%	93%
Dec-04	100%	100%	100%	100%	100%	100%	100%
Jan-05	100%	100%	100%	99%	99%	100%	100%
Feb-05	100%	99%	99%	100%	100%	99%	99%
Mar-05	100%	94%	94%	93%	93%	94%	94%
Apr-05	100%	92%	92%	68%	68%	92%	92%
May-05	100%	100%	100%	100%	100%	100%	100%
Jun-05	100%	100%	99%	99%	99%	100%	100%
Jul-05	100%	100%	100%	100%	99%	100%	100%
Aug-05	100%	100%	97%	100%	100%	100%	100%
Sep-05	99%	100%	100%	99%	99%	100%	100%
Oct-05	100%	100%	97%	100%	99%	100%	100%
Nov-05	100%	73%	70%	73%	73%	73%	73%
Dec-05	100%	100%	100%	100%	100%	100%	100%
Jan-06	100%	100%	100%	96%	95%	100%	100%
Feb-06	100%	100%	96%	96%	96%	100%	100%
Mar-06	100%	100%	100%	100%	100%	100%	100%
Apr-06	100%	100%	100%	100%	100%	100%	100%
May-06	100%	100%	100%	99%	100%	100%	100%
Jun-06	100%	100%	100%	100%	100%	100%	100%
Jul-06	100%	100%	100%	100%	100%	100%	100%
Aug-06	97%	100%	100%	100%	100%	100%	100%
Sep-06	67%	100%	100%	100%	100%	100%	100%
Oct-06	0%	100%	100%	97%	97%	100%	100%
Nov-06	48%	100%	100%	100%	100%	100%	0%
Dec-06	100%	100%	100%	100%	100%	100%	100%
Jan-07	99%	100%	100%	100%	100%	100%	100%
Feb-07	55%	100%	100%	100%	100%	100%	100%
Mar-07	0%	100%	100%	100%	100%	100%	100%
Apr-07	0%	100%	100%	97%	97%	100%	100%
May-07	0%	100%	100%	97%	97%	100%	100%
Jun-07	100%	100%	100%	100%	100%	100%	100%
Jul-07	99%	100%	97%	83%	83%	100%	100%
Aug-07	100%	100%	78%	100%	100%	100%	100%
Sep-07	100%	100%	100%	100%	100%	100%	100%
Oct-07	30%	100%	99%	99%	98%	100%	100%
Nov-07	0%	100%	99%	100%	100%	100%	100%
Dec-07	0%	100%	98%	100%	92%	100%	100%

Table C.3 Completeness of the data for meteorological readings at Airport station

APPENDIX D: Monthly Averages (2004 – 2007 Time Series)

D.1 Air Quality Data at Airport

Month	O3 (Airport)	PM2.5 (Airport)	NO (Airport)	NO2 (Airport)	CO (Airport)
Jan-04		5.8	7.3	28.2	335.2
Feb-04		11.0	22.5	50.0	424.5
Mar-04		9.0	28.2	41.3	421.5
Apr-04		5.6	2.9	27.5	297.3
May-04		7.6	5.1	24.9	254.9
Jun-04	45.4		2.1	19.1	173.2
Jul-04	41.7	10.5	3.6	21.1	282.3
Aug-04	36.3	10.1	4.5	18.8	308.0
Sep-04	30.8	7.6	9.6	21.8	220.5
Oct-04	28.5	7.2	18.3	28.7	227.0
Nov-04	23.4	7.0	21.9	32.9	238.5
Dec-04	32.5	8.3	17.7	35.1	260.5
Jan-05	33.2	8.4	13.1	38.5	284.7
Feb-05	31.2	18.9	30.7	54.9	466.7
Mar-05	57.9	6.7	6.6	30.9	210.3
Apr-05	58.6	5.5	5.0	26.5	212.9
May-05	54.7	5.1	4.8	21.0	200.2
Jun-05	61.3	17.1	4.7	22.0	377.8
Jul-05	52.1	9.4	3.1	17.5	320.7
Aug-05	51.6	10.3	3.7	17.4	378.7
Sep-05	45.0	9.4	3.4	16.9	334.8
Oct-05	29.1	7.8	6.8	22.0	325.6
Nov-05	29.4	6.9	11.8	25.7	350.8
Dec-05	30.4	7.1	13.4	32.3	378.7
Jan-06	27.2	9.8	19.0	39.2	473.4
Feb-06	44.9	6.6	8.3	28.2	385.5
Mar-06	55.7	5.9	5.0	24.0	357.7
Apr-06	57.6	4.2	3.2	21.0	366.4
May-06	52.7	6.8	3.8	20.7	334.0
Jun-06	51.4	7.9	2.7	17.9	305.4
Jul-06	60.6	10.5	1.4	14.2	382.4
Aug-06	43.2	6.8	3.6	15.8	346.7
Sep-06	32.4	6.1	5.0	16.2	339.0
Oct-06	29.4	4.3	8.6	19.9	296.2
Nov-06	21.0	8.0	16.9	25.0	404.3
Dec-06	31.1	5.4	7.1	24.5	326.0
Jan-07	37.9	6.1	9.2	26.0	350.4
Feb-07	46.6	6.2	7.8	26.4	326.7
Mar-07	49.3	5.9	9.0	27.9	335.4
Apr-07	53.4	4.7	3.6	23.0	273.7
May-07	64.9	7.5	2.6	18.9	324.9
Jun-07	60.4	9.0	2.2	15.5	349.0
Jul-07	52.6	9.4	2.5	15.2	354.0
Aug-07	47.8	7.6	5.5	17.3	346.5
Sep-07	46.3	7.2	4.5	16.5	322.3
Oct-07	33.9	6.2	12.6	23.3	360.8
Nov-07	36.0	5.3	10.2	24.1	315.3
Dec-07	35.2	6.0	11.5	32.7	326.4

Table D.1 Monthly averages (2004 – 2007) of air quality data at Airport

D.2 Air Quality Data at Maisonneuve

Month	O3 (Maison)	PM2.5 (Maison)	NO (Maison)	NO2 (Maison)	CO (Maison)
Jan-04	26.1	5.9	41.5	40.8	467.3
Feb-04	21.3	10.3	51.5	50.8	560.7
Mar-04	26.7	8.7	42.3	62.9	503.7
Apr-04	32.5	6.5	33.7	55.9	441.5
May-04	29.2	8.1	30.8	52.3	413.7
Jun-04	36.4	8.9	23.2	41.8	402.4
Jul-04	31.7	11.2	19.2	39.7	350.5
Aug-04	25.1	11.3	25.0	40.0	394.8
Sep-04	19.1	10.0	34.1	41.4	445.1
Oct-04	13.9	7.9	42.3	44.3	456.5
Nov-04	11.9	7.5	49.9	45.0	495.1
Dec-04	18.6	9.2	41.9	47.4	502.4
Jan-05	20.3	8.7	41.7	53.1	511.4
Feb-05	19.2	18.2	60.2	67.4	649.1
Mar-05	37.3	7.9	29.8	55.4	418.7
Apr-05	39.3	6.9	24.3	49.1	426.6
May-05	35.5	6.7	22.9	41.1	389.9
Jun-05	40.7	15.7	19.3	39.6	531.8
Jul-05	36.1	12.2	15.2	34.0	530.0
Aug-05	34.4	12.0	19.5	41.9	558.6
Sep-05	28.1	11.4	21.9	38.9	525.0
Oct-05	17.9	11.3	29.9	38.6	518.3
Nov-05	15.9	7.9	35.6	44.0	613.9
Dec-05	16.2	7.5	36.5	46.9	572.8
Jan-06	17.3	9.9	40.7	51.5	623.5
Feb-06	25.8	7.5	30.5	48.6	569.6
Mar-06	31.8	8.1	28.4	52.1	532.7
Apr-06	38.0	5.5	18.7	41.8	450.2
May-06	36.3	8.0	19.4	37.0	480.8
Jun-06	33.5	7.0	19.9	36.7	561.0
Jul-06	42.3		14.4	34.5	559.2
Aug-06	27.5		21.4	33.8	583.2
Sep-06	18.9	9.7	24.1	33.5	532.3
Oct-06	18.4	7.4	31.5	36.6	515.0
Nov-06	12.2	9.0	40.1	41.0	602.6
Dec-06	18.2	6.2	30.5	41.4	517.6
Jan-07	22.6	6.0	29.6	41.9	509.1
Feb-07	30.7	6.9	29.4	48.6	380.3
Mar-07	32.7	6.4	27.8	45.6	355.7
Apr-07	39.3	5.6	18.1	26.5	277.5
May-07	47.1	8.3	17.4	40.1	273.1
Jun-07	39.4	10.2	19.4	37.6	404.8
Jul-07	36.3	10.8	14.7	34.6	392.8
Aug-07	31.1	7.3	18.5	35.9	400.5
Sep-07	30.6	8.8	16.8	34.2	384.4
Oct-07	19.9	6.4	29.8	42.1	454.2
Nov-07	20.4	5.1	26.1	42.2	338.1
Dec-07	21.4	5.7	27.6	45.1	140.3

Table D.2 Monthly averages (2004 – 2007) of air quality data at Maisonneuve

D.3 Meteorological Data at Airport

Month	SR	Temp	DP	Press	Precip
Jan-04	553.3	-14.8	-20.0	101.0	0.0
Feb-04	460.6	-7.1	-12.7	101.6	0.0
Mar-04	252.6	0.1	-6.8	101.5	0.1
Apr-04	164.7	6.2	-3.2	101.0	0.1
May-04	214.7	14.0	6.9	101.1	0.1
Jun-04	357.1	17.9	10.6	101.0	0.1
Jul-04	631.4	21.6	16.0	100.9	0.2
Aug-04	695.2	19.6	14.5	101.1	0.1
Sep-04	767.0	16.5	11.5	101.6	0.1
Oct-04	883.6	9.3	4.5	101.2	0.0
Nov-04	1201.0	2.2	-2.0	101.5	0.1
Dec-04	808.0	-7.1	-10.1	101.2	0.2
Jan-05	626.8	-10.8	-15.6	102.0	0.1
Feb-05	328.6	-6.2	-10.9	101.6	0.1
Mar-05	193.0	-2.9	-9.8	100.6	0.1
Apr-05	166.7	7.8	-1.1	100.9	0.3
May-05	149.2	11.9	4.4	101.2	0.1
Jun-05	269.7	21.7	14.7	100.9	0.2
Jul-05	435.6	22.7	15.7	101.1	0.2
Aug-05	615.6	22.0	15.6	101.1	0.2
Sep-05	643.6	17.8	12.6	101.3	0.1
Oct-05	759.1	10.2	6.3	101.2	0.2
Nov-05	838.1	4.4	0.1	101.0	0.1
Dec-05	741.8	-5.2	-8.4	101.0	0.1
Jan-06	515.7	-4.5	-7.6	100.9	0.2
Feb-06	308.7	-6.9	-12.3	100.8	0.1
Mar-06	168.1	-0.6	-7.5	101.0	0.0
Apr-06	138.1	8.0	-0.7	101.0	0.1
May-06	165.3	14.6	8.2	100.7	0.2
Jun-06	319.3	19.5	12.9	100.9	0.1
Jul-06	446.7	22.9	16.1	100.9	0.1
Aug-06	468.4	19.7	12.9	101.1	0.2
Sep-06	596.1	15.4	10.9	101.1	0.1
Oct-06		8.1	4.2	100.8	0.2
Nov-06	590.3	4.6	1.4	101.5	0.1
Dec-06	600.9	-0.8	-4.2	101.4	0.1
Jan-07	502.8	-6.9	-11.5	101.1	0.1
Feb-07	396.9	-10.6	-16.4	100.8	0.0
Mar-07		-2.4	-9.1	101.5	0.1
Apr-07		5.9	-0.6	100.7	0.2
May-07		14.1	4.4	101.5	0.1
Jun-07	115.3	20.1	12.8	100.9	0.1
Jul-07	125.8	20.6	15.2	100.9	0.2
Aug-07	145.3	20.5	14.3	101.0	0.1
Sep-07	501.1	17.2	11.3	101.4	0.1
Oct-07	411.6	11.6	7.5	101.2	0.1
Nov-07		1.4	-2.7	101.2	0.2
Dec-07		-6.0	-9.0	101.4	

Table D.3 Monthly averages (2004 – 2007) of meteorological data at Airport

APPENDIX E Typical Monthly Averages Observed in 2004 – 2007 Time Series

E.1 Air Quality Data at Airport

Month	O3 (Airport)	PM2.5 (Airport)	NO (Airport)	NO2 (Airport)	CO (Airport)
1	32.8	7.5	12.1	33.0	360.9
2	40.9	10.6	17.5	40.2	401.2
3	54.3	6.8	9.2	31.0	330.2
4	56.5	5.0	3.7	24.5	287.6
5	57.4	6.7	4.0	21.3	280.0
6	56.1	11.1	3.0	18.5	320.3
7	51.7	9.9	2.7	17.0	334.7
8	44.9	8.7	4.3	17.3	345.1
9	38.7	7.6	5.6	17.9	304.2
10	30.2	6.4	11.6	23.5	303.1
11	27.5	6.8	15.2	26.9	327.3
12	32.3	6.7	12.4	31.1	322.8
Total	42.9	7.7	8.4	25.2	326.3
n	30832	32896	33893	34326	34241

Table E.1 Averages by month of air quality data at Airport

E.2 Air Quality Data at Maisonneuve

Month	O3 (Maison)	PM2.5 (Maison)	NO (Maison)	NO2 (Maison)	CO (Maison)
1	21.6	7.6	38.6	47.0	528.3
2	24.2	10.8	43.1	53.9	540.7
3	32.1	7.7	32.1	54.0	453.0
4	37.3	6.1	23.7	45.6	394.9
5	37.0	7.8	22.6	42.6	389.8
6	37.5	10.9	20.5	39.0	475.0
7	36.6	11.4	15.9	35.7	458.0
8	29.5	10.4	21.1	37.9	484.3
9	24.2	10.0	24.2	37.0	471.7
10	17.5	8.0	33.4	40.4	486.1
11	15.1	7.4	37.9	43.0	512.0
12	18.6	7.5	34.1	45.2	432.6
Total	27.6	8.6	28.8	43.4	468.7
n	34881	30795	34671	34341	34529

Table E.2 Averages by month of air quality data at Maisonneuve

E.3 Meteorological Data at Airport

Month	SR	Temp	DP	Press	Precip
1	549.7	-9.2	-13.7	101.3	0.1
2	371.7	-7.7	-13.1	101.2	0.1
3	204.6	-1.4	-8.3	101.2	0.1
4	156.5	7.0	-1.4	100.9	0.2
5	176.4	13.7	5.9	101.1	0.1
6	265.3	19.8	12.7	100.9	0.1
7	410.2	21.9	15.8	100.9	0.2
8	467.8	20.4	14.3	101.1	0.2
9	629.7	16.7	11.6	101.3	0.1
10	767.0	9.8	5.6	101.1	0.2
11	934.7	3.1	-0.9	101.3	0.1
12	717.0	-4.8	-7.9	101.3	0.7
Total	456.2	7.6	1.7	101.1	0.2
n	28963	34692	34239	34145	34042

Table E.3 Averages by month of meteorological data at Airport

APPENDIX F Hourly Averages (2004 – 2007 Time Series) by Season

Hour	O3 (Airport)	PM2.5 (Airport)	NO (Airport)	NO2 (Airport)	CO (Airport)
0	41.4	8.8	2.5	21.8	329.9
1	40.6	8.9	3.0	20.5	316.1
2	38.7	9.0	2.2	19.8	308.0
3	36.1	9.2	2.3	20.7	306.0
4	33.4	9.6	3.9	22.5	310.0
5	32.5	10.2	7.3	24.2	338.3
6	36.1	10.1	9.7	23.9	351.2
7	41.9	9.8	8.9	21.7	346.9
8	49.3	9.3	6.7	18.9	331.6
9	57.3	9.1	4.8	15.6	312.9
10	66.9	9.0	2.9	12.3	296.7
11	73.1	8.6	2.2	10.9	279.3
12	77.3	8.3	2.1	10.5	275.5
13	78.5	8.3	2.0	10.8	275.0
14	79.4	8.3	2.0	11.0	276.0
15	79.0	8.1	1.7	11.2	268.2
16	76.7	8.0	1.7	13.2	277.1
17	73.9	8.4	1.5	15.2	285.8
18	68.2	8.7	1.1	17.8	299.1
19	57.1	9.1	1.4	25.3	321.3
20	50.0	9.7	1.2	26.9	340.9
21	45.1	9.4	2.1	28.0	344.6
22	42.4	9.0	2.4	26.4	347.3
23	41.3	8.8	2.5	24.2	341.7
Total	54.8	9.0	3.3	18.9	311.7
n	7652	7228	8297	8278	8279

Table F.1 Hourly averages of air quality data at Airport (summer)

Hour	O3 (Airport)	PM2.5 (Airport)	NO (Airport)	NO2 (Airport)	CO (Airport)
0	28.4	7.6	11.1	30.7	345.7
1	29.2	7.4	10.8	29.2	323.8
2	29.5	6.9	10.1	28.0	314.5
3	29.4	6.3	9.3	27.4	295.6
4	29.1	6.0	9.2	27.3	281.6
5	26.9	6.0	10.4	29.3	283.8
6	24.1	6.5	14.8	33.7	325.7
7	22.8	7.1	20.1	36.5	370.9
8	26.8	7.4	22.6	33.3	384.0
9	31.9	6.9	20.9	28.9	367.8
10	36.5	6.1	17.7	24.0	310.8
11	39.4	5.7	16.2	22.6	297.7
12	41.5	5.9	13.8	21.3	292.4
13	41.5	6.2	12.6	22.6	287.7
14	40.5	6.7	11.6	24.3	311.9
15	37.1	6.6	11.1	27.7	326.5
16	31.3	6.7	11.2	33.4	347.7
17	28.0	7.3	11.9	36.8	388.4
18	27.3	7.8	12.1	37.2	384.9
19	27.3	8.0	12.5	36.4	380.2
20	27.3	8.2	12.6	36.1	369.3
21	27.3	8.5	11.7	34.7	371.2
22	27.3	8.3	11.6	33.8	365.4
23	27.5	8.0	12.0	32.8	363.5
Total	30.7	7.0	13.2	30.4	337.2
n	8030	8627	8770	8770	8720

Table F.2 Hourly averages of air quality data at Airport (winter)

Hour	O3 (Maison)	PM2.5 (Maison)	NO (Maison)	NO2 (Maison)	CO (Maison)
0	33.9	7.6	11.2	34.1	364.1
1	35.3	7.6	8.9	30.4	327.4
2	33.8	7.6	9.2	30.1	316.3
3	34.4	7.8	6.7	27.3	227.7
4	30.8	8.0	8.8	29.1	228.0
5	25.0	8.4	19.6	35.9	289.1
6	21.2	9.2	31.6	42.0	382.3
7	23.3	9.4	35.4	43.1	440.3
8	27.7	9.2	33.9	42.8	431.8
9	32.9	8.8	29.8	41.8	473.6
10	40.7	9.5	27.2	40.5	463.0
11	47.2	10.5	23.0	38.0	487.1
12	51.1	9.6	21.4	37.9	465.5
13	51.5	8.9	21.5	39.2	465.4
14	50.1	8.9	21.1	40.7	482.2
15	48.4	9.5	21.5	42.7	542.8
16	45.2	10.3	22.1	45.3	598.5
17	47.1	12.0	17.8	41.5	535.2
18	46.0	13.9	14.2	39.6	508.1
19	39.6	15.0	15.4	42.7	525.5
20	32.1	15.0	20.5	47.0	561.8
21	30.5	12.0	19.1	45.5	511.6
22	29.7	9.4	17.2	42.8	499.6
23	31.1	8.0	15.1	38.9	455.1
Total	37.0	9.8	19.6	39.1	440.7
n	8777	7222	8676	8676	8772

Table F.3 Hourly averages of air quality data at Maisonneuve (Summer)

Hour	O3 (Maison)	PM2.5 (Maison)	NO (Maison)	NO2 (Maison)	CO (Maison)
0	19.8	5.9	22.6	40.6	425.3
1	21.1	5.9	20.6	39.0	336.2
2	22.1	5.3	20.2	37.6	298.6
3	22.5	4.9	17.5	36.3	287.6
4	23.3	4.5	15.8	35.2	222.2
5	21.8	4.6	17.8	36.6	226.3
6	18.4	5.1	26.0	41.6	280.5
7	15.0	5.9	41.1	47.2	378.0
8	15.1	6.6	53.3	49.1	452.4
9	16.7	6.7	54.0	48.5	471.6
10	18.6	6.6	55.5	47.2	524.8
11	19.6	7.2	54.5	47.0	541.4
12	21.4	8.3	47.5	45.2	574.1
13	21.3	8.4	47.1	46.1	582.8
14	20.5	7.3	47.6	47.1	588.2
15	17.8	7.4	47.8	49.7	636.1
16	15.1	8.1	48.9	52.0	737.9
17	13.6	9.7	49.2	53.2	784.4
18	14.5	11.3	42.4	51.4	678.4
19	15.9	11.7	35.0	48.7	615.0
20	16.9	11.9	32.9	47.4	566.3
21	16.5	10.6	33.8	47.3	577.0
22	17.4	8.7	29.9	45.3	513.4
23	18.4	6.9	25.4	43.0	483.1
Total	18.5	7.5	36.8	45.1	490.4
n	8761	8252	8678	8678	8660

Table F.4 Hourly averages of air quality data at Maisonneuve (Winter)

Hour	SR	Temp	DP	Press	Precip
0	1.0	16.4	11.1	101.0	0.1
1	1.0	15.9	11.1	101.0	0.1
2	1.0	15.4	11.0	101.0	0.1
3	0.9	15.0	10.9	101.0	0.1
4	0.9	14.6	10.8	101.0	0.1
5	0.9	14.5	10.8	101.0	0.1
6	1.2	15.4	11.1	101.0	0.1
7	20.6	16.3	11.2	101.1	0.1
8	143.7	17.3	11.5	101.1	0.1
9	427.2	18.3	11.7	101.1	0.1
10	734.8	19.3	11.9	101.1	0.1
11	985.2	20.2	12.0	101.1	0.1
12	1122.7	21.0	12.0	101.0	0.2
13	1138.8	21.5	11.9	101.0	0.1
14	1011.3	21.9	11.9	101.0	0.1
15	776.9	22.1	11.7	100.9	0.2
16	475.0	22.0	11.6	100.9	0.2
17	179.7	21.7	11.6	100.9	0.2
18	30.8	21.2	11.5	100.9	0.2
19	1.7	20.3	11.4	100.9	0.1
20	1.3	19.3	11.4	100.9	0.1
21	1.2	18.5	11.5	101.0	0.1
22	1.1	17.7	11.4	101.0	0.1
23	1.1	17.1	11.3	101.0	0.1
Total	294.0	18.5	11.4	101.0	0.1
n	8080	8832	8722	8596	8589

Table F.5 Hourly averages of meteorological data at Airport (Summer)

Hour	SR	Temp	DP	Press	Precip
0	0.4	-4.2	-7.8	101.3	1.1
1	0.4	-4.4	-7.8	101.3	0.7
2	0.4	-4.6	-7.9	101.3	0.1
3	0.4	-4.7	-7.9	101.3	0.1
4	0.4	-4.8	-8.0	101.3	0.1
5	10.6	-5.0	-8.1	101.3	0.1
6	134.8	-5.1	-8.2	101.3	0.1
7	449.4	-5.2	-8.2	101.3	0.1
8	855.3	-5.1	-8.1	101.3	0.1
9	1301.1	-4.5	-7.9	101.3	0.2
10	1680.1	-4.0	-7.8	101.3	0.1
11	1949.1	-3.4	-7.6	101.3	0.1
12	2076.4	-2.9	-7.5	101.2	0.1
13	2063.1	-2.6	-7.5	101.2	0.1
14	1883.8	-2.4	-7.3	101.2	0.1
15	1657.3	-2.4	-7.3	101.2	0.2
16	1279.2	-2.6	-7.4	101.2	0.7
17	857.7	-3.0	-7.5	101.3	0.5
18	449.6	-3.2	-7.5	101.3	0.6
19	142.2	-3.5	-7.7	101.3	0.7
20	15.8	-3.7	-7.7	101.3	0.4
21	0.5	-3.9	-7.8	101.3	0.5
22	0.4	-4.1	-7.9	101.3	0.7
23	0.4	-4.3	-7.9	101.3	0.3
Total	700.8	-3.9	-7.8	101.3	0.3
n	6964	8584	8538	8541	8470

Table F.6 Hourly averages of meteorological data at Airport (Winter)

APPENDIX G O_3 and $PM_{2.5}$ Averages at Airport and Maisonneuve by Wind Direction (2004 – 2007 Time Series)

Season	Period	WD	O3 (Airport)	O3 (Maison)	PM2.5 (Airport)	PM2.5 (Maison)
Summer	Day	0	61.4	34.3	6.0	8.3
		1	62.2	40.0	6.5	7.6
		2	74.2	52.7	7.5	8.4
		3	79.6	53.3	9.7	11.8
		4	85.9	54.2	9.5	11.6
		5	93.3	62.1	11.5	12.6
		6	68.9	40.8	5.8	6.8
		7	60.8	31.4	4.5	6.2
		8	86.6	49.5	10.2	11.3
	Night	0	28.2	24.7	6.7	5.3
		1	31.3	26.9	7.6	6.2
		2	34.7	35.8	8.3	6.7
		3	36.5	30.5	10.1	9.2
		4	49.5	37.0	13.3	12.1
		5	52.9	42.7	11.0	10.6
		6	44.5	36.5	7.8	7.4
		7	28.1	22.5	4.9	4.1
		8	16.4	22.3	12.0	9.3
Winter	Day	0	28.5	14.2	13.0	14.7
		1	26.4	19.0	9.4	9.7
		2	29.8	23.0	5.1	5.2
		3	41.1	19.8	4.9	8.0
		4	39.0	13.4	5.4	8.6
		5	40.5	17.7	6.6	7.4
		6	50.8	24.7	3.2	4.8
		7	45.9	17.7	3.4	5.2
		8	31.4	13.8	12.6	15.2
	Night	0	21.0	16.2	11.9	9.4
		1	22.3	21.4	7.8	6.1
		2	20.6	22.6	7.0	6.3
		3	32.4	18.7	5.5	6.0
		4	28.4	11.3	7.3	8.0
		5	30.7	19.3	7.4	6.2
		6	38.0	27.0	4.7	3.6
		7	39.0	25.5	6.3	4.9
		8	9.8	12.4	14.2	9.6

Table G.1 O_3 and $PM_{2.5}$ Averages by Wind Direction

APPENDIX H Hourly Averages by Season by Period (2004 – 2007 Time Series)

H.1 Summer

Summer/Day	O3 (Airport)	PM2.5 (Airport)	NO (Airport)	NO2 (Airport)	CO (Airport)
Moments					
Mean	**77.3**	**8.3**	**1.9**	**11.3**	**275.2**
Std Dev	28.8	8.5	3.0	8.1	117.1
Std Err Mean	0.7	0.2	0.1	0.2	2.6
upper 95% Mean	78.6	8.7	2.1	11.6	280.2
lower 95% Mean	76.1	7.9	1.8	10.9	270.1
Variance	827.4	72.2	8.7	65.7	13712.6
Skewness	0.2	1.9	6.4	1.6	0.2
Kurtosis	0.1	4.4	65.1	4.0	0.3
n	1903.0	1789.0	2062.0	2058.0	2058.0
Percentiles					
100.0%	170.0	55.0	46.0	77.0	799.9
99.5%	162.5	44.0	21.7	41.7	599.9
97.5%	137.4	33.0	8.0	33.0	499.9
90.0%	115.0	19.0	4.0	22.0	399.9
75.0%	96.0	11.0	2.0	15.0	399.9
50.0%	76.0	5.0	1.0	9.0	300.0
25.0%	58.0	3.0	1.0	6.0	200.0
10.0%	43.0	1.0	0.0	3.0	100.0
2.5%	21.0	0.0	0.0	2.0	100.0
0.5%	9.5	0.0	0.0	1.0	0.0
0.0%	5.0	0.0	0.0	0.0	0.0

Table H.1 Hourly averages of air quality data at Airport (summer/day)

Summer/Day	O3 (Maison)	PM2.5 (Maison)	NO (Maison)	NO2 (Maison)	CO (Maison)
Moments					
Mean	**48.9**	**9.6**	**21.8**	**40.6**	**507.2**
Std Dev	23.7	8.7	14.5	15.1	230.1
Std Err Mean	0.5	0.2	0.3	0.3	4.9
upper 95% Mean	49.9	10.0	22.4	41.3	516.8
lower 95% Mean	47.9	9.2	21.2	40.0	497.5
Variance	560.6	76.2	209.0	229.3	52944.7
Skewness	0.4	1.7	1.6	0.7	0.6
Kurtosis	0.4	3.5	4.1	1.0	0.8
n	2192.0	1793.0	2168.0	2168.0	2190.0
Percentiles					
100.0%	145.0	54.0	122.0	119.0	1799.7
99.5%	127.1	46.0	84.0	94.2	1204.3
97.5%	98.0	33.0	61.0	73.8	999.8
90.0%	78.0	22.0	40.0	60.0	799.9
75.0%	65.0	13.0	29.0	50.0	699.9
50.0%	48.0	7.0	18.0	40.0	499.9
25.0%	32.0	3.0	11.0	29.0	299.9
10.0%	19.0	2.0	7.0	22.0	200.0
2.5%	6.0	0.0	4.0	15.0	100.0
0.5%	1.0	0.0	2.0	12.9	100.0
0.0%	0.0	0.0	1.0	10.0	0.0

Table H.2 Hourly averages of air quality data at Maisonneuve (summer/day)

Summer/Day	SR	Temp	DP	Press	Precip	WS	WDI
Moments							
Mean	**918.7**	**21.5**	**11.9**	**101.0**	**0.1**	**17.8**	**1.3**
Std Dev	667.1	5.8	6.3	0.6	0.9	8.3	0.7
Std Err Mean	14.9	0.1	0.1	0.0	0.0	0.2	0.0
upper 95% Mean	947.9	21.7	12.1	101.0	0.2	18.2	1.3
lower 95% Mean	889.6	21.2	11.6	101.0	0.1	17.5	1.3
Variance	445034.6	33.1	39.2	0.4	0.8	68.9	0.5
Skewness	0.6	-0.5	-0.8	-0.2	11.4	0.5	-0.8
Kurtosis	-0.5	-0.4	0.3	0.6	171.9	0.0	-1.0
n	2017.0	2208.0	2177.0	2144.0	2143.0	2208.0	2208.0
Percentiles							
100.0%	2804.0	32.7	23.2	103.1	19.3	52.0	2.0
99.5%	2739.6	32.0	22.5	102.7	6.0	42.9	2.0
97.5%	2389.2	30.6	21.1	102.3	1.8	37.0	2.0
90.0%	1888.2	28.4	19.0	101.7	0.0	30.0	2.0
75.0%	1382.5	25.8	16.8	101.4	0.0	24.0	2.0
50.0%	818.0	22.4	12.7	101.0	0.0	17.0	1.7
25.0%	328.0	17.6	8.2	100.6	0.0	11.0	1.0
10.0%	138.0	12.7	3.4	100.2	0.0	7.0	0.0
2.5%	61.4	9.2	-3.2	99.6	0.0	4.0	0.0
0.5%	28.1	6.8	-7.4	99.1	0.0	0.0	0.0
0.0%	15.0	5.7	-9.6	98.9	0.0	0.0	0.0

Table H.3 Hourly averages of meteorological data at Airport (summer/day)

Summer/Night	O3 (Airport)	PM2.5 (Airport)	NO (Airport)	NO2 (Airport)	CO (Airport)
Moments					
Mean	**39.1**	**9.0**	**2.7**	**22.3**	**322.7**
Std Dev	26.7	8.4	10.7	16.5	138.6
Std Err Mean	0.6	0.2	0.2	0.3	2.8
upper 95% Mean	40.2	9.4	3.1	22.9	328.2
lower 95% Mean	38.0	8.7	2.3	21.6	317.2
Variance	715.3	69.7	115.3	271.3	19198.6
Skewness	0.7	1.9	7.4	1.5	0.8
Kurtosis	0.4	4.7	66.4	2.8	2.2
n	2241.0	2125.0	2435.0	2428.0	2428.0
Percentiles					
100.0%	152.0	56.0	148.0	108.0	1099.8
99.5%	123.8	48.0	87.5	89.0	885.4
97.5%	102.0	32.0	28.0	66.0	599.9
90.0%	74.0	20.0	5.0	45.0	499.9
75.0%	55.0	12.0	1.0	29.0	399.9
50.0%	37.0	7.0	0.0	18.0	299.9
25.0%	18.0	3.0	0.0	11.0	200.0
10.0%	5.0	1.0	0.0	7.0	200.0
2.5%	0.0	0.0	0.0	4.0	100.0
0.5%	0.0	0.0	0.0	2.0	0.0
0.0%	0.0	0.0	0.0	0.0	0.0

Table H.4 Hourly averages of air quality data at Airport (summer/night)

Summer/Night	O3 (Maison)	PM2.5 (Maison)	NO (Maison)	NO2 (Maison)	CO (Maison)
Moments					
Mean	**32.7**	**8.0**	**11.0**	**33.2**	**345.4**
Std Dev	21.2	7.7	11.3	15.6	304.3
Std Err Mean	0.4	0.2	0.2	0.3	6.0
upper 95% Mean	33.5	8.3	11.5	33.8	357.1
lower 95% Mean	31.9	7.7	10.6	32.6	333.6
Variance	449.5	59.1	127.0	243.2	92581.4
Skewness	1.0	1.7	4.7	1.3	10.9
Kurtosis	1.6	3.8	47.8	3.8	228.0
n	2575.0	2122.0	2547.0	2547.0	2575.0
Percentiles					
100.0%	129.0	46.0	198.0	173.0	7598.7
99.5%	112.1	44.0	66.3	87.3	1199.8
97.5%	85.0	28.0	39.3	72.0	899.9
90.0%	60.0	19.0	22.0	54.0	599.9
75.0%	44.0	11.0	14.0	41.0	499.9
50.0%	30.0	6.0	8.0	30.0	299.9
25.0%	17.0	3.0	5.0	22.0	200.0
10.0%	8.0	1.0	2.0	17.0	100.0
2.5%	1.0	0.0	1.0	12.0	0.0
0.5%	0.0	0.0	1.0	8.0	0.0
0.0%	0.0	0.0	0.0	5.0	0.0

Table H.5 Hourly averages of air quality data at Maisonneuve (summer/night)

Summer/Night	SR	Temp	DP	Press	Precip	WS	WDI
Moments							
Mean	**1.0**	**16.0**	**11.1**	**101.0**	**0.1**	**11.6**	**1.1**
Std Dev	2.9	5.3	6.2	0.6	0.8	7.0	0.8
Std Err Mean	0.1	0.1	0.1	0.0	0.0	0.1	0.0
upper 95% Mean	1.1	16.2	11.3	101.0	0.1	11.8	1.1
lower 95% Mean	0.9	15.8	10.8	101.0	0.1	11.3	1.1
Variance	8.6	28.1	38.3	0.4	0.6	48.4	0.6
Skewness	4.2	-0.4	-0.7	-0.2	11.9	0.7	-0.2
Kurtosis	18.5	-0.4	0.1	1.0	183.0	0.4	-1.6
n	2359.0	2576.0	2549.0	2512.0	2508.0	2576.0	2576.0
Percentiles							
100.0%	22.0	27.0	22.3	102.8	17.4	43.0	2.0
99.5%	19.0	26.2	21.6	102.7	5.9	33.0	2.0
97.5%	12.0	24.8	20.2	102.3	1.4	28.0	2.0
90.0%	2.0	22.6	18.3	101.7	0.0	20.6	2.0
75.0%	1.0	20.0	15.9	101.4	0.0	15.0	1.7
50.0%	0.0	16.6	11.8	101.0	0.0	11.0	1.0
25.0%	0.0	12.4	7.6	100.6	0.0	7.0	0.3
10.0%	0.0	8.6	1.9	100.3	0.0	4.0	0.0
2.5%	0.0	4.6	-3.0	99.6	0.0	0.0	0.0
0.5%	0.0	2.3	-7.4	99.1	0.0	0.0	0.0
0.0%	0.0	0.1	-9.3	98.7	0.0	0.0	0.0

Table H.6 Hourly averages of meteorological data at Airport (summer/night)

H.2 Winter

Winter/Day	O3 (Airport)	PM2.5 (Airport)	NO (Airport)	NO2 (Airport)	CO (Airport)
Moments					
Mean	**38.5**	**6.3**	**12.7**	**25.4**	**310.8**
Std Dev	19.4	7.3	24.1	19.4	213.6
Std Err Mean	0.4	0.2	0.5	0.4	4.6
upper 95% Mean	39.4	6.6	13.7	26.2	319.8
lower 95% Mean	37.7	6.0	11.7	24.5	301.8
Variance	377.1	53.2	578.4	375.0	45624.2
Skewness	-0.3	2.3	5.5	1.2	2.3
Kurtosis	-1.0	6.6	45.6	1.0	10.8
n	1986.0	2130.0	2166.0	2166.0	2162.0
Percentiles					
100.0%	87.0	47.0	329.0	116.0	2199.6
99.5%	72.0	41.0	147.2	88.2	1199.8
97.5%	68.0	28.0	73.0	73.0	899.9
90.0%	63.0	15.0	33.0	54.0	599.9
75.0%	55.0	8.0	12.0	35.0	399.9
50.0%	42.0	4.0	5.0	20.0	299.9
25.0%	23.0	2.0	2.0	10.0	200.0
10.0%	9.0	0.0	1.0	6.0	100.0
2.5%	3.0	0.0	0.0	3.0	0.0
0.5%	1.0	0.0	0.0	2.0	0.0
0.0%	0.0	0.0	0.0	1.0	0.0

Table H.7 Hourly averages of air quality data at Airport (winter/day)

Winter/Day	O3 (Maison)	PM2.5 (Maison)	NO (Maison)	NO2 (Maison)	CO (Maison)
Moments					
Mean	**19.3**	**7.8**	**48.9**	**47.9**	**610.6**
Std Dev	12.0	7.3	32.4	14.2	296.3
Std Err Mean	0.3	0.2	0.7	0.3	6.4
upper 95% Mean	19.8	8.1	50.3	48.5	623.1
lower 95% Mean	18.8	7.5	47.5	47.3	598.1
Variance	145.1	53.0	1050.7	200.4	87815.5
Skewness	0.4	2.2	2.2	0.3	0.8
Kurtosis	-0.6	6.7	9.6	0.0	2.5
n	2185.0	2052.0	2157.0	2157.0	2152.0
Percentiles					
100.0%	54.0	62.0	327.0	108.0	2299.6
99.5%	49.0	37.7	224.6	91.0	1723.2
97.5%	45.0	29.0	127.0	77.0	1199.8
90.0%	37.0	17.0	86.0	66.0	999.8
75.0%	27.0	10.0	63.0	57.0	799.9
50.0%	18.0	6.0	43.0	47.0	599.9
25.0%	9.0	3.0	27.0	38.0	399.9
10.0%	4.0	1.0	17.0	30.0	299.9
2.5%	2.0	0.0	10.0	23.0	0.0
0.5%	1.0	0.0	5.8	18.0	0.0
0.0%	0.0	0.0	2.0	13.0	0.0

Table H.8 Hourly averages of air quality data at Maisonneuve (winter/day)

Winter/Day	SR	Temp	DP	Press	Precip	WS	WDI
Moments							
Mean	**1817.8**	**-2.7**	**-7.4**	**101.2**	**0.2**	**18.8**	**1.1**
Std Dev	890.1	8.3	9.1	1.1	4.2	10.1	0.8
Std Err Mean	21.3	0.2	0.2	0.0	0.1	0.2	0.0
upper 95% Mean	1859.6	-2.4	-7.1	101.3	0.4	19.2	1.1
lower 95% Mean	1776.0	-3.1	-7.8	101.2	0.1	18.4	1.1
Variance	792285.9	68.7	83.1	1.1	17.5	101.1	0.6
Skewness	0.1	-0.4	-0.5	-0.2	43.6	0.5	-0.2
Kurtosis	-0.2	-0.3	0.0	-0.2	1964.6	0.1	-1.7
n	1743.0	2147.0	2137.0	2134.0	2117.0	2147.0	2208.0
Percentiles							
100.0%	4339.0	18.7	15.1	104.1	188.8	63.0	2.0
99.5%	4251.2	15.7	12.5	103.8	4.2	48.0	2.0
97.5%	3749.2	11.0	7.5	103.2	1.8	41.0	2.0
90.0%	2887.4	7.4	3.1	102.6	0.0	32.0	2.0
75.0%	2418.0	3.6	-1.0	102.0	0.0	26.0	1.7
50.0%	1840.0	-1.6	-6.1	101.2	0.0	19.0	1.7
25.0%	1206.0	-8.9	-13.3	100.6	0.0	11.0	0.3
10.0%	538.0	-13.5	-19.0	99.8	0.0	7.0	0.0
2.5%	177.8	-21.1	-29.4	99.0	0.0	0.0	0.0
0.5%	84.7	-24.8	-32.6	98.5	0.0	0.0	0.0
0.0%	24.0	-26.8	-34.3	98.3	0.0	0.0	0.0

Table H.9 Hourly averages of meteorological data at Airport (winter/day)

Winter/Night	O3 (Airport)	PM2.5 (Airport)	NO (Airport)	NO2 (Airport)	CO (Airport)
Moments					
Mean	**28.6**	**7.2**	**10.6**	**29.9**	**327.1**
Std Dev	19.5	7.7	25.7	20.9	238.0
Std Err Mean	0.4	0.2	0.5	0.4	4.7
upper 95% Mean	29.4	7.5	11.6	30.7	336.4
lower 95% Mean	27.8	6.9	9.6	29.1	317.9
Variance	378.5	59.1	662.8	438.8	56645.0
Skewness	0.1	2.2	4.5	0.7	2.8
Kurtosis	-1.2	7.0	26.7	-0.3	13.1
n	2359.0	2532.0	2576.0	2576.0	2555.0
Percentiles					
100.0%	78.0	64.0	264.0	116.0	2199.6
99.5%	70.0	45.0	174.5	86.1	1699.7
97.5%	63.0	27.7	87.0	74.6	999.8
90.0%	55.0	17.0	31.0	62.0	599.9
75.0%	44.0	10.0	7.0	45.0	399.9
50.0%	29.0	5.0	1.0	25.0	299.9
25.0%	10.0	2.0	0.0	13.0	200.0
10.0%	3.0	1.0	0.0	6.0	100.0
2.5%	0.0	0.0	0.0	3.0	100.0
0.5%	0.0	0.0	0.0	2.0	0.0
0.0%	0.0	0.0	0.0	1.0	0.0

Table H.10 Hourly averages of air quality data at Airport (winter/night)

Winter/Night	O3 (Maison)	PM2.5 (Maison)	NO (Maison)	NO2 (Maison)	CO (Maison)
Moments					
Mean	**20.7**	**6.0**	**21.7**	**39.6**	**366.4**
Std Dev	13.2	6.5	21.1	14.9	255.5
Std Err Mean	0.3	0.1	0.4	0.3	5.1
upper 95% Mean	21.2	6.3	22.5	40.1	376.4
lower 95% Mean	20.2	5.8	20.9	39.0	356.5
Variance	174.8	41.6	446.5	220.6	65264.0
Skewness	0.3	2.5	3.0	0.5	1.5
Kurtosis	-0.9	13.1	12.4	-0.1	5.6
n	2567.0	2411.0	2544.0	2544.0	2546.0
Percentiles					
100.0%	58.0	73.0	182.0	98.0	2599.6
99.5%	53.0	30.9	139.5	82.0	1299.8
97.5%	47.0	22.0	84.0	72.0	999.8
90.0%	39.0	14.0	44.0	60.0	699.9
75.0%	31.0	9.0	26.0	50.0	499.9
50.0%	20.0	4.0	15.0	38.0	299.9
25.0%	9.0	2.0	9.0	28.0	200.0
10.0%	4.0	0.0	6.0	21.0	100.0
2.5%	2.0	0.0	3.0	16.0	0.0
0.5%	1.0	0.0	1.0	12.0	0.0
0.0%	0.0	0.0	0.0	10.0	0.0

Table H.11 Hourly averages of air quality data at Maisonneuve (winter/night)

Winter/Night	SR	Temp	DP	Press	Precip	WS	WDI
Moments							
Mean	**0.4**	**-4.5**	**-7.9**	**101.3**	**0.4**	**15.5**	**1.0**
Std Dev	0.8	8.3	9.2	1.0	9.2	9.5	0.8
Std Err Mean	0.0	0.2	0.2	0.0	0.2	0.2	0.0
upper 95% Mean	0.4	-4.1	-7.5	101.3	0.8	15.9	1.1
lower 95% Mean	0.4	-4.8	-8.2	101.2	0.1	15.2	1.0
Variance	0.7	68.8	85.3	1.0	84.4	90.4	0.6
Skewness	3.6	-0.5	-0.6	-0.1	30.9	0.9	-0.1
Kurtosis	19.1	-0.3	0.0	-0.4	1033.0	1.1	-1.7
n	2026.0	2506.0	2490.0	2492.0	2467.0	2505.0	2576.0
Percentiles							
100.0%	9.0	16.7	15.4	103.9	350.6	59.0	2.0
99.5%	5.9	12.9	9.1	103.7	4.0	48.0	2.0
97.5%	3.0	8.6	6.7	103.2	1.6	37.0	2.0
90.0%	1.0	5.0	2.5	102.6	0.0	28.0	2.0
75.0%	1.0	1.7	-1.2	102.0	0.0	20.0	1.7
50.0%	0.0	-3.1	-6.2	101.3	0.0	13.0	1.0
25.0%	0.0	-10.3	-14.2	100.6	0.0	9.0	0.3
10.0%	0.0	-15.9	-20.3	99.9	0.0	6.0	0.0
2.5%	0.0	-23.1	-29.8	99.3	0.0	0.0	0.0
0.5%	0.0	-25.9	-32.4	98.6	0.0	0.0	0.0
0.0%	0.0	-27.5	-34.4	98.2	0.0	0.0	0.0

Table H.12 Hourly averages of meteorological data at Airport (winter/night)

Appendix I Sample Model Outputs For Case Study 1 (Day Period)

Response OP (Airport) Summer Day

Summary of Fit	
R2	0.68
R2 (Adj)	0.67
RMSE	17.44
Mean of Response	78.93
Observations	506

Analysis of Variance	DF	SS	MS	F Ratio	Prob > F
Model	7	314801	44972	148	<.0001
Error	498	151470	304		
C. Total	505	466272			

Parameter Estimates	Estimate	Std Error	t Ratio	Prob>|t|
Intercept	-629.04	149.50	-4.21	<.0001
PM2.5 (Airport)	1.84	0.13	14.52	<.0001
NO (Airport)	-1.66	0.23	-7.32	<.0001
CO (Airport)	0.036	0.011	3.29	0.0011
Temp	2.81	0.24	11.66	<.0001
DP	-2.90	0.29	-10.09	<.0001
Press	6.50	1.49	4.37	<.0001
WDI	4.53	1.09	4.13	<.0001

Table I.1 Model output MLR

	PC1	**PC2**	**PC3**	**PC4**	**PC5**	**PC6**	**PC7**	**PC8**	**PC9**	**PC10**	**PC11**
Eigenvalue	2.97	2.09	1.39	1.05	0.90	0.81	0.53	0.49	0.34	0.30	0.12
Percent	27.02	19.00	12.66	9.59	8.15	7.36	4.86	4.45	3.13	2.73	1.05
Cum Percent	27.02	46.02	58.68	68.27	76.42	83.78	88.64	93.09	96.22	98.95	100.00
PM2.5 (Airpo	0.45	0.17	-0.05	-0.19	0.19	0.15	0.09	-0.36	0.60	-0.41	-0.08
NO (Airport)	0.18	-0.49	0.03	-0.22	-0.25	-0.12	0.32	0.60	0.13	-0.34	0.02
NO2 (Airport	0.28	-0.50	0.05	-0.15	-0.01	0.00	0.16	-0.28	0.18	0.71	-0.02
CO (Airport)	0.47	-0.16	-0.18	-0.06	0.06	0.07	0.08	-0.29	-0.70	-0.25	0.27
SR	0.10	0.04	0.42	0.59	-0.56	0.07	0.25	-0.24	0.06	-0.10	0.10
Temp	0.39	0.39	0.19	-0.04	0.05	0.15	-0.11	0.41	0.09	0.28	0.60
DP	0.50	0.19	-0.04	0.20	-0.05	0.10	-0.12	0.29	-0.17	0.15	-0.71
Press	-0.12	0.15	0.62	-0.24	0.39	0.16	0.51	0.02	-0.23	0.01	-0.18
Precip	0.03	-0.22	-0.16	0.66	0.63	-0.06	0.20	0.16	0.12	-0.03	0.10
WS	-0.18	0.16	-0.52	0.00	-0.17	0.61	0.49	0.07	0.01	0.14	0.02
WDI	0.09	0.40	-0.25	-0.05	-0.08	-0.72	0.47	-0.05	-0.01	0.14	0.00

Table I.2 Model output PCA

Response OP (Airport) Summer Day

Summary of Fit	
R2	0.68
R2 (Adj)	0.67
RMSE	17.47
Mean of Response	78.93
Observations	506

Analysis of Variance	DF	SS	MS	F Ratio	Prob > F
Model	9	314833	34981	115	<.0001
Error	496	151439	305		
C. Total	505	466272			

Parameter Estimates	Estimate	Std Error	t Ratio	Prob>|t|
Intercept	78.93	0.78	101.61	<.0001
Prin Comp 1	6.42	0.45	14.23	<.0001
Prin Comp 2	10.96	0.54	20.38	<.0001
Prin Comp 3	4.29	0.66	6.52	<.0001
Prin Comp 4	-7.58	0.76	-10.01	<.0001
Prin Comp 5	7.69	0.82	9.36	<.0001
Prin Comp 8	-8.57	1.11	-7.71	<.0001
Prin Comp 9	8.87	1.33	6.69	<.0001
Prin Comp 10	-3.81	1.42	-2.69	0.0075
Prin Comp 11	19.38	2.29	8.47	<.0001

Table I.3 Model output PCR

# BFs	TotVar	DirVar	EffPar	GCV	Learn MSE	Test MSE
19	9	9	40.00	278.48	245.91	278.22
18	9	9	37.95	276.05	245.41	278.21
17	9	9	35.89	273.66	244.92	280.36
16	9	9	33.84	271.41	244.54	280.39
15	9	9	31.79	269.85	244.74	278.88
14	9	9	29.74	268.52	245.15	278.46
** 13	8	8	27.68	267.70	246.02	274.81
12	8	8	25.63	266.90	246.89	277.49
11	7	7	23.58	267.61	249.16	274.97
10	7	7	21.53	268.47	251.58	279.33
9	7	7	19.47	269.82	254.48	275.59
8	6	6	17.42	273.43	259.55	279.00
7	6	6	15.37	279.15	266.66	280.35
6	5	5	13.32	290.07	278.86	296.82
5	4	4	11.26	307.07	297.07	336.73
4	4	4	9.21	329.41	320.69	331.50
3	3	3	7.16	365.38	357.95	370.62
2	2	2	5.11	507.81	500.58	522.28
1	1	1	3.05	565.75	561.17	655.35
0	0	0	1.00	925.14	921.49	852.28

Table I.4 Model identification MARS 1

Response OP (Airport) Summer Day

Summary of Fit	
R2	0.74
R2 (Adj)	0.73
RMSE	15.68
Mean of Response	78.93
Observations	506

Analysis of Variance	DF	SS	MS	F Ratio	Prob > F
Model	13	345231	26556	108	<.0001
Error	492	121041	246		
C. Total	505	466272			

Parameter Estimates	Estimate	Std Error	t Ratio	Prob>|t|
Constant	107.34	5.40	19.86	<.0001
BF2	-2.64	0.16	-16.25	<.0001
BF4	-3.48	0.73	-4.76	<.0001
BF5	6.90	1.56	4.42	<.0001
BF6	22.42	8.72	2.57	0.0104
BF8	2.74	0.42	6.50	<.0001
B11	-3.12	0.47	-6.64	<.0001
BF12	2.73	0.31	8.92	<.0001
BF14	-2.57	0.23	-11.35	<.0001
BF15	20.96	6.53	3.21	0.0014
BF16	-2.87	1.24	-2.31	0.0212
BF17	-1.33	0.35	-3.80	0.0002
BF19	0.00	0.00	-1.66	0.0981
BF20	-0.23	0.09	-2.65	0.0083

BF2 = max (0 , 24 - PM2.5 (AIRPORT))
BF4 = max(0, 6 - NO2 (AIRPORT))
BF5 = max (0, PRESS - 99.69)
BF6 = max (0, 99.69 - PRESS)
BF8 = max (0, 11.00 - NO (AIRPORT))
BF11 = max(0, DP - 13.80)
BF12 = max (0, 13.80 - DP)
BF14 = max (0, 28.40 - TEMP)
BF15 = max (0, WDI - 1.71)
BF16 = max (0, 1.71 - WDI)
BF17 = max (0, NO2 (AIRPORT) - 24.00)
BF19 = max (0, SR - 85.00)
BF20 = max (0, 85 - SR)

Table I.5 Model output MARS 1

# BFs	TotVar	DirVar	EffPar	GCV	Learn MSE	Test MSE
20	7	7	54.00	275.73	229.54	310.39
19	7	7	51.35	272.55	229.09	312.95
18	7	7	48.70	269.47	228.68	312.25
17	7	7	46.05	266.83	228.60	313.42
16	7	7	43.40	264.40	228.67	314.71
15	7	7	40.75	263.55	230.09	320.57
14	7	7	38.10	263.13	231.87	319.52
13	7	7	35.45	264.57	235.31	307.84
12	7	7	32.80	266.76	239.45	301.54
11	7	7	30.15	271.64	246.07	300.45
**10	7	7	27.50	277.20	253.40	295.57
9	7	7	24.85	284.71	262.62	299.58
8	6	6	22.20	292.77	272.49	316.68
7	5	5	19.55	299.68	281.42	320.44
6	4	4	16.90	317.61	300.91	358.46
5	4	4	14.25	322.79	308.53	371.09
4	4	4	11.60	362.97	349.98	419.57
3	4	4	8.95	426.75	415.07	525.53
2	3	3	6.30	463.77	454.99	595.38
1	1	1	3.65	567.10	561.17	655.35
0	0	0	1.00	925.14	921.49	852.28

Table I.6 Model identification MARS 2

Response OP (Airport) Summer Day

Summary of Fit	
R2	0.73
R2 (Adj)	0.73
RMSE	15.91
Mean of Response	78.93
Observations	506

Analysis of Variance	DF	SS	MS	F Ratio	Prob > F
Model	10	340838	34084	135	<.0001
Error	495	125434	253		
C. Total	505	466272			

Parameter Estimates	Estimate	Std Error	t Ratio	Prob>|t|
Constant	95.41	4.36	21.88	<.0001
BF2	-1.87	0.17	-11.29	<.0001
BF$	-4.65	0.74	-6.25	<.0001
BF5	7.82	1.50	5.22	<.0001
BF7	0.21	0.02	9.53	<.0001
BF9	-0.28	0.02	-11.77	<.0001
BF10	-0.92	0.21	-4.36	<.0001
BF12	4.06	0.77	5.29	<.0001
BF13	4.72	1.02	4.63	<.0001
BF18	-0.06	0.01	-5.52	<.0001
BF20	2.63	0.45	5.88	<.0001

BF2 = max (0, 24.00 - PM2.5 (AIRPORT))
BF3 = max (0, NO2 (AIRPORT) - 6.00)
BF4 = max (0, 6.00 - NO2 (AIRPORT))
BF5 = max (0, PRESS - 99.69)
BF7 = max (0, TEMP - 12.80) * BF3
BF9 = max (0, DP - 6.40) * BF3
BF10 = max (0, 6.40 - DP) * BF3
BF12 = max (0, 3.99 - NO (AIRPORT))
BF13 = max (0, WDI + 0.01)
BF18 = max (0, 30.30 - TEMP) * BF2
BF20 = max (0, 9.40 - DP)

Table I.7 Model output MARS 2

	Train		Test	
Hidden Nodes	R2	SSE	R2	SSE
1	0.70	139299	0.54	193565
2	0.77	108684	0.56	185535
**3	0.80	91626	0.58	178059
4	0.82	84669	0.57	182572
5	0.84	73998	0.54	192690
6	0.86	67053	0.49	213601
7	0.87	62547	0.51	206640
8	0.87	58456	0.51	206314
9	0.90	47335	0.54	195838
10	0.90	45519	0.55	189983

Table I.8 Model identification ANN

Hidden Node	Multiplier	Constant	PM2.5 (Airport)	NO (Airport)	NO2 (Airport)	CO (Airport)	
1	-1.89	-12.05	-0.10	0.48	-0.06	0.00	
2	0.75	1644.35	3.11	-0.89	1.44	-0.07	
3	3.79	-48.48	0.02	0.01	-0.04	0.00	
Hidden Node	**SR**	**Temp**	**DP**	**Press**	**Precip**	**WS**	**WDI**
1	0.00	0.05	-0.09	0.18	-0.35	0.03	-1.80
2	-0.01	0.48	-1.27	-15.92	-4.60	-0.75	-15.34
3	0.00	0.14	-0.20	0.49	-0.07	0.00	-0.13

Table I.9 Model output ANN

Hidden Nodes	Train		Test	
	R2	SSE	R2	SSE
1	0.70	139299	0.54	193539
2	0.77	108923	0.56	184648
3	0.80	91988	0.57	180726
4	0.83	80759	0.60	171082
5	0.84	74892	0.55	190681
6	0.86	67038	0.56	184314
**7	0.86	63908	0.67	141034
8	0.88	54770	0.51	207795
9	0.90	47915	0.50	210271
10	0.90	45247	0.64	153146

Table I.10 Model identification PC-ANN

Hidden Node	Multiplier	Constant	PC1	PC2	PC3	PC4	PC5	PC6	PC7	PC8	PC9	PC10	PC11
1	-3.41	-1.09	-0.29	-0.53	-0.53	-0.54	-0.76	-0.23	0.33	-0.92	0.27	-0.44	-1.70
2	-0.76	8.06	0.18	-2.85	2.79	1.23	-0.29	11.16	-5.55	2.22	-2.44	-4.70	-9.36
3	0.62	0.62	3.45	-6.86	-2.78	15.07	12.48	0.28	8.41	11.27	-1.27	-3.52	1.04
4	-2.96	0.28	-0.13	0.04	0.24	0.87	0.97	-0.08	-0.80	1.13	-1.08	2.20	0.89
5	0.87	4.67	-5.66	3.85	0.78	-5.55	2.95	-4.59	5.87	-2.23	-1.81	-1.72	4.96
6	0.83	-2.00	0.47	2.26	1.32	2.24	2.54	-0.25	-8.01	-3.51	-7.75	13.11	-2.67
7	1.31	-0.07	0.32	0.62	0.12	-1.54	0.82	1.62	-2.63	-3.83	2.68	1.96	0.53

Table I.11 Model output PC-ANN

	Train		Test	
Hidden Nodes	R2	SSE	R2	SSE
1	0.54	212917	0.46	228598
2	0.61	183478	0.53	198867
**3	0.64	168788	0.55	188601
4	0.67	155358	0.52	202941
5	0.68	151507	0.47	223958
6	0.70	140717	0.50	211097
7	0.71	137117	0.50	211988
8	0.71	133552	0.45	232686
9	0.73	124098	0.41	250347
10	0.73	123792	0.45	231049

Table I.12 Model identification PC*-ANN

Hidden Node	Multiplier	Constant	PC1	PC2	PC3	PC4
1	3.16	1.42	-0.42	-2.12	0.38	-0.4385472
2	-2.77	1.55	-1.06	-1.41	0.44	-0.5604144
3	-8.21	0.75	-0.06	-0.35	-0.10	0.235713

Table I.13 Model output PC*-ANN

Appendix J Sample Error Diagnostics
For Case Study 1 (Day Period)

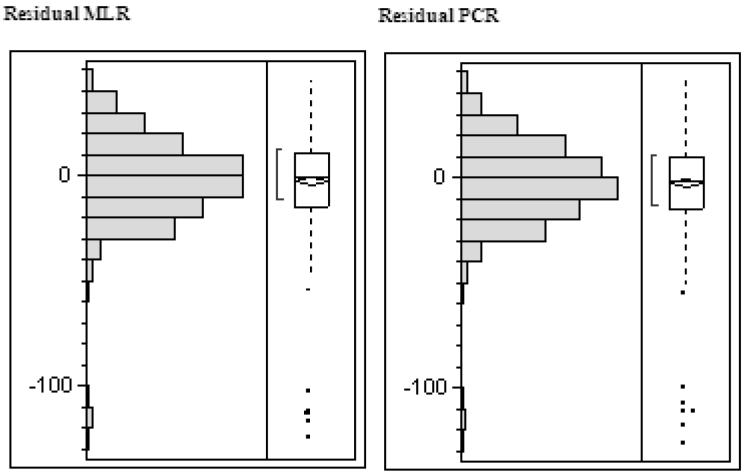

Quantiles

100.0%	maximum	45.4
99.5%		44.1
97.5%		33.5
90.0%		21.7
75.0%	quartile	10.6
50.0%	median	-1.1
25.0%	quartile	-15.2
10.0%		-24.0
2.5%		-40.3
0.5%		-115.5
0.0%	minimum	-125.3

Moments

Mean	-2.516235
Std Dev	21.336894
Std Err Mean	0.9580548
upper 95% Mean	-0.633879
lower 95% Mean	-4.39859
N	496

Quantiles

100.0%	maximum	48.4
99.5%		45.8
97.5%		33.4
90.0%		21.4
75.0%	quartile	10.3
50.0%	median	-1.7
25.0%	quartile	-15.6
10.0%		-26.4
2.5%		-41.7
0.5%		-115.3
0.0%	minimum	-126.5

Moments

Mean	-3.001421
Std Dev	21.352732
Std Err Mean	0.958766
upper 95% Mean	-1.117668
lower 95% Mean	-4.885174
N	496

Figure J.1 Residual Moments (MLR, PCR)

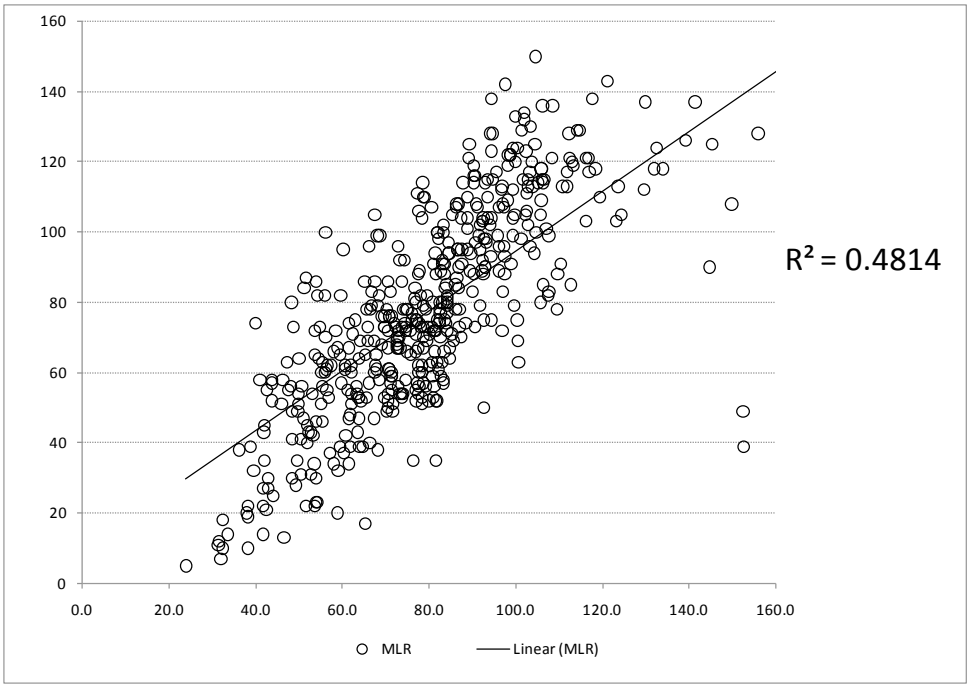

Figure J.2 Plot O_3 observed by O_3 predicted (MLR) in $\mu g/m^3$

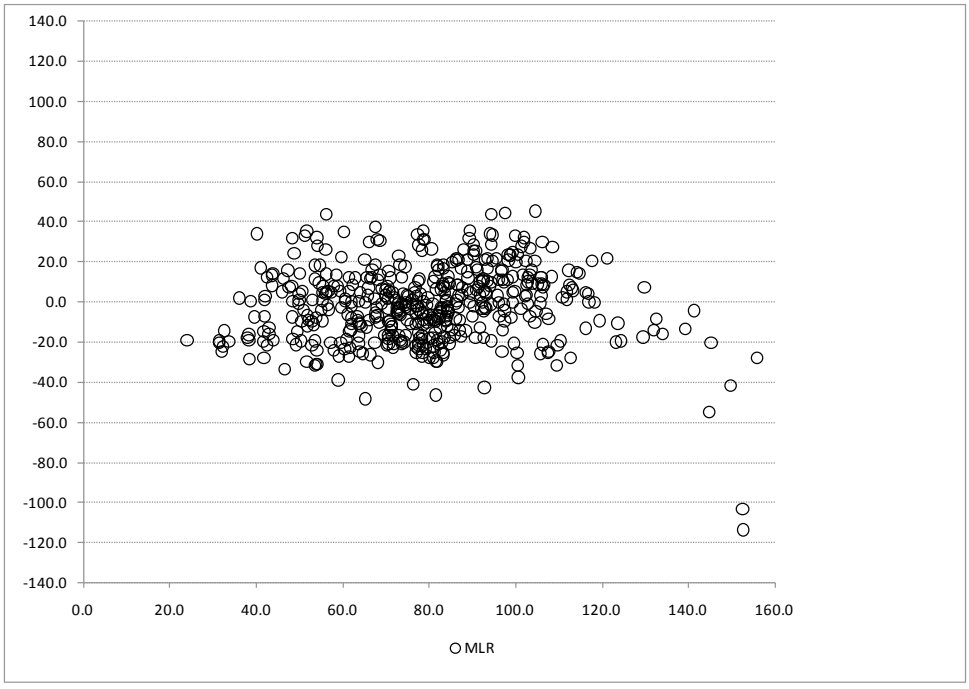

Figure J.3 Plot Residual by O_3 predicted (MLR) in $\mu g/m^3$

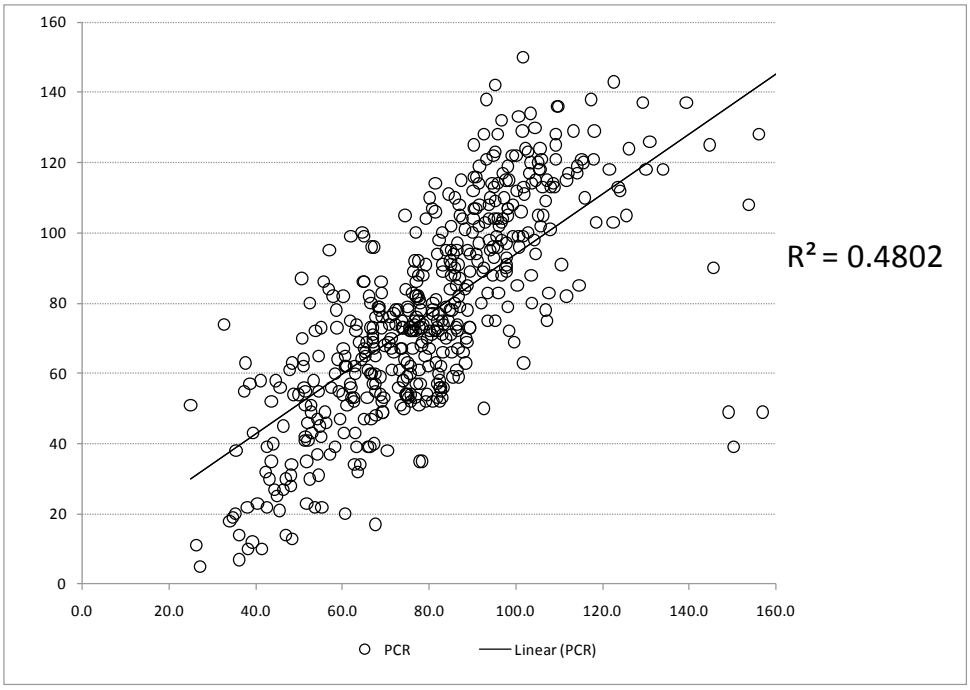

Figure J.4 Plot O_3 observed by O_3 predicted (PCR) in µg/m^3

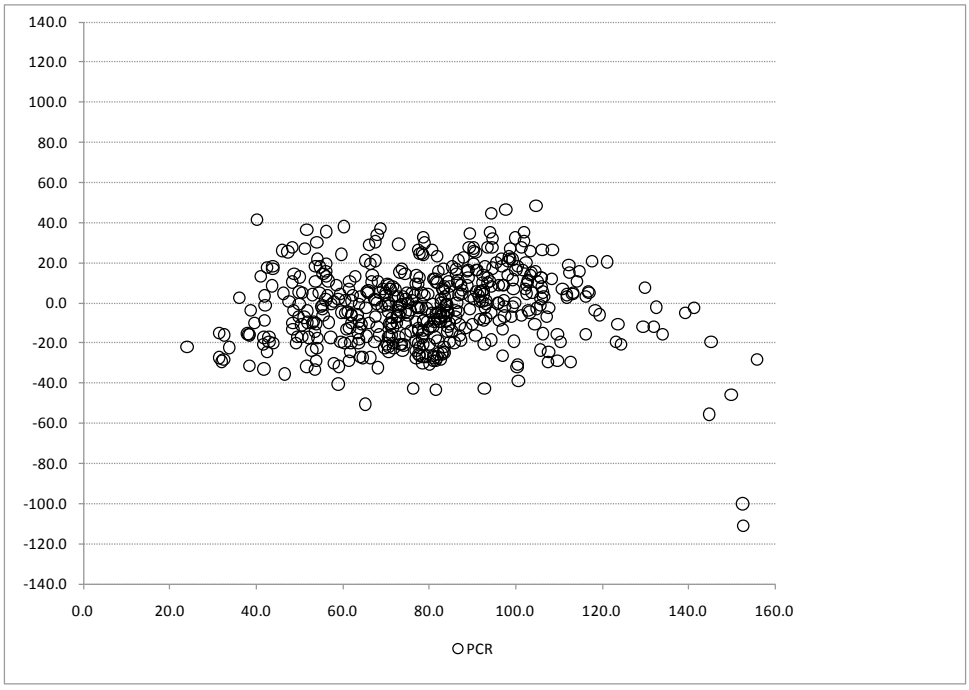

Figure J.5 Plot Residual by O_3 predicted (PCR) in µg/m^3

Residual MARS 1

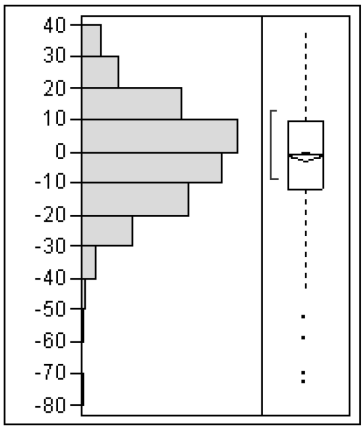

Quantiles

100.0%	maximum	39.46
99.5%		37.10
97.5%		31.56
90.0%		18.93
75.0%	quartile	9.85
50.0%	median	-0.81
25.0%	quartile	-11.87
10.0%		-20.85
2.5%		-34.83
0.5%		-64.69
0.0%	minimum	-72.93

Moments

Mean	-1.294454
Std Dev	16.543362
Std Err Mean	0.7428189
upper 95% Mean	0.1650131
lower 95% Mean	-2.75392
N	496

Residual MARS 2

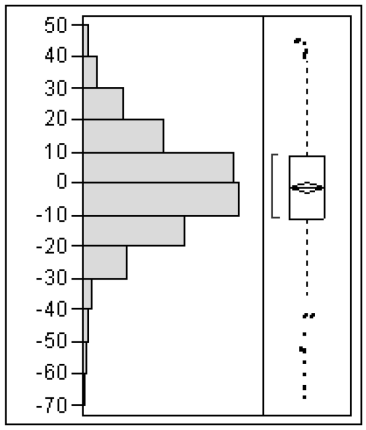

Quantiles

100.0%	maximum	44.78
99.5%		44.06
97.5%		30.80
90.0%		20.15
75.0%	quartile	9.04
50.0%	median	-1.33
25.0%	quartile	-11.04
10.0%		-21.28
2.5%		-39.17
0.5%		-62.78
0.0%	minimum	-67.69

Moments

Mean	-1.298896
Std Dev	17.16036
Std Err Mean	0.7705229
upper 95% Mean	0.2150032
lower 95% Mean	-2.812794
N	496

Figure J.6 Residual Moments (MARS 1, MARS 2)

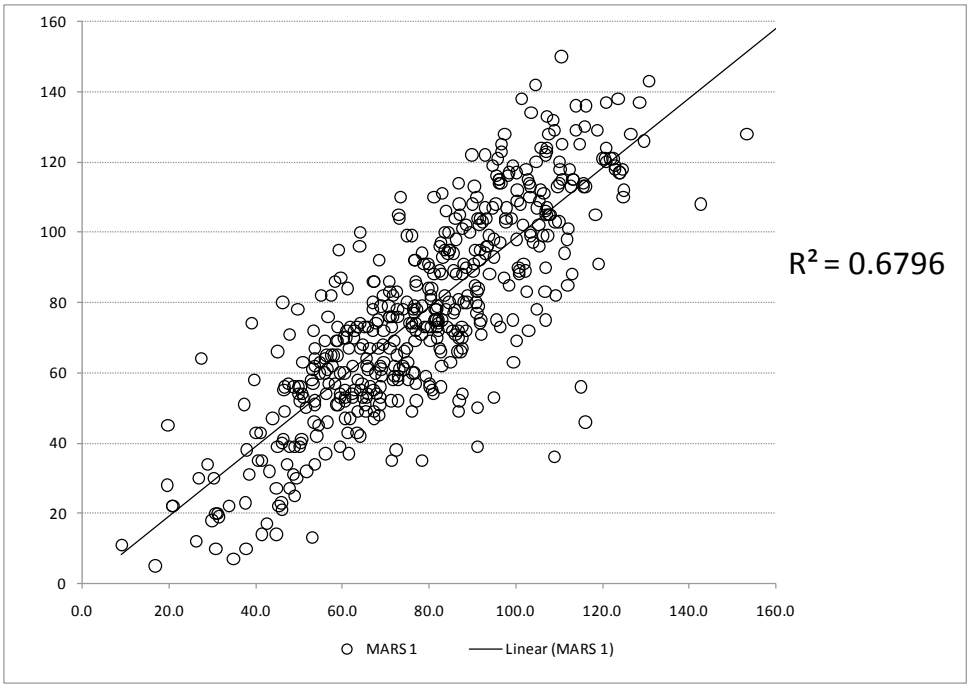

Figure J.7 Plot O_3 observed by O_3 predicted (MARS 1) in $\mu g/m^3$

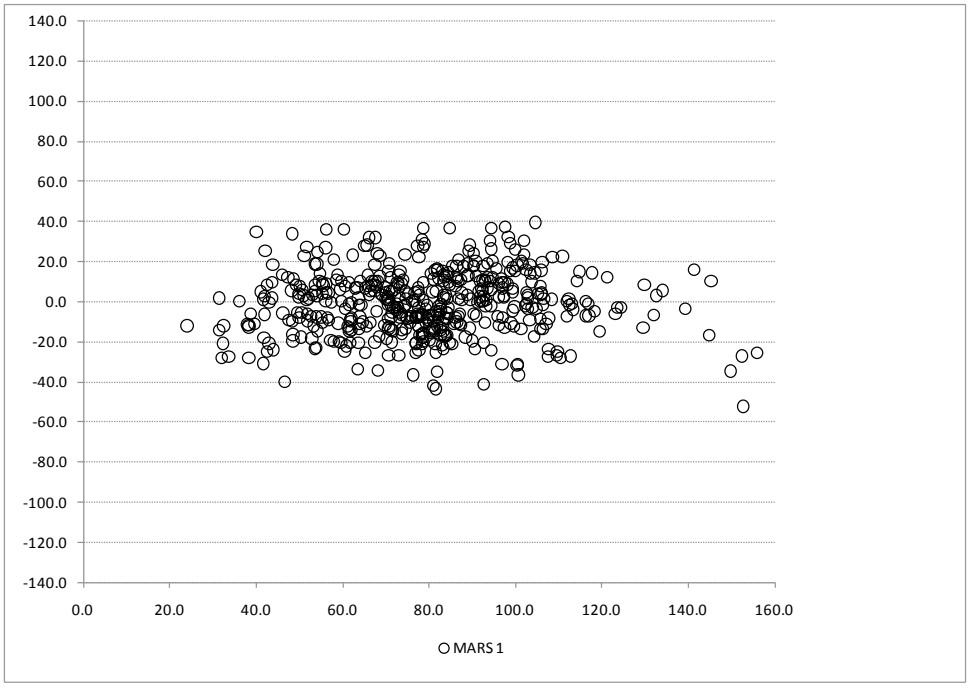

Figure J.8 Plot Residual by O_3 predicted (MARS 1) in $\mu g/m^3$

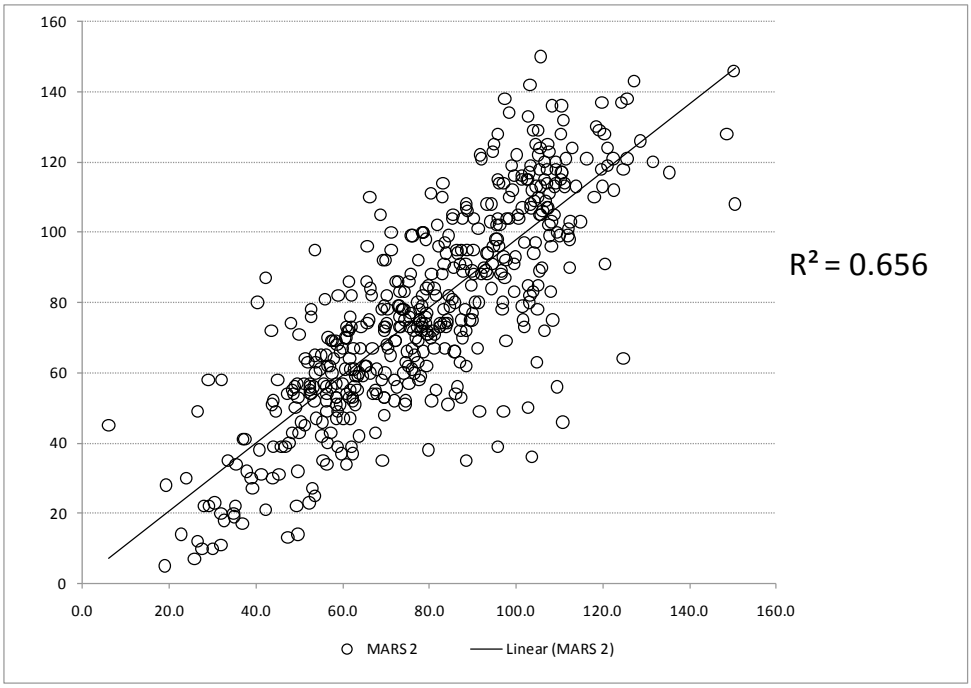

Figure J.9 Plot O_3 observed by O_3 predicted (MARS 2) in $\mu g/m^3$

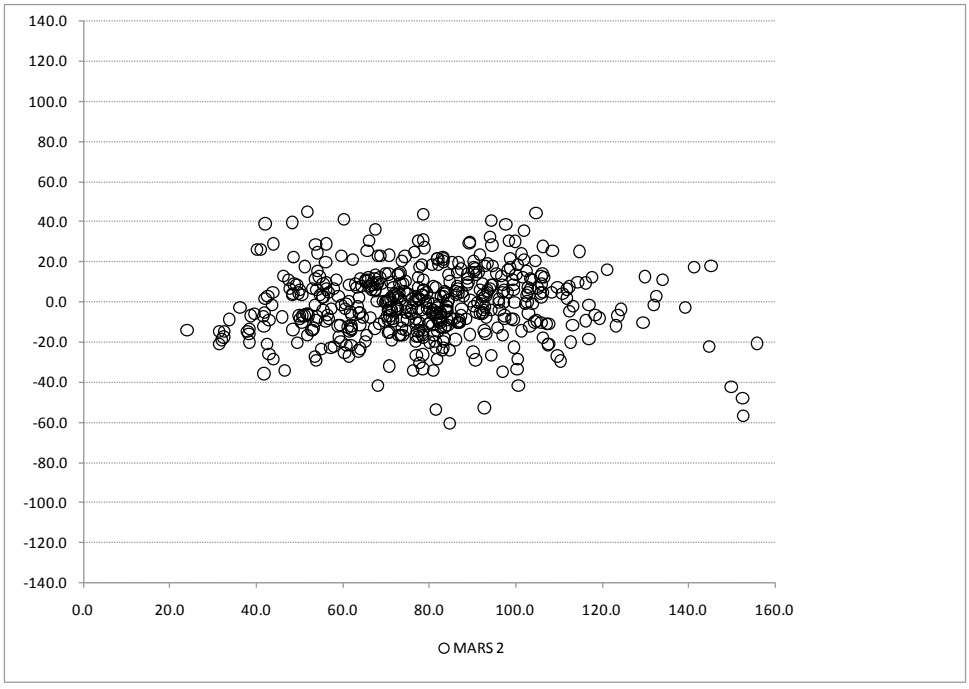

Figure J.10 Plot Residual by O_3 predicted (MARS 2) in $\mu g/m^3$

Residual ANN

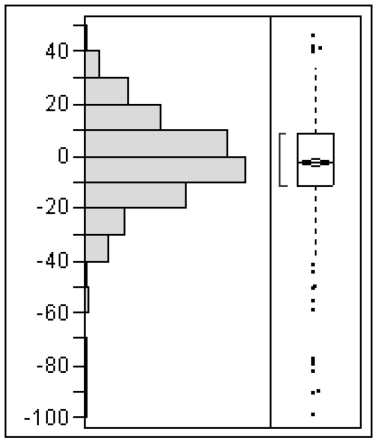

Residual PC-ANN

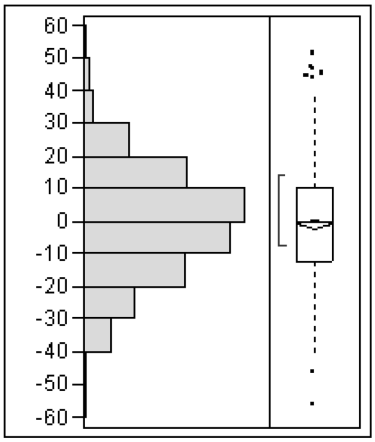

Quantiles

100.0%	maximum	45.81
99.5%		40.83
97.5%		30.38
90.0%		20.49
75.0%	quartile	8.05
50.0%	median	-2.01
25.0%	quartile	-11.46
10.0%		-23.33
2.5%		-40.85
0.5%		-90.63
0.0%	minimum	-99.29

Moments

Mean	-2.487075
Std Dev	18.802072
Std Err Mean	0.844238
upper 95% Mean	-0.828344
lower 95% Mean	-4.145807
N	496

Quantiles

100.0%	maximum	51.29
99.5%		46.70
97.5%		33.51
90.0%		20.23
75.0%	quartile	10.08
50.0%	median	-0.0828
25.0%	quartile	-11.92
10.0%		-23.37
2.5%		-33.83
0.5%		-44.45
0.0%	minimum	-56.13

Moments

Mean	-0.832116
Std Dev	16.858938
Std Err Mean	0.7569887
upper 95% Mean	0.6551907
lower 95% Mean	-2.319424
N	496

Figure J.11 Residual Moments (ANN, PC-ANN)

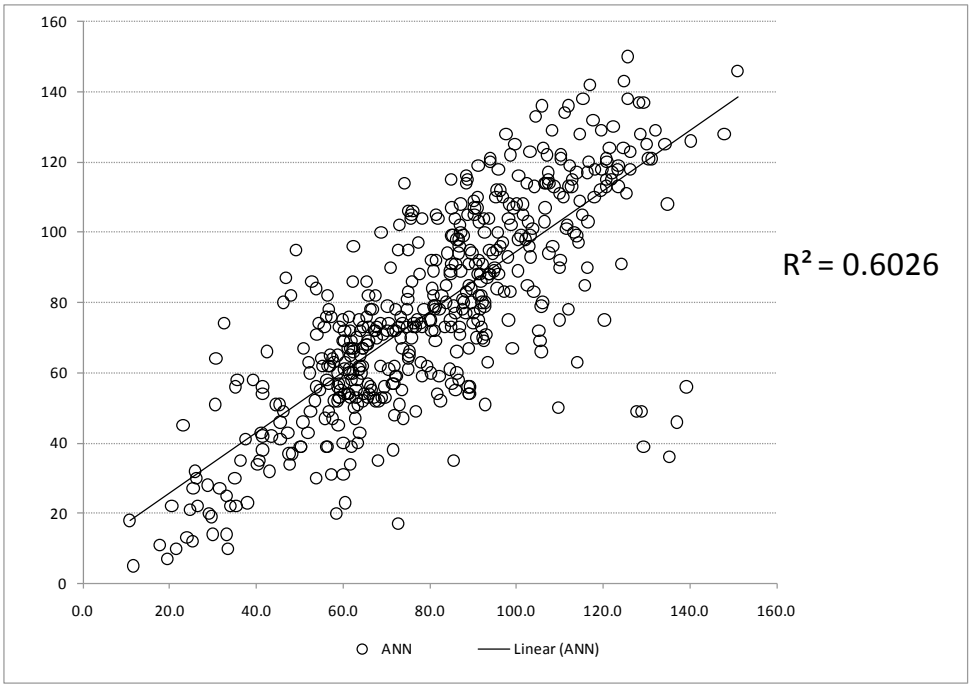

Figure J.12 Plot O_3 observed by O_3 predicted (ANN) in $\mu g/m^3$

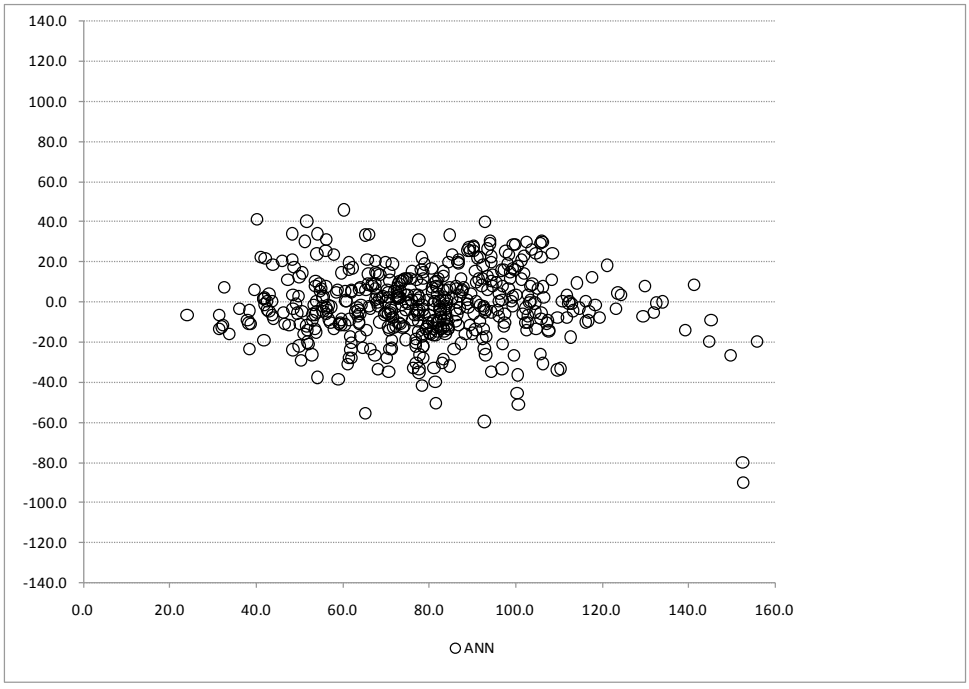

Figure J.13 Plot Residual by O_3 predicted (ANN) in $\mu g/m^3$

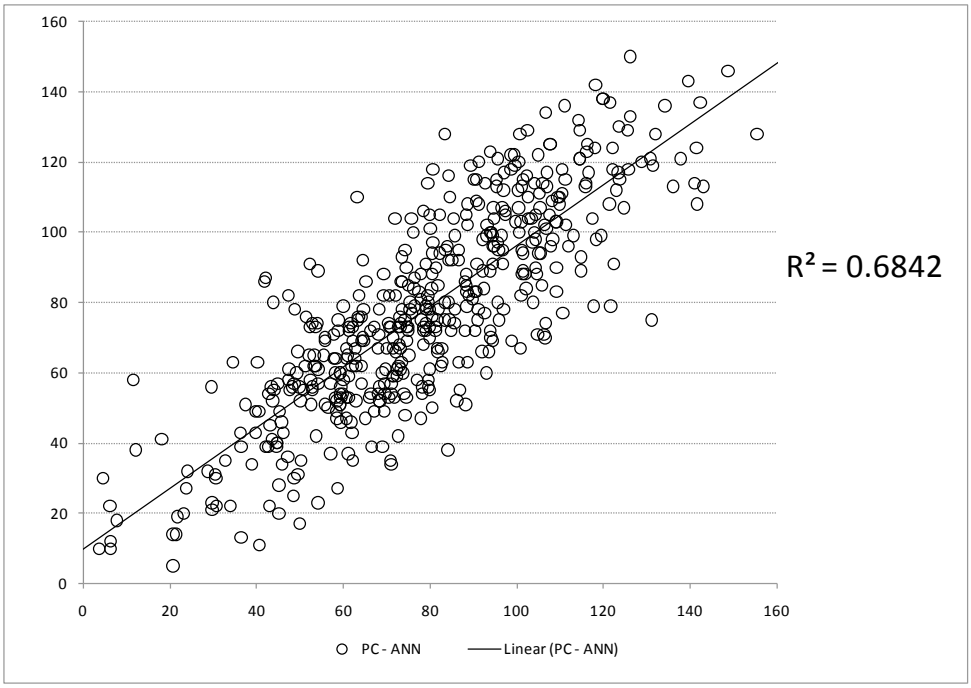

Figure J.14 Plot O_3 observed by O_3 predicted (PC-ANN) in $\mu g/m^3$

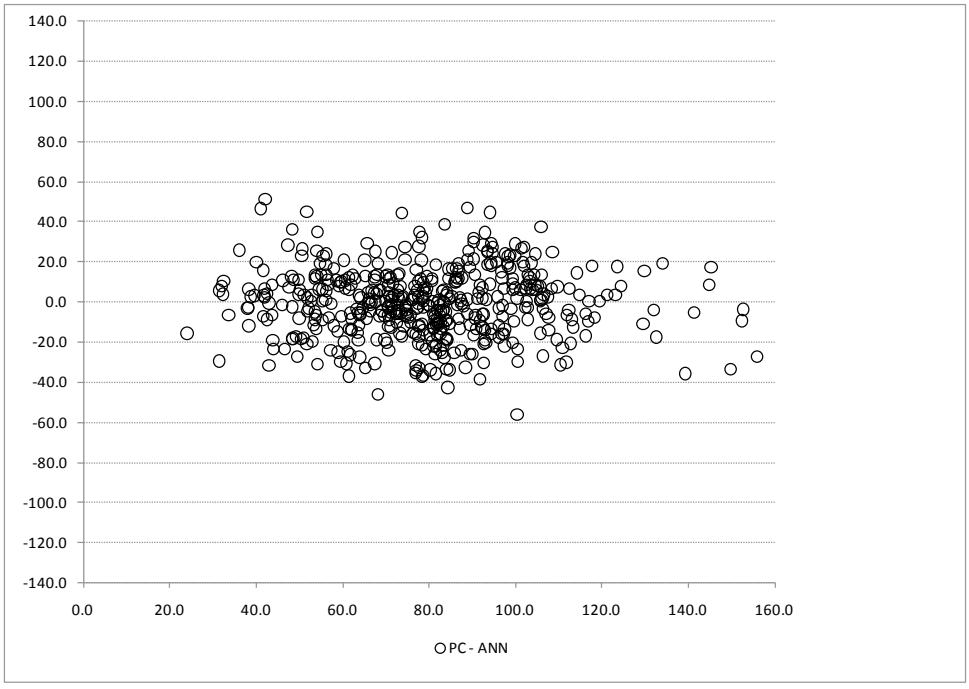

Figure J.15 Plot Residual by O_3 predicted (PC-ANN) in $\mu g/m^3$

Residual PC*-ANN

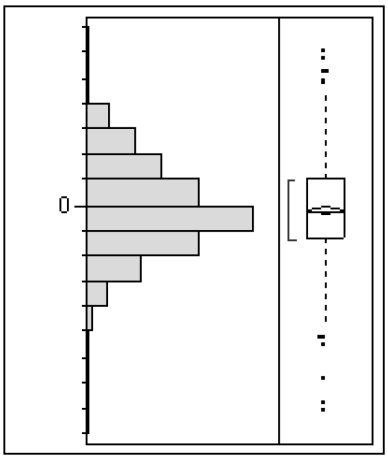

Quantiles

100.0%	maximum	60.14
99.5%		54.62
97.5%		36.84
90.0%		23.66
75.0%	quartile	9.88
50.0%	median	-3.03
25.0%	quartile	-13.58
10.0%		-24.46
2.5%		-40.19
0.5%		-73.53
0.0%	minimum	-81.70

Moments

Mean	-1.817008
Std Dev	19.434622
Std Err Mean	0.8726403
upper 95% Mean	-0.102472
lower 95% Mean	-3.531544
N	496

Figure J.16 Residual Moments (PC*-ANN)

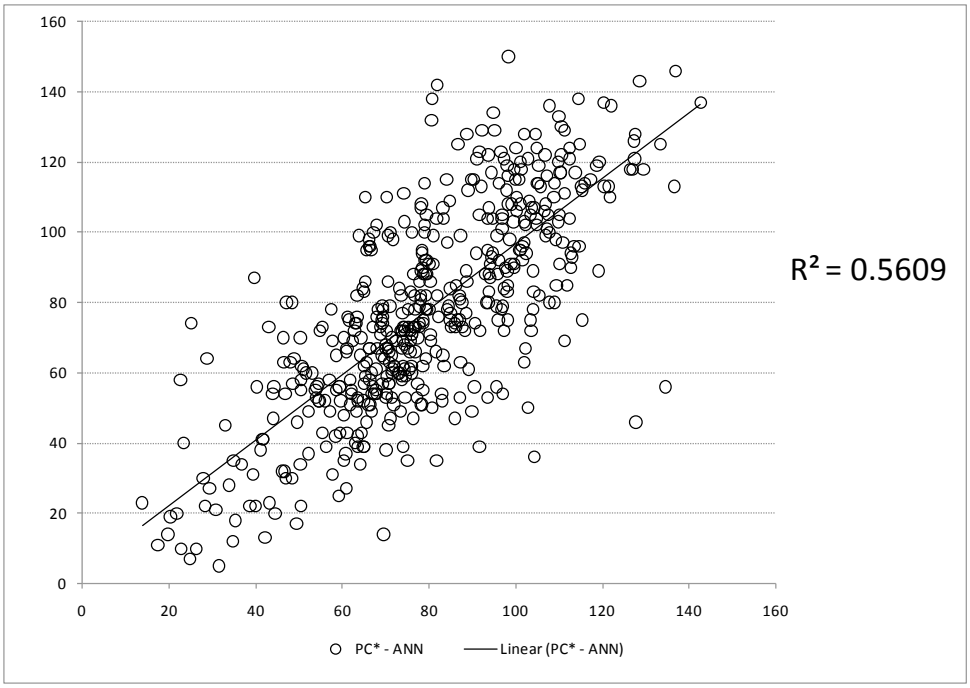

Figure J.17 Plot O_3 observed by O_3 predicted (PC*-ANN) in $\mu g/m^3$

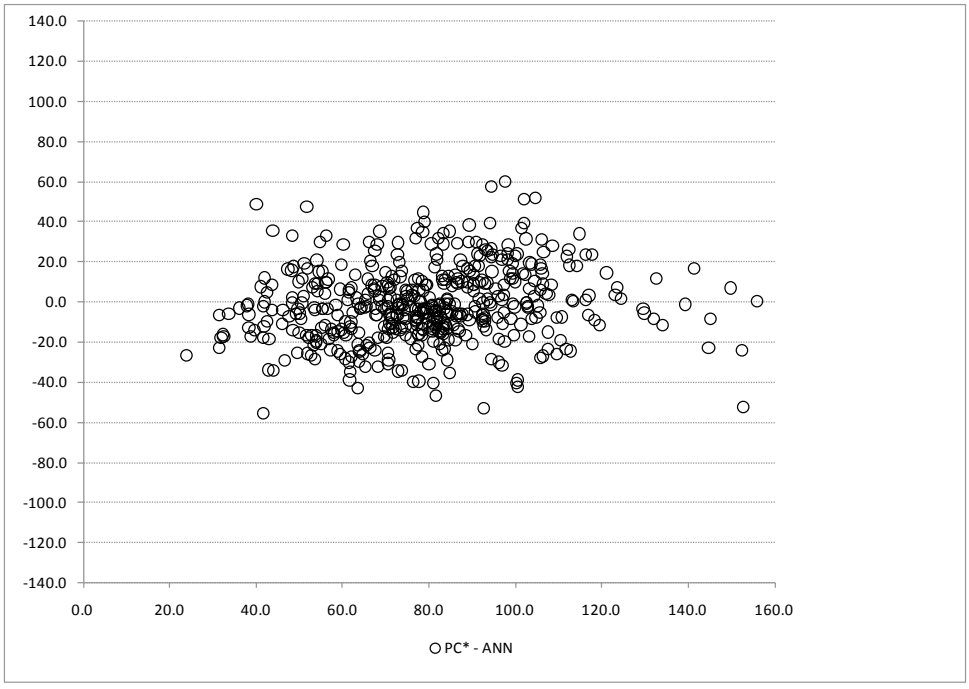

Figure J.18 Plot Residual by O_3 predicted (PC*-ANN) in $\mu g/m^3$